Engineered micro-devices for the isolation of circulating tumor cells in clinical routine

Alejandro Kayum Jimenez Zenteno

▶ **To cite this version:**

Alejandro Kayum Jimenez Zenteno. Engineered micro-devices for the isolation of circulating tumor cells in clinical routine. Micro and nanotechnologies/Microelectronics. Université Toulouse 3 Paul Sabatier (UT3 Paul Sabatier), 2018. English. NNT : . tel-02137588

HAL Id: tel-02137588

https://laas.hal.science/tel-02137588v1

Submitted on 23 May 2019

HAL is a multi-disciplinary open access archive for the deposit and dissemination of scientific research documents, whether they are published or not. The documents may come from teaching and research institutions in France or abroad, or from public or private research centers.

L'archive ouverte pluridisciplinaire **HAL**, est destinée au dépôt et à la diffusion de documents scientifiques de niveau recherche, publiés ou non, émanant des établissements d'enseignement et de recherche français ou étrangers, des laboratoires publics ou privés.

THÈSE

En vue de l'obtention du

DOCTORAT DE L'UNIVERSITÉ DE TOULOUSE

Délivré par l'Université Toulouse 3 - Paul Sabatier

Présentée et soutenue par

Alejandro Kayum JIMENEZ ZENTENO

Le 21 septembre 2018

Micro-dispositifs pour l'isolement des cellules tumorales circulantes en routine clinique

---

Ecole doctorale : **SDM - SCIENCES DE LA MATIERE - Toulouse**
Spécialité : **Nanophysique**

Unité de recherche :
LAAS - Laboratoire d'Analyse et d'Architecture des Systèmes

Thèse dirigée par
Christophe VIEU et Aline CERF

Jury

M. Emmanuel DELAMARCHE, Rapporteur
Mme Julia R. GREER, Rapporteur
Mme Catherine PICART, Examinateur
M. Scott VERBRIDGE, Examinateur
M. Utkan DEMIRCI, Examinateur
M. Jérémie GRISOLIA, Examinateur
M. Christophe VIEU, Directeur de thèse
Mme Aline CERF, Co-directeur de thèse

Acknowledgments

Gratitude matters. I thank both Aline Cerf and Christophe Vieu for giving me the opportunity to explore this life-changing experience usually called a doctorate. I appreciate their guidance all along during this challenging research work, first as an intern and later back as a Ph.D. student. To them my sincere gratitude. My sincere thanks also to the whole *Engineering in Life Science Applications* (ELiA) research group.

I would also like to thank all members of the *Technique and Equipments Applied to Micro and nanotechnologies* (TEAM) group, particularly to David Bourrier, for his valuable support to face and conduct the technological achievements of this research work. I also extend my thanks to Charline Blatche and Xavier Dollat from the *Instrumentation Conception Caractérisation* (I2C) group.

My deepest thank to my friends and colleagues Aurore Esteve, Elise Bou, and Hélène Cayron, with whom I had the pleasure to collaborate very closely during this project. Besides them, I also thank my other fellows for being more than labmates: Emma, Maxime, Lin, Julie, Kevin, Adrian, Lucie, Cécile, Matthieu, Angelo, Dolores, Roberto.

Of course, I cannot leave my family aside. Thanks mom and dad, Angélica and Pascual, to always encourage my dreams. Thanks, Yunuem, Yareni and Tania for always being by my side despite the distance.

I acknowledge the financial support from the French National Research Agency (ANR-15-CE19-0020) and the facilities of the French National Nanofabrication Network (RENATECH). I also thank the National Council of Science and Technology (CONACYT) of Mexico for the doctoral fellowship granted.

Table of Contents

Introduction

Cancer is a family of diseases resulting from the combination of genetic changes and environmental risk factors, and it is one of the major public health concerns throughout the world. During the last decades, novel methods for tumor detection at a favorable stage have favored an earlier implementation of treatment strategies in patients. In the field of cancer diagnosis, there is a growing expectation around the use of liquid biopsies, blood-based cancer screening, for the monitoring of the disease progression and treatment response, serving as a means to guide personalized therapies.

Circulating tumor cells (CTCs), cancer cells rarely found in the bloodstream, are considered to be the main source of metastases, and have been recognized as a blood-based cancer biomarker. Several technologies have been recently developed to isolate these rare cells from blood. However, so far only a few methods have received regulatory approval, limiting the application of liquid biopsy in daily clinical practice.

In this PhD work, we present novel microfiltration devices for the isolation of CTCs from whole blood. Our approach, based on microfabrication technologies, offers the possibility of being adapted to clinical requirements in order to facilitate the screening of significantly higher volumes of blood than current technologies and under physiologically relevant flow conditions. This multidisciplinary project covers areas such as microfabrication techniques, fluid dynamics, and cancer cell biophysics. The work presented in this manuscript is organized into three chapters.

In chapter I, we provide an extensive review of the different stages involved in the tumor dissemination emphasizing those in which CTCs are involved. We also introduce the concept of liquid biopsy and contextualize the role of CTCs in the field. In this chapter, we further review the main biophysical and biochemical properties of CTCs, and these are compared to the ones of blood cells. In addition, we introduce the most commonly used techniques for the isolation and identification of CTCs from blood samples. The last part of this chapter is dedicated to underline the relevance of CTCs as prognostic biomarker and the current challenges in the field of liquid biopsy.

Chapter II sets the theoretical basis of blood microfiltration, which serves as the fundaments to design the first three-dimensional capture microdevice adapted to the *in vivo* constraints. We then describe the implementation of a fluidic test-bench, which is used to provide the first formal demonstration of cancer cell capture from whole blood samples. We also discuss possible hydrodynamic effects near and within the capture microdevice influencing cancer cell trapping, as well as the detection limit. Finally, this chapter also evaluates the possibility to translate our proposed design to real in vivo settings.

Finally, in chapter III we introduce novel microengineered cell capture microdevices based in electrochemical deposition of metals. We evaluate the cell capture performance under *in vitro* and *in vivo* conditions, confirming the feasibility of our proposed approach. We further extrapolate this concept and fabrication technique to a portable microfilter, which fulfills the requirements of point-of-care systems.

Chapter I

Liquid Biopsy: an emerging-concept towards precision medicine

Chapter I

Liquid Biopsy: an emerging-concept towards precision medicine

1.1 Cancer as a disease

Cancer is referred as a generic term for a large group of related diseases characterized by the continual and **unregulated proliferation** of cells. It is believed that cancer onset is the result from a series of genetic changes directly linked with cell division and growth deregulation. Cells growing in an uncontrolled manner, invade normal tissues and organs resulting in an **abnormal neoplasm formation**, commonly referred as tumor.

In oncology, tumors are classified according to the type of cell from which cancer originates and are grouped into three main categories: **carcinomas**, **leukemias/lymphomas**, and **sarcomas**.[1] Carcinomas account for 80-90% of all cancers and are originated from epithelial cells. Leukemias and lymphomas form the second major group covering approximately 8% of malignancies, and arise from blood-forming cells at the bone marrow site and from cells of the immune system, respectively. The third group refers to cancer originated in supportive and connective tissues such as bone and muscle and represents a rare group in humans. Hereinafter and along this manuscript, the term tumor will just refer to the carcinoma type.

Similarly to other medical conditions, some symptoms may indicate the presence of a tumor and depending on its type, imaging procedures and direct sampling of tissue will allow **diagnosis** of cancer. Pathological analysis from solid tissue, **biopsy**, determines the malignancy of tumors. A tumor is considered as malignant when it is capable of both invading surrounding normal tissue and spreading throughout the body. Only diagnosed **malignant tumors** are **referred as cancers**, and they are commonly classified under the TNM staging system which mainly considers the size and extent of the primary tumor (T), the spread extent to the lymph nodes (N), and the presence of metastasis (M).[2]

There are more than **100 types** of cancers, usually named by the organs or tissues where they form, but only a few occur frequently. The incidence, prevalence, and mortality from major types of cancer were estimated for 184 countries worldwide in 2012, latest year available, by the GLOBOLCAN project from the International Agency for Research on Cancer (IARC). Those cancer statistics exhibit that **breast, colorectal,** and **lung** cancers are the most incident cases in women while **lung, prostate,** and **colorectal** are the most frequent in men.[3]

Although the formation of a tumor in a **primary site** implies a health risk for patients, the formation of **distant metastases** is the deadliest phase of cancer progression as it is not possible to prevent it yet and treatments are much less successful. Patients with metastatic disease often have one or more clinically detectable micrometastatic/macrometastatic foci, however it is likely that many others could be present but not detectable. One of the reasons of the **poor outcome** of treatments is that current **treatment strategies** are usually based on the pathological and molecular characterization of the primary tumor and not from the overall setting including metastatic lesions. Thus, there is a **clinical need** to obtain information of the hardly accessible and/or undetectable metastases in order to provide more effective therapies in patients.

1.2 Tumor progression and cancer dissemination pathway

The development of a tumor is a **multistep process** as a consequence of multiple abnormalities which accumulate over time. Tumor onset is thought to be the result of a genetic alteration at the cellular level. Broadly, malignant cells will proliferate and interact with many other surrounding cells forming what is known as a **tumor microenvironment**. This heterogeneous cellular environment contains cells of the immune system, fibroblasts, vasculature and lymphatic nodes, as well as extracellular matrix.[4] Altogether the latter interact in a **dynamic** manner but little is known about their **biological interactions** and functions during tumor progression even though they are widely investigated today. The net contribution of the interaction between the tumor and its microenvironment regulate, either positively or negatively, tumor survival and progression. At early stages, the microenvironment tends to exert anti-malignant functions, whereas at late stages it exerts pro-malignant ones.[5]

According to the Darwinian model, **tumors evolve** towards greater malignancy over time promoting an invasive behavior and dissemination in later stages of tumor evolution, thus, the development of **distant metastases** is the final step in tumor progression.[6,7] This model successfully explains the steps of tumor progression and it has naturally been extended to account for cancer metastasis, however, it faces conceptual problems to explain clinical observations suggesting that metastatic seeding occurs prior to the formation of an identifiable primary tumor.[7–10] These clinical observations are the basis of a new model of cancer spreading. Currently, both hypotheses are widely studied, however, the second one faces greater challenges given its clinical nature.

In 1889, Stephen Paget stated the 'seed and soil' hypothesis in order to elucidate the formation of metastases in certain organs, e.g. breast and prostate cancer often metastasize in bone, establishing that tumor cells (*seeds*) from a primary tumor have a preference for specific organs (*soil*) concluding that metastases form only when the seed and soil are compatible.[11] This phenomenon is also known as metastatic organotropism. Accordingly, the metastatic cascade mainly comprises the physical translocation of a cancer cell from the primary tumor to the microenvironment of a distant tissue, and having as end stage its colonization. This process consists in a series of complex steps, which must be successfully completed, involving (**Figure 1.1**):

b) angiogenesis, forming new blood vessels,
c) intravasation, where tumor cells detach and leave the primary tumor via the bloodstream or the lymphatic system,
d) tumor cells survival in the bloodstream and arrest in capillaries of distant organs,
e) extravasation of tumor cells, and
f) colonization and formation of a secondary tumor.

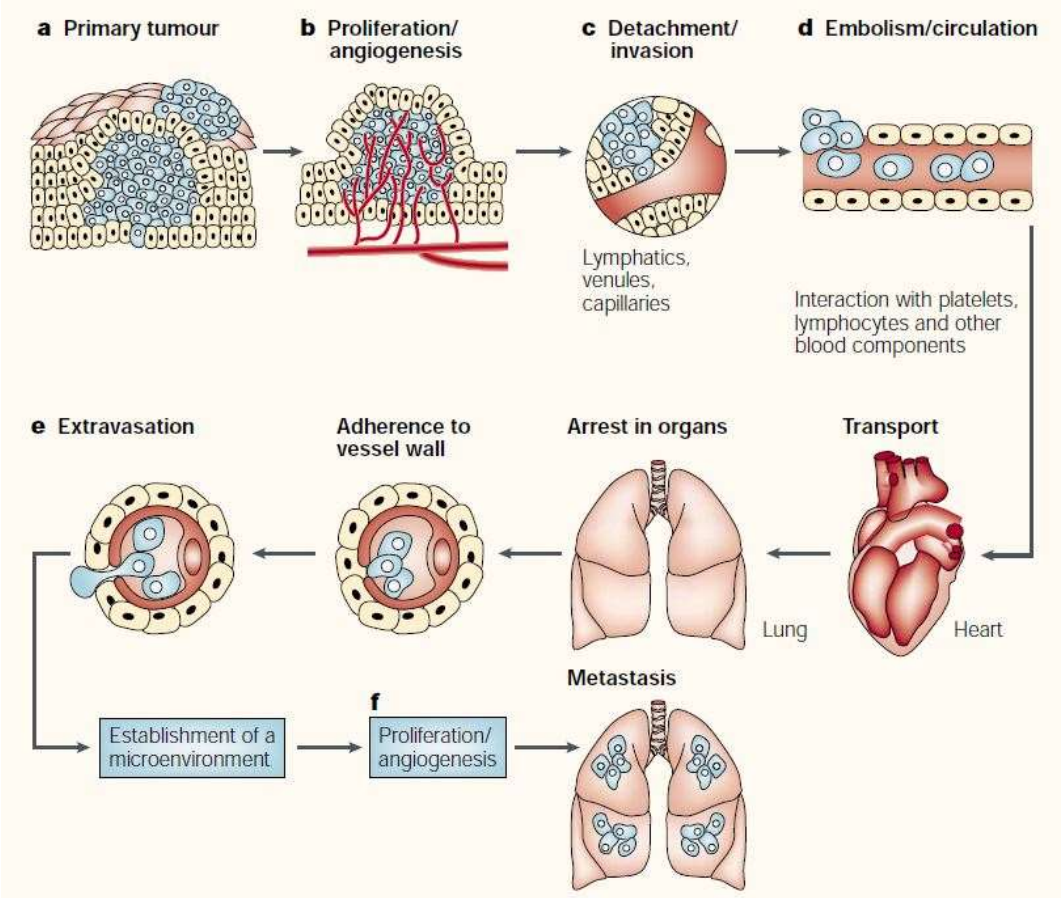

Figure 1.1 The main steps in the formation of metastasis. Figure extracted from *IJ Fidler, Nature Reviews Cancer, 2003*.[12]

At early stages of tumor formation, neoplastic cells are supplied with nutrients and oxygen by simple diffusion. When the tumor reaches a specific size, 1-2 mm, vascularization is needed for the tumor to grow, in fact, **angiogenesis** is a prerequisite for massive tumor growth and metastatic progression.[13] This neo-vasculature can also provide an **escape route** from which cells can leave the tumor and enter into the body's circulatory blood system. Tumor cells must first detach from the primary tumor and invade towards blood vessels, penetrating the basement membrane and the endothelium, and finally disseminating through the blood vessel. Cancer invasion is initiated and maintained by signaling pathways that control **cytoskeletal dynamics** in tumor cells and regulate the mechanism of cell adhesion (cell-matrix and cell-cell). This suggests the **microenvironment** plays a significant role in determining cancer cell migration.[14,15]

Depending on the tumor environment, **cancer cell migration** can occur individually, when cell-cell junctions are absent, or collectively as multicellular groups, when cell-cell adhesions are retained. Cancer invasion not always is the result of an active cell migration. When the surrounding tissue does not hinder the expansion of the tumor, the expansive growth may displace cells by volume expansion and pushing, this phenomenon accounting for a **passive migration** mode.[14] On the other hand, the process of cancer cell individualization and acquisition of an invasive migratory phenotype is

associated with the activation of the **epithelial-to-mesenchymal transition (EMT)** program, which allows an **active migration** of cancer cells **Figure 1.2**. It has been observed that invading cells often display characteristic EMT markers, such as downregulation of E-cadherin and upregulation of Vimentin expression, while losing some epithelial characteristics, such as polarity.[16] However, the downregulation of E-cadherin expression is likely tunable as evidenced by the identification of hybrid phenotypes, suggesting that cells could undergo a partial EMT process during migration.[17] Tumor cells transitioning between epithelial and mesenchymal phenotypes, (i.e., partial EMT) have mixed epithelial (e.g., adhesion) and mesenchymal (e.g., migration) properties, thereby allowing them to move collectively as clusters.[18] More recently, a cooperative model has also been proposed in which EMT and non-EMT cells cooperate to complete the migration process and subsequent metastasis.[19,20]

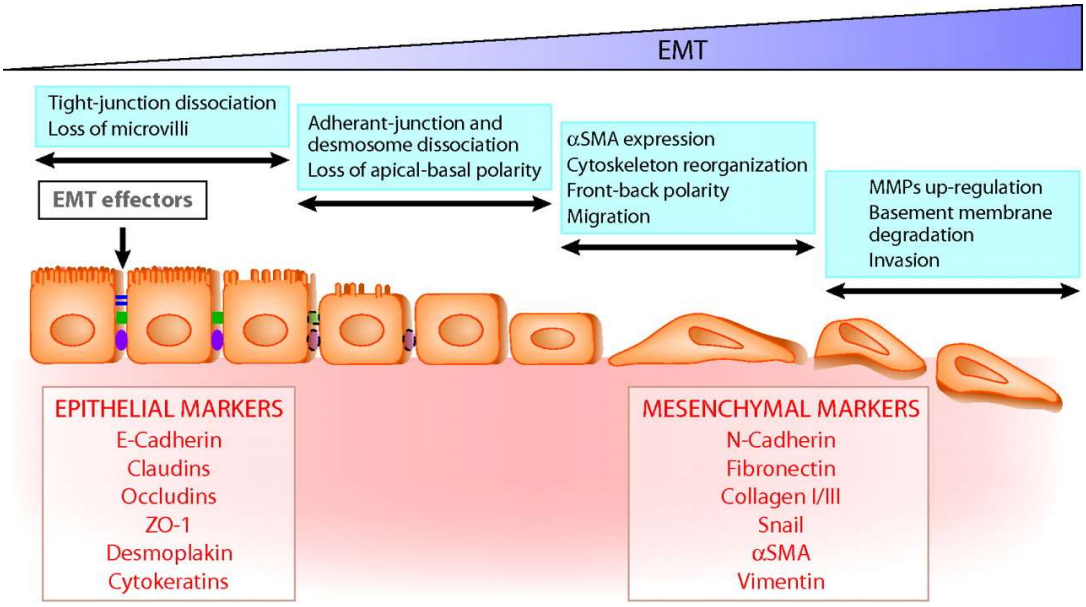

Figure 1.2 Epithelial-to-mesenchymal transition. Figure adapted from *LS. Aroeira et al, J Am Soc Nephrol., 2007*.[21]

Migratory cells that detached from the primary tumor and successfully intravasate into blood vessels are likely to follow the **hematogenous route** for spreading through the body. Although the circulatory system is frequently considered as the major route for cancer dissemination, evidence suggests that the lymphatic system also plays a role in it.[22] Gaining access to the circulatory system provide tumor cells, in this stage of cancer spreading also known as **circulating tumor cells (CTCs)**, direct access to virtually all organs of the body.

The amount of cells released by the tumor and entering the blood circulation is estimated to be in the range of millions, 3 to 4 millions of cells/day per gram of primary tumor in murine models,[23] but just a few would survive within the bloodstream. Once into the blood circulation, major CTC death occurs due to anoikis, a programmed cell death that occurs when they detach from the extracellular matrix.[24] CTCs are also directly exposed to the innate immune system and most of them are cleared

by natural killer (NK) cells through immune-cell-mediated lysis. Nevertheless, a small subpopulation of CTCs might evade or survive encounters with immune cells by means of diverse mechanisms.[25] Additionally, CTCs must survive the effects of fluid shear within the blood flow in order to contribute to metastatic seeding. Based on these observations, we can infer that the persistence of CTCs in blood circulation is limited, certainly, its half-life has been estimated to be in the range of 1-2.4 h, in breast cancer patients.[26] Further discussion regarding CTCs is presented in section 1.3.1.

Cancer cells in blood circulation will disseminate following blood-flow patterns. In fact, in 1920, James Ewing challenged the 'seed and soil' hypothesis suggesting that circulatory patterns between a primary tumor and determined secondary organs were sufficient to initiate organ-specific metastasis.[27] Both hypotheses are not mutually exclusive, but rather, complementary and it is believed that both contribute to the formation of site-specific metastasis, as evidenced by various autopsy studies and murine in vivo models.[28–31] Thus, routing dictated by the innate blood circulation and the local microenvironment of the host organ determine the formation of a secondary tumor.

CTCs usually get trapped in the first (or second) capillary bed they encounter during their first pass through the heart, this due to size restriction since they are generally 2 to 4-fold larger in diameter than capillaries (~8-µm diameter), **Figure 1.3a**. Other physical factors such as hemodynamic forces and deformability of the cancer cell will determine their arresting in the microvasculature.[32] It is thought that physical trapping within capillaries is one of the mechanisms exploited by tumor cells for extravasation. However, CTCs can undergo adhesive lodging in pre-capillary vessels (venules) that are larger than the cancer cell, via adhesion molecules which facilitate direct interaction with the endothelium, **Figure 1.3b**.[31,33] Only those cells that find a stable adhesion and chemoattractive gradient arising from a particular tissue will extravasate into a new site.

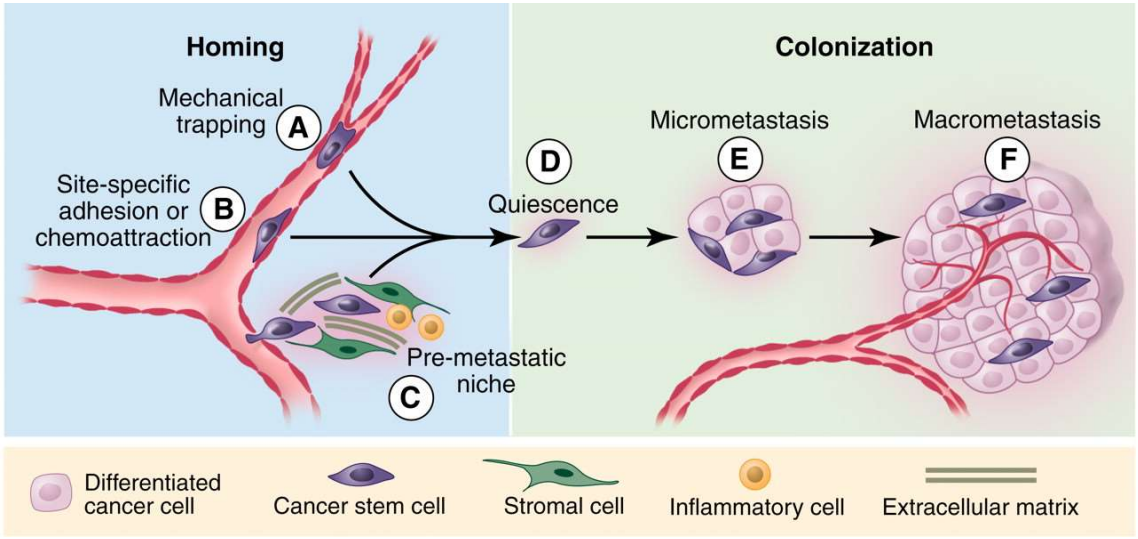

Figure 1.3 Homing and colonization of circulating tumor cells. Figure adapted from C.*L. Chaffer and R.A Weinberg, Science., 2011*.[34]

Infiltrated cancer cells may invade the local extracellular matrix, and colonize the targeted distant tissue. In addition, CTCs can also re-infiltrate their primary tumors of origin (self-seeding) and affect tumor progression.[35] Molecular interactions between the local microenvironment and the extravasated CTCs, also known as **disseminated tumor cells (DTCs)**, are critical and will determine DTCs survival and adaptation. This stage of the metastatic cascade is considered to be the less efficient, only a small subset (<0.01%)[36] of infiltrated cancer cells is able to initiate cell division and proliferate, and the vast majority will undergo apoptosis within 24 hours of extravasation.[37,38] Accordingly, cells that survive to the new microenvironment would form **micrometastases** and an even smaller portion of them will continue their growth to form macroscopic metastases, **Figure 1.3e-f** . This suggests that only a subset of CTCs has a metastasis-initiating capacity.[39,40] It is thought that CTCs with an epithelial-like phenotype are more suitable for colonization, meaning that metastases might arise from CTCs with preserved epithelial characteristics or from cells that have undergone EMT and upon reaching a secondary organ undergo the reverse process, **mesenchymal-to-epithelial transition (MET)**.

Moreover, infiltrated CTCs can adopt a **dormancy state**, meaning that viable DTCs may persist and survive within the host tissue for long periods of time in a quiescent-nonproliferative state, **Figure 1.3d**. The mechanisms governing this quiescent state remain elusive and are the subject of intense investigation.[41,42] In line with this idea, the parallel-progression model of cancer metastasis is reinforced proposing that early dissemination of cancer cells from the primary tumor may occur and may undergo parallel progression.[43] To add an extra layer of complexity, it was recently suggested that distant tissue microenvironment could undertake a series of molecular and cellular changes to form a **pre-metastatic niche** before the arrival of tumor cells, and subsequently, both facilitate tumor cell colonization and promote metastasis.[44] This phenomenon could be driven by the interplay among primary tumor-derived factors, tumor-mobilized bone marrow-derived cells, and local stromal components.[45]

As here depicted, the fate of metastasis relies on the translocation of tumor cells and their colonization in a distant host environment. From a therapeutic standpoint, understanding the mechanisms of physical translocation would provide insights and new therapeutic strategies for preventing metastasis in patients who are diagnosed with early cancer lesions. The comprehension of mechanisms leading to a successful colonization could lead to more effective therapies in patients with already-established metastases. Therefore, the successful translation of new research findings into clinical routine depends, among many other things, on the sampling of clinically accessible biological targets.

1.3 Liquid biopsy: blood-based cancer biomarkers

Biopsy comprises a group of medical procedures based on **obtaining body tissue** by needle biopsy, endoscope-based procedures or surgical intervention for its examination and cancer diagnosis. Biopsies can be performed at different regions of the human body and the procedure is adapted depending on the accessibility of the targeted tissue or organ. These medical procedures imply a certain degree of risk and complications, ranging from pain at the site of incision, bleeding, drug reaction, damage to nearby tissue, and infection. Pathological analysis of tissue biopsies is not always accurate because it only reflects a **single point in time** of the whole **intratumoral heterogeneity**.

Hence, repeated biopsies at different time points may be required, which is often impractical and represents a risk to the patient. Additionally, analysis from single-tumor biopsy limits its application for prognosis and for the evaluation of treatment efficacy.[46] Thus, there is a clinical need for accessing cancer-related biological information in a consistent, less invasive, and repeated manner in order to improve the clinical management of patients.

Biomarkers are defined as a measured characteristic that correlates with a normal or abnormal biological state in a living organism. The quantification of the appropriate biomarker can be used to differentiate between an affected patient and a healthy subject. In oncology, biomarkers could provide relevant information for diagnosis of patients and prognosis of cancer. Moreover, they could also predict response to treatment and enable monitoring of the disease progression. Ultimately, cancer biomarkers could potentially be used for early detection of cancer.[47,48] As biomarkers play a critical role in all stages of cancerous pathology, there is therefore, a continuous search for reliable biomarkers that can be easily implemented in clinical settings and that can improve disease outcome and patient survival. To this end, efforts have focused on investigating the biological material of diverse biological body fluids such as blood, urine, saliva, seminal plasma, cerebrospinal fluid, to name a few.[49,50]

In this context, the analysis of cancer biomarkers, at the cellular and molecular level, carried by the bloodstream, gave rise to the emerging concept of ***liquid biopsy***. Liquid biopsy arises as a minimally invasive approach fitting into current clinical practice and offering advantages over traditional tissue biopsies such as increased temporal and spatial representativeness of the heterogeneity of solid tumors, and more frequent sampling.[51] These added features would mainly enable real-time monitoring of the disease and study of the biological behavior of the tumor, particularly valuable during disease follow-up for the application of a treatment plan being both tailored at the patient scale which the community now refers to as **precision medicine**. Liquid biopsy has become recognized as a novel source of cancer biomarkers (**Figure 1.4**), and these blood-based signatures can be addressed by analyzing tumor-derived materials such as CTCs, cell-free fragments of nucleic acids (DNA, mRNA, miRNA, and lncRNAs), proteins, peptides, or extracellular vesicles. More recently, tumor-educated platelets have also been reported as another source of tumor signature in blood.[52]

Among the vast range of tumor-derived material in the bloodstream, circulating tumor cells, circulating free DNA (cfDNA), and extracellular vesicles dominate the research field of liquid biopsy. Historically, the presence of epithelial cells in blood was first documented by Thomas Ashworth in 1869. Nonetheless, the detection of epithelial cancer cells hidden among hematopoietic cells was intensively investigated and recognized in bone marrow during the 90's in the field of minimal residual disease (MRD) monitoring.[53,54] Following those findings, researchers focused on peripheral blood as an easier access to cancer epithelial cells, later named CTCs.[55–58] Along this line, the presence of fragments of cell-free DNA in human blood was first described in 1948 by Mandel and Métais, but it was until 1989 that Stroun reported at least some cfDNA in the plasma of patients with cancer originates from cancer cells.[59] A few years later, the term circulating tumor DNA (ctDNA) was introduced when it was formally confirmed that mutant DNA fragments in the plasma were of tumor origin.[60] The relative ease of isolating cell-free DNA from plasma samples and the advent of digital PCR and next-generation sequencing-based technologies have accelerated research activity in this field.[61] More recently, in the last decade, tumor-secreted extracellular vesicles are emerging as a source of intracellular components such as proteins and RNA.[62,63] In the following paragraphs, a

broad introduction of these blood-based biomarkers will be given, except for CTCs which will be further explained since they are the main biological target of this manuscript.

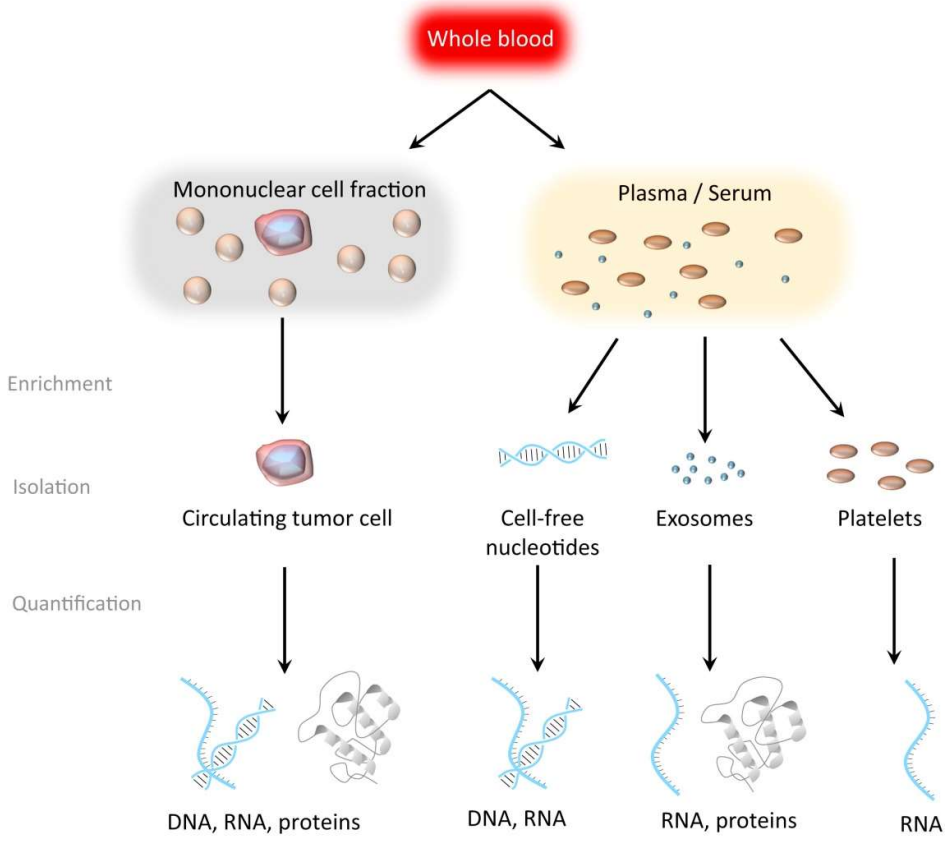

Figure 1.4 Tumor-derived materials of liquid biopsy. Figure extracted from *S.A. Joosse and K. Pantel, Cancer Cell, 2015*.[52]

1.3.1 Circulating tumor DNA (ctDNA)

Cell-free DNA is continuously released in fragments into the blood circulation through processes such as apoptosis and necrosis, and possibly also active secretion, by both normal and cancerous cells, **Figure 1.5**. Circulating free DNA (cfDNA) has a half-life in the circulation ranging from 16 minutes to 2.5 hours and a characteristic length in integer multiples of 180-200 base pairs.[61,64] On the other hand, circulating tumor DNA (ctDNA) only represents a small fraction (<1%) of total cfDNA and these molecules are shorter than non-mutant cfDNA (134-144bp).[61] Thus, the size of DNA fragments is one of the accessible parameters to discriminate between tumor-derived and nontumor DNA, but still, the biology behind cfDNA fragmentation is still unclear.[65] However, longer fragments of cfDNA could potentially provide complementary information.

As a cancer biomarker, ctDNA is attractive due to the ease with which plasma can be collected and analyzed using a simple workflow. However, its analysis requires highly sensitive techniques such as conventional PCR-based assays and more advanced technologies as targeted/whole-genome

sequencing, since tumor-specific mutations can represent as low as 0.01% of the total cfDNA.[66] These assays provide information about cfDNA levels or genomic signatures such as point mutations, copy number alterations, and methylation changes, **Figure 1.5**.[61] The quantitative information obtained allows for the assessment of molecular heterogeneity, monitoring of tumor dynamics, identification of genetic determinants for therapy, tracking of genomic evolution and development of acquired resistance.[61,64] A hallmark of ctDNA analyses is its high degree of specificity, because mutations found in cfDNA are in essence unique signatures of cancer. In terms of sensitivity, ctDNA levels are in enough quantity in most patients with advanced cancer to be detected. However its extrapolation towards early-stage disease and minimal residual disease remains elusive.

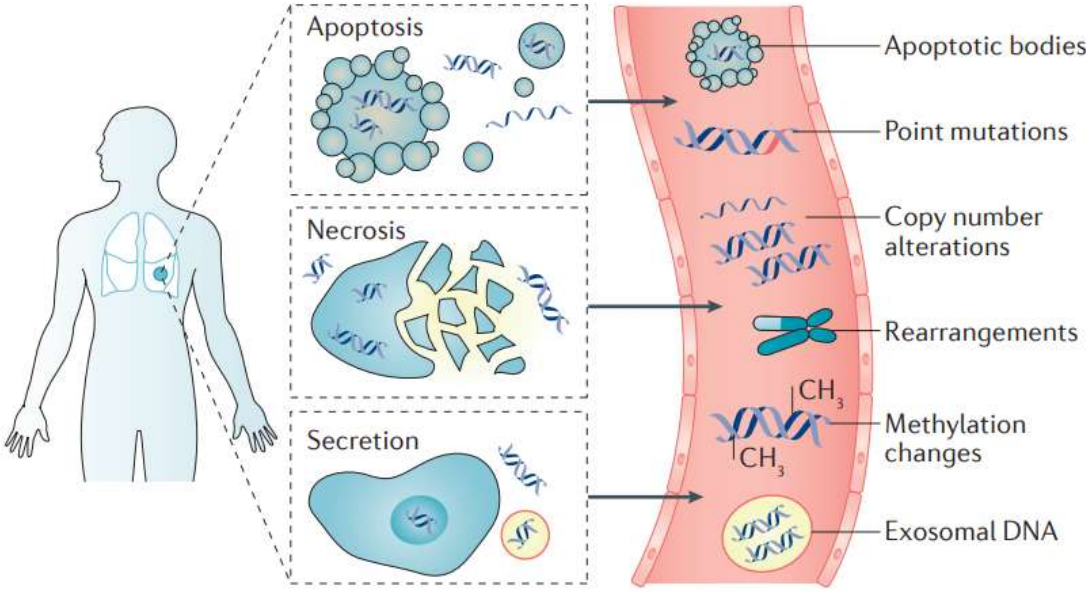

Figure 1.5 Origins and range of alterations in cell-free DNA. Figure taken from *J.C.M. Wan, Nature Reviews Cancer, 2017*.[61]

1.3.2 Extracellular vesicles (EVs): Exosomes

Tumor-secreted extracellular vesicles (EVs) mainly comprise microvesicles and exosomes, and are recognized as critical mediators of intercellular communication between tumor cells and stromal cells in local and distant microenvironments. Moreover, they are also implicated in cell-cell communication between cancer cells. Thereby, tumor-secreted vesicles are thought to participate in multiple steps during cancer invasion and perhaps contribute to early steps involved in metastasis.[63] Emerging evidence suggests that EVs, particularly exosomes, derived from cancer cells and the molecular information they contain can be used as cancer biomarkers.

Exosomes are small, 30–150 nm in diameter, membranous vesicles that contain multiple molecules inside, such as nucleic acids (DNA, mRNA, miRNA, and lncRNAs), proteins (receptors, transcription factors, enzymes, extracellular matrix proteins), and lipids. A representation of the tumor

transcriptome can be addressed by analyzing exosomal nucleic acids. Particularly, exosomal miRNAs have been the subject of increased attention as a potential cancer biomarker for diagnosis and monitoring of therapeutic efficiency, due to its stability.[62,67] A limiting factor to establish the routine application of exosomes as cancer biomarkers has been limited by fundamental technical and methodological challenges relying on their small size and the extensive sample preparation required prior to analysis.[68] Nevertheless, given their rich molecular content, exosomes could provide a complementary proteomic and genetic profile of the cell of origin, a trait that cfDNA cannot achieve by itself.

1.3.3 Circulating tumor cells (CTCs)

1.3.3.1 Intravascular transit of CTCs

As previously stated, tumor cells can reach the systemic circulation, ~4 million of cells/day per gram of primary tumor,[23] as individual cells or as clusters, and clear from circulation within a couple of hours.[26] These epithelial cells exposed to non-adherent conditions are more likely to undergo anoikis, a programmed cell death. However, tumor cells with an increased malignant potential could develop anoikis resistance through diverse mechanisms, being these features mainly acquired during tumor development and cell invasion in the primary tumor.[24] In addition to the developed anoikis resistance, other threats present in the blood environment must be overcome by CTCs, which includes evading the immune system and withstanding the hemodynamic forces.

The survival of the rarely found **CTCs in the blood circulation** mainly depends on the **favorable interactions** these might have with the abundant background of normal blood cells. This interplay mainly takes place with leukocytes and platelets, cells related to the immune surveillance and coagulation respectively, and both together, represent approximately 1% of the total blood cell population, **Figure 1.6.** Certainly, a direct cell-cell interaction with blood cells is unavoidable and only cancer cells adapted to the circulatory environment may survive.

In order to **escape immune surveillance,** tumor cells can shed/restrict the presentation of ligands involved in their recognition and interrogation by immune system cells, mainly **natural killer (NK)** cells and cytotoxic T lymphocytes, this representing an advantage to circumvent its elimination. NK cells are well recognized in controlling the growth of cancer cells at the tissue level, however, their role in preventing metastatic spread has not been clearly demonstrated yet, but recent evidence suggests the necessity of direct cell–cell contact for the elimination of CTCs.[25,69] Recently, studies have also suggested the direct adherence of CTCs on top of **neutrophils**, indicating that CTCs could potentially use immune cells as a bridge to facilitate extravasation,[70,71] as well as the presence of circulating giant macrophages capable of binding CTCs in peripheral blood,[72] indicating that CTCs interact with almost all leukocytes.

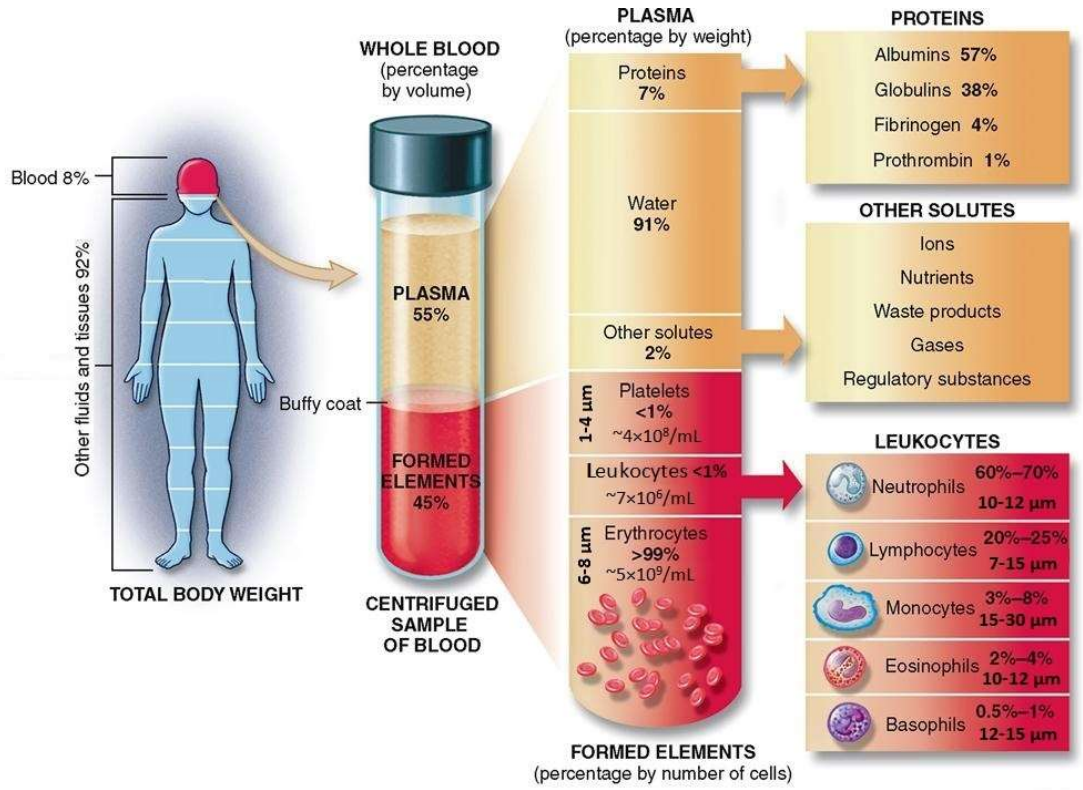

Figure 1.6 Composition of blood. Whole blood constitutes about 8% of total body weight, and from this, plasma represents about 55%. Formed elements account for about 45% of the total blood volume: erythrocytes or red blood cells (RBCs), Leukocytes or white blood cells (WBCs), and platelets. Figure adapted from *basicmedicalkey.com*.[73]

In line with these observations, **platelets**, the second most abundant population of blood cells, have been shown to actively interact with cancer cells contributing to the hematogenous spread of cancer during invasion, translocation, and extravasation.[74] Early studies evidenced a relation between blood coagulation and cancer disease, since **thrombosis** is a frequent complication of cancer and it is the second most common cause of death in cancer patients.[75] The association between platelets and CTCs during translocation, known as tumor cell-induced **platelet aggregation**, confers several advantages to the **immunoevasion**. It has been reported that the aggregation/adhesion of platelets around tumor cells may form a protective 'cloak' that could shield CTCs from natural killer cell-mediated cytotoxicity and TNF-α mediated cytolysis.[76,77] Adherent platelets may also protect cancer cells from hemodynamic shear stress exerted by blood flow. Moreover, platelet aggregation may also contribute to the **activation of EMT** program on CTCs and aid the extravasation of CTCs by enhancing their adhesion to the endothelium.[78,79]

In addition to the physicochemical interactions between blood cells and CTCs, cancer cells undergo shear stress mainly generated from blood flow but also from collisions between CTCs, blood cells, and endothelial cells lining the vessel wall.[80] It has been hypothesized that **hemodynamic shear stress** in human circulation (0.5-4 dynes cm^{-2} in venous circulation, 4-30 dynes cm^{-2} in arterial circulation) could affect cancer cell survival within the bloodstream inducing significant membrane-cytoskeletal changes and triggering apoptosis. Indeed, in accordance with this hypothesis, it has recently been shown that cancer cell lines with **higher metastatic potentials** are more **resistant to shear stress**.[81–83] However, it remains unclear whether hemodynamic shear stress can modulate the biophysical properties and functions of CTCs and confer them a metastasis-initiating capacity.

As here reviewed, blood circulation is an aggressive environment for foreign tumor cells. Besides the aforementioned survival mechanisms, the survival of tumor cells disseminated through the blood circulation might be enhanced when cancer cells translocate as **clusters**, also called tumor microemboli. Clusters are rare in the circulation, 2-5% of the total CTC population,[84,85] compared with single CTCs and it is thought that they arise from the solid tumor and not from intravascular aggregation events.[86] The number of cells within clusters, in cancer patients, varies from two to over 100 cells, where the majority of them exist as small 2–4 cell-aggregates.[87,88] CTC clusters demonstrate increased **anoikis resistance** due to a combination of **mesenchymal properties** as compared to single CTC, and persistent epithelial cell-cell junctions.[89] Further, the cooperation between cells within CTC clusters may confer resistance to hemodynamic forces within the circulation. In addition to their capacity to **survive in the bloodstream**, CTC clusters are also suggested to have an increased **metastatic potential**.[84]

1.3.3.2 Biophysical differences of CTCs and blood cells

The presence of cancer cells in the blood of metastatic patients has been quantified since the early 1950s, evidencing its low frequency, one cancer cell in among 10^5-10^6 peripheral blood mononuclear cells.[90,91] Their identification by microscopic pathological analysis indicated that CTCs preserve the cytomorphologic features of tumor cells in tissue, characterized by a **high nuclear-to-cytoplasm ratio**, and irregular size and shape, when compared to normal epithelial cells. Cancer cells are frequently found having gigantic nuclei and being multinucleated, as a sign of abnormal division.[92] It is worth noting that CTCs exhibit a high degree of pleomorphism, cell **variations in size and shape**, similar to those seen in primary and metastatic tumor tissue.[85,93,94] Given those characteristics, cancer cells are normally larger than normal blood cells. Indeed, S. H. Seal, a pioneer in the field of CTCs, was the first suggesting that cancer cells are generally, but not always, larger than the normal cellular elements of the blood and also more rigid.[95] However, the presence of a population of small CTCs should not be ignored.

It is generally accepted that the vast majority of tumor cells, but not all, have **distinct biophysical properties** compared to **normal blood cells**. In terms of size, CTCs range from **<4 to >30 µm in diameter**, **Figure 1.7**, and this dimension varies depending on the tissue of origin as well as among patients, **Table 1.1**. When compared to blood cells, CTC diameter is usually larger than the one of erythrocytes and platelets, and it mostly **overlaps** with the diameter of leukocytes. Additionally, and in line with reported observations, CTC volume is at least 2-fold the one of leukocytes.

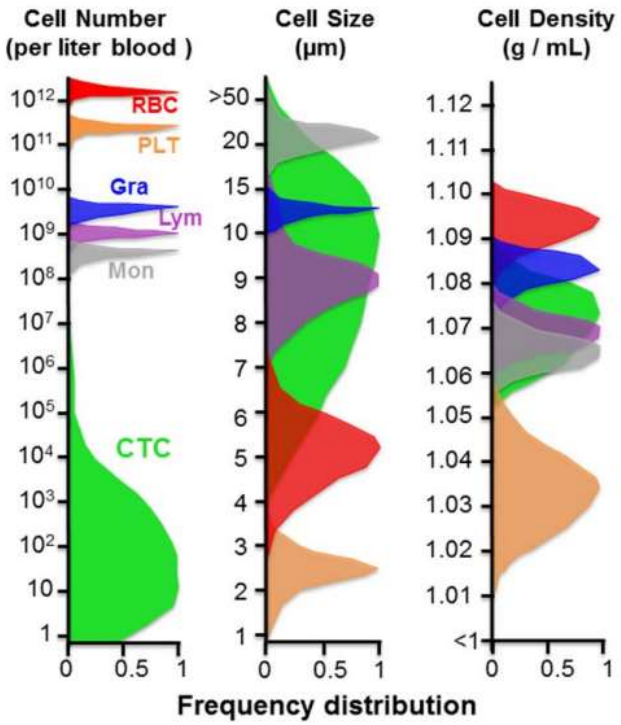

Figure 1.7 Frequency distribution of CTCs compared to blood cells. Comparison by cell number, size and density. CTC frequency obtained from analysis using CellSearch system. Erythrocytes (RBC), platelets (PLT), granulocytes (Gra), lymphocytes (Lym) and monocytes (Mon) per liter of blood in human subjects. Figure taken from *H.N. Stoecklein et al. Expert Review of Molecular Diagnostics, 2016*.[96]

Cancer cell deformability has also been investigated since this property is associated with an invasive and migratory phenotype. Deformability and rigidity measurements, using various techniques, evidenced that malignant cancer cells are often more deformable than non-malignant cells, the latter related to their mesenchymal phenotype.[97–99] However, the majority of these biomechanical measurements have been performed on patient tumor cells under adhesion conditions**,** which may change the cytoskeletal properties, a determinant factor of cellular mechanics, and measurements do not necessarily reflect the properties of CTCs in blood circulation. More recently, the mechanical properties of **suspended cancer cells** prior and after exposure to **fluid shear stress** were measured, indicating that transformed cancer cells adapt to the magnitude of the stress, by increasing their rigidity.[100] This is in agreement with results obtained by computational modeling, where it is suggested that a CTC with a stiff cell cortex would better survive during its passive transport in the blood flow. Interestingly, the model showed that dynamic changes in the stiffness of cytoskeleton during intravenous transport are required for successful adherence to the endothelium.[101]

Based on the aforementioned, a high degree of cytoskeletal **deformability** seems to be a predominant trait of malignant cancer cells at the **tumor level** since it may confer to cancer cells the ability to invade surrounding tissue and gain vascular access, while a more **solid-like cytoskeleton** may be able to develop the required internal stresses to **counteract hematological forces** and resist lethal deformations.[102] Nevertheless, relating these insights derived from the biophysical characterization of stiffness/deformability of cultured cancer cells back to metastatic processes that occur in vivo remain at the level of speculation.

Regarding CTC and blood cell differences in deformability, the fact that a significant fraction of CTCs is physically retained in the microvasculature is perhaps the clearest evidence that cancer cells have stiffer mechanical characteristics in comparison to normal blood cells. This increased stiffness could be related to the higher nuclear-to-cytoplasm ratio of cancer cells which gives them a greater resistance to deformation, knowing that the nucleus is more solid-like than the rest of the cell. Some efforts have been made to directly compare the intrinsic cell deformability of tissue **tumor cells and leukocytes**, finding that cancer cells are significantly stiffer,[103,104] despite that, the deformability of patient-derived CTCs is still uncertain. In this context, the deformability of CTCs versus blood cells in suspension has been recently explored by Bagnall et al., suggesting that tumor cells and **CTCs could be less deformable than blood cells**.[105] However, it is not excluded the fact that some of the CTCs in circulation may be as deformable as blood cells. Indeed, deformability trait would enable CTCs to escape from the mechanical trapping of the capillaries, similar to red blood cells, and spread to all tissues and organs.

1.3.3.3 Membrane surface markers of CTCs

In terms of **biochemical properties**, CTCs also differ from blood and normal epithelial cells. Most of the scientific research has focused on this field, given that the identification of specific biochemical signatures driving their altered behavior could be used as therapeutic targets to treat or reverse the malignant disease. The alterations in the cell surface membrane of cancer cells are believed to be the result of changes in their genome. Most of **tumor-associated markers** are proteins, however patterns of gene expression are also considered as tumor markers but these are cancer-type dependent.[106] Vast efforts have targeted the accessible cell-surface receptors at the membrane level, since this is the main structure through which cells communicate and interact with other cells and their microenvironment. The **extracellular molecules** present in cancer cells may range from cell **adhesion molecules, cytokines/growth factors, hormone receptors, and neurotransmitter receptors**.

At the cell level, the identification of **cell surface markers**, also known as surface antigens, has been used to **classify CTCs** according to the expression-level of specific molecules. The three most accepted families of antigen signatures that may be present alone or in different combinations on CTCs are the **epithelial, mesenchymal** and **stem-like markers**.[107] However, variations of diverse extracellular molecules can be also found depending on the cancer type, the stage of the disease, and the disease evolution during treatment.[108] Additionally, noncancerous conditions can also cause the overexpression of these molecules.

Due to the epithelial nature of **carcinomas**, some CTCs could express the **Epithelial Cell Adhesion Molecule (EpCAM),** a cell surface glycoprotein normally found in **neoplastic epithelial cells** and at lower levels in normal epithelia.[109,110] However, the downregulation of EpCAM commonly occurs

during epithelial-to-mesenchymal transition which is a process widely associated with the enhanced ability of cells to enter the blood circulation, survive within the bloodstream, and develop treatment resistance.[16,17,20,111,112] Additionally, cancer of **non-epithelial origin** such as **melanoma** and **glioblastoma** do not express this molecule. Together with EpCAM, other epithelial markers could be also expressed, such as E-cadherin, Cytokeratin (CK), and Zonula occludens (ZO).[112]

Epithelial carcinoma cells can be transformed into a more mesenchymal state, and during this process **hybrid phenotypes** can be present.[17] For this reason, it is difficult to find CTCs having a pure mesenchymal phenotype. EpCAM could still be expressed on those hybrid phenotypes but it is dependent on the EMT stage and when downregulated, it can be co-expressed together with mesenchymal markers such as N-cadherin, Vimentin, ZEB1, and Twist1, just to mention a few.[112] EpCAM could finally disappear in the same manner as E-cadherin.

Among the whole CTC population, it has been suggested that only a specific subpopulation of them may have the ability to self-renew and differentiate in order to create new tumors at distant sites from the primary one.[113] In this context, **Cancer Stem Cells (CSCs)** possess all of these fundamental requisites for cancer cell invasion and metastasis, thus there is special interest in recognizing this CTC subpopulation. The CTC population identified as CSC has usually mixed epithelial, mesenchymal and stemness properties and the diversity of surface markers can be increased according to the organ/tissue of origin. Apart from epithelial and/or mesenchymal markers, specific molecular signatures of CSCs have been suggested to identify this population of cells. For example, CD44, CD24 and Aldehyde dehydrogenase-1 (ALDH1) surface antigens have been used to identity CSCs in breast cancer.[114] However, stemness markers on CTCs are still under deep investigation and discussion.

Taken together, these findings evidence that our knowledge of the biophysical, biochemical and behavioral characteristics of CTCs is in contrast to our understanding of the normal constituents of the peripheral blood. More in-depth studies using a variety of platforms and patient-derived CTCs are necessary to fully reveal their properties, since **CTCs provide the unique opportunity to study the whole cell, allowing DNA, RNA and protein-based molecular profiling**, which can be used as cancer biomarkers and also to identify cells with an increased tumor-initiating capacity. However, one of the main challenges concerns to the isolation of such abnormal cell type from the vast blood cell population and, perhaps at the same level of importance, keeping them alive to perform systematic and detailed proteomic characterization, as well as functional analysis. Along with this line, an overview of the technological efforts that have been recently developed to face these challenges is presented below.

Cell Type	Value	Isolation/Detection Platform	Isolation Principle	Reference
Diameter, µm				
Prostate CTC	8 - 16	HB-Chip	Antibody-coated Chip Surface, EpCAM	Stott et al., 2010.[115]
Prostate CTC	3 - >10 3 -10 (150/199 counts) >10 (49/199 counts)	FACS	Positive Immunomagnetic Sorting, EpCAM	Moreno et al., 2001.[116]
Prostate CTC	21.1 ± 8.4 15.9 ± 6.9, CK+ 26.2 ± 6.5, CK-	Vortex HT	Size-based Sorting	Renier et al., 2017.[117]
Prostate CTC	7.97 ± 1.81	CellSearch	Positive Immunomagnetic Sorting, EpCAM	Park et al., 2014.[118]
Melanoma CTC	>12	CTC-iChip	Negative Immunomagnetic Sorting, CD45	Ozkumur et al., 2013.[119]
Breast CTC	9 - 19	CTC-iChip	Negative Immunomagnetic Sorting, CD45	Ozkumur et al., 2013.[119]
Breast CTC	32.0 ± 5.8, Primary Tumor 33.9 ± 8.3, Metastatic Disease 29.8 ± 6.5, Dormancy Candidates	MACS	Positive Immunomagnetic Sorting, EpCAM	Meng et al., 2004.[120]
Various metastatic carcinomas	<4 - >30	CellSearch	Positive Immunomagnetic Sorting, EpCAM	Allard et al., 2004.[121]
Volume, µm³				
Breast CTC	851.6 ± 45.8	HD-CTC		Phillips et al., 2012.[122]
Ovarian CTC	518.3 ± 24	HD-CTC		Phillips et al.,2012.[123]
Leukocyte	234.1 ± 4.1			Phillips et al., 2012.[122]
Erythrocyte	100.6 ± 4.0			Phillips et al., 2012.[122]

Table 1.1 Biophysical properties of CTCs for different carcinomas. Values are means ± SD, unless otherwise noted. HB-Chip: Herringbone-Chip, HD-CTC: high-definition CTC, CTC-iChip: inertial focusing CTC-Chip, MACS: high-gradient magnetic cell sorting, FACS: fluorescence-activated cell sorting, Vortex HT: High Throughput Vortex Chip, CK+: Positive to Cytokeratin, CK-: Negative to Cytokeratin.

1.4 Methods and technologies for CTC separation from blood samples

Currently, CTCs must be first isolated prior to any phenotypic or genotypic analysis to confirm their nature. The separation of extremely rare CTCs from blood samples is the initial step of the non-standardized CTC-workflow and the advent of techniques and processes to achieve it has been driven by the relatively easy access to blood samples directly from cancer patients. The guidelines for phlebotomy, drawing or removing blood from the circulatory system, allow the frequent access of specific volumes of blood. These samples are collected in 2 -10mL sterile tubes which preserve the specimen for a determined period of time. Thus, CTC separation processes used in clinical and research laboratories fit into the conventional volumes.

Cell separation has been widely used in clinics and research laboratories for the analysis of heterogeneous cell populations such as immune cells from the peripheral blood. The basic principle of separating CTCs from blood cells is to utilize one or more properties, biochemical or biophysical, that are unique to this cell type. Two main groups are commonly proposed to classify the technologies dedicated to the separation of CTCs. Those platforms taking advantage of the cell surface markers of cancer cells are classified under the **immunoaffinity** group. The second one, **biophysical** group, benefit from the biophysical differences of CTCs with respect to blood cells. Additionally, cell separation can also be classified as positive and negative selection. Positive selection aims at isolating the target cell type (i.e., CTC) from the entire population (i.e., blood cells) while a negative one, is an indirect method for CTC separation based on the removal/depletion of the unwanted cell types. Some platforms also combine both, positive and negative, selection approaches to reduce the background of blood cells and improve the purity of separated cells.

Extensive reviews of technologies for the isolation and identification of CTCs have been published elsewhere. One of the most recent reviews presented by Ferreira et al,[124] extensively compares those technologies. The following section aims to briefly introduce some of the current and most used methods for CTC enrichment, in order to provide to the reader a general overview. Microfiltration technologies are further discussed in Chapter II.

1.4.1 Immunoaffinity-based technologies

Immunoaffinity-based separation strategy, or immunocapture, is the most widely used approach for the isolation of CTCs from blood samples. This method uses engineered antibodies directed against antigens expressed by the targeted cells. A particular **antibody or cocktail of antibodies** can be coated onto a surface and be in turn placed directly in contact with the blood sample allowing the antigen-antibody interaction. This interaction binds the targeted cell to the functionalized surface and enables cell separation. It is important to emphasize that currently **there is no CTC-specific antigen**, which makes their separation from blood cells challenging.

When a positive selection of CTCs is performed, the antibodies against cancer cells are typically bound to the functionalized surface of either magnetic micro/nano beads or specific devices. As previously introduced, **EpCAM antigen** is found to be expressed in cancer cells of epithelial origin and not in normal blood cells, thus, this antigen is widely used as target for affinity-based CTC enrichment, keeping in mind that no CTC-specific antigen has been evidenced up to now. Conversely,

when a negative selection is aimed, the cell surface marker commonly targeted is the CD45 antigen, expressed in WBCs. This method is usually preferred when no bias from selection markers is desired.

Cell separation platforms based on the magnetic principle, pre-mix blood samples with antibody-coated magnetic beads and subsequently expose them to a controllable magnetic field. This magnetic field acts as a filter, the magnetic beads carry the targeted cells towards the magnets, where they are retained, while unlabelled cells flow through or are washed out. Based on ferrofluid nanoparticles coated with **anti-EpCAM antibody**, the **CellSearch System (Menarini Silicon Biosystems)** is the first and only clinically validated blood test cleared by the U.S. Food and Drug Administration (FDA) for detecting and enumerating CTCs. CTCs are magnetically separated from centrifugated blood samples in a fully-automated system, which can also perform their recognition. Currently, this system is considered as the gold standard within the field, since emerging technologies for CTC isolation are usually compared to it. In a similar fashion, **AdnaTest (Adnagen AG)** uses antibody-coated magnetic beads but rather than using a single antibody uses a **cocktail of antibodies** specific to a given cancer type. Additionally, this assay allows the evaluation of gene expression on isolated cells. Other available technologies based on magnetic separation from clinically acceptable blood volumes are the **Magnetic-Activated Cell Sorting (MACS, Miltenyi Biotec)** and **MagSweeper**[125] platforms.

With the technological advances in **microfluidics**, which allows the precise control of fluids, several platforms have been developed, combining micro-scale channels with magnetic array-patterns, for CTC capture. Some examples are the commercially available **LiquidBiopsy Platform (Cynvenio)** and **IsoFlux (Fluxion Biosciences)** platforms which offer fully-automated magnetic-based CTC isolation. Some other examples are the **Ephesia chip**,[126] and the **Magnetic Sifter**[127] fluidic platforms.

In this field, a vast range of microfluidic-based platforms have also been proposed using integrated micropatterned surfaces decorated with anti-bodies. As a hallmark, microfluidic devices would allow the precise control of the flow which increases the likelihood of cell-antibody interactions, and consequently CTC capture. The first platform using this approach was the **CTC-Chip** which integrates an array of anti-EpCAM coated microposts along the flow path.[128] Following the same idea, other microfluidic platforms have used antibody cocktails to enhance the cell capture, such as **OncoCEE (Biocept)**. Some other platforms, such as the **Herringbone-Chip (HB-Chip)**[115], the **Geometrically Enhanced Mixing (GEM) chip**,[129] and the **Geometrically Enhanced Differential Immunocapture (GEDI)** platform,[130] have focused on enhancing the possible interactions between the cell and the antibody-coated surface.

1.4.2 Physical properties based technologies

Some isolation platforms have taken advantage of the common features observed on CTCs, such as density, size, deformability and electric charge to separate them from normal blood cells. Those antibody-free methods are sub classified in the following paragraphs.

1.4.2.1 Centrifugation

The fractionation of whole blood using density-based gradient centrifugation has been used for almost 100 years to separate CTCs from the background of blood cells,[131] and remains a simple and inexpensive method. Centrifugation of whole blood results in the fractionation of cells in three

layers, where plasma and RBCs are on the top and bottom layer, respectively, and a mixture of WBCs, platelets, and CTCs is located at the middle layer. Although it was not originally designed for the isolation of CTCs, early studies reported the use of **Ficoll-Paque (GE Healthcare)** density gradient media to improve the fractionation of blood. More recently, **OncoQuick (Greiner Bio-One)** developed a specialized separation tube to allow a further depletion of erythrocytes, granulocytes, lymphocytes and mononuclear cells towards the bottom layer. **RosetteSep™ (STEMCELL Technologies)**, combines centrifugation with immunoaffinity-based enrichment, crosslinking unwanted cells to RBCs, to increase the purity of targeted CTCs. Based on the principle of centrifugation as well, **Accucyte® (RareCyte)** is another available platform for blood fractionation. However, in all these technologies the fraction corresponding to enriched CTCs still contains platelets and some WBCs sharing similar characteristics to those enriched CTCs. Thus, centrifugation-based platforms are usually a pre-enrichment step for subsequent specialized CTC-isolation platforms.

1.4.2.2 Microfiltration

Microfiltration of blood has been used since S. H. Seal observed some of the intrinsic properties of cancer cells as being relatively larger than WBCs and less deformable than blood cells.[95] These traits enable flowing blood cells through micrometric range constrictions designed to retain CTC population only. Using this approach, no functional modifications of the surface are required since cells are trapped by their intrinsic size and deformability. Based on this principle, **ISET® (Rarecells Diagnostics)** and **ScreenCell® (ScreenCell)** use track-etched membranes containing 8-µm pores randomly placed to isolate CTCs from buffer-diluted blood samples. One of the limiting factors of this approach is clogging when whole blood is processed, thus high pore density and relatively increased driving pressures are needed. To face these limitations, micropatterned membranes based on a photolithographic technique have also been proposed controlling the size, shape/geometry, and distribution of pores on different materials such as Silicon,[132,133] Silicon/Silicon-Nitride **(VyCAP microsieve, VyCAP)**,[134] Nickel,[135] and polymers like SU-8 **(CellSieve™, Creatv MicroTech)**,[136] and Parylene-C.[137,138]The size of pore ranges from 5 to 12 µm having typically circular shapes and a total number of pores in the range of 10^3-10^5. Another associated issue related to microfiltration is the mechanical stress on CTCs once they are trapped into the pores, thus limiting their viability. Filtration membranes in a stacked bilayer configuration were presented as a strategy to diminish stress on captured cells.[139,140]

In the field of microfluidics, some platforms have proposed the use of arrays of pillars or traps[141–143], stair-like architectures **(Parsortix, ANGLE)**, and pneumatically-controlled isolation gaps[144] integrated within microchannels in order to retain CTCs by size. Similarly, CTC-clusters have the intrinsic characteristic of being larger than individual CTCs. Thus, taking advantage of this biophysical trait, a microfluidic device, **Cluster-Chip**, was optimized for the isolation of CTC-clusters based on an array of pillars.[87]

1.4.2.3 Hydrodynamic cell sorting

Microfluidic channels having specific geometrical dimensions and controlled flow rate generate hydrodynamic forces (inertial forces) that allow sorting cells by their size.[145] For example, **Vortex HT Chip (Vortex Biosciences)** uses inertial focusing to position CTCs along the microchannel and then trap them into vortices generated by the sudden expansion of the channel.[146] Similarly, the **CTChip® FR (Clearbridge Biomedics)** uses spiral microchannels to exploit the centrifugal forces (Dean drag

force) in combination with the inertial focusing to separate CTCs from the rest of blood constituents.[147]

In this context, some platforms have used **deterministic lateral displacement (DLD)** to separate large cells from blood samples. This technology uses a specific arrangement of micropillars along the channel to control the trajectory of cells. By controlling parameters such as shape and distance in-between pillars, the separation of small blood cells (RBCs and Platelets) from large ones (WBCs and CTCs) is reached.[148] This strategy has also been used to separate CTC-clusters from blood using a two-stage microfluidic platform.[149] The same research group, has combined DLD, inertial focusing and magnetophoresis within the **CTC-iChip** to isolate CTCs from whole blood samples.[150]

1.4.2.4 Dielectrophoresis (DEP)

This approach uses the electrical properties of cells to exert forces on them via an external electric field. Those forces can be repulsive or attractive relative to the position of the electric field source and depend on both the dielectric characteristics of the cells (diameter, membrane, density, conductivity, volume) and their surrounding environment. **ApoStream® (ApoCell)** uses dielectrophoretic forces to attract CTCs near the electric field and repel WBCs in continuous flow.[151] The platform requires centrifugated samples and the adjustment of the suspension medium conductivity. **DEPArray™ (Menarini Silicon Biosystems)** is a platform based on repellent forces to manipulate and recover individual cells within an array of electrodes. However this platform is not dedicated to the isolation of CTCs from whole blood samples, it is rather employed for the identification of cells from pre-concentrated samples.

1.5 Methods and technologies for cell identification

The isolation of CTCs from blood samples using the technologies above described is the initial step in the CTC-based liquid biopsy workflow. In order to use these cells and the biological information they contain, their interrogation and **identification as cancerous cells** are required. The conventional methods currently used for CTC identification are based on **cytometric** and **polymerase chain reaction (PCR)** techniques.

In the early 1950s the papanicolaou staining (by George Papanikolaou in 1928) became widespread, allowing the visual assessment and identification of specific proteins on cancer cells and tissue fragments under a fluorescence microscope. At the same time, cytopathology had become a major tool for cancer diagnosis. These protocols were initially applied for the identification and discrimination of CTCs from blood cells. Currently, **no standardized detection method exists** for CTCs; nonetheless, the **cytomorphological** analysis combined with **immunocytochemistry** protocols is the most frequently used strategy since it allows the visual inspection and enumeration of cells.

Along this line and given the lack of CTC-specific markers, CTCs have been commonly discriminated from blood cells by the positive expression of the epithelial cell adhesion molecule (**EpCAM+**), cytokeratins (**CK+**) which are intracellular structural proteins found in epithelial cells, and the negative expression of CD45 (**CD45-**) which is specific to leukocytes and used to discard contamination of blood cells having similar morphology to CTCs. Complementarily, the cell nucleus is stained with DAPI (**DAPI+**) to exclude cellular fragments and cytomorphological analysis is also carried out. For instance, the FDA-cleared **CellSearch platform** identifies CTCs among the enriched

cells based on the expression of cytokeratin 4–6, 8, 10, 13, 18 and 19, lack of CD45 expression, presence of a nucleus, and a cytomorphology of neoplastic cells with a minimum diameter of 4 μm.[133] However, the expression/absence of these markers only allows classifying these cells as **rare epithelial cells in whole blood** but does not ensure either their **tumor derived-origin** or **malignancy**. Since, it has been reported that other rare non-tumor cells with similar antigen expression could also be present in blood circulation due to various pathological conditions, such as inflammatory diseases.[152] Despite this, the detection of these EpCAM- and cytokeratin-positive cellular events is known to have prognostic significance in a variety of metastatic cancer types. Further discussion regarding the clinical significance is presented in the following section of this chapter.

The expression of these **fluorochrome-conjugated antibodies** on CTCs is verified by measuring the fluorophore intensity with high-definition (HD) fluorescence-based optical systems such as fluorescence microscopy (static) and flow cytometry (in flow). Using this approach, the associated detection rates are strongly dependent on the technology used to this end. Sample imaging using fluorescence microscopes is a time-consuming step, particularly when large areas are required to be inspected. In order to address this point, platforms as CellSearch and DEPArray incorporated semi-automated fluorescence imaging systems into their workflow. Some other independent technologies such as **FASTcell™ (SRI Biosciences)**, **Epic platform (Epic Sciences)**, and **CytoTrack (CytoTrack)** combine HD imaging with computer algorithms for the identification of CTCs. In the same line**, ImageStream® (Amnis-Merck)** combines conventional flow cytometry with fluorescence imaging to identify CTCs from a background of cells in suspension. Moreover, systems based in flow cytometry, a standard procedure in many laboratories, offer a fast method to process samples, but, these systems require a relatively large quantity of cells to sample.

Isolated cells are usually further characterized to evaluate their tumor-derived nature. Techniques such as **Fluorescent In Situ Hybridization (FISH)** are frequently applied for the localization of a specific segment of a nucleic acid. Dual color or tricolor fluorescent probes are used for the detection of chromosomal abnormalities such as the presence or absence of specific DNA sequences related to the tumor. For example this tool has been used to determine whether CTCs express the same genomic changes as the primary tumor.[54] Along the same line, **RNA–in Situ Hybridization (RNA-ISH)** has also been used to confirm the differential expression in epithelial versus mesenchymal phenotype, confirming CTC heterogeneity.[88]

In general, **imaging-based techniques** allow morphological identification, molecular characterization, and cell counting. However, they are susceptible to false-positive or false-negative results due to either the intrinsic biology of CTCs or staining artifacts. Moreover, these techniques require carefulness in setting appropriate signal thresholds with respect to fluorescence intensity making it prone to low specificity and subjective interpretation of the acquired data which can preclude accurate CTC identification.

Thereby, aside from the visual identification of CTCs by protein expression-based techniques, some **nucleic acid-based techniques** have also been used to identify CTCs, in particular **PCR-based assays**. Following the extraction of nucleic acids, the analysis of **mRNA** provides real-time information about intracellular activity since they are the direct products of transcription, RNA synthesis. **Quantitative reverse transcription polymerase chain reaction (qRT-PCR)** has been used to find tumor-associated

expression patterns using mRNA strands transcripted into cDNA. This technique has shown to be highly sensitive and specific to quantify specific CTC mutations at the mRNA level.[153–155] However, some protocols used for CTC analysis induce RNA degradation, such as formaldehyde fixation, limiting the isolation of high-quality RNA.[156] More recently, **next-generation sequencing (NGS)** enabled the massive parallel processing of the whole genome dramatically reducing the sequencing time. Thus wide gene expression interrogation of patient-derived CTCs is possible even at the single-cell level.[157–159] However, this type of analysis does not provide direct information about CTC counts and its associated heterogeneity. Thus, to address these issues single-cell level interrogation is a must.

1.6 Clinical significance of CTCs: enumeration as a prognostic biomarker

Several reports have underlined the presence of CTCs in the blood of patients with metastatic disease across all major types of carcinomas,[121] and as here reviewed, they are considered to be the main source of metastases. CTCs are believed to be representative of the tumor, both primary and metastatic sites, and thus, their presence in the bloodstream is associated with and increased risk of disease malignancy. Their isolation, detection, and enumeration based on a determined volume of blood at multiple time points have been set as the acknowledged workflow to offer quantitative information during the evolution of the disease.

Enumeration of CTCs has been widely performed using the **CellSearch system** which has been set as the gold standard for CTC counts. Broadly, reports focused on monitoring changes in the number of CTCs in peripheral blood both **before and after a new treatment**, observing that an increase in the number of CTC counts, over a specific threshold, is associated with cancer progression. In clinical studies, the obtained data has been used as a **prognostic biomarker** to estimate the overall survival and the progression-free survival using Kaplan-Meier analysis. Estimation of the **overall survival** provides information related to the length of time that a determined patient would survive, using as a starting point the date of diagnosis or the start of a treatment. Complementarily, the **progression-free survival** corresponds to the length of time that the patient lives with no signs of worsening, relapse, right after a specific treatment. Both measurements are quantitative information to evaluate the response to treatment.

Multicenter studies have proven the **prognostic value** of CTC counts in **metastatic patients (M_1)** with breast, prostate, and colorectal cancer.[160–162] Results from **breast** and **prostate** cancer patients evidenced that levels of circulating tumor cells **≥ 5 per 7.5 ml of whole blood**, as compared with the group with <5 circulating tumor cells per 7.5 ml, had a shorter median progression-free and shorter overall survival. Based on this criterion, patients are stratified in favorable or unfavorable groups according to levels of CTCs, where 5 CTCs in 7.5 mL is the cutoff value. Different cutoff values have been established for each carcinoma, for instance, colorectal cancer has a cutoff value of 3 CTCs in 7.5 mL. Moreover, these clinical studies correlate the expression of **CD45-, EpCAM+, CK 8, 18+ and/or 19+** on CTCs with a more aggressive phenotype and a poor patient outcome. Other studies using small cohorts of patients have also evidenced the prognostic value of CTC counts in **non-small-cell lung, small-cell lung, ovarian, renal,** and **melanoma** metastatic patients.[163–167]

In the clinical prognostic line, complementary clinical studies have focused in non-metastatic cancer patients with **early-stage disease,** e.g. **M_0** patients. Those reports have evidenced that CTC detection

both before and after adjuvant **chemotherapy**, administrated **after primary surgery**, is linked to an increased **risk of relapse** in breast, prostate, colorectal, bladder, and liver cancer.[168–172] However, the very low CTC number and incidence at this stage of the disease raises doubts about whether or not CTC counts are a reliable indicator of an unfavorable prognosis. Moreover, it also suggests that the largest amount of CTCs is more likely to originate from metastatic sites rather than from primary lesions.

The use of CTC counts as a **predictive biomarker**, assessing the likelihood of the disease to respond to a therapeutic intervention, is uncertain and still under investigation. Vast efforts have been accomplished to demonstrate the clinical validity of CTC quantification for monitoring of **chemotherapy** for breast and castration-resistant prostate metastatic cancers.[173,174] However, some drugs belonging to the ***targeted therapy*** family may modify CTC counts impacting the predictive value of CTCs.[175,176] Despite providing valuable information for prognosis, these **non-interventional** studies have not been able to demonstrate their capacity for therapeutic decision-making yet. Along with this line, few **interventional trials**, also called clinical trials**,** are currently carried out by different groups, aiming to demonstrate that the use of CTC enumeration and monitoring could drive clinical decisions and improve the clinical outcome of metastatic cancer patients.[177]

1.7 The current outlook of CTCs in *liquid biopsy*

It is evident that remarkable improvements have been made in the detection of early cancer lesions, surgical techniques, and treatment of the primary tumor to improve the outcome of patients with cancer. A major challenge is the treatment and monitoring of patients with already-established metastases which reflects our limited understanding of the biology of cancer in the metastatic setting. As here reviewed, there is an evident **clinical need** to repeatedly obtain biological information related to both the primary tumor and the metastatic lesion in order to provide more effective therapies to patients. Blood-based cancer biomarkers provide an opportunity to face this need. From the liquid biopsy spectrum, **CTCs** are the only one which can provide disease-related **genomic, proteomic,** and **functional information**.

The analysis of CTCs goes beyond the biological understanding of the metastatic process, where its main goal is to be implemented as a cancer biomarker in clinical routine. From a therapeutic standpoint, in patients with **early cancer lesions** it would be a major breakthrough to repeatedly isolate as many CTCs from blood as possible and identify these molecular and functional signatures that allow their physical translocation. Thus, the deep characterization of these cancer cells having metastasis-initiating capacity would provide insights and new **therapeutic strategies for preventing metastasis**. Similarly, in patients with **already-established metastases** the characterization of isolated cells must aim to identify patient-specific therapeutic targets that could lead to **more effective therapies**.

1.7.1 Isolation of a widely heterogeneous CTC population

Aside from the biological and medical constraints, the implementation of the CTC-derived data for the therapeutic management of patients in clinical routine is also hindered by **technical limitations**. Despite the extensive development of technologies for CTC isolation from blood, so far, there is no technology or method capable to identify and/or isolate **all tumor cell types** present in human blood circulation.

As reviewed along this chapter, many of the CTC isolation methods rely on the detection of cells that express epithelial-related markers in blood. Moreover, most recent clinical trials enumerate CTCs using platforms based on this approach, i.e. CellSearch, targeting the population of cells expressing the cell surface glycoprotein EpCAM. However, it has been extensively postulated that during detachment and dissemination of tumor cells, **EpCAM** may be **downregulated** due to the activation of the EMT program, thus some CTCs that either express low levels or completely suppress this antigen are omitted by these methods. Moreover, EMT-like events could occur during the intravascular transit due to EMT inducers secreted by platelets. In general, EpCAM-based isolation systems are an alternative to enumerate tumor-derived cells from epithelial cancer types that often express high levels of EpCAM, but they do not ensure **detection of the entire pool of CTCs** present in blood circulation. Thus, EpCAM cannot be taken as a universal marker for CTC detection.

The transient and variable expression of EpCAM in CTCs points out a **dynamic** and **heterogeneous** population where the mechanisms driving EpCAM and other different molecular expressions, are not well understood. This opens up new opportunities for **multimarker-based** and **antigen-independent** methods in the pathway of **capturing more** and a **phenotypically wider range** of tumor-derived cells. As a consequence, improved identification methods would be required to discriminate between subpopulations, particularly those relevant for patients with either early (i.e., metastasis-initiating phenotype) or metastatic (i.e., drug-resistance phenotype) cancer lesions.

1.7.2 Processing larger volumes of blood

Intrinsically, low CTC counts are closely related to the amount of blood screened. CTC enumeration from the processing of **clinically relevant blood volumes** of 7.5 mL, suffers from low statistical power, mainly because this volume represents less than 0.2% of the total blood volume. Different reports have emphasized the need for a larger volume of blood in combination with high sensitivity assays in order to increase **CTC counts** and **detection rates**.[56,178–182] For example, CTC counts in metastatic patients range from one to **few tens**, reaching up to thousands in very particular cases, and detection rates vary in the interval of 30-80%, depending on the cancer type. These numbers are even lower in nonmetastatic cancer. However, the volume of blood taken from the patient cannot be substantially increased.

In line with this need, **CellCollector (GILUPI Nanomedizin)** arose as technology claiming to access large volumes of blood by placing it intravenously.[183,184] This device is a structured medical guidewire coated with a hydrogel layer which in turn, is covalently coupled with antibodies against EpCAM. Authors estimate that the device is exposed to approximately 1 L of blood during 30-min in the vein. In small patient cohorts, this technology has shown greater numbers of CTCs and in more patients as compared with the CellSearch system.[185–188] Complementarily, an EpCAM-independent strategy, **diagnostic leukapheresis**, has been recently proposed to increase the volume of blood sampled. This density-based method, processes up to 62% of the total blood via continuous centrifugation, and collects mononuclear cells with high levels of CTCs. The approach combined with CellSearch technology, revealed a significantly higher detection rate, from 28% to 72%, in a side-by-side comparison between the 7.5 mL peripheral blood, and the matched 2 mL diagnostic leukapheresis product.[96,189] Alternatively and along the same line, some techniques for *in vivo* detection of CTCs,[190–192] and early recruitment of metastatic cells,[193] have also been reported.

Despite that sophisticated methods have been proposed in the field of microfluidics to increase sensitivity (efficiency 80–100%) and selectivity (purity <70%), their intrinsic nature as **point-of-care platforms** limits the processing of large blood volumes (throughput ≤10 mL h^{-1}). This evidences even more that no single platform is currently capable of detecting more CTCs at larger rates. For this reason, recent studies have combined different CTC-detection platforms aiming to yield clinically useful information.[188,194] Thus, in the perspective of utilizing CTCs in clinical routine, it is clear that **beyond CTC-enumeration**, it will be of utmost importance to harvest more CTCs and to identify those having clinical relevance, in order to complement enumeration data.

In addition to the single-sampling-point processing of large blood volumes, blood sampling strategies are also required at multiple times and at different venipuncture sites in order to elucidate the actual kinetics of CTC dissemination and phenotypic and molecular changes in the blood of cancer patients. Typically, in clinical settings, blood samples from cancer patients are collected at monthly intervals. However, a recent report based on case studies and hypothetical simulation models,[195] has suggested that weekly, or even more frequent, sampling could result in better diagnosis and patient management.

1.7.3 Blood processing: blood collection and sample preparation

Liquid biopsy, similar to other clinical procedures involving the handling of biological samples, such as blood, requires to be processed immediately (<24 hours) or be stabilized with fixatives. Logistics for blood transportation and storage led to the development of dedicated containers with additives, such as anti-coagulants or pH-buffers, in order to avoid platelet aggregation and deterioration of leukocytes. In addition to their rareness, CTCs are subjected to different stress factors during their transit in the human bloodstream, but perhaps to one of a greater impact during the blood draw. In fact, relatively high numbers of apoptotic CTCs have been reported in blood samples from peripheral blood,[196,197] evidencing their fragility.

It has been reported that cancer cell numbers in blood samples rapidly decline over a time span of 5 hours, revealing that the time from blood draw to cell harvest is critical.[198] Other reports have shown that a significant RNA degradation occurs within a period of 2 to 4 hours.[199–201] These reports highlight the need for an adequate sample preservation for subsequent gene expression profiling. Along with this line, diverse strategies have been proposed for the stabilization of CTCs in blood samples,[202–204] such as CellSave tubes (CellSearch System, Menarini Silicon Biosystems) the most employed approach allowing up to 96 hours of blood preservation at room temperature conditions.

In addition to collection and blood preservation issues, a common trait of CTC isolation platforms is the use of cell fixatives. However, the use of a fixative solution sacrifices cell viability and degrades RNA.[205,206] Another predominant trait of CTC isolation platforms is the requirement of extensive sample preparation, such as RBC lysis, centrifugation, staining, multi-step washing, etc., just to list a few. Thus, those platforms are prone to CTC loss during the isolation process. For instance, in a direct comparison between CellSearch and Flow cytometry platforms, a 3.3-fold loss of CTCs was reported due to the isolation and staining procedures where flow cytometry yielded better results.[182]

1.7.4 Functional studies on CTCs

Beyond CTC enumeration from blood samples, to date, there is no strong data demonstrating its clinical utility to drive therapeutic decisions. The latter is perhaps the major obstacle to their implementation as cancer biomarker in clinical routine. The long-term culture of CTCs and the establishment of CTC lines, are the first step enabling the acquisition of qualitative and quantitative information related to the biological activity of CTCs. The data obtained from this type of studies, could offer, for instance, the possibility to identify the biological properties of metastatic cells, develop new anticancer drugs, or understand drug resistance mechanisms.

In this context, the isolation of viable CTCs is a necessary prerequisite. A platform dedicated to the detection of viable CTCs and subsequent short-term culture of CTCs has been recently introduced, EPISPOT technology, and it is based on the releasing of CK19 marker from tumor cells.[207] This platform has allowed the establishment of CTC-derived cell lines from blood samples with different cancerous pathologies.[208] Another alternative is the use of *in vivo* models, xenograft, to create clinically relevant cancer pathologies from CTCs. This technique has also allowed the identification of a subset of CTC population with increased metastatic potential, and the evaluation of anticancer drugs.[39,208]

However, the routine implementation of these techniques is currently hampered by the difficulty to systematically and frequently isolate viable CTCs in large numbers, as well as the technical difficulties encountered to culture CTCs.

1.8 Thesis objectives

Herein, we aimed at the development, from conception to validation, of novel microengineered technologies for the physical isolation of circulating tumor cells from whole blood. Generally speaking, our main objective is designing CTC capture devices adapted to the following specifications:

- CTC capture at physiologically relevant flow conditions, similar to those found in superficial human veins, in terms of flow velocity and pressure.
- Processing of whole blood, requiring no prior preparation/treatment.
- Use of conventional techniques for the fabrication of devices.
- Fulfillment of medical requirements and easy implementation of devices in clinical routine.

Based on the above general specifications, our strategy consisted in the implementation of two CTC capture approaches:

1) Directly from the bloodstream. Using CTC capture engineered devices that could be directly introduced within superficial human veins for a limited time span.
2) As a point-of-care device. Using CTC capture engineered devices adapted to conventional blood-contact medical consumables and clinical protocols.

These novel concepts and devices were conceived in the context of microengineering, to fulfill the medical and biological needs of the liquid biopsy community.

Bibliography of Chapter I

1. Cooper, G. M. The Development and Causes of Cancer. (2000).
2. AJCC - What is Cancer Staging? Available at: https://cancerstaging.org/references-tools/Pages/What-is-Cancer-Staging.aspx. (Accessed: 10th May 2018)
3. Cancer today. Available at: http://gco.iarc.fr/today/home. (Accessed: 10th May 2018)
4. Balkwill, F. R., Capasso, M. & Hagemann, T. The tumor microenvironment at a glance. *J Cell Sci* **125,** 5591–5596 (2012).
5. Klein-Goldberg, A., Maman, S. & Witz, I. P. The role played by the microenvironment in site-specific metastasis. *Cancer Lett.* **352,** 54–58 (2014).
6. Cairns, J. Mutation selection and the natural history of cancer. *Nature* **255,** 197–200 (1975).
7. Gupta, P. B., Mani, S., Yang, J., Hartwell, K. & Weinberg, R. A. The Evolving Portrait of Cancer Metastasis. *Cold Spring Harb. Symp. Quant. Biol.* **70,** 291–297 (2005).
8. Hellman, S. Karnofsky Memorial Lecture. Natural history of small breast cancers. *J. Clin. Oncol.* **12,** 2229–2234 (1994).
9. Klein, C. A. Parallel progression of primary tumours and metastases. *Nat. Rev. Cancer* **9,** 302–312 (2009).
10. Rhim, A. D. *et al.* EMT and Dissemination Precede Pancreatic Tumor Formation. *Cell* **148,** 349–361 (2012).
11. Paget, S. THE DISTRIBUTION OF SECONDARY GROWTHS IN CANCER OF THE BREAST. *The Lancet* **133,** 571–573 (1889).
12. Fidler, I. J. The pathogenesis of cancer metastasis: the 'seed and soil' hypothesis revisited. *Nat. Rev. Cancer* **3,** 453–458 (2003).
13. Folkman, J. How Is Blood Vessel Growth Regulated in Normal and Neoplastic Tissue?—G. H. A. Clowes Memorial Award Lecture. *Cancer Res.* **46,** 467–473 (1986).
14. Friedl, P. & Alexander, S. Cancer Invasion and the Microenvironment: Plasticity and Reciprocity. *Cell* **147,** 992–1009 (2011).
15. Clark, A. G. & Vignjevic, D. M. Modes of cancer cell invasion and the role of the microenvironment. *Curr. Opin. Cell Biol.* **36,** 13–22 (2015).
16. Thiery, J. P. Epithelial–mesenchymal transitions in tumour progression. *Nat. Rev. Cancer* **2,** 442–454 (2002).
17. Christiansen, J. J. & Rajasekaran, A. K. Reassessing Epithelial to Mesenchymal Transition as a Prerequisite for Carcinoma Invasion and Metastasis. *Cancer Res.* **66,** 8319–8326 (2006).
18. Jolly, M. K. *et al.* Implications of the Hybrid Epithelial/Mesenchymal Phenotype in Metastasis. *Front. Oncol.* **5,** (2015).
19. Tsuji, T., Ibaragi, S. & Hu, G. Epithelial-Mesenchymal Transition and Cell Cooperativity in Metastasis. *Cancer Res.* **69,** 7135–7139 (2009).
20. Celià-Terrassa, T. *et al.* Epithelial-mesenchymal transition can suppress major attributes of human epithelial tumor-initiating cells. *J. Clin. Invest.* **122,** 1849–1868 (2012).
21. Aroeira, L. S. *et al.* Epithelial to Mesenchymal Transition and Peritoneal Membrane Failure in Peritoneal Dialysis Patients: Pathologic Significance and Potential Therapeutic Interventions. *J. Am. Soc. Nephrol.* **18,** 2004–2013 (2007).
22. Wong, S. Y. & Hynes, R. O. Lymphatic or Hematogenous Dissemination: How Does a Metastatic Tumor Cell Decide? *Cell Cycle Georget. Tex* **5,** 812–817 (2006).

23. Butler, T. P. & Gullino, P. M. Quantitation of Cell Shedding into Efferent Blood of Mammary Adenocarcinoma. *Cancer Res.* **35,** 512–516 (1975).
24. Paoli, P., Giannoni, E. & Chiarugi, P. Anoikis molecular pathways and its role in cancer progression. *Biochim. Biophys. Acta BBA - Mol. Cell Res.* **1833,** 3481–3498 (2013).
25. Mohme, M., Riethdorf, S. & Pantel, K. Circulating and disseminated tumour cells — mechanisms of immune surveillance and escape. *Nat. Rev. Clin. Oncol.* **14,** 155–167 (2017).
26. Meng, S. *et al.* Circulating Tumor Cells in Patients with Breast Cancer Dormancy. *Clin. Cancer Res.* **10,** 8152–8162 (2004).
27. Ewing, J. *Neoplastic diseases; a treatise on tumors*. (Philadelphia London, W. B. Saunders company, 1922).
28. Gassmann, P., Hemping-Bovenkerk, A., Mees, S. T. & Haier, J. Metastatic tumor cell arrest in the liver-lumen occlusion and specific adhesion are not exclusive. *Int. J. Colorectal Dis.* **24,** 851–858 (2009).
29. Weiss, L. Comments on hematogenous metastatic patterns in humans as revealed by autopsy. *Clin. Exp. Metastasis* **10,** 191–199 (1992).
30. Disibio, G. & French, S. W. Metastatic patterns of cancers: results from a large autopsy study. *Arch. Pathol. Lab. Med.* **132,** 931–939 (2008).
31. Chambers, A. F., Groom, A. C. & MacDonald, I. C. Metastasis: Dissemination and growth of cancer cells in metastatic sites. *Nat. Rev. Cancer* **2,** 563–572 (2002).
32. Follain, G. *et al.* Hemodynamic Forces Tune the Arrest, Adhesion, and Extravasation of Circulating Tumor Cells. *Dev. Cell* **45,** 33–52.e12 (2018).
33. Li, J. & King, M. R. Adhesion receptors as therapeutic targets for circulating tumor cells. *Front. Oncol.* **2,** (2012).
34. Chaffer, C. L. & Weinberg, R. A. A Perspective on Cancer Cell Metastasis. *Science* **331,** 1559–1564 (2011).
35. Kim, M.-Y. *et al.* Tumor Self-Seeding by Circulating Cancer Cells. *Cell* **139,** 1315–1326 (2009).
36. Fidler, I. J. Metastasis: Quantitative Analysis of Distribution and Fate of Tumor Emboli Labeled With 125I-5-Iodo-2' -deoxyuridine. *JNCI J. Natl. Cancer Inst.* **45,** 773–782 (1970).
37. Luzzi, K. J. *et al.* Multistep Nature of Metastatic Inefficiency: Dormancy of Solitary Cells after Successful Extravasation and Limited Survival of Early Micrometastases. *Am. J. Pathol.* **153,** 865–873 (1998).
38. Kim, J. *et al.* Rapid apoptosis in the pulmonary vasculature distinguishes non-metastatic from metastatic melanoma cells. *Cancer Lett.* **213,** 203–212 (2004).
39. Hodgkinson, C. L. *et al.* Tumorigenicity and genetic profiling of circulating tumor cells in small-cell lung cancer. *Nat. Med.* **20,** 897–903 (2014).
40. Baccelli, I. *et al.* Identification of a population of blood circulating tumor cells from breast cancer patients that initiates metastasis in a xenograft assay. *Nat. Biotechnol.* **31,** 539–544 (2013).
41. Goss, P. E. & Chambers, A. F. Does tumour dormancy offer a therapeutic target? *Nat. Rev. Cancer* **10,** 871–877 (2010).
42. Kang, Y. & Pantel, K. Tumor Cell Dissemination: Emerging Biological Insights from Animal Models and Cancer Patients. *Cancer Cell* **23,** 573–581 (2013).
43. Klein, C. A. Parallel progression of primary tumours and metastases. *Nat. Rev. Cancer* **9,** 302–312 (2009).
44. Kaplan, R. N. *et al.* VEGFR1-positive haematopoietic bone marrow progenitors initiate the pre-metastatic niche. *Nature* **438,** 820–827 (2005).

45. Liu, Y. & Cao, X. Characteristics and Significance of the Pre-metastatic Niche. *Cancer Cell* **30,** 668–681 (2016).
46. Gerlinger, M. *et al.* Intratumor heterogeneity and branched evolution revealed by multiregion sequencing. *N. Engl. J. Med.* **366,** 883–892 (2012).
47. Welcome to EDRN — EDRN Public Portal. Available at: https://edrn.nci.nih.gov/. (Accessed: 19th May 2018)
48. GRAIL - Detecting Cancer Early, When It Can Be Cured. *GRAIL* Available at: https://grail.com/. (Accessed: 19th May 2018)
49. Nakamura, K. *et al.* Clinical relevance of circulating cell-free microRNAs in ovarian cancer. *Mol. Cancer* **15,** 48 (2016).
50. Di Meo, A., Bartlett, J., Cheng, Y., Pasic, M. D. & Yousef, G. M. Liquid biopsy: a step forward towards precision medicine in urologic malignancies. *Mol. Cancer* **16,** 80 (2017).
51. Esposito, A., Criscitiello, C., Locatelli, M., Milano, M. & Curigliano, G. Liquid biopsies for solid tumors: Understanding tumor heterogeneity and real time monitoring of early resistance to targeted therapies. *Pharmacol. Ther.* **157,** 120–124 (2016).
52. Joosse, S. A. & Pantel, K. Tumor-Educated Platelets as Liquid Biopsy in Cancer Patients. *Cancer Cell* **28,** 552–554 (2015).
53. Braun, S. *et al.* Cytokeratin-Positive Cells in the Bone Marrow and Survival of Patients with Stage I, II, or III Breast Cancer. *http://dx.doi.org/10.1056/NEJM200002243420801* (2009). Available at: https://www.nejm.org/doi/10.1056/NEJM200002243420801?url_ver=Z39.88-2003&rfr_id=ori%3Arid%3Acrossref.org&rfr_dat=cr_pub%3Dwww.ncbi.nlm.nih.gov. (Accessed: 22nd May 2018)
54. Fehm, T. *et al.* Cytogenetic Evidence That Circulating Epithelial Cells in Patients with Carcinoma Are Malignant. *Clin. Cancer Res.* **8,** 2073–2084 (2002).
55. Weitz, J. *et al.* Dissemination of tumor cells in patients undergoing surgery for colorectal cancer. *Clin. Cancer Res. Off. J. Am. Assoc. Cancer Res.* **4,** 343–348 (1998).
56. Racila, E. *et al.* Detection and characterization of carcinoma cells in the blood. *Proc. Natl. Acad. Sci. U. S. A.* **95,** 4589–4594 (1998).
57. Gertler, R. *et al.* Detection of Circulating Tumor Cells in Blood Using an Optimized Density Gradient Centrifugation. in *Molecular Staging of Cancer* 149–155 (Springer, Berlin, Heidelberg, 2003).
58. Sabbatini, R. *et al.* Detection of circulating tumor cells by reverse transcriptase polymerase chain reaction of maspin in patients with breast cancer undergoing conventional-dose chemotherapy. *J. Clin. Oncol. Off. J. Am. Soc. Clin. Oncol.* **18,** 1914–1920 (2000).
59. Stroun, M. *et al.* Neoplastic Characteristics of the DNA Found in the Plasma of Cancer Patients. *Oncology* **46,** 318–322 (1989).
60. Sorenson, G. D. *et al.* Soluble normal and mutated DNA sequences from single-copy genes in human blood. *Cancer Epidemiol. Biomark. Prev. Publ. Am. Assoc. Cancer Res. Cosponsored Am. Soc. Prev. Oncol.* **3,** 67–71 (1994).
61. Wan, J. C. M. *et al.* Liquid biopsies come of age: towards implementation of circulating tumour DNA. *Nat. Rev. Cancer* **17,** 223–238 (2017).
62. Kosaka, N., Yoshioka, Y., Fujita, Y. & Ochiya, T. Versatile roles of extracellular vesicles in cancer. *J. Clin. Invest.* **126,** 1163–1172
63. Becker, A. *et al.* Extracellular Vesicles in Cancer: Cell-to-Cell Mediators of Metastasis. *Cancer Cell* **30,** 836–848 (2016).

64. Diaz, L. A. & Bardelli, A. Liquid Biopsies: Genotyping Circulating Tumor DNA. *J. Clin. Oncol.* **32,** 579–586 (2014).
65. Mouliere, F. & Rosenfeld, N. Circulating tumor-derived DNA is shorter than somatic DNA in plasma. *Proc. Natl. Acad. Sci. U. S. A.* **112,** 3178–3179 (2015).
66. Leung, F. *et al.* Circulating Tumor DNA as a Cancer Biomarker: Fact or Fiction? *Clin. Chem.* **62,** 1054–1060 (2016).
67. Soung, Y. H., Ford, S., Zhang, V. & Chung, J. Exosomes in Cancer Diagnostics. *Cancers* **9,** (2017).
68. Ko, J., Carpenter, E. & Issadore, D. Detection and isolation of circulating exosomes and microvesicles for cancer monitoring and diagnostics using micro-/nano-based devices. *The Analyst* **141,** 450–460 (2016).
69. Brodbeck, T., Nehmann, N., Bethge, A., Wedemann, G. & Schumacher, U. Perforin-dependent direct cytotoxicity in natural killer cells induces considerable knockdown of spontaneous lung metastases and computer modelling-proven tumor cell dormancy in a HT29 human colon cancer xenograft mouse model. *Mol. Cancer* **13,** 244 (2014).
70. Spicer, J. D. *et al.* Neutrophils Promote Liver Metastasis via Mac-1–Mediated Interactions with Circulating Tumor Cells. *Cancer Res.* **72,** 3919–3927 (2012).
71. Lambert, A. W., Pattabiraman, D. R. & Weinberg, R. A. Emerging Biological Principles of Metastasis. *Cell* **168,** 670–691 (2017).
72. Adams, D. L. *et al.* Circulating giant macrophages as a potential biomarker of solid tumors. *Proc. Natl. Acad. Sci. U. S. A.* **111,** 3514–3519 (2014).
73. Themes, U. F. O. Blood. *Basicmedical Key* (2016).
74. Yan, M. & Jurasz, P. The role of platelets in the tumor microenvironment: From solid tumors to leukemia. *Biochim. Biophys. Acta BBA - Mol. Cell Res.* **1863,** 392–400 (2016).
75. Caine, G. J., Stonelake, P. S., Lip, G. Y. & Kehoe, S. T. The Hypercoagulable State of Malignancy: Pathogenesis and Current Debate. *Neoplasia N. Y. N* **4,** 465–473 (2002).
76. Palumbo, J. S. *et al.* Platelets and fibrin(ogen) increase metastatic potential by impeding natural killer cell–mediated elimination of tumor cells. *Blood* **105,** 178–185 (2005).
77. Philippe, C. *et al.* Protection from tumor necrosis factor-mediated cytolysis by platelets. *Am. J. Pathol.* **143,** 1713–1723 (1993).
78. Rickles, F. R. & Falanga, A. Molecular Basis for the Relationship Between Thrombosis and Cancer. *Thromb. Res.* **102,** V215–V224 (2001).
79. Labelle, M., Begum, S. & Hynes, R. O. Direct signaling between platelets and cancer cells induces an epithelial-mesenchymal-like transition and promotes metastasis. *Cancer Cell* **20,** 576–590 (2011).
80. Wirtz, D., Konstantopoulos, K. & Searson, P. C. The physics of cancer: the role of physical interactions and mechanical forces in metastasis. *Nat. Rev. Cancer* **11,** 512–522 (2011).
81. Barnes, J. M., Nauseef, J. T. & Henry, M. D. Resistance to Fluid Shear Stress Is a Conserved Biophysical Property of Malignant Cells. *PLoS ONE* **7,** (2012).
82. Fu, A. *et al.* High expression of MnSOD promotes survival of circulating breast cancer cells and increases their resistance to doxorubicin. *Oncotarget* **7,** 50239–50257 (2016).
83. Regmi, S., Fu, A. & Luo, K. Q. High Shear Stresses under Exercise Condition Destroy Circulating Tumor Cells in a Microfluidic System. *Sci. Rep.* **7,** 39975 (2017).
84. Fabisiewicz, A. & Grzybowska, E. CTC clusters in cancer progression and metastasis. *Med. Oncol.* **34,** 12 (2017).

85. Marrinucci, D. *et al.* Case study of the morphologic variation of circulating tumor cells. *Hum. Pathol.* **38,** 514–519 (2007).
86. Aceto, N. *et al.* Circulating Tumor Cell Clusters Are Oligoclonal Precursors of Breast Cancer Metastasis. *Cell* **158,** 1110–1122 (2014).
87. Sarioglu, A. F. *et al.* A microfluidic device for label-free, physical capture of circulating tumor cell-clusters. *Nat. Methods* **12,** 685–691 (2015).
88. Yu, M. *et al.* Circulating Breast Tumor Cells Exhibit Dynamic Changes in Epithelial and Mesenchymal Composition. *Science* **339,** 580–584 (2013).
89. Giuliano, M. *et al.* Perspective on Circulating Tumor Cell Clusters: Why It Takes a Village to Metastasize. *Cancer Res.* (2018). doi:10.1158/0008-5472.CAN-17-2748
90. Engell, H. C. Cancer Cells in the Blood. *Ann. Surg.* **149,** 457–461 (1959).
91. Ross, A. A. *et al.* Detection and viability of tumor cells in peripheral blood stem cell collections from breast cancer patients using immunocytochemical and clonogenic assay techniques [see comments]. *Blood* **82,** 2605–2610 (1993).
92. N & Db, I. Cancer Cell Nucleus: An Insight. *J. Mol. Biomark. Diagn.* **8,** 1–8 (2017).
93. Marrinucci, D. *et al.* Cytomorphology of Circulating Colorectal Tumor Cells:A Small Case Series. *J. Oncol.* **2010,** (2010).
94. Marrinucci, D. *et al.* Circulating Tumor Cells From Well-Differentiated Lung Adenocarcinoma Retain Cytomorphologic Features of Primary Tumor Type. *Arch. Pathol. Lab. Med.* **133,** 1468–1471 (2009).
95. Seal, S. H. A sieve for the isolation of cancer cells and other large cells from the blood. *Cancer* **17,** 637–642
96. Stoecklein, N. H., Fischer, J. C., Niederacher, D. & Terstappen, L. W. M. M. Challenges for CTC-based liquid biopsies: low CTC frequency and diagnostic leukapheresis as a potential solution. *Expert Rev. Mol. Diagn.* **16,** 147–164 (2016).
97. Suresh, S. Nanomedicine: Elastic clues in cancer detection. *Nat. Nanotechnol.* **2,** 748–749 (2007).
98. Cross, S. E., Jin, Y.-S., Rao, J. & Gimzewski, J. K. Nanomechanical analysis of cells from cancer patients. *Nat. Nanotechnol.* **2,** 780–783 (2007).
99. Swaminathan, V. *et al.* Mechanical Stiffness Grades Metastatic Potential in Patient Tumor Cells and in Cancer Cell Lines. *Cancer Res.* **71,** 5075–5080 (2011).
100. Chivukula, V. K., Krog, B. L., Nauseef, J. T., Henry, M. D. & Vigmostad, S. C. Alterations in cancer cell mechanical properties after fluid shear stress exposure: a micropipette aspiration study. *Cell Health and Cytoskeleton* (2015). Available at: https://www.dovepress.com/alterations-in-cancer-cell-mechanical-properties-after-fluid-shear-str-peer-reviewed-fulltext-article-CHC. (Accessed: 28th May 2018)
101. Rejniak, K. A. Investigating dynamical deformations of tumor cells in circulation: predictions from a theoretical model. *Front. Oncol.* **2,** (2012).
102. Coughlin, M. F. *et al.* Cytoskeletal stiffness, friction, and fluidity of cancer cell lines with different metastatic potential. *Clin. Exp. Metastasis* **30,** (2013).
103. Guo, Q., Park, S. & Ma, H. Microfluidic micropipette aspiration for measuring the deformability of single cells. *Lab. Chip* **12,** 2687–2695 (2012).
104. Rosenbluth, M. J., Lam, W. A. & Fletcher, D. A. Force microscopy of nonadherent cells: a comparison of leukemia cell deformability. *Biophys. J.* **90,** 2994–3003 (2006).
105. Bagnall, J. S. *et al.* Deformability of Tumor Cells versus Blood Cells. *Sci. Rep.* **5,** 18542 (2015).

106. Tumor Markers. *National Cancer Institute* Available at: https://www.cancer.gov/about-cancer/diagnosis-staging/diagnosis/tumor-markers-fact-sheet. (Accessed: 18th June 2018)
107. Barriere, G. *et al.* Circulating tumor cells and epithelial, mesenchymal and stemness markers: characterization of cell subpopulations. *Ann. Transl. Med.* **2,** (2014).
108. Gkountela, S., Szczerba, B., Donato, C. & Aceto, N. Recent advances in the biology of human circulating tumour cells and metastasis. *ESMO Open* **1,** e000078 (2016).
109. Armstrong, A. & Eck, S. L. EpCAM: A New Therapeutic Target for an Old Cancer Antigen. *Cancer Biol. Ther.* **2,** 320–325 (2003).
110. Raimondi, C., Nicolazzo, C. & Gradilone, A. Circulating tumor cells isolation: the 'post-EpCAM era'. *Chin. J. Cancer Res.* **27,** 461–470 (2015).
111. Francart, M.-E. *et al.* Epithelial-mesenchymal plasticity and circulating tumor cells: Travel companions to metastases. *Dev. Dyn. Off. Publ. Am. Assoc. Anat.* **247,** 432–450 (2018).
112. Rao, C. G. *et al.* Expression of epithelial cell adhesion molecule in carcinoma cells present in blood and primary and metastatic tumors. *Int. J. Oncol.* **27,** 49–57 (2005).
113. Li, F., Tiede, B., Massagué, J. & Kang, Y. Beyond tumorigenesis: cancer stem cells in metastasis. *Cell Res.* **17,** 3–14 (2007).
114. Li, W. *et al.* Unraveling the roles of CD44/CD24 and ALDH1 as cancer stem cell markers in tumorigenesis and metastasis. *Sci. Rep.* **7,** 13856 (2017).
115. Stott, S. L. *et al.* Isolation of circulating tumor cells using a microvortex-generating herringbone-chip. *Proc. Natl. Acad. Sci. U. S. A.* **107,** 18392–18397 (2010).
116. Moreno, J. G. *et al.* Changes in circulating carcinoma cells in patients with metastatic prostate cancer correlate with disease status. *Urology* **58,** 386–392 (2001).
117. Renier, C. *et al.* Label-free isolation of prostate circulating tumor cells using Vortex microfluidic technology. *Npj Precis. Oncol.* **1,** 15 (2017).
118. Park, S. *et al.* Morphological Differences between Circulating Tumor Cells from Prostate Cancer Patients and Cultured Prostate Cancer Cells. *PLoS ONE* **9,** (2014).
119. Ozkumur, E. *et al.* Inertial Focusing for Tumor Antigen–Dependent and –Independent Sorting of Rare Circulating Tumor Cells. *Sci. Transl. Med.* **5,** 179ra47 (2013).
120. Meng, S. *et al.* Circulating Tumor Cells in Patients with Breast Cancer Dormancy. *Clin. Cancer Res.* **10,** 8152–8162 (2004).
121. Allard, W. J. *et al.* Tumor Cells Circulate in the Peripheral Blood of All Major Carcinomas but not in Healthy Subjects or Patients With Nonmalignant Diseases. *Clin. Cancer Res.* **10,** 6897–6904 (2004).
122. Phillips, K. G. *et al.* Quantification of cellular volume and sub-cellular density fluctuations: comparison of normal peripheral blood cells and circulating tumor cells identified in a breast cancer patient. *Front. Oncol.* **2,** (2012).
123. Phillips, K. G. *et al.* Optical Quantification of Cellular Mass, Volume, and Density of Circulating Tumor Cells Identified in an Ovarian Cancer Patient. *Front. Oncol.* **2,** (2012).
124. Ferreira, M. M., Ramani, V. C. & Jeffrey, S. S. Circulating tumor cell technologies. *Mol. Oncol.* **10,** 374–394 (2016).
125. Talasaz, A. H. *et al.* Isolating highly enriched populations of circulating epithelial cells and other rare cells from blood using a magnetic sweeper device. *Proc. Natl. Acad. Sci. U. S. A.* **106,** 3970–3975 (2009).
126. Autebert, J. *et al.* High purity microfluidic sorting and analysis of circulating tumor cells: towards routine mutation detection. *Lab. Chip* **15,** 2090–2101 (2015).

127. Earhart, C. M., Wilson, R. J., White, R. L., Pourmand, N. & Wang, S. X. Microfabricated magnetic sifter for high-throughput and high-gradient magnetic separation. *J. Magn. Magn. Mater.* **321,** 1436–1439 (2009).
128. Nagrath, S. *et al.* Isolation of rare circulating tumour cells in cancer patients by microchip technology. *Nature* **450,** 1235–1239 (2007).
129. Sheng, W. *et al.* Capture, release and culture of circulating tumor cells from pancreatic cancer patients using an enhanced mixing chip. *Lab. Chip* **14,** 89–98 (2014).
130. P. Gleghorn, J. *et al.* Capture of circulating tumor cells from whole blood of prostate cancer patients using geometrically enhanced differential immunocapture (GEDI) and a prostate-specific antibody. *Lab. Chip* **10,** 27–29 (2010).
131. Mandlebaum, F. S. The diagnosis of malignant tumors by paraffin sections of centrifuged exudates. *J. Lab. Clin. Med.* **2,** 580 (1917).
132. Lim, L. S. *et al.* Microsieve lab-chip device for rapid enumeration and fluorescence in situ hybridization of circulating tumor cells. *Lab. Chip* **12,** 4388–4396 (2012).
133. Wit, S. de *et al.* The detection of $EpCAM^+$ and $EpCAM^-$ circulating tumor cells. *Sci. Rep.* **5,** 12270 (2015).
134. Swennenhuis, J. F. *et al.* Self-seeding microwell chip for the isolation and characterization of single cells. *Lab. Chip* **15,** 3039–3046 (2015).
135. Hosokawa, M. *et al.* Size-Selective Microcavity Array for Rapid and Efficient Detection of Circulating Tumor Cells. *Anal. Chem.* **82,** 6629–6635 (2010).
136. Adams, D. L. *et al.* The systematic study of circulating tumor cell isolation using lithographic microfilters. *RSC Adv.* **9,** 4334–4342 (2014).
137. Zheng, S. *et al.* Membrane microfilter device for selective capture, electrolysis and genomic analysis of human circulating tumor cells. *J. Chromatogr. A* **1162,** 154–161 (2007).
138. Harouaka, R. A. *et al.* Flexible Micro Spring Array Device for High-Throughput Enrichment of Viable Circulating Tumor Cells. *Clin. Chem.* **60,** 323–333 (2014).
139. Zheng, S. *et al.* 3D microfilter device for viable circulating tumor cell (CTC) enrichment from blood. *Biomed. Microdevices* **13,** 203–213 (2011).
140. Zhou, M.-D. *et al.* Separable Bilayer Microfiltration Device for Viable Label-free Enrichment of Circulating Tumour Cells. *Sci. Rep.* **4,** 7392 (2014).
141. Mohamed, H., Murray, M., Turner, J. N. & Caggana, M. Isolation of tumor cells using size and deformation. *J. Chromatogr. A* **1216,** 8289–8295 (2009).
142. Tan, S. J., Yobas, L., Lee, G. Y. H., Ong, C. N. & Lim, C. T. Microdevice for the isolation and enumeration of cancer cells from blood. *Biomed. Microdevices* **11,** 883–892 (2009).
143. Kuo, J. S. *et al.* Deformability considerations in filtration of biological cells. *Lab. Chip* **10,** 837–842 (2010).
144. Beattie, W., Qin, X., Wang, L. & Ma, H. Clog-free cell filtration using resettable cell traps. *Lab. Chip* **14,** 2657–2665 (2014).
145. Carlo, D. D. Inertial microfluidics. *Lab. Chip* **9,** 3038–3046 (2009).
146. Sollier, E. *et al.* Size-selective collection of circulating tumor cells using Vortex technology. *Lab. Chip* **14,** 63–77 (2013).
147. Hou, H. W. *et al.* Isolation and retrieval of circulating tumor cells using centrifugal forces. *Sci. Rep.* **3,** 1259 (2013).
148. Loutherback, K. *et al.* Deterministic separation of cancer cells from blood at 10 mL/min. *AIP Adv.* **2,** (2012).

149. Au, S. H. *et al.* Microfluidic Isolation of Circulating Tumor Cell Clusters by Size and Asymmetry. *Sci. Rep.* **7,** 2433 (2017).
150. Karabacak, N. M. *et al.* Microfluidic, marker-free isolation of circulating tumor cells from blood samples. *Nat. Protoc.* **9,** 694–710 (2014).
151. Gupta, V. *et al.* ApoStream™, a new dielectrophoretic device for antibody independent isolation and recovery of viable cancer cells from blood. *Biomicrofluidics* **6,** 24133 (2012).
152. Pantel, K. *et al.* Circulating Epithelial Cells in Patients with Benign Colon Diseases. *Clin. Chem.* **58,** 936–940 (2012).
153. Andreopoulou, E. *et al.* Comparison of assay methods for detection of circulating tumor cells in metastatic breast cancer: AdnaGen AdnaTest BreastCancer Select/Detect™ versus Veridex CellSearch™ system. *Int. J. Cancer* **130,** 1590–1597
154. Xi, L. *et al.* Optimal markers for real-time quantitative reverse transcription PCR detection of circulating tumor cells from melanoma, breast, colon, esophageal, head and neck, and lung cancers. *Clin. Chem.* **53,** 1206–1215 (2007).
155. Stott, S. L. *et al.* Isolation and characterization of circulating tumor cells from patients with localized and metastatic prostate cancer. *Sci. Transl. Med.* **2,** 25ra23 (2010).
156. Evers, D. L., Fowler, C. B., Cunningham, B. R., Mason, J. T. & O'Leary, T. J. The Effect of Formaldehyde Fixation on RNA. *J. Mol. Diagn. JMD* **13,** 282–288 (2011).
157. Yu, M. *et al.* RNA sequencing of pancreatic circulating tumour cells implicates WNT signalling in metastasis. *Nature* **487,** 510–513 (2012).
158. Cann, G. M. *et al.* mRNA-Seq of Single Prostate Cancer Circulating Tumor Cells Reveals Recapitulation of Gene Expression and Pathways Found in Prostate Cancer. *PLOS ONE* **7,** e49144 (2012).
159. Boral, D. *et al.* Molecular characterization of breast cancer CTCs associated with brain metastasis. *Nat. Commun.* **8,** 196 (2017).
160. Cristofanilli, M. *et al.* Circulating Tumor Cells, Disease Progression, and Survival in Metastatic Breast Cancer. *http://dx.doi.org/10.1056/NEJMoa040766* (2009). Available at: https://www.nejm.org/doi/10.1056/NEJMoa040766?url_ver=Z39.88-2003&rfr_id=ori%3Arid%3Acrossref.org&rfr_dat=cr_pub%3Dwww.ncbi.nlm.nih.gov. (Accessed: 18th June 2018)
161. Bono, J. S. de *et al.* Circulating Tumor Cells Predict Survival Benefit from Treatment in Metastatic Castration-Resistant Prostate Cancer. *Clin. Cancer Res.* **14,** 6302–6309 (2008).
162. Cohen, S. J. *et al.* Relationship of Circulating Tumor Cells to Tumor Response, Progression-Free Survival, and Overall Survival in Patients With Metastatic Colorectal Cancer. *J. Clin. Oncol.* **26,** 3213–3221 (2008).
163. Hofman, V. *et al.* Detection of circulating tumor cells as a prognostic factor in patients undergoing radical surgery for non-small-cell lung carcinoma: comparison of the efficacy of the CellSearch Assay™ and the isolation by size of epithelial tumor cell method. *Int. J. Cancer* **129,** 1651–1660
164. Naito, T. *et al.* Prognostic Impact of Circulating Tumor Cells in Patients with Small Cell Lung Cancer. *J. Thorac. Oncol.* **7,** 512–519 (2012).
165. Poveda, A. *et al.* Circulating tumor cells predict progression free survival and overall survival in patients with relapsed/recurrent advanced ovarian cancer. *Gynecol. Oncol.* **122,** 567–572 (2011).

166. Rossi, E. *et al.* Dynamic changes of live/apoptotic circulating tumour cells as predictive marker of response to Sunitinib in metastatic renal cancer. *Br. J. Cancer* **107,** 1286–1294 (2012).
167. Klinac, D. *et al.* Monitoring changes in circulating tumour cells as a prognostic indicator of overall survival and treatment response in patients with metastatic melanoma. *BMC Cancer* **14,** 423 (2014).
168. Rack, B. *et al.* Circulating Tumor Cells Predict Survival in Early Average-to-High Risk Breast Cancer Patients. *JNCI J. Natl. Cancer Inst.* **106,** (2014).
169. Thalgott, M. *et al.* Detection of Circulating Tumor Cells in Locally Advanced High-risk Prostate Cancer During Neoadjuvant Chemotherapy and Radical Prostatectomy. *Anticancer Res.* **35,** 5679–5685 (2015).
170. Denève, E. *et al.* Capture of Viable Circulating Tumor Cells in the Liver of Colorectal Cancer Patients. *Clin. Chem.* **59,** 1384–1392 (2013).
171. Gazzaniga, P. *et al.* Circulating tumor cells detection has independent prognostic impact in high-risk non-muscle invasive bladder cancer. *Int. J. Cancer* **135,** 1978–1982 (2014).
172. Schulze, K. *et al.* Presence of EpCAM-positive circulating tumor cells as biomarker for systemic disease strongly correlates to survival in patients with hepatocellular carcinoma. *Int. J. Cancer* **133,** 2165–2171
173. Bidard, F.-C. *et al.* Clinical validity of circulating tumour cells in patients with metastatic breast cancer: a pooled analysis of individual patient data. *Lancet Oncol.* **15,** 406–414 (2014).
174. Scher, H. I. *et al.* Circulating tumor cell biomarker panel as an individual-level surrogate for survival in metastatic castration-resistant prostate cancer. *J. Clin. Oncol. Off. J. Am. Soc. Clin. Oncol.* **33,** 1348–1355 (2015).
175. Bidard, F.-C. *et al.* Clinical value of circulating endothelial cells and circulating tumor cells in metastatic breast cancer patients treated first line with bevacizumab and chemotherapy. *Ann. Oncol.* **21,** 1765–1771 (2010).
176. Giordano, A. *et al.* Artificial neural network analysis of circulating tumor cells in metastatic breast cancer patients. *Breast Cancer Res. Treat.* **129,** 451–458 (2011).
177. Bidard, F.-C. *et al.* Clinical application of circulating tumor cells in breast cancer: overview of the current interventional trials. *Cancer Metastasis Rev.* **32,** 179–188 (2013).
178. Lalmahomed, Z. S. *et al.* Circulating Tumor Cells and Sample Size: The More, the Better. *J. Clin. Oncol.* **28,** e288–e289 (2010).
179. Tibbe, A. G. J., Miller, M. C. & Terstappen, L. W. M. M. Statistical considerations for enumeration of circulating tumor cells. *Cytometry A* **71A,** 154–162
180. Rosenblatt, J. I., Hokanson, J. A., McLaughlin, S. R. & Leary, J. F. Theoretical basis for sampling statistics useful for detecting and isolating rare cells using flow cytometry and cell sorting. *Cytometry* **27,** 233–238 (1997).
181. Allan, A. L. & Keeney, M. Circulating tumor cell analysis: technical and statistical considerations for application to the clinic. *J. Oncol.* **2010,** 426218 (2010).
182. Coumans, F. A. W., Ligthart, S. T., Uhr, J. W. & Terstappen, L. W. M. M. Challenges in the Enumeration and Phenotyping of CTC. *Clin. Cancer Res.* **18,** 5711–5718 (2012).
183. Saucedo-Zeni, N. *et al.* A novel method for the in vivo isolation of circulating tumor cells from peripheral blood of cancer patients using a functionalized and structured medical wire. *Int. J. Oncol.* **41,** 1241–1250 (2012).
184. Chen, S. *et al.* Catch and Release: rare cell analysis from a functionalised medical wire. *Sci. Rep.* **7,** 43424 (2017).

185. Mandair, D. *et al.* A comparison of CellCollector with CellSearch in patients with neuroendocrine tumours. *Endocr. Relat. Cancer* **23,** L29–L32 (2016).
186. Gorges, T. M. *et al.* Enumeration and Molecular Characterization of Tumor Cells in Lung Cancer Patients Using a Novel In Vivo Device for Capturing Circulating Tumor Cells. *Clin. Cancer Res. Off. J. Am. Assoc. Cancer Res.* **22,** 2197–2206 (2016).
187. Markou, A. *et al.* Multiplex Gene Expression Profiling of In Vivo Isolated Circulating Tumor Cells in High-Risk Prostate Cancer Patients. *Clin. Chem.* clinchem.2017.275503 (2017). doi:10.1373/clinchem.2017.275503
188. Kuske, A. *et al.* Improved detection of circulating tumor cells in non-metastatic high-risk prostate cancer patients. *Sci. Rep.* **6,** 39736 (2016).
189. Fischer, J. C. *et al.* Diagnostic leukapheresis enables reliable detection of circulating tumor cells of nonmetastatic cancer patients. *Proc. Natl. Acad. Sci.* **110,** 16580–16585 (2013).
190. Galanzha, E. I. *et al.* In vivo magnetic enrichment and multiplex photoacoustic detection of circulating tumour cells. *Nat. Nanotechnol.* **4,** 855–860 (2009).
191. Chang, Y.-C. *et al.* Fiber-optic multiphoton flow cytometry in whole blood and in vivo. *J. Biomed. Opt.* **15,** 47004 (2010).
192. He, W., Wang, H., Hartmann, L. C., Cheng, J.-X. & Low, P. S. In vivo quantitation of rare circulating tumor cells by multiphoton intravital flow cytometry. *Proc. Natl. Acad. Sci. U. S. A.* **104,** 11760–11765 (2007).
193. Azarin, S. M. *et al. In vivo* capture and label-free detection of early metastatic cells. *Nat. Commun.* **6,** 8094 (2015).
194. El-Heliebi, A. *et al.* In Situ Detection and Quantification of AR-V7, AR-FL, PSA, and KRAS Point Mutations in Circulating Tumor Cells. *Clin. Chem.* clinchem.2017.281295 (2016). doi:10.1373/clinchem.2017.281295
195. Leong, S. M. *et al.* Sampling circulating tumor cells for clinical benefits: how frequent? *J. Hematol. Oncol.J Hematol Oncol* **8,** 75 (2015).
196. Méhes, G., Witt, A., Kubista, E. & Ambros, P. F. Circulating Breast Cancer Cells Are Frequently Apoptotic. *Am. J. Pathol.* **159,** 17–20 (2001).
197. Apoptosis of circulating tumor cells in prostate cancer patients - Larson - 2004 - Cytometry Part A - Wiley Online Library.
198. Ring, A. *et al.* EpCAM based capture detects and recovers circulating tumor cells from all subtypes of breast cancer except claudin-low. *Oncotarget* **6,** 44623–44634 (2015).
199. Becker, S., Becker-Pergola, G., Fehm, T., Wallwiener, D. & Solomayer, E.-F. Time is an important factor when processing samples for the detection of disseminated tumor cells in blood/bone marrow by reverse transcription-PCR. *Clin. Chem.* **50,** 785–786 (2004).
200. Benoy, I. H. *et al.* Detection of circulating tumour cells in blood by quantitative real-time RT-PCR: effect of pre-analytical time. *Clin. Chem. Lab. Med.* **44,** 1082–1087 (2006).
201. Molloy, T. J., Bosma, A. J. & van't Veer, L. J. Towards an optimized platform for the detection, enrichment, and semi-quantitation circulating tumor cells. *Breast Cancer Res. Treat.* **112,** 297–307 (2008).
202. Wong, K. H. K. *et al.* Whole blood stabilization for the microfluidic isolation and molecular characterization of circulating tumor cells. *Nat. Commun.* **8,** 1733 (2017).
203. Wong, K. H. K. *et al.* The Role of Physical Stabilization in Whole Blood Preservation. *Sci. Rep.* **6,** 21023 (2016).

204. Qin, J., Alt, J. R., Hunsley, B. A., Williams, T. L. & Fernando, M. R. Stabilization of circulating tumor cells in blood using a collection device with a preservative reagent. *Cancer Cell Int.* **14,** 23 (2014).

205. Reinholz, M. M. *et al.* Cytokeratin-19 and mammaglobin gene expression in circulating tumor cells from metastatic breast cancer patients enrolled in North Central Cancer Treatment Group trials, N0234/336/436/437. *Clin. Cancer Res. Off. J. Am. Assoc. Cancer Res.* **17,** 7183–7193 (2011).

206. Medeiros, F., Rigl, C. T., Anderson, G. G., Becker, S. H. & Halling, K. C. Tissue handling for genome-wide expression analysis: a review of the issues, evidence, and opportunities. *Arch. Pathol. Lab. Med.* **131,** 1805–1816 (2007).

207. Alix-Panabières, C. EPISPOT Assay: Detection of Viable DTCs/CTCs in Solid Tumor Patients. in *Minimal Residual Disease and Circulating Tumor Cells in Breast Cancer* 69–76 (Springer, Berlin, Heidelberg, 2012).

208. Alix-Panabières, C., Bartkowiak, K. & Pantel, K. Functional studies on circulating and disseminated tumor cells in carcinoma patients. *Mol. Oncol.* **10,** 443–449 (2016).

Chapter II

Engineered polymer-based microdevices for the isolation of CTCs

Chapter II
Engineered polymer-based microdevices for the isolation of CTCs

2.1 Conceptual and theoretical framework

2.1.1 Concept: *in vivo* microfiltration of blood for CTC trapping

As introduced in Chapter I, there is a clinical need for a repeated access to CTCs present in the bloodstream of cancer patients. Apart of high sensitive technologies, it has been extensively suggested that the interrogation of a large volume of blood could potentially increase CTC counts and detection rates. At the time of writing this dissertation, the only technology for the *in vivo* isolation of CTCs directly from the bloodstream, CellCollector®, relies on the expression of EpCAM antigen in CTCs. According to different reports, immunoaffinity-based technologies only based on EpCAM are prone to selection bias, due to the heterogeneous and dynamic expression of this antigen and other antigens in CTCs.

In this chapter, we introduce an innovative intravascular medical device for the physical trapping of CTCs from human blood, under physiological venous flow conditions. Conceptually, the device can be inserted via a medical catheter into a superficial vein of a patient's forearm, a standard procedure in clinical routine, and then exposed to the bloodstream for a short period of time, **Figure 2.1**. Cancer cells are discriminated from normal blood cells based solely on their intrinsic mechanical properties. Thus, the trapping device takes advantage of the hemodynamic conditions of the superficial human veins, as a continuous source of blood, to perform the physical cell separation through an array of micrometric pores. In addition to the cell separation, the trapping device enables the retention of these trapped cells to subsequently retrieve them along with the device, to further identify them.

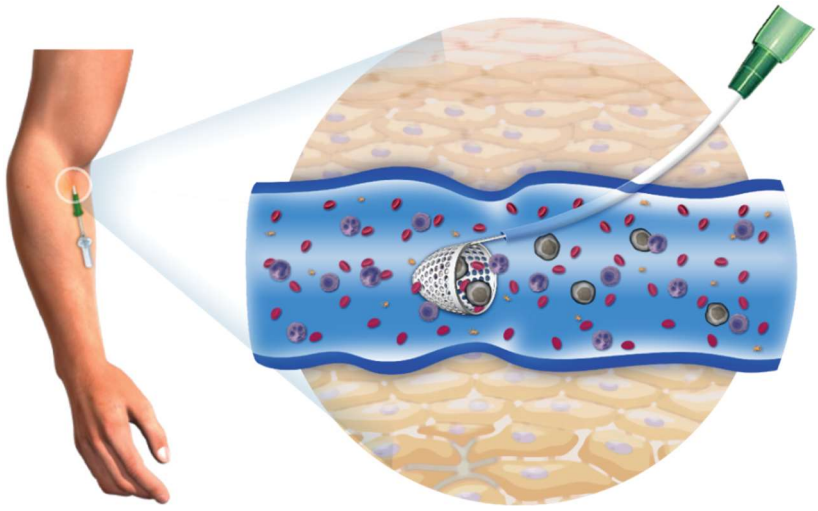

Figure 2.1 Schematic representation of the in vivo microfiltration concept. An intravascular medical device is engineered to be introduced into the superficial veins of the human forearm and perform the selective capture of CTCs based on their intrinsic physical traits.

We hypothesize, that this novel approach could possibly offer several advantages over current conventional CTC isolation platforms. First, this technology could potentially give access to high volumes of unprocessed blood and isolate a wide range of CTC phenotypes preserving cell integrity, since isolation is performed under normal physiological conditions and it does not depend on the cellular expression of any specific antigen. Secondly, due to its potential adaptability to clinical constraints, this technology could enable more frequent blood-interrogation to precisely monitor at different time points cancer evolution over time. Third, isolated cells are concentrated within a small area enabling fast identification and it could potentially serve as a platform for functional studies.

Along this chapter, we mainly focused on the development of the technology and on its *in vitro* assessment, providing insights for the understanding of physical mechanisms that would enable a successful *in vivo* capture of the targeted cells. The experiments and results here presented served to evaluate the proposed hypotheses abovementioned.

2.1.2 Microfiltration of blood for CTC capture: lessons learned from *ex vivo* platforms

Microfiltration of blood has been extensively used for the *ex vivo* isolation of CTCs, as introduced in section 1.4.2.2, and summarized in **Table 2.1**. Conventional setups generally utilize a holey surface, or filter, of a few square millimeters containing micrometric pores placed in a configuration known as dead-end, **Figure 2.2a**. This configuration allows cell filtration when a pressure-driven flow enters perpendicular to the holey surface, such that larger and less deformable cells, either naturally or due to cell fixatives, can be captured within pores. The holey surface completely occludes the lumen of the setup forcing in this way the transit of the total volume of the sample in a single pass. Typical configurations sandwich the filter in customized holders and the blood sample is processed using either gravity, syringes, peristaltic pumps or vacuum systems (**Figure 2.2b-c**). However, the presence of the filter represents a substantial increase in the hydraulic resistance of the system, so a controlled pumping system is usually preferred to ensure a constant and controlled flow during the filtration process.

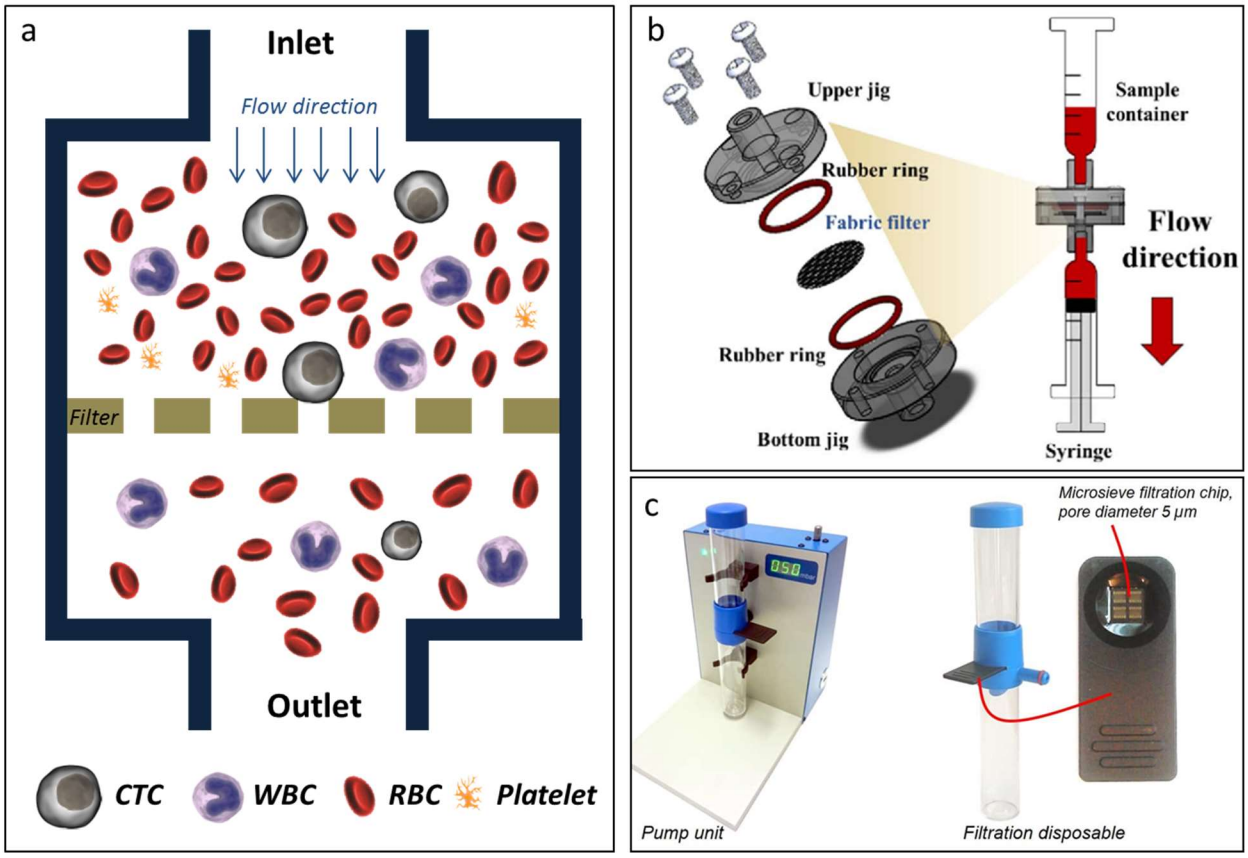

Figure 2.2 Typical setup used for the *ex vivo* CTC isolation from blood samples using engineered holey membranes. **a** Schematic representation, transverse view, of the dead-end configuration for blood microfiltration, drawings are not to scale. **b** Setup using a customized filter holder and syringes as a pumping system. Image taken from *J. Bu, Biosens Bioelectron, 2017*.[1] **c** Semi-automated blood filtration system using a vacuum pump, where the filter (microsieve) is adapted into a disposable cartridge. Image taken from VyCAP official website.[2]

The CTC separation process using narrow constrictions can be represented by the liquid-drop model, also known as cortical shell-liquid core, commonly used in the context of micropipette aspiration.[3,4] Hereinafter, the constriction will refer to a circular pore having a diameter d_p. The model applies for those cells having a similar or larger diameter to the one of the constriction, namely leukocytes and CTCs. Generally, this simplified model assumes that cells behave like a liquid drop, adopting a spherical shape in suspension and deforming/spreading on a surface.

The interaction of any cell type with a pore of the filter depends on the **intrinsic mechanical properties** of each cell, and its capture during the filtration process is mainly determined by the **degree of deformation** and the external **pressure exerted** on them. At the initial phase of the separation process, **Figure 2.3a**, the cellular material arrives to the holey surface following the stream direction and driven by the **pressure difference across the filter, ΔP**. Ideally, cells are pulled by ΔP towards the filter, where cells with a smaller diameter than d_p will pass through the pore, i.e., RBCs, while larger cells will interact with the constriction, **Figure 2.3b**. The latter will tend to deform in order to move into the pore, this deformation trait is determined by the **apparent overall viscosity of the cell,** which depends on cellular features such as cell membrane, cytoplasm, and nucleus.

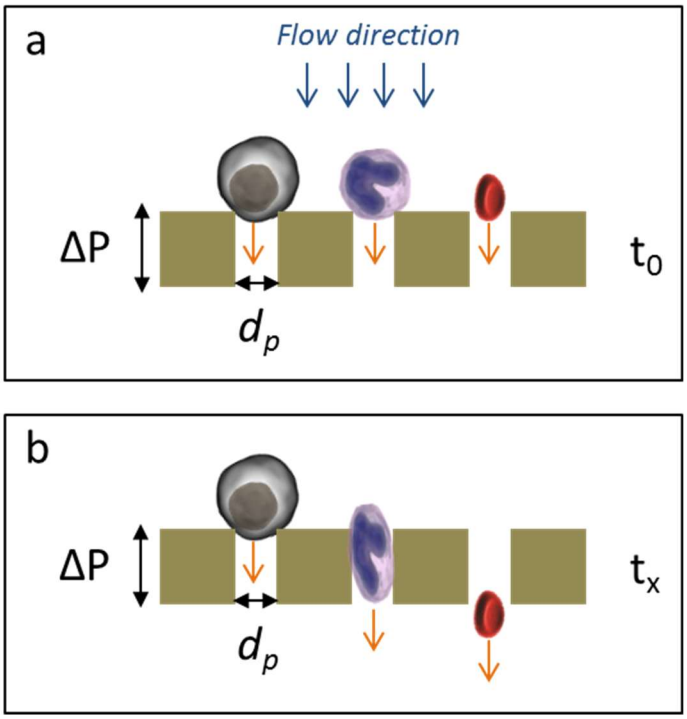

Figure 2.3 The filtration processes of blood cells. **a** Initial phase of the separation, t_0, where the pressure difference across the filter ΔP drives cell arrival. **b** At a given ΔP and due to the intrinsic mechanical properties of each cell, cells will pass through the pores at a determined rate.

Cells with a **higher apparent viscosity** will have a **slower transit** through the constriction at a determined ΔP, thus at a specific pressure condition, known as **critical pressure**, the full entrapment of a cell within the pore is feasible. Below a critical pressure, the surface tension of the cell membrane will balance the force pushing the cell into the filter pore. Conversely, at pressures above this critical pressure, the cell will move into the pore at a rate determined by the apparent viscosity.[5] It has been reported that for constrictions with d_p= 5 µm the critical pressure of granulocytes (8.5 to 9.4 µm in diameter) is about 10-20 Pa, while for some **cancer cell lines it is 160-800 Pa** using a d_p= 6.5 µm.[6,7] Therefore, for a successful CTC separation, the operating pressure during the filtration process needs to be kept below the critical pressure of CTCs and above the critical pressure of normal blood cells. Additionally, using a theoretical model Zhang, et al.[8] reported different values of critical pressure as a function of pore radius and geometrical cross-sections, suggesting that a circular cross-section is most suitable for high efficiency CTC separation.

According with large-deformation studies performed in human neutrophils, the most abundant type of WBCs, the apparent overall viscosity and stiffness of cells varies continuously with the degree of deformation.[9] This phenomenon is described by the **shear thinning liquid drop model**, in which the apparent viscosity of the cytoplasm increases while decreasing the aspiration pressure. In other words, cells are more resistant to deform when the suction pressure decreases near the value of the critical pressure. Accordingly, Coumans *et al.*,[5] suggested that, if the shear thinning phenomenon also holds true for CTCs, the range of ΔP in which **CTC filtration is more effective** must be **slightly above the critical pressure of CTCs**. Under this condition and assuming that the critical pressure of CTCs is higher than the one of blood cells, all blood cells will pass through the pores and CTCs will be retained due to their intrinsic surface tension.

In practice, blood filtration for CTC capture is usually performed at **higher ΔP values** than the critical pressure of all types of cells, ranging from 0.1 psi up to ≥14 psi (700 Pa to 100 kPa), mainly due to the limited porosity of the used filters, which are in the range of 2-40%.[10] Performing whole blood processing using those filters and under lower pressure conditions, may lead to pore clogging given the complexity of blood. Therefore, most of the technologies summarized in **Table 2.1** use diluted blood samples or perform sample preparation such as RBCs lysis.

Additionally, working at ΔP values usually reported, CTCs and blood cells will start deforming and translocating through pores, at a transit rate determined by their apparent viscosity, and thus all cell types would eventually pass through the filter. Given this, the processing of large volumes of blood or their processing for a prolonged time, will result in a reduced recovery of CTCs. This is probably one of the reasons why some of current platforms only process a few mL of whole blood. Therefore, in practical terms, the selection of an adequate **working pressure/flow rate** for a specific type of filter, defined by its porosity and pore size, and a determined **volume of blood** seems to be instrumental to maximize CTC capture.

Taken the abovementioned, the **selectivity** of filtration systems is not only determined by the **size of targeted cells in relation with the one of pores**, but also influenced by the **operating conditions** of the filtering system and the **sample processing time**.

Material	Pore Diameter, µm	Filter Area	Pore Distribution	Blood Volume	Processing Time or Rate	Pumping System	Reference
Polycarbonate (ISET®)	FS: 8.0 NFS: 10-12	6.0-mm diameter	Random	1 mL of WB + Buffer	3 min	Vacuum pump	Vona et al., 2000.[11]
Polycarbonate (ScreenCell®)	FS: 7.5±0.36 NFS: 6.5±0.33	---	Random, $1x10^5/cm^2$	RBC lysis, 1-3 mL WB + Buffer	50 sec	Evacuated Tubes	Desitter et al., 2011.[12]
Parylene-C	NFS: 10.0	600x600 μm^2	16 000 pores	1 mL of WB	10 min	Syringes (3450 Pa)	Zheng, S. et al. 2007.[13]
Parylene-C (3D microfilter)	NFS, Top: 9 Bottom: 8 Gap:6.5	1.0x1.0 cm^2	$2.89x10^5/cm^2$, 14.5% porosity	1 mL of WB + 9 mL PBS	3-5 min	Syringes, 0.5 psi (3450 Pa)	Zheng, S. et al., 2011.[14]
SU-8 (CellSieve™)	FS : 7.0	9.0 mm diameter	160 000 pores, 12.5% porosity	7.5 mL of WB + Buffer	3 min	Vacuum pump, 18.5 mbar (1850 Pa)	Adams et al., 2014.[10]
Nickel	NFS: 9.0	6.0x6.0 mm^2	10 000 pores	3-7.5 mL of WB	200 µL min^{-1}, 5-10 min	Peristaltic Pump (Vaccum Line)	Hosokawa *et al.*, 2010.[15,16]
Nickel, Gold (MCA)	NFS: 8.0 x 100.0 rectangular Slits	---	---	3 mL of WB	600 µL min^{-1}	Peristaltic pump (Vaccum Line)	Yagi *et al*., 2017.[17]
Silicon	NFS: 10.0	5.0-mm diameter	5000/mm^2, 40% porosity	1 mL of WB + 2 mL PBS	1 µL min^{-1}	Peristaltic pump, (~500 Pa)	Shi Lim et al., 2012.[18]
Silicon (VyCAP)	NFS: 5.0	8.0×8.0 mm^2	111 800 pores, 10% porosity	7.5 mL of WB + Buffer	2-15 min	Vacuum pump, 100 mbar (10 000 Pa)	Wit et al, 2015.[19]
Silicon/Silicon Nitride (VyCAP)	NFS: 5.0	8.0×8.0 mm^2	6400 pores	---	1 µL min^{-1}	Vacuum pump, 10 mbar (1000 Pa)	Swennenhuis et al., 2015.[20]
Silicon/Silicon Nitride (VyCAP)	NFS: 5.0 ± 0.2	8.0×8.0 mm^2	160 000 pores	Max : 40 mL of WB	Few minutes	Vacuum pump, 10 mbar (1000 Pa)	VyCAP official website.[2]

Table 2.1 Microfiltration technologies for CTC isolation. FS: Fixed samples, NFS: Non-fixed samples, WB: Whole blood, PBS: phosphate buffered saline, MCA: Microcavity array. The buffer solutions and volumes are different for each platform.

An associated effect of filtration systems is **cell damage**. Experiments using micropipette aspiration have shown that an increment above 3% in the cell membrane surface will result in permanent cell damage.[21,22] The mechanical stress induced on cells during the filtration process is directly related to the experimental pressure condition and size/geometry of the constriction. Following the cell capture process, the main source of mechanical stress arises from the static pressure of the filtration system.[14] One alternative to reduce damaging of isolated CTCs is reducing the operating pressure conditions and accordingly, if possible, adjusting the size of pores. However, this strategy is prone to sample clogging on the filter and long processing times. Some other strategies have also been suggested, such as multilayer filters (*3D microfilter*)[14] and flexible micro-spring arrays,[23] in order to minimize the mechanical stress on cells. Thus, a compromise between pore size/geometry and operating pressure condition is always needed for any filtration setup.

To our knowledge, there is currently no filtration system designed for CTC capture in which the flow conditions are adapted to operate within the range of the theoretical critical pressure of CTCs. Having this as a premise, here we envision providing, for the first time, experimental evidence of cancer cells capture from blood samples at physiologically relevant flow conditions, meeting abovementioned requirements of critical pressure.

2.1.3 Targeted specifications and design parameters

As introduced at the beginning of this chapter, our main objective is to assess the physical trapping of CTCs directly from the human bloodstream using an engineered device containing an array of micrometric pores. It is worth clearly establishing what is the framework and constraints involved in this development.

The **first constraint** is related to physical dimensions. We aim at performing the *in vivo* CTC capture procedure at the superficial **basilic vein**, one of the most common venipuncture sites in the human forearm. Despite the patient-to-patient variability, Doppler ultrasound measurements of the vascular system have evidenced that the internal diameter of the basilic vein ranges from 2 to 7 mm.[24–26] Given this, we envisioned inserting our device within the basilic vein using either a peripheral venous catheter or a venipuncture needle. As part of the early prototyping step, we preferred the use of venipuncture needles as insertion cannula, as it maintains a constant diameter throughout its length and has a greater mechanical rigidity. Thus, the **overall geometrical dimensions** of the device were constrained by the inner diameter of an **18G hypodermic needle** (860-920 μm).[27] Foreseeing its future application as a potential medical consumable and considering its practical use in clinical routine, we limited the overall dimensions of the device to <500 μm.

Our blood filtering approach does not aim to interrogate the total blood volume circulating through the basilic vein since it would imply the total occlusion of the venous cross-section, and consequently would represent a risk for the patient. However, we do pursue maximizing the amount of blood interrogated by the capture device without having side effects related to blood flow disturbance. Accordingly, the rationale behind the geometric design of the capture device is based on creating a **derivation of the main flow stream**, in which blood filtration and CTC trapping will be carried out.

Based on this premise, we envisaged a 3D tubular geometry**,** **Figure 2.4.** The cylinder is longitudinally aligned along the stream direction where the incoming bloodstream is diverted, creating a confined zone characterized by a **lower velocity.** This secondary flow stream will in turn pass through a **holey membrane** placed at the end-wall of the tubular geometry. Hereinafter, the whole set formed by the tubular geometry and the holey membrane will be referred as the **microdevice**.

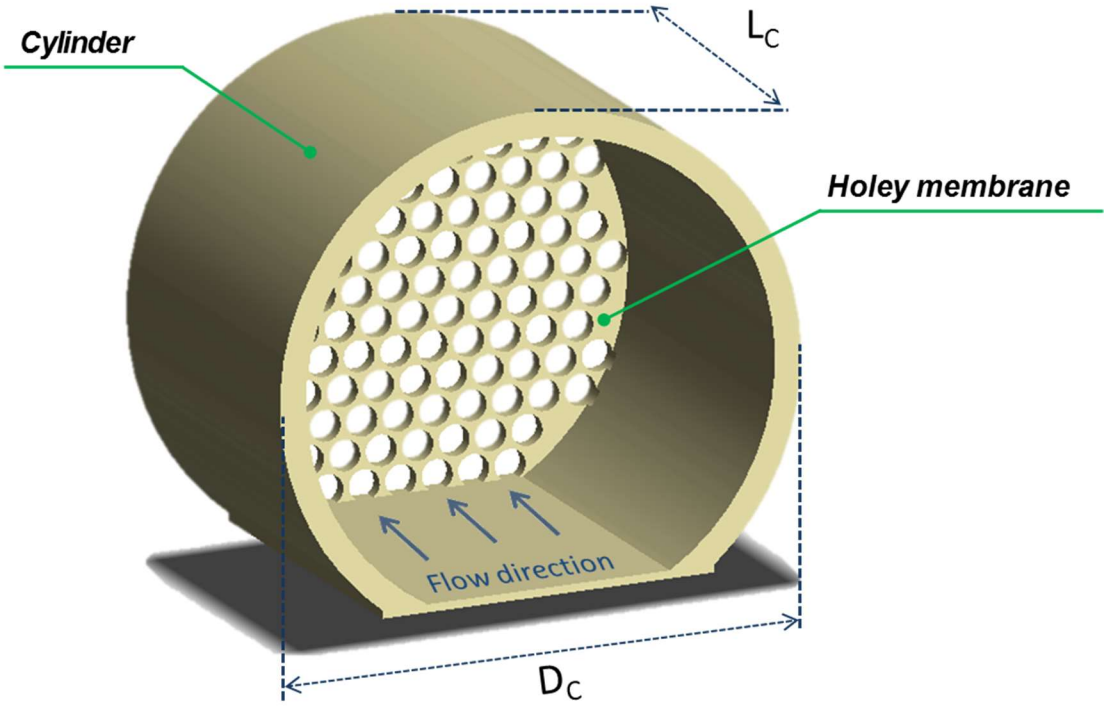

Figure 2.4 The microdevice defined by a cylinder, which creates a derivation of the main flow stream, and the holey membrane, which performs the blood filtration.

We set the diameter of the cylinder $D_C=2r_c$ constitutive of the microdevice as $\boldsymbol{D_C}$**= 200 µm**, foreseeing the use of different hypodermic needles having smaller inner diameters (e.g., 20G or 21G). The length of the cylinder L_C should allow a non-disturbed region within the microdevice so that the velocity profile after the middle length of the cylinder is fully-developed. Based on pipe flow theory, the distance needed to have a fully-developed flow, known as entrance-length, is roughly equal to the pipe radius r_c=100 µm and independent from the flow rate at low Reynolds number (Re≤30).[28] Therefore, L_C must ideally be set higher than the radius of the cylinder, establishing it as $\boldsymbol{L_C}$**= 150 µm**.

The overall hydraulic resistance of the microdevice is defined as the sum of two contributions: the hollow cylinder resistance R_C and the holey membrane resistance R_M, as $R_H=R_C+R_M$. The intrinsic hydraulic resistance of the microdevice is given by $R_H=8\eta/\pi\ (L/\ r_c^4+t/nr_p^4)$, (refer to Appendix A for full description of the formula) from where we inferred that the **holey membrane** contributes the most to the overall resistance of the microdevice, having as **design variables** the number (**n**) and radius ($\mathbf{r_p}$) of pores, as well as the thickness of the holey membrane ($\mathbf{t_m}$).

From those variables, the most important one is the size of the pore. As observed in **Table 2.1**, most of the filters range from 5 to 12 µm, depending on the targeted cancer cell type, sample preparation, and working conditions. At the time this project started, our laboratory had a few cell lines of cancerous

origin from where we decided to use **human prostate cancer cell line (PC3)** which are genetically modified to express green fluorescent protein (GFP). The mean diameter of this cancer cell line usually ranges from 12 to 21 µm. Given this, the pore diameter $d_p=2r_p$ was nominally set to $\boldsymbol{d_p}$**=12 µm** to ensure cancer cell selectivity and reduce at most the contamination with undesirable cell components such as red blood cells and leukocytes mainly.

The total number and geometrical arrangement of micrometric pores constitutive of the holey membrane were optimized to minimize the initial **hydraulic resistance** $\mathbf{R_{H0}}$ and, thus, favour the flow within the microdevice. The **number of pores (n)** was maximized to cover the maximum of the available holey membrane area. An hexagonal geometrical arrangement allows maximizing the number of pores keeping a center-to-center equidistant distance of 14 µm between pores. This arrangement enabled a total of ***n*=137,** thus defining the overall cell capture capacity of the holey membrane.

Other parameters, such as the thicknesses of the cylinder ($\mathbf{t_c}$) and the holey membrane ($\mathbf{t_m}$), were determined by the technique used for the microdevice fabrication in order to define the mechanical properties of the microdevice.

2.2 Proof-of-concept using a rapid prototyping technique

2.2.1 Direct laser writing technique for 3D fabrication of the microdevice

Considering the specific characteristics of our design and the equipment availability in our facilities, we assessed the fabrication feasibility of the microdevice using rapid prototyping techniques. **Direct-laser-writing (DLW)** by two-photon polymerization is a unique technique offering high accuracy three-dimensional (3D) structuring. This additive manufacturing technique allows the 3D microfabrication based on the local polymerization of a photosensitive material through a nonlinear absorption of photons.[29] We used the commercially available equipment Photonic Professional (Nanoscribe® GmbH) at an early stage of this project, and later the updated version **Photonic Professional GT**. Given the optical characteristics of this technology, established by a highly focused and ultra-fast laser (λ=780 nm, 100 fs, 50 mW), it was feasible fabricating micro- and meso-scale 3D structures having sub-micrometer resolution (100-200 nm), which perfectly fitted our needs. This equipment allows layer-by-layer fabrication controlling the position, in x-y-z directions, of the laser beam according to a pattern established by a computer program.

Our tailored 3D microdevices were designed using Computer Aided Design (CAD) software (Autodesk Inventor® 2015) and exported into a compatible format file (stl). The DeScribe® software (Nanoscribe® GmbH) allowed the controlled discretization of the 3D design by layers, *slicing*, and each of these planes by lines, *hatching*. Both, slicing and hatching were set to 200 nm. Other settings such as the laser power and the scan speed are accessible as controllable parameters in order to determine the exposure dose. The negative tone photoresist (**IP-Dip,** Nanoscribe® GmbH) was drop-casted onto the glass substrate (fused silica or ITO-coated) in the dip-in laser lithography (DiLL) configuration. In this configuration, the sample is facing down and the lens of the objective (63x**,** Carl Zeiss, NA= 1.4) dips in the index-matched resist. We performed a set of writing tests in order to determine reasonable thicknesses for both the cylinder and the membrane wall, which enabled obtaining a microdevice with good adherence to the substrate and reasonable mechanical stability. Typically, we swept the laser power from 30 to 80%, where 100% corresponds to 50 mW, and the scan speed from 25 mm s^{-1} to 50 mm s^{-1}. The writing time of each microdevice at early stages of this project was about 32h, later reduced to <10 min when the GT module was acquired by our laboratory.

After polymerization, the microstructures were developed, following the process suggested by the supplier, using SU-8 developer for 20 minutes, isopropyl alcohol rinsing during 2 min, and blow drying with nitrogen gas. Some samples were also dried using a critical point drying process, to avoid surface tension effects, however no significant differences were observed. A typical sweeping test is shown in **Figure 2.5a**, the scanning electron microscope (SEM) inspection evidenced certain writing conditions where the structure is not mechanically stable and the adhesion to the underlying substrate is compromised. In addition, a high exposure dose, **Figure 2.5b**, induce the formation of microbubbles during fabrication resulting in crater-like aberrations. Therefore, the optimal laser power was set to 65% and the scan speed to 50 mm s^{-1}, while slicing and hatching distances were kept to 200 nm. The resulting microdevice exhibited stable mechanical properties and an acceptable adhesion to the substrate, both physical features rendering it adapted to withstand flow conditions.

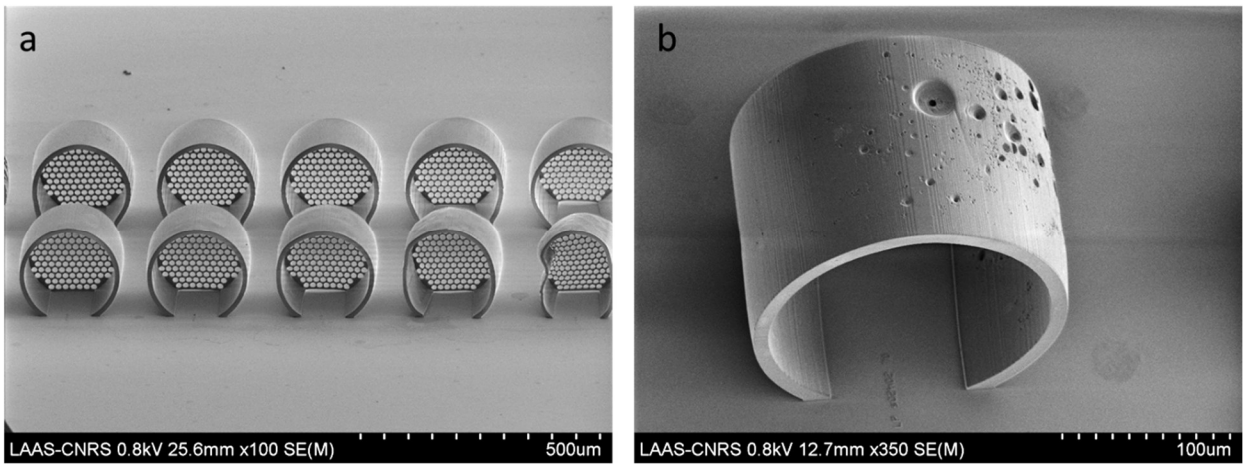

Figure 2.5 Scanning electron micrographs of the writing sets for the optimization of the DLW conditions. **a** From left to right, the laser power varies from 65% to 45%. The front row corresponds to writings jobs using a scan speed of 50 mm s^{-1} while the back one corresponds to 25 mm s^{-1}. **b** At the surface of the cylinder we can observe the effect of overexposure, creating crater-like artifacts. Those artifacts are randomly located, sometimes observed in the holey membrane surface.

Along with exposure-dose optimization, the geometrical variables t_m and t_c were also determined. Finding that for IP-Dip material and established writing conditions, the minimum thickness of the holey membrane is **t_m= 6 µm**. Lower values of t_m mainly induce detachment from the substrate and poor mechanical properties. Under the established thickness and writing conditions, the roundness of the pores is acceptable having a mean (± standard deviation) diameter ***D_p*=11.5±0.08 µm**. Nanogroove patterns of ≈200 nm are observed along the thickness of the pore due to the slicing and hatching parameters set during the fabrication of the microdevice, **Figure 2.6**. The wall thickness of the cylinder was set to **t_c = 10 µm**, as a good compromise between mechanical stability and total writing time, since it mainly defines the bulk body of the microdevice.

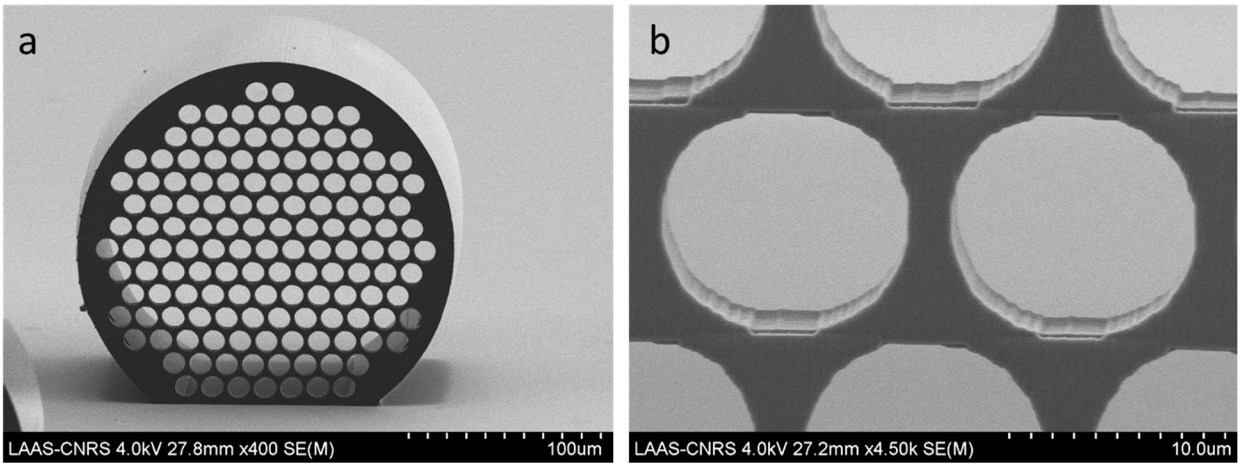

Figure 2.6 Scanning electron micrographs of the holey membrane. **a** Rear view of the microdevice composed of 137 pores. **b** Magnification of the pores area evidencing the nanogrooves resulting from hatching and slicing.

2.2.2 Validation of cell capture using a microdevice-integrated fluidic platform

2.2.2.1 Fabrication of the fluidic platform

Firstly, we aimed at validating our design under flow conditions similar to those found in the human veins. We conceived the fabrication of a fluidic platform in which the geometric and flow conditions replicate those found in the **basilic vein** of the human forearm. The reported **mean velocity** ranges from a minimum value of 0.072 ± 0.007 ms^{-1} to a maximum of 0.24 ± 0.027 ms^{-1}.[26] In addition, the **mean pressure** is reported to be of about 10mmHg which is equivalent to 1333.22 Pa.[30,31] This fluidic bench was conceived to allow **controlled experimental conditions**, **real-time observation** of the capture events, and **in situ microscopy characterization**.

In principle, this platform must have had similar dimensions as the basilic vein, circular cross-section and a diameter ranging from 2 to 7 mm. However, these characteristics represented a major challenge from a technical standpoint, particularly because real-time optical observations were needed to confirm cell capture. Thus, the fluidic platform was adapted to the molding techniques available in our laboratory, setting it to have overall dimensions of **1 mm-tall** channel with a **square section**, and a total length of **12 mm**. Under these conditions, the pumping system was adapted to fulfill the requirements of velocity magnitude. It is worth noting that a change in the cross-section geometry, from circular to square, and a scaling-down of the channel cross-section, is expected to impact the shape of the velocity profile only, which does not play a significant role here.

From fluid mechanics theory, it is known there is an inherent **near-zero velocity** at the wall surfaces of the channel and the **maximum of the velocity profile** is located at the center of the channel cross-section. We hypothesized that placing the device near the region where the maximum of the velocity profile is, would improve cell capture efficiency. In order to achieve this, we proposed the use of a lift-base which may place the microdevice in the middle of the channel cross-section.

In order to fabricate the fluidic platform, the lift-base was first patterned using SU-8 photoresist with 300x300 µm in lateral dimensions and ~350 µm in height. The **SU-8 pillar** was fabricated in conventional 25x25 mm glass substrates, compatible with the standard DLW process. This customized glass-pillar substrate was subsequently used for the fabrication of the microdevice onto the pre-fabricated SU-8 pillar. The fabrication parameters and protocol were carried out as explained in section 2.2.1, considering a proper positioning of the laser onto the pillar, for which the mechanical stage and visualization through the camera were used. The inlet of the microdevices was preferentially aligned with the upstream edge of the pillar. Note that, the DLW system was able to automatically recognize the interface formed by the SU-8 pillar and the IP-Dip photoresist, which ensured the right positioning in the z-axis. Right after development and drying, the microdevices were inspected both optically and by SEM, **Figure 2.7a**, since occasionally a weak adhesion was found at the bottom of the holey membrane region.

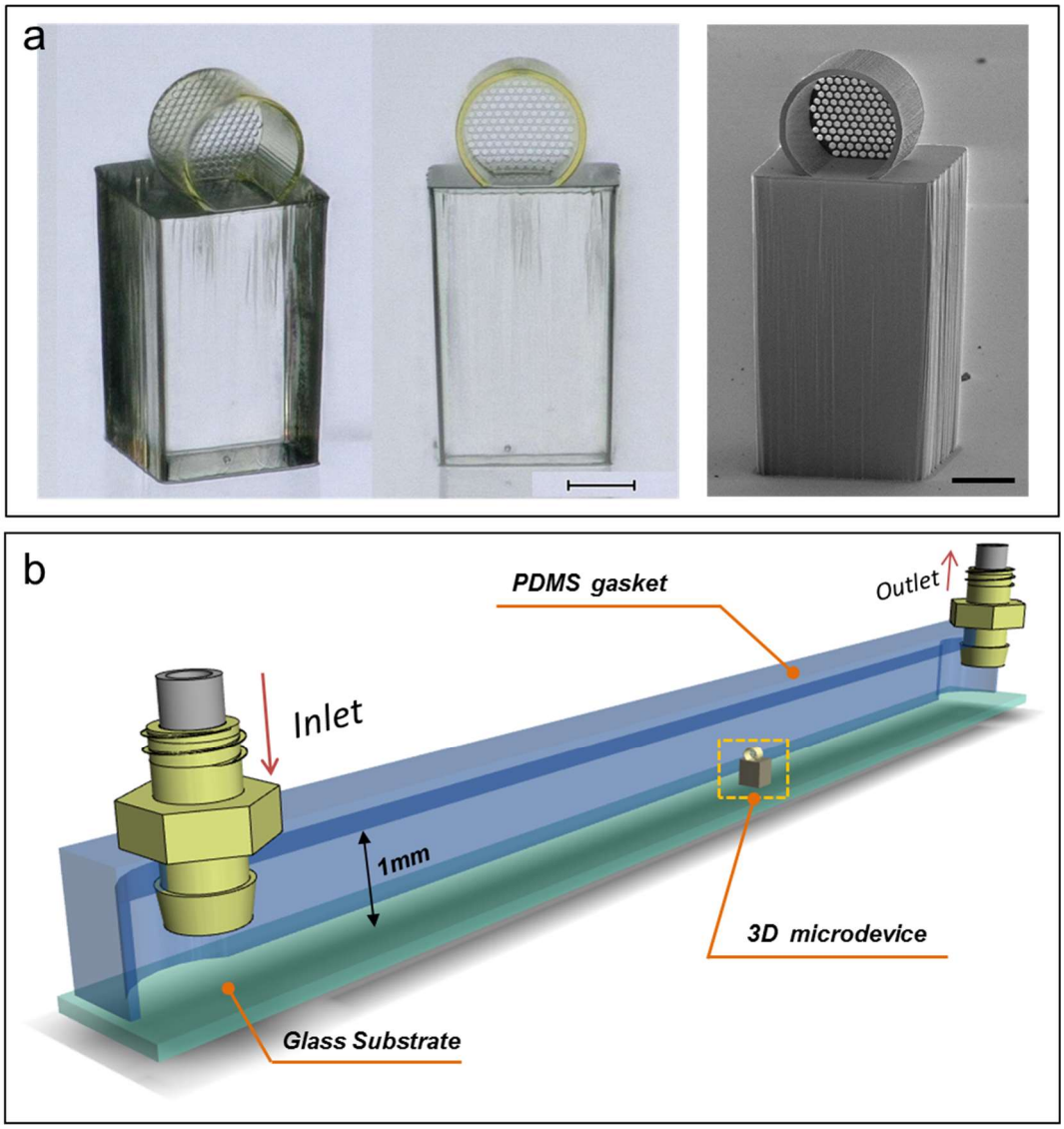

Figure 2.7 Customized test-bench integrating the 3D microdevice. **a** Optical and SEM images of the 3D microdevice onto a SU-8 pillar. Scale bars correspond to 100 µm. **b** Schematic representation of the fluidic platform.

Independently, the fluidic channel gasket made of PDMS was molded (10:1 w/w ratio, 1 hour at 100°C). This PDMS gasket was then punched to form the inlet and outlet of the fluidic circuit. Finally, the whole assembly consisting of glass, SU-8 pillar, and microdevice was bonded to the PDMS gasket using plasma treatment (air plasma, 50W, 0.5 mbar, 5 min). The alignment of both parts was manually performed being careful to place the microdevice at the center position with respect to the longitudinal axis of the channel, **Figure 2.7b**.

2.2.2.2 Fluid dynamics within the fluidic platform

Before evaluating the capture capabilities of the proposed design under real flow conditions, an *in silico* evaluation was carried out with the objective of predicting the flow field and dynamics, within and around the 3D microdevice. Steady-state fluid dynamic simulations were performed using ANSYS Fluent (ANSYS Fluent® v15). The fluidic platform was simplified and represented by a computational domain of 5 mm in length, **Figure 2.8a**. At first, the fluid was modeled **as water** (ρ=997.13 kg m^{-3}, μ=0.000891 kg m^{-1} s^{-1}), the pressure at the inlet boundary set to P=1333.33 Pa, and the reference velocities, v_{min}=0.072 m s^{-1} and v_{max}=0.275 m s^{-1}, were targeted. A non-uniform mesh of the model was generated (ANSYS Meshing) with a refined resolution in the microdevice region to ensure significant data.

From simulations, we first observed that the proposed test-bench would allow a velocity field having a **fully developed parabolic profile**, as expected in real experimental conditions. Given the range of velocities, the flow behaves as laminar along the channel where the centerline velocity, hereinafter named freestream velocity $\boldsymbol{v_{freestream}}$, has a magnitude roughly twice the targeted mean one. For example, for a targeted mean velocity within the channel of v_{min}=0.072 m s^{-1}, we obtained a $v_{freestream}$=0.134 m s^{-1}, **Figure 2.8c1**. Generally speaking, the whole set formed by the microdevice and pillar modifies, upstream and downstream, the flow field. Taking as a reference the position of this set, upstream, the velocity field is disturbed at a distance 3-fold the length L_c of the microdevice ($L_{upstream}$) approximately. The initial profile is recovered at 12 to 15-fold the same characteristic distance ($L_{downstream}$).

The microdevice-pillar set can be considered as a surface-mounted 'bluff body', **non-streamlined shape**, which in the fluid dynamics field is characterized to divert the flow, and as a result of its shape and specific flow conditions, could induce a phenomenon known as 'flow separation'. This phenomenon is related to the inability of the streamlines to follow the geometric shape of the obstacle, so the flow becomes detached from the obstacle's surface and potentially creates downstream vortices (vortex-shedding), **Figure 2.8b**. Following this idea, at the simulations level **we did not observe vortex-shedding** at any position downstream the microdevice **in the range of velocities of interest**. The flow permeability of the holey membrane seems to be closely implicated in the reduction of these undesired effects.[32] However, further investigation is still required.

We expected the 3D microdevice would promote a redistribution of the flow, and a portion of it would pass through. The numerical model confirmed this assumption and evidenced that the velocity distribution within the microdevice is not uniform. Roughly, velocity magnitude tends to be higher at the half bottom, **Figure 2.8c2**. Along the length of the cylinder L_C=150 µm, first the velocity at the inlet L0 has its minimum value and then increases up to its maximum value at a distance L1=L_C/2, **Figure 2.8c3** and **Figure 2.8c4**. Thus, the overall velocity within the microdevice ranges from 10 mm s^{-1} to 60 mm s^{-1}, when v_{min}=0.072 m s^{-1}, and from 100 mm s^{-1} to 180 mm s^{-1} when v_{max}=0.275 m s^{-1} (data not shown).

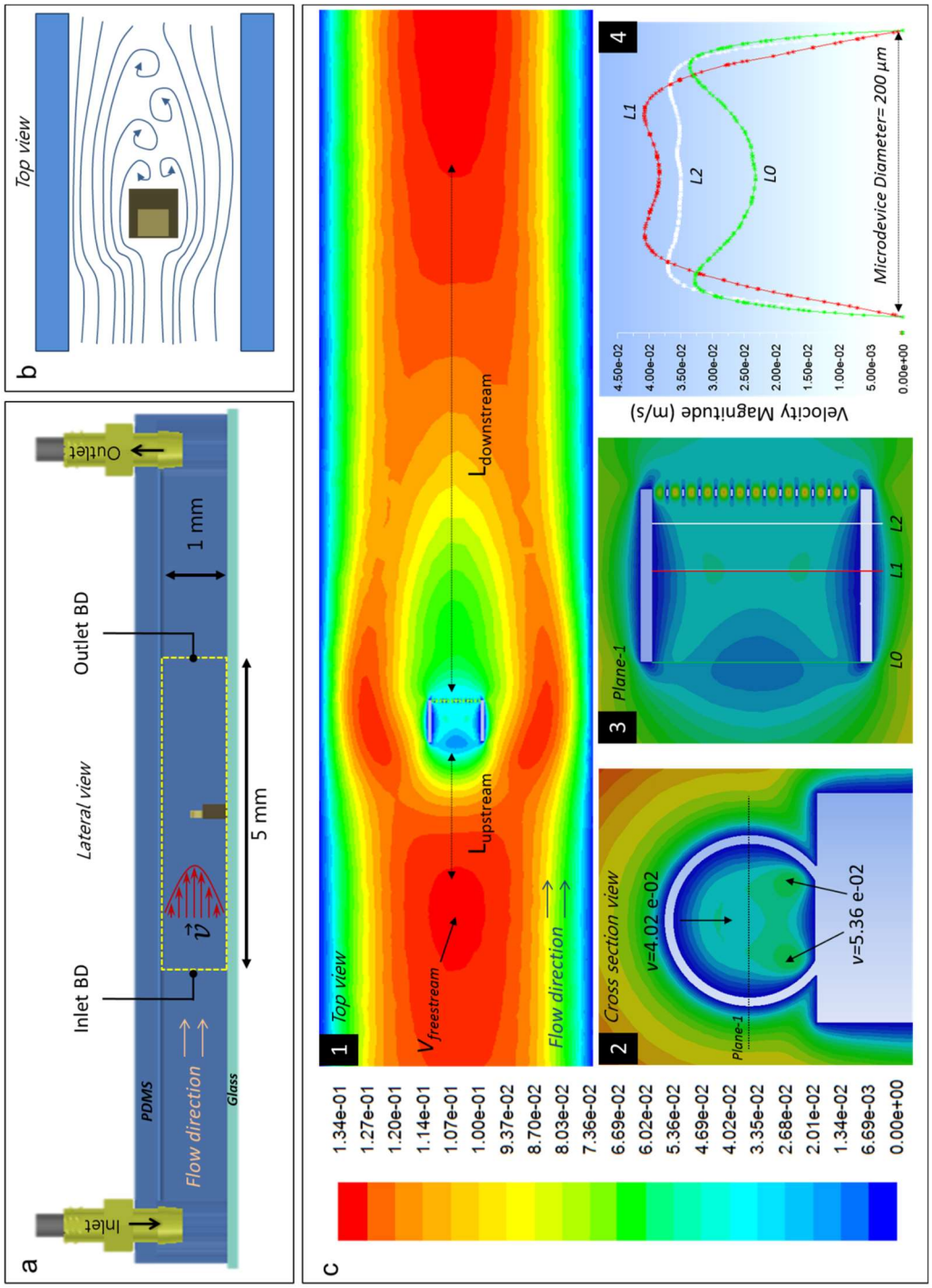

Figure 2.8 Fluid-dynamics within the fluidic platform. **a** Computation domain representing the fluidic platform. The inlet and outlet boundaries (BD) where set at a distance ~2.5 mm from the microdevice. **b** Schematic representation of vortex-shedding. **c** Velocity distribution along the channel and within the microdevice. Images (1-3) show the contours of velocity magnitude where the colormap is in m s^{-1}. Image (4) shows the velocity profile at three positons along the length of the cylinder and at the middle plane position, plane-1.

Additionally, we estimated the total volume of liquid passing through the microdevice per unit of time, (**effective flow rate Q_{eff}**). The numerical model reveals that Q_{eff} ranges from 45 to 145 µl per min at v_{min} and v_{max} respectively, (blue plot of **Figure 2.9**), when the liquid is modelled as water. In addition we also evaluated a blood-like liquid in which we considered a constant viscosity approximately 4-fold the one of water (Newtonian model, ρ=1060.0 kg m^{-3}, μ=0.004 kg m^{-1} s^{-1}). Using these conditions, we observed an increased flow rate within the same rate of velocities, (red plot of **Figure 2.9**), which is probably related to a lower Reynolds number resulting in a faster development of the velocity profile within the microdevice.

We also analyzed the pressure distribution within the microdevice, **Figure 2.10**, at v_{min} and v_{max}. The magnitude of the total pressure, the sum of static and dynamic pressures, gradually increases along L_C, and reaches its maximum value at the inner surface of the holey membrane L_S. This behavior was observed independently from the nature of the simulated liquid. The combined contribution of the pressure near L_S and the one at the rear of the holey membrane L_C defines the **pressure difference across the filter ΔP**. The value of ΔP ranges from 40 to 200 Pa when water is considered and from 200 to 700 Pa in the case of blood, **Figure 2.10b-c**.

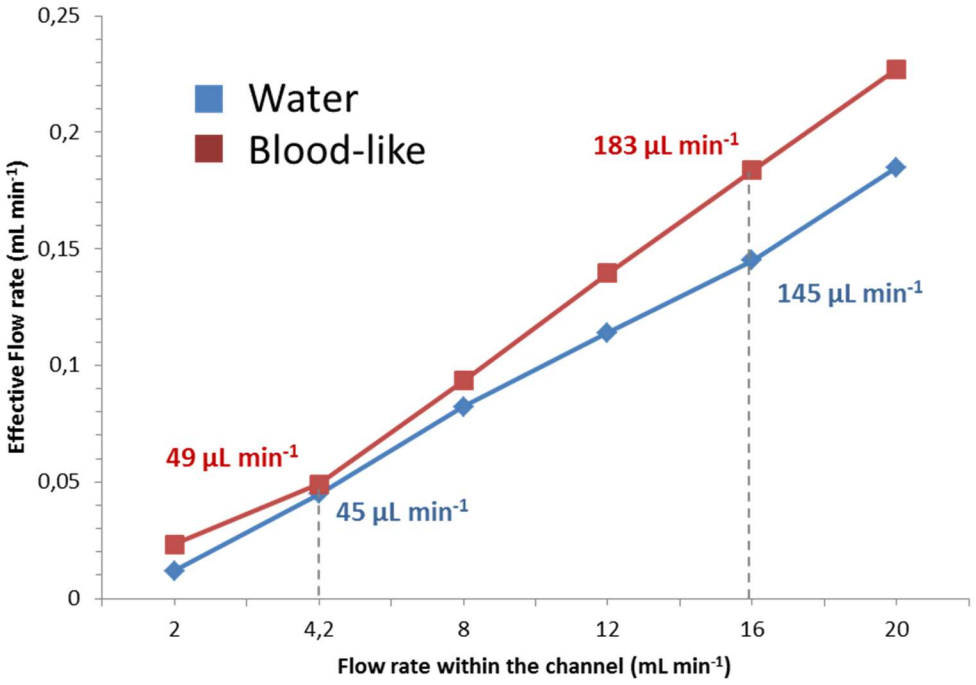

Figure 2.9 Estimation of the effective flow rate Q_{eff} passing through the microdevice. The plot shows Q_{eff} as a function of the flow rate within the 1-mm channel. The velocities v_{min} and v_{max} are represented by their equivalent flow rate within the channel, 4.2 and 16 mL per min respectively.

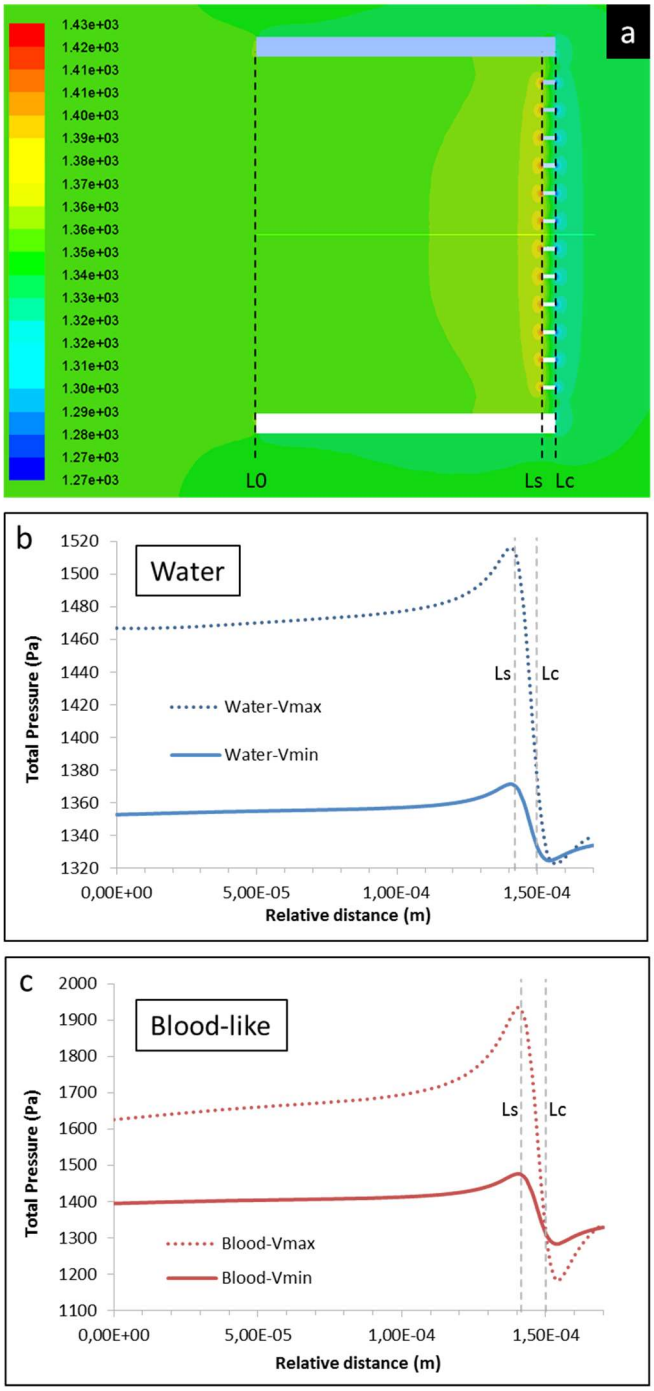

Figure 2.10 Pressure distribution within the microdevice. **a** Representative image of the pressure distribution within the microdevice at v_{min} and liquid considered as water, colormap in Pa. The position L0 represents the inlet of the microdevice, and L_S and L_C the inner and outer surfaces of the holey membrane respectively. **b** Plots representing the total pressure along the microdevice and considering water as fluid. **c** Plots representing the total pressure along the microdevice and considering blood as fluid. Dashed vertical lines represent the positions L_S and L_C, and the difference of pressure at these intersection points defines ΔP.

2.2.2.3 Cell capture using the microdevice-integrated fluidic platform

The capture capabilities of the 3D microdevice in flow were analyzed in the above described fluidic platform adapted to an external peristaltic pumping system. In order to observe the capture events, we needed an optically transparent fluid, so we used cell culture medium as a model liquid. We first prepared controlled suspensions of human prostate cancer cell line (**PC3**), genetically-modified to express green fluorescent protein **(GFP)**. During fluidic experiments, 3D polymeric microdevices were **monitored** through the SU-8 pillar by live inverted fluorescence microscopy (Olympus IX71, LCPlanarFI 20X), **Figure 2.11a**, and image sequences were recorded (EMCCD camera, Andor Ixon +, exposure time: 50 ms, read-out time: 38.19 ms). Due to the auto-fluorescence of photoresist constitutive of the microdevice (IP-Dip: λexc = 405 nm, λem= 478 nm),[33] the GFP emission of PC3 cells (λexc = 475 nm, λem = 504 nm) could not be clearly discriminated, **Figure 2.11b2**. Thus, we required an **adapted labeling** of the cancer cells, for what we used the far-red fluorescent DNA staining **DRAQ5** (λexc = 646 nm, λem= 681 nm), which could be easily identified from the fluorescent background emitted by the microdevice.

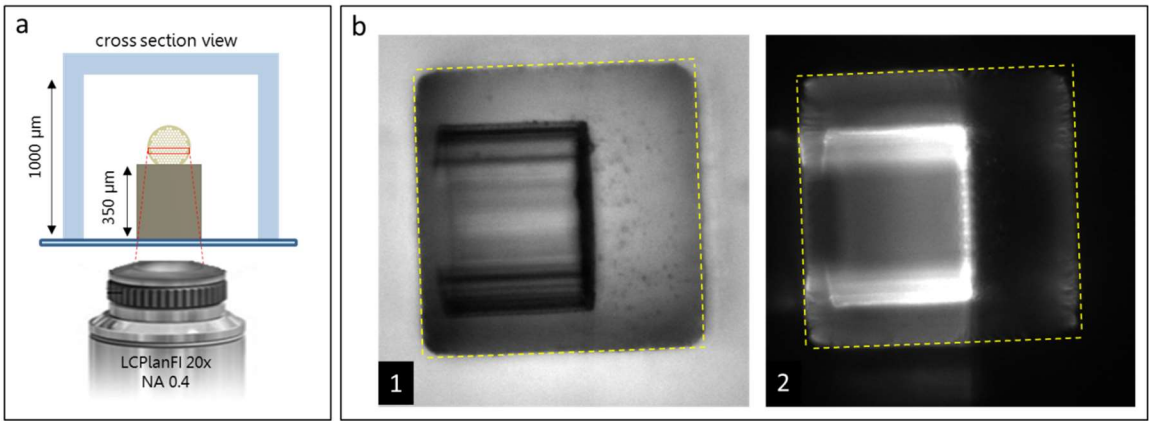

Figure 2.11 Configuration used for real-time monitoring of the capture events. **a** Schematic representation of the configuration, the observation was performed through the SU-8 pillar. The focus point of the objective was placed approximately at the middle of the microdevice, depicted by the red area. The thickness of the glass substrate is 700 µm and is not represented in the scheme. Drawings are not to scale. **b** Representative images of the microdevice onto the pillar, (1) bright field and (2) GFP-emission range, when observed through the SU-8 pillar. Dashed lines highlight edges of the pillar (approximately 300x300 µm), where the inlet of the microdevice is observed near the left edge.

In order to remove air bubbles from the channel and avoid them forming within the capture microdevice, the fluidic platform **was rinsed in reverse flow** to avoid unwanted debris trapping, with 30 mL of ethanol followed by 30 mL of RPMI-1640 cell culture medium. The cell culture medium was kept in the fluidic circuit, in static conditions, and the absence of air bubbles inside the PDMS channel and the 3D microdevice was verified using an optical microscope. The pumping system (FH100®, Thermo Scientific) was set to reach either v_{min} or v_{max} through the channel adjusting the rotation speed at **10 rpm** and **40 rpm** respectively.

Prior to fluidic experimentation, cells were labelled with the abovementioned nucleic acid marker DRAQ5™ (BioStatus Limited®, 0.5%v, 3min incubation at 37°C) before detachment from the cell culture flask. Stained cells were manually counted with a counting chamber and serial dilutions were performed to obtain the targeted cell concentrations. Cell suspensions were prepared in volumes of 10 mL. The mean diameter of PC3 cells was measured using an automated cell counter (Scepter™, Merk Millipore) and it was found to range from **12 to 21 µm**.

Suspensions containing PC3 cells were flowed through the channel and the first 2 to 3 mL were discarded, in order to remove the culture medium not containing cells previously introduced. Afterwards, the suspensions were flowed in a closed-loop configuration where inlet and outlet tubing were placed in the same container. Suspensions were manually agitated before and during the experiments to avoid cell sedimentation. After cell flowing, a rinsing step was performed with 30 mL of RPMI-1640 cell culture medium and then, captured cells were fixed using formaldehyde at 4% (Formalin solution, neutral buffered, 10%, SIGMA-ALDRICH®). A final rinsing step with phosphate buffered saline (PBS 1X) was performed and samples were kept in PBS solution for further characterization.

2.2.2.4 Assessing fouling of the holey membrane

As established in section 2.1.2, one of the associated issues of dead-end filtration systems is **clogging**. Following the principle of dead-end filtration, the progressive obstruction of pores, as cells are captured, is expected, resulting in a decline of the effective flow passing through the microdevice over time and ultimate clogging of the holey membrane. This limiting mechanism was evaluated in order to **estimate a reasonable timespan** which would allow capture of CTCs without reaching clogging stage. For this, highly concentrated suspensions were used, containing **25000 cells mL^{-1}** and **1000 cells mL^{-1}**.

We analyzed the recorded sequence of images in order to account for the capture events. From these images we observed the intrinsic **pulsation** induced by the peristaltic pump at early stages of trapping. Cells arriving at the holey membrane temporarily oscillated backward and forward in a range minor to 30 µm. This transitory pulsation phenomenon diminished as cells were captured. Nevertheless, we did not observe backflow of cells due to pulsations, thus, all cells arriving at the region near the holey membrane stayed trapped. **Figure 2.12** shows the cumulative capture events $\mathbf{C_C}$ as a function of time **t**.

When a highly concentrated suspension was flowed (25000 cells mL^{-1}), at both v_{min}=0.072 m s^{-1} and v_{max}=0.275 m s^{-1}, a significant decrease in the capture rate Cc/Δt, being captured cells over unit of time, was observed at 30-40% of the overall holey membrane capacity (n_p=137), blue plots of **Figure 2.12a**. This trait was observed at **t ≈ 8** min and t ≈ 2 min for velocity = $\mathbf{v_{min}}$ and velocity = v_{max} respectively. For both, v_{min} and v_{max}, it seems that the saturation plateau was reached at similar captured-cell range, Cc=60-80 approximately. These observations suggest that the capture performance of the 3D microdevice is **diminished at approximately 60%** of its potential cell capture capacity. However, it does not mean that capture will be null after this threshold but rather the cell capture will be less frequent. When we analyzed the data from a suspension at 1000 cells mL^{-1}, the cell capture dynamics followed a similar trend as the one at 25000 cells mL^{-1}, plotted in orange color in **Figure 2.12a**. However, the afore observed saturation plateau was not reached after 10 min, at any of the two velocities tested.

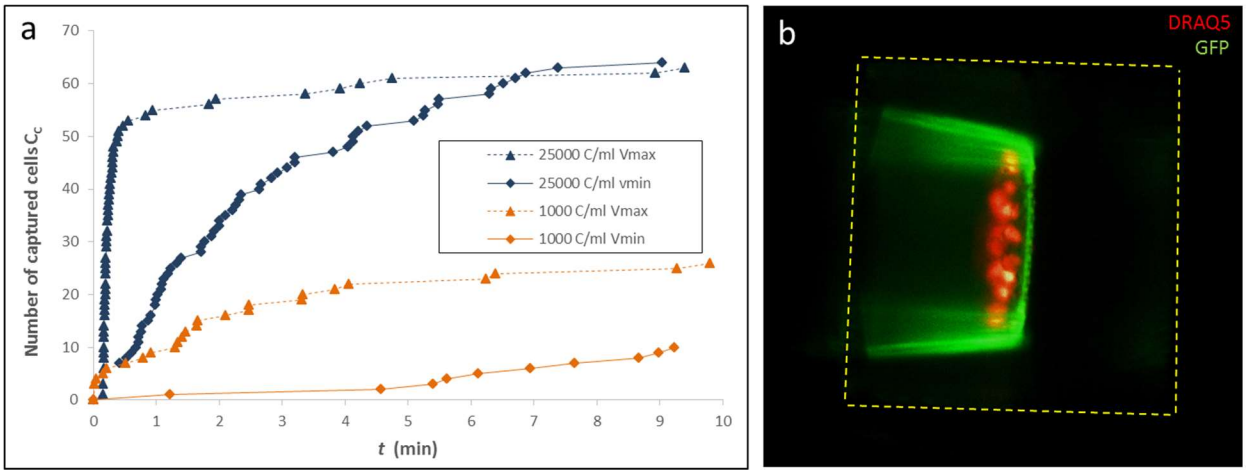

Figure 2.12 Cell capture dynamics using the 3D microdevice. **a** Suspensions containing either 25000 cells mL^{-1} (blue) or 1000 cells mL^{-1} (orange) in cell culture medium were flowed at v_{min}=0.072 m s^{-1} and v_{max}=0.275 m s^{-1}. **b** Overlay of GFP (green) and DRAQ5 (red) expression after cell capture, for the suspension of 25000 cells mL^{-1}. Trapped cells stay adhered to the surface of the holey membrane. Dashed lines highlight edges of the pillar (approximately 300x300 µm).

These results taken together, we theorize that the fluid velocity within the channel is directly proportional to the number of cells captured, so higher speeds increase the likelihood of cell capture. However, considering that, in practice, venous flow velocity is not a controllable variable, the *in vitro* **assessment of the capture performance must be at v_{min}**, being the less favorable trapping condition. As a consequence, a longer exposure of the 3D microdevice to the flow could be required. We suggested that an acceptable time span of **10 minutes** would achieve cell capture at a relatively low-concentration range avoiding both saturation of the holey membrane and overexposure of the microdevice to the flow. Thus, to meet future medical applications hereinafter, the duration of all of our fluidic experiments was restricted to 10 min and the mean velocity within the channel to v_{min}=0.072 m s^{-1}, unless otherwise noted.

It is worth noting that, at the time of capture, cells seem to remain at the surface of the holey membrane and not within the pores, **Figure 2.12b**. In addition, at the end of the fluidic experiments and before cell fixation, trapped cells also seem **strongly adherent** to the holey membrane surface. They were not usually detached by either direct or reversed flow rate. We believe this is related to two factors, one being that cells have the capacity to adhere, and second cells have a long enough time span to adhere.

We further inspected these samples by **confocal fluorescence microscopy** (Upright Leica SP8). Confocal characterization did not represent a simple task, since accessing the holey membrane containing the trapped cells required a non-conventional placement of the sample at an acceptable distance from the

objective. After trying various configurations, the most convenient strategy consisted in making a cut mark at the back of the glass substrate so that, at the end of the experimentation and cell fixation, the fluidic channel could be split at a distance of approximately 2 mm from the microdevice. This cross-sectional splitting of the channel allowed positioning it in a vertical configuration where the whole area of the holey membrane was readily accessible. The microdevice was usually kept in PBS solution and conventional mounting media was placed onto it. The use of a 25x immersion objective showed the best results in terms of spatial resolution. Signal in the GFP spectral range (λexc=475 nm, λem=504 nm) was acquired for microdevice imaging, and DRAQ5 range (λexc=646 nm, λem=681 nm) for trapped cells.

The inspection of the holey membrane revealed that cells are uniformly distributed all over the surface and cells blocking the pores are the cause of the observed decrease in permeability, **Figure 2.13a-c**. We also confirmed that most of trapped cells remain at the surface of the holey membrane and only a few of them within the pores, as evidenced by the 3D confocal inspection **Figure 2.13d**. Moreover, cells seem to preserve their rounded shape, even at v_{max}=0.275 m s^{-1} flow condition. Less often, some cells stacked on top of others, as the one pointed by the arrow in **Figure 2.13**. These observations suggest that trapping conditions, velocity magnitude and transmembrane pressure, are gentle enough to preserve cell integrity.

Additionally, the visual access to the whole holey membrane surface using confocal microscopy allowed direct cell counting. We observed a discrepancy in PC3 counts between capture events accounted by video microscopy tracking and confocal characterization. The real number of trapped cells is higher by confocal counting than the accounted by video microscopy. We believe this difference arises from the inability of the microscope to account for all capture events due to the limited depth of field of the objective. Thus, just a thin region from the whole microdevice is monitored. From this experimental data, we concluded that the holey membrane permeability is significantly diminished when the number of trapped cells reaches a range **C_C=90-100 over the total number n_p=137 of potential capture events**.

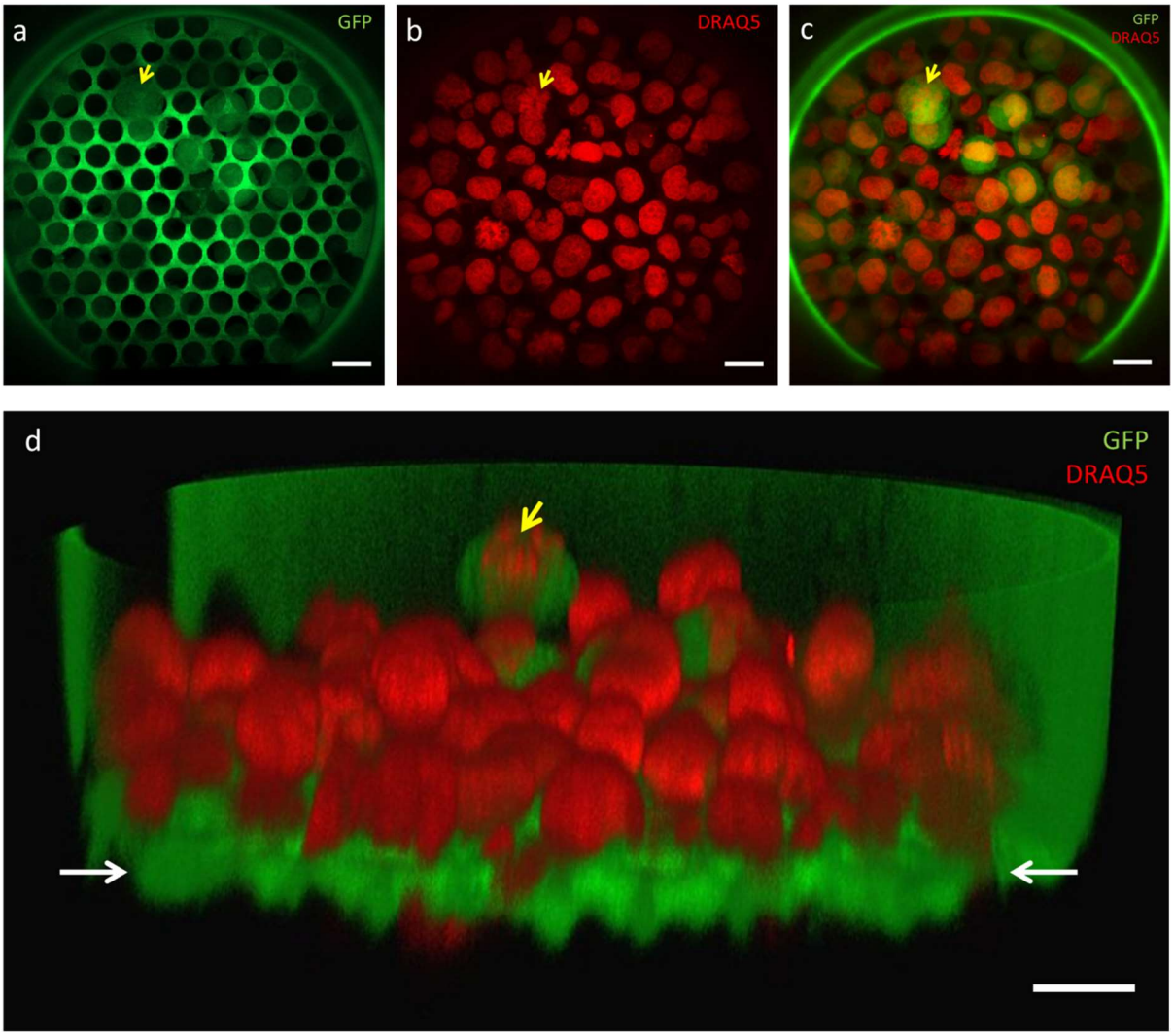

Figure 2.13 Confocal images of a representative sample processed at v_{max}=0.275 m s^{-1} at a concentration of 25000 cells per mL. **a-c** Front view images of the holey membrane. The intense auto-fluorescence of the microdevice inhibits the visualization of the GFP emission of PC3 cells as evidenced in (a). However, DRAQ5 emission from the cell nuclei was clearly identified (b). Image (c) shows the overlay of the two emissions and a total of C_C=103 cells were identified. **d** Lateral view of the 3D confocal reconstruction. The scanned section corresponds to ~70 µm out of a total of L_C=150 µm. From the bottom to the top, first, we observe the holey membrane indicated between white arrows, and right onto it the nucleus of the trapped cells. The yellow arrow points to one of the few cells stacked in onto another one. Scale bars are 20 µm.

2.2.2.5 Hydrodynamic effects due to fouling of the holey membrane

We numerically evaluated possible hydrodynamic effects within the microdevice due to fouling of the holey membrane. We represented the trapping process by the direct obstruction of pores of the holey membrane upon different possible scenarios. Accordingly, we observed the flow patterns within the microdevice and computed Q_{eff}. This analysis was just applied for a fluid modeled as water and at v_{min}.

The result is summarized in **Figure 2.14a**, evidencing a gradual decrease of Q_{eff} as the number of blocked pores is increased, and drop down to 50% when 80/137 pores were blocked, trace highlighted in red color. Interestingly, at this condition we clearly observed the formation of a stagnation-like region near the inlet of the microdevice and velocity vectors displayed a pattern similar to symmetrical vortices, **Figure 2.14b2**. This phenomenon is weakly observed starting from 60/137 blocked pores, trace highlighted in orange color. We believe this behavior is the result of the combined effect of an adverse pressure gradient and a low local velocity magnitude.

We theorize that these hydrodynamic effects observed in the numerical models are closely associated with the diminished capture rate observed in fluidic experiments, **Figure 2.12a**. Our experimental data suggest that the saturation plateau occurs at C_C=90-100, while simulations evidence a significant drop in Qeff and a stagnation-like region when >80 pores are blocked. The difference between the experimental data and the theoretical model could be explained by pulsations induced by the peristaltic pump, since mechanical oscillations have shown to improve the performance of microfiltration.[34,35]

Additionally, we consider that the symmetrical-vortices pattern, as evidenced by velocity vectors, do not induce any backflow of the trapped cells. This is reinforced by our experimental evidence, where we did not observe the detachment and backflow of any trapped cells. However, it is not discarded that this stagnation-like region could induce flow instabilities.

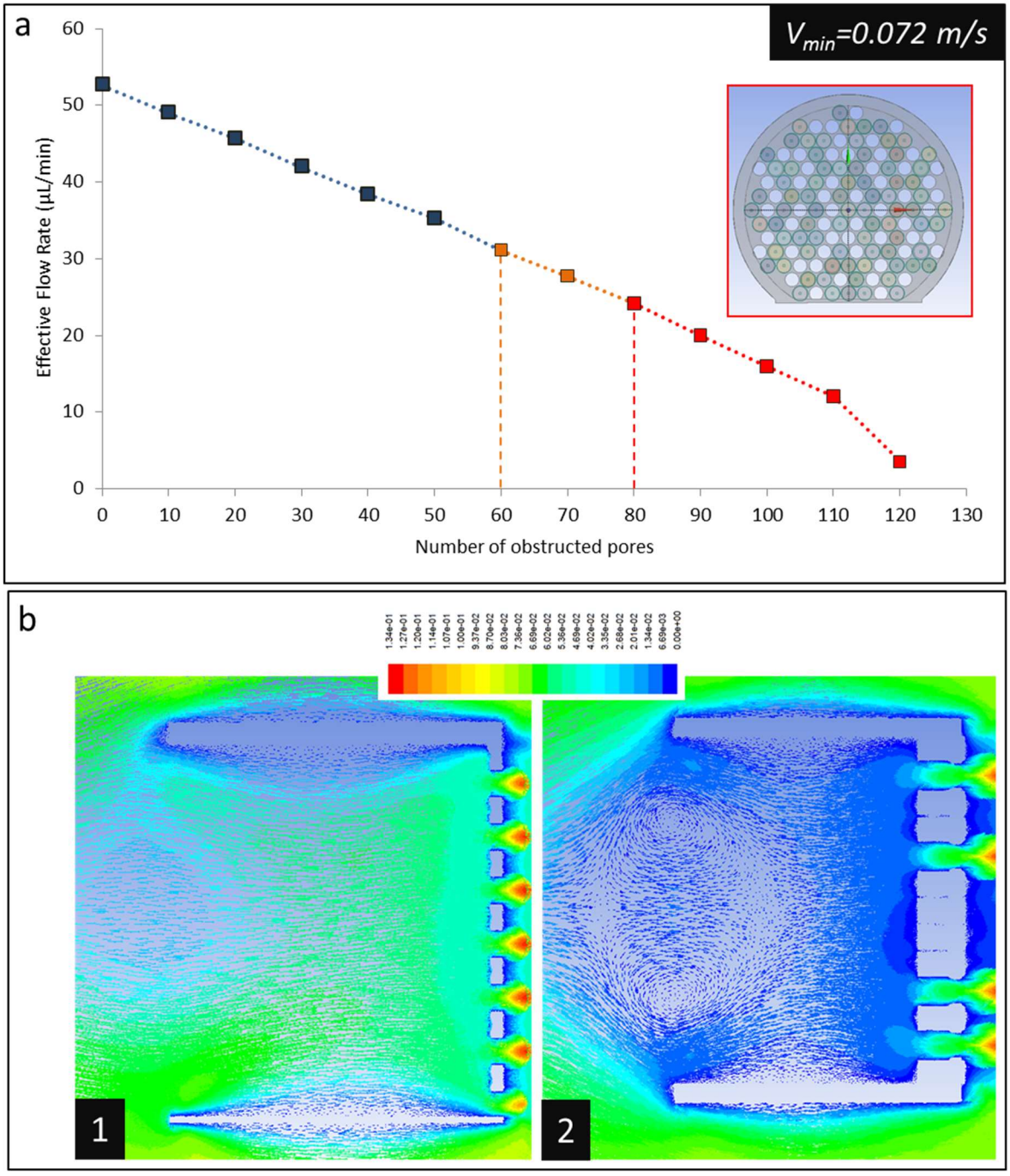

Figure 2.14 The impact of pore-blocking in flow dynamics. **a** Plot of Qeff as function of the number of pores blocked. The velocity within the channel is v_{min} and the fluid model is water. The insert depicts the geometrical model when 80 pores are obstructed corresponding to the condition where we observe a symmetrical-vortices pattern. **b** Velocity vectors in the confined area within the microdevice. Image (1) corresponds to the velocity vectors at zero obstructed pores, while image (2) corresponds to a total of 80. In image (1) all vectors point towards the holey membrane and in image (2) a symmetrical-vortices pattern is evidenced, colormap is in m s^{-1}.

2.2.2.6 Assessing changes in cell morphology due to velocity magnitude

As mentioned in section 2.2.2.4, we observed that the morphology of trapped cells was preserved during the trapping process. We evaluated whether changes in the velocity magnitude could have an impact on the morphology of trapped cells. We processed 40 mL of a suspension at 5000 cells mL^{-1}, at both v_{min}=0.072 m s^{-1} and v_{max}=0.275 m s^{-1}. Similarly to abovementioned samples, cells were fixed at the end of the trapping process and afterward dehydrated using successive baths of ethanol dilutions in PBS 1X (25% to 100% v/v) for SEM imaging (Hitachi S-4800, 10 nm gold-sputtering).

SEM characterization exhibited that most of the captured cells maintain a spherical shape and remain adherent to the surface of the holey membrane at both tested velocity conditions, **Figure 2.15**. A more rounded morphology was observed at v_{min} which is possibly associated with the lower pressure differential across the filter ΔP, **Figure 2.15a**. Some particular flattened-shape cells were rarely identified, pointed with yellow arrows in **Figure 2.15b**, which could be an artifact resulting from the dehydration step. In addition, we observed a smaller size and shifted-position when compared to confocal images, which is also associated with the dehydration step.

Electron micrographs evidenced cell pseudopod protrusions, which confirmed the strong adhesion of cells to the underlying resist. We think these protrusions resulted from the favorable hydrodynamic conditions within the microdevice and by the intrinsic nano-roughened surface of the holey membrane, 200 nm, as suggested by some authors.[36–38] These findings suggest that the capture process does not affect the cell viability after capture.

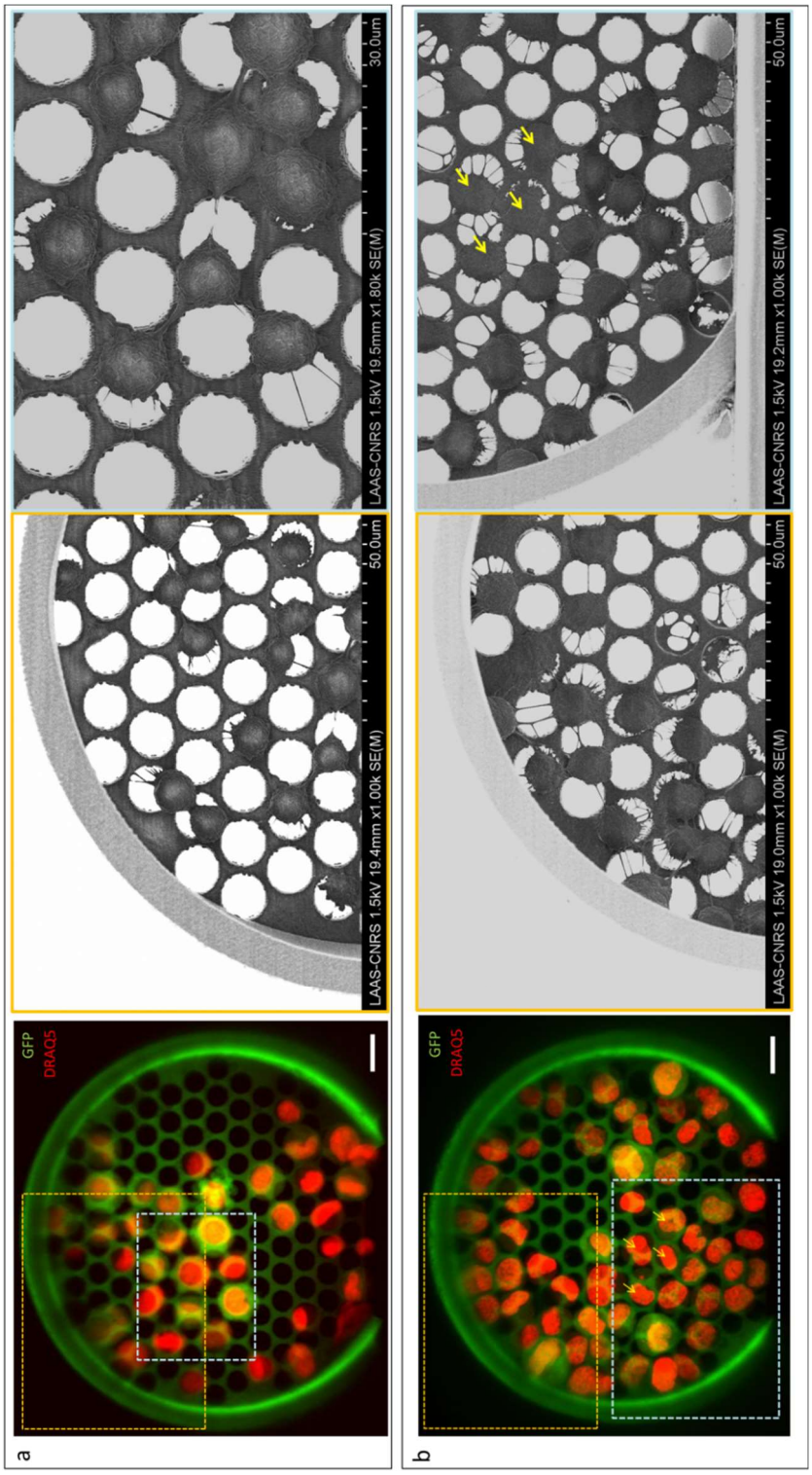

Figure 2.15 Direct identification of trapped cells by confocal imaging and SEM. **a** Confocal image and corresponding electron micrographs of selected areas of sample processed at v_{min}. **b** Sample processed at v_{max}. Scale bars are 20 µm.

2.2.2.7 Assessing cell viability of captured cells

As suggested by morphological imaging, trapped cells seem to preserve their integrity and viability. To verify this hypothesis we proceeded to the culturing of the trapped cells. After cell trapping, we introduced a 500 µL of trypsin, within the fluidic channel, in order to promote the detachment of cells from the holey membrane, and then cells were recovered by reverse flow. The collected volume was divided among three different wells of a 96-well plate, and monitored for two weeks.

We observed the proliferation of cells, starting from <10 cell per well until reaching confluence, with a duplication rate of 44h. **Figure 2.13** shows representative images of the cultured cells at different time points. This result suggests that captured cells are representative in terms of phenotypic and genotypic characteristics of the initial population of cells, and opens up the possibility of molecular and phenotypic analysis of the trapped cells.

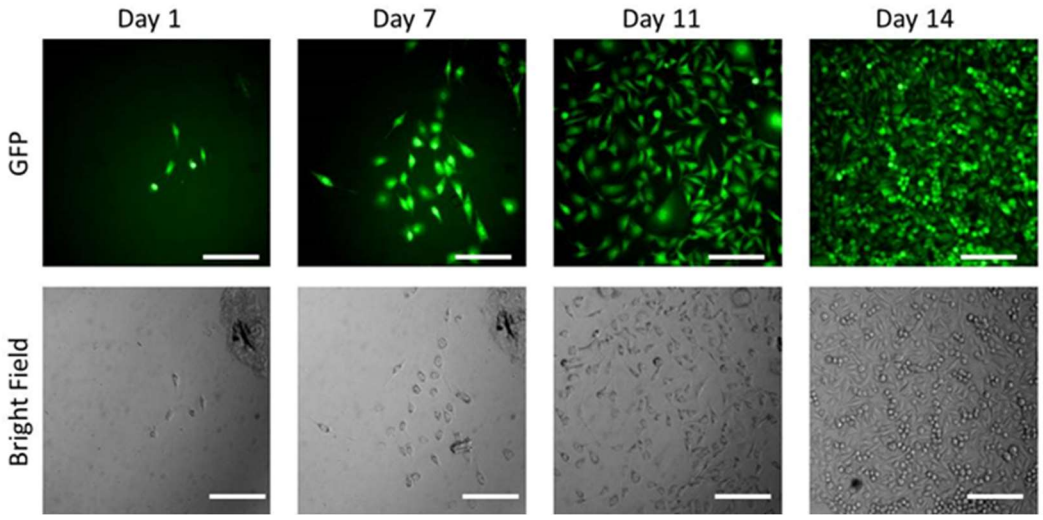

Figure 2.16 Proliferation of captured cells. Representative images, GFP expression and bright field, of cultured cells at days 1,7,11, and 14. Scale bars are 200 µm. Image adapted from H. Cayron manuscript, LAAS-CNRS 2016.[39]

2.2.2.8 Assessing the detection limit

We performed a set of experiments in order to investigate the detection limit of the 3D microdevice. We processed cell suspensions at concentrations ranging from 10 to 25000 cells per mL of model cells (DRAQ5-stained PC3-GFP) for 10 min at v_{min}. The capture events were monitored by video microscopy, and confirmed using both confocal and SEM.

Results are summarized in **Figure 2.14**, where we can observe a direct relation between the number of captured cells Cc and the cell concentration of the processed suspension. Cells were detected down to a concentration of 10 cells mL^{-1}, where the number of recovered cells was one. Below a cell concentration of 500 cells mL^{-1} the number of C_C was not higher than a single cell.

We believe that this number of captured cells is the consequence of the relatively low amount of liquid screened by a single microdevice (effective flow rate Qeff ≈500 µL) for a 10 min experiment, imposed by the established filtration time and the velocity of the fluid within the channel.

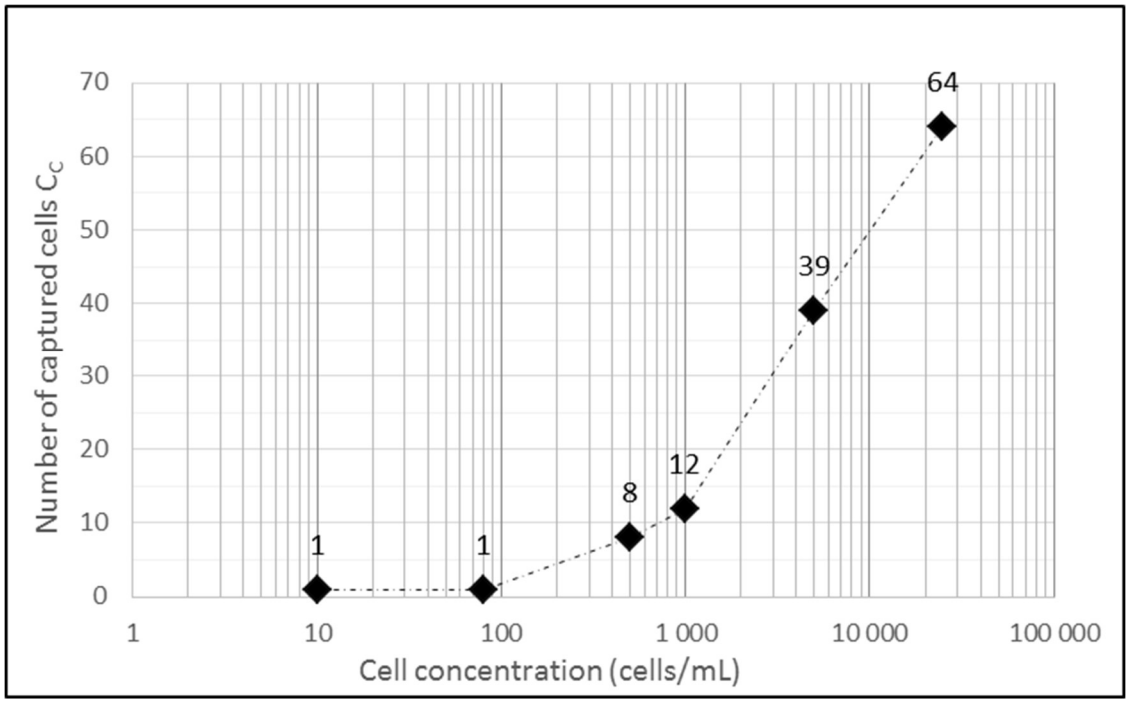

Figure 2.17 Number of trapped cells as a function of cell concentration in the processed suspension. Cell suspensions ranged from 10 to 25000 cells per mL.

2.2.2.9 Assessing clogging of pores by blood cells

There are significant differences between our model fluid (i.e., cell culture medium) and whole blood. Particularly, blood is considered as a complex fluid due to its heterogeneity in cell composition, the number of cells (~10^9 cells per mL), and rheological properties.

We firstly evaluated possible clogging of the holey membrane, and non-specific adhesion of blood-related components onto the microdevice. We obtained blood samples from healthy donors collected in ethylenediaminetetraacetic acid (EDTA) tubes supplied by the EFS-Toulouse (etablissement francais du sang in Toulouse France). Blood was flowed through the fluidic platform for 10 min at v_{min} and subsequently rinsed with cell culture medium. We characterized those samples using confocal and electron microscopy, following the same protocols as previous samples.

The overall inspection of the samples did not evidence massive accumulation of blood cells either on the surroundings or within the microdevice, **Figure 2.18a**. At the holey membrane level, interestingly most of the pores are completely free, and we did not observe significant clogging of pores by red blood cells or other morphologies resembling to white blood cells. However, we observed minor platelet aggregates and nondescript debris onto the surface or within the membrane pores, **Figure 2.18b**. The degree of contamination observed was usually lower than the one showed in **Figures 2.18a** and **2.18b**. We also evaluated whether the undesired debris could hide or overlap with the identification of DRAQ5-stained PC3-GFP cells, and as depicted in **Figure 2.18c,** these debris do not emit fluorescent signal in the range of interest.

Furthermore, we assessed the use of heparin coating to inhibit the adhesion of platelets and the potential formation of blood clots. However, we did not observe significant improvement in the number of platelet aggregates, since the EDTA-treated blood used already prevents these effects. Thus, we continued using microdevices without any surface treatment.

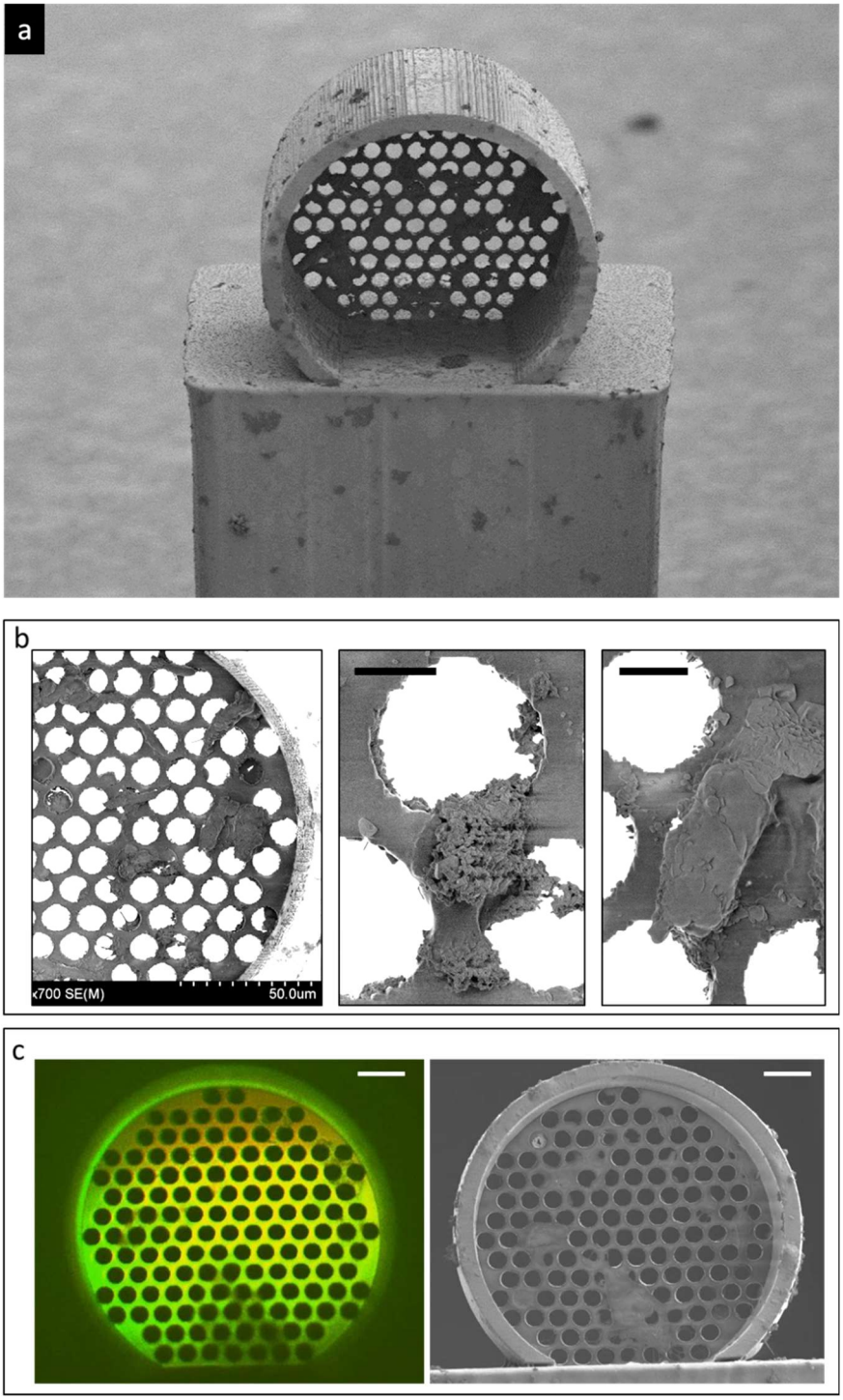

Figure 2.18 Representative images of the microdevice after the exposure to whole blood flow. **a** General view of the microdevice onto the pillar, where few platelet aggregates are observed onto the cylinder and pillar surfaces. **b** Scanning electron micrographs of the holey membrane region and magnifications of the type of contamination regularly found. **c** Confocal image of the microdevice (DRAQ and GFP emission) and its corresponding SEM image.

2.2.2.10 Assessing the capture of PC3 cells from blood samples

Having established the feasibility of using whole blood in our fluidic platform without considerable fouling of the holey membrane, we then assessed whether our findings in PC3 capture from cell culture media were transposable to blood samples. Similarly to cell culture medium experiments, we spiked controlled concentrations of DRAQ5-stained PC3-GFP cells into whole blood from healthy donors. We set the velocity within the channel to v_{min} and experimental time was limited to 10 minutes, as previous experiments. Microscope observation during fluidic experiments through the pillar was not possible, in the configuration previously used, since blood is an opaque fluid and does not allow obtaining a reasonable signal intensity from stained cells.

We aimed to evaluate the capture performance at a relatively high PC3 concentration, but even more interestingly, at low concentrations. When we processed suspensions containing 25000 PC3 cells per mL, in a total of 8 mL of whole blood, we first observed a decrease in the intensity of the fluorescence emitted by cells, particularly DRAQ5 emission. This represented a challenge for the identification, by confocal imaging, of PC3 cells from other blood-related cells and debris. However, we could identify PC3 cells by increasing the intensity of the excitation signal and an adequate image processing. For example, some of these cells clearly express GFP and DRAQ5, pointed cells in yellow in **Figure 2.19a1**.

The trapping of undesired cells, such as WBCs, is a parameter commonly investigated in this field. Usually staining protocols are applied for the recognition of WBC, targeting the positive expression of CD45. At this stage of the project, we were not able to perform the immunofluorescence recognition of WBC, thus we proceeded to one-to-one comparison using confocal and SEM images in order to evaluate contamination, **Figure 2.19a2**. We found a negligible contamination of red blood cells or leukocytes, having most of pores free. However, as previously remarked, platelet aggregates are observed. Less frequently, some samples also exhibit a thin layer of an organic material covering both cells and free-pores, as observed in **Figure 2.19a2**. We believe these organic materials correspond to proteins deposited after cell capture and during the fixation and dehydration steps. Despite this, in most samples we were able to recognize the rounded morphology of trapped cells, as shown in **Figure 2.19b**, similar to the one found in culture media experiments. Therefore and hereinafter, we defined as C_C these cells expressing the double staining in confocal characterization, and also found by SEM imaging having >5µm as characteristic diameter.

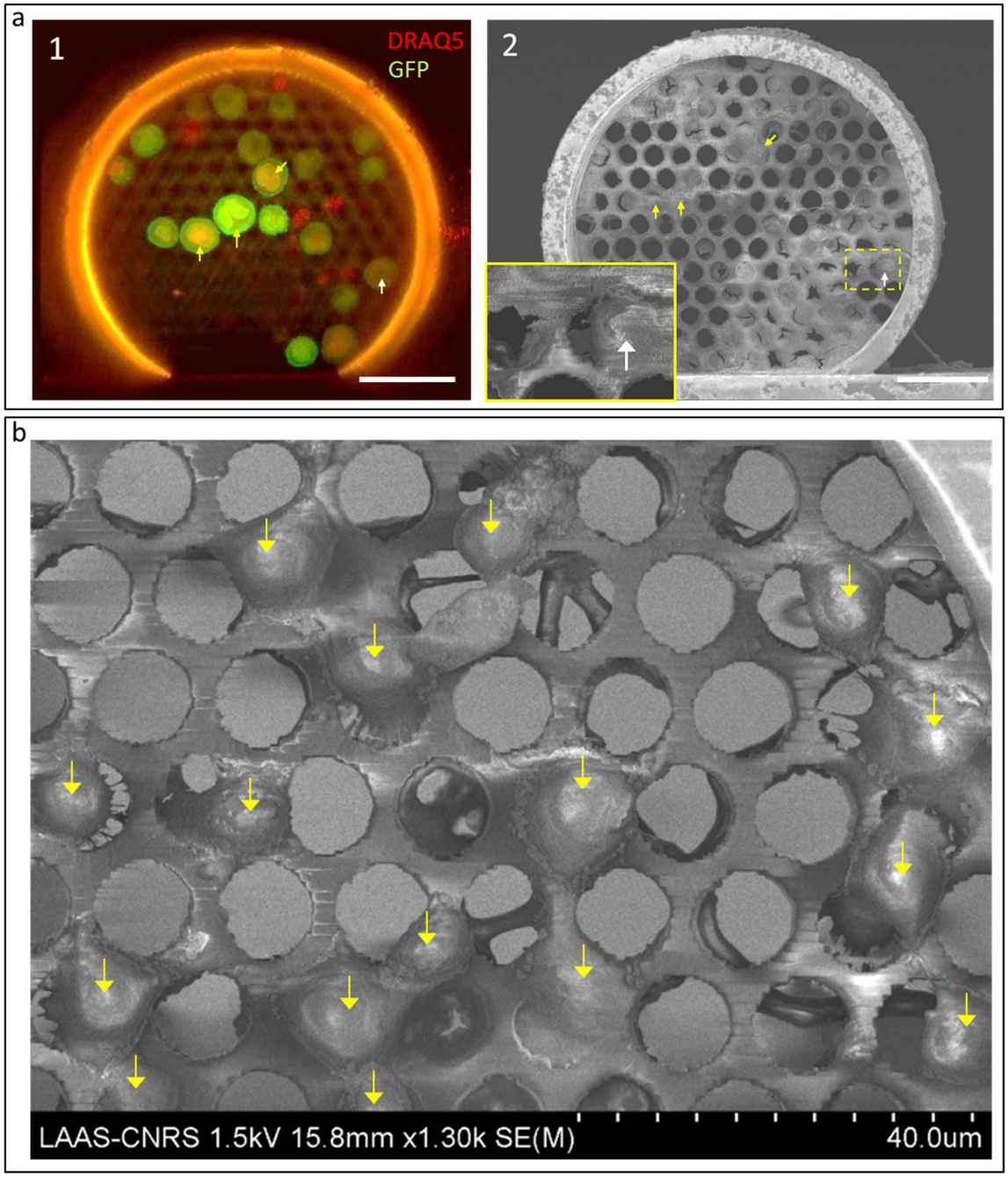

Figure 2.19 Representative images of captured PC3 cells from whole blood, at 25000 cells per mL, using the capture microdevice. **a** Confocal (1) and SEM (2) images of captured cells. Yellow arrows point to some cells where GFP and DRAQ expression was evident. The inset of image (2) corresponds to a magnification of the dashed area where a layer of organic material is observed onto a cell (white arrow) and pores. Scale bars are 50 µm. **b** Scanning electron micrograph of the holey membrane where we observe the captured PC3 cells. Yellow arrows point to cells first identified by confocal imaging and then matched using SEM.

Using the C_C values obtained from culture media experiments as a baseline, we compared the number of trapped cells. For blood experiments, at 25000 cells mL^{-1}, C_C ranged from 13 to 36 cells across the four experiments performed. Notice that fewer PC3 cells were captured in whole blood than in cell culture medium suspensions (minus 60-70%). We believe that this reduction in the number of cells captured is due to the combination of two factors enhanced by blood cells: concentration polarization and cell transit time.

Concentration polarization is a phenomenon usually observed in microfiltration systems.[40,41] As blood entering the microdevice approaches the holey membrane, blood components gradually build-up in concentration in a region near the surface of the holey membrane giving rise to a fouling layer, **Figure 2.20**. Thus, a temporary accumulation of blood cells occurs, mostly RBCs ≈5 million per mm^3, leading to an apparent fouling and transient pore-blocking. This phenomenon reduces the effective flow passing through the microdevice due to a local increase of blood viscosity.[18] The degree of this apparent fouling is determined by the ability of each cell to move into the pore and transit through it at a determined rate. As introduced in section 2.1.2, each blood cell has a specific transit time mainly determined by its apparent viscosity and ΔP, where cells having a higher apparent viscosity will have a slower transit through the pore. Generally, since RBCs and WBCs transit faster through pores than cancer cells, $t_{RBC} < t_{WBC} < t_{cancer\ cell}$, it is expected that a longer filtration time could lead to an increased number of captured PC3 cells.

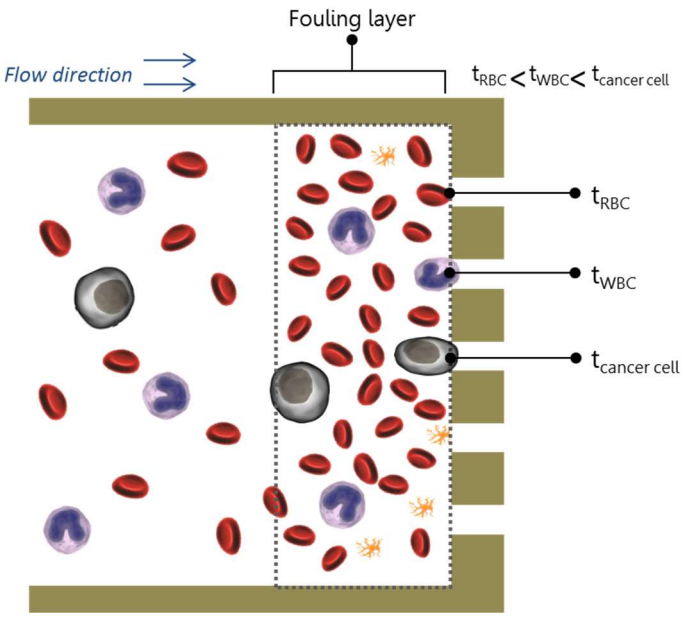

Figure 2.20 Schematic and hypothetical representation of blood filtration using the 3D microdevice, top view. A fouling layer is formed near the holey membrane due to the different transit time of each cell.

Given the observations in cell capture numbers at high PC3 concentrations, we also assessed the performance of the microdevice at relatively low concentrations. Similarly, we processed 8 mL of whole blood spiked with DRAQ5-stained PC3-GFP aiming to obtain concentration of 1000 cells mL^{-1}. From five experiments no cells were found in three samples, and the number of captured cells was C_C=2 and C_C=4 respectively in the other two samples, **Figure 2.21**. Those results confirmed our observations at high cell concentrations: in blood, a lower amount of PC3 cells are captured compared to culture media experiments. Interestingly, given the success rate of this set of experiments, three of five experiments, we believe this cell concentration is at the microdevice's detection limit.

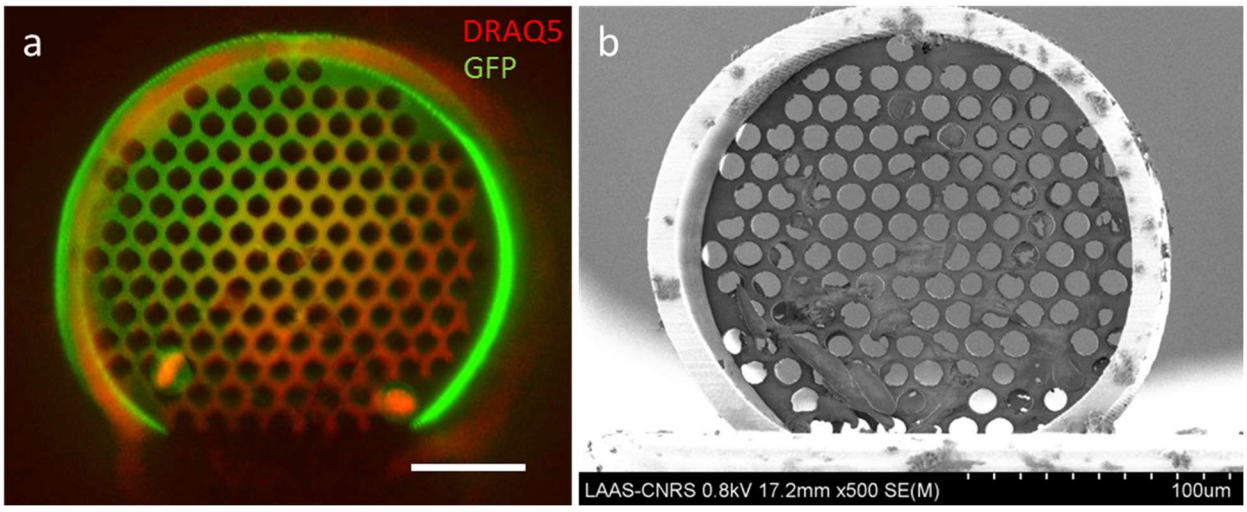

Figure 2.21 Representative images of captured PC3 cells from whole blood, at 1000 cells per mL, using the capture microdevice. **a** Confocal image evidencing two PC3 cells. **b** Corresponding SEM image, where in addition to captured cells, several blood debris are also observed.

2.3 Engineering the intravascular prototype

2.3.1 The venipuncture and insertion strategy

The fluidic test-bench allowed demonstrating the feasibility of cancer cell capture under different flow conditions. However, our final objective is the integration of the 3D microdevice onto customized substrates which would allow its insertion within the vein through venipuncture needles. To that end, we proposed a **double-needle insertion system**, which is composed of a puncture needle, an insertion strip-needle guide, and the capture microdevice, **Figure 2.22**.

The concept is based on the fabrication of the 3D microdevice onto a customized metallic strip, and subsequent integration along with the insertion needle in order to form the strip-needle guide. This assembly is placed, in turn, inside the puncture needle. This way, overall microdevice-guide ensemble is able to move freely through the 18G puncture needle, allowing for the microdevice to be inserted and retracted. This configuration could enable the protection of the microdevice during skin/vein penetration by the puncture needle, and once within the vein, its exposure to the bloodstream. The strip-needle guide is attached to the plunger of a plastic syringe to enable its manual insertion and retraction.

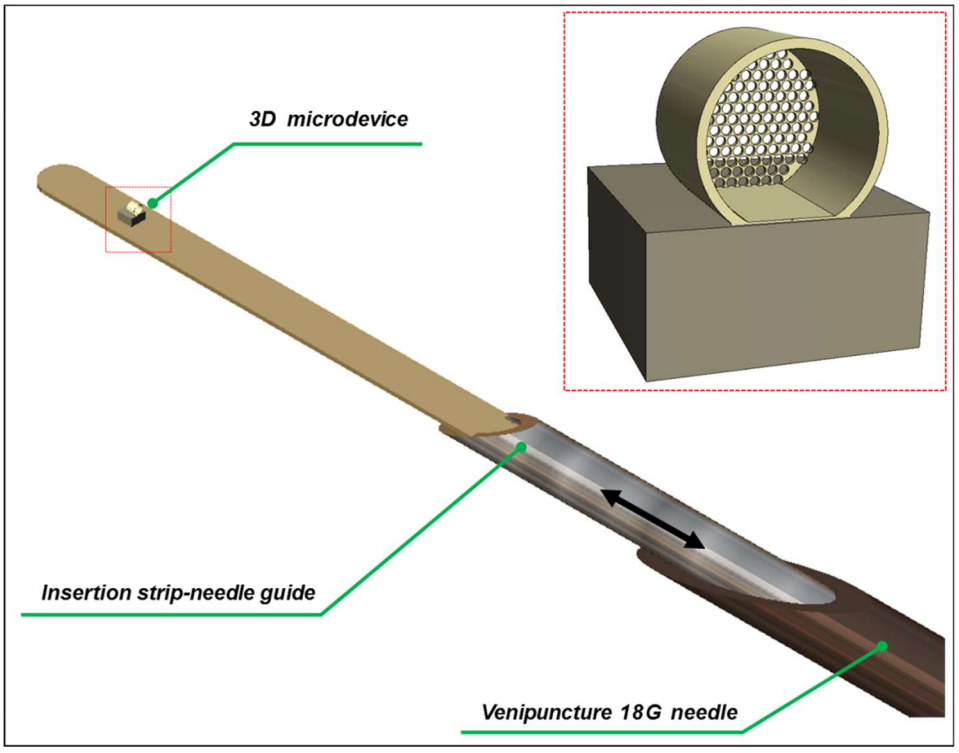

Figure 2.22 Double-needle insertion system for the intravascular access of the 3D microdevice. The 3D microdevice and the micropillar are integrated onto the insertion strip-needle guide, which allows the insertion and retrieval of the microdevice. This assembly was designed to fit inside an 18G hypodermic needle which is used as puncture needle.

In order to fabricate the proposed double-needle insertion system we first fabricated the customized metallic strips. We used an 80 µm-thick Nickel-Titanium alloy (Nickel Titanium-Naval Ordnance Laboratory, Nitinol) sheet to fabricate strips with total dimensions of 12 mm-length and 700 µm-width, having rounded and sharp ends at each extremity (Water jet cutting). We used the DLW system to fabricate the 3D microdevice. Unlike the protocol presented in section 2.2.1, we sticked the metallic strip onto the glass substrate and the laser was manually positioned onto the desired strip area, approximately 1 mm from the rounded edge, **Figure 2.23**. We included the base-pillar as in the test-bench, but this time it was fabricated along with the microdevice. Fabricated IP-Dip structures directly onto the Nitinol strip showed good mechanical adhesion.

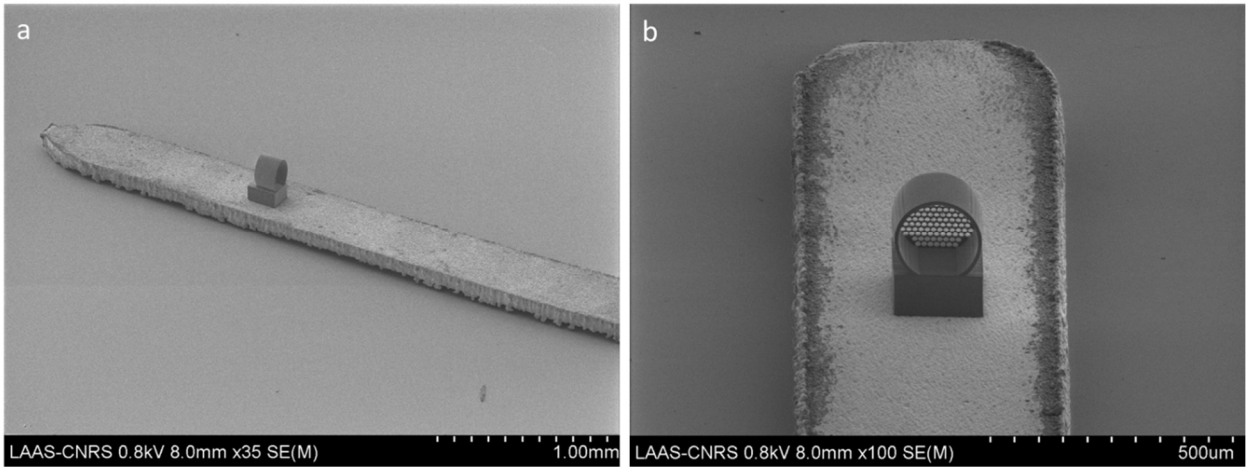

Figure 2.23 SEM images of the microdevice fabricated onto a metallic strip. **a** Perspective view of the overall strip with the pillar and microdevice at an approximate distance of 1 mm from the front edge. **b** Front view of the microdevice and strip.

In order to form the strip-needle guide we directly glued the Nitinol strip (Cyanoacrylate instant adhesive, Würth) to the end-tip of a 20G needle (Terumo, 20Gx 2 3/4”). Afterwards, this guide was attached to the plunger of a 1 mL syringe having a 18G venipuncture needle (~650 µm inner diameter, Terumo, 18Gx 1 1/2”). The final assembly is shown in **Figure 2.24a** and the system in a semi-retracted position is displayed in **Figure 2.24b.**

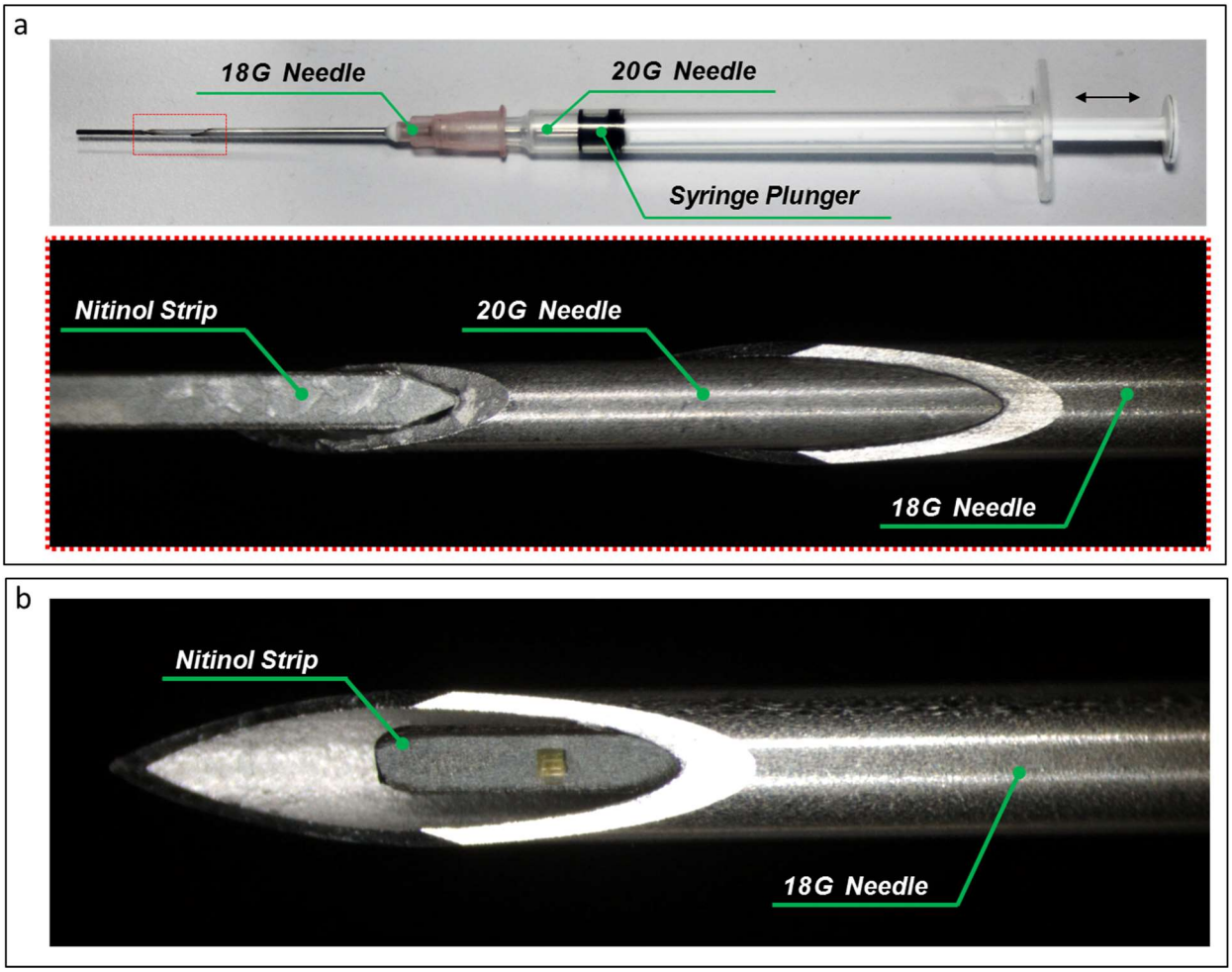

Figure 2.24 Assembly of the double-needle insertion system. **a** Overall assembly including the syringe. The dotted area is magnified in the insert where is observed the joint between the Nitinol strip and the 20G needle forming the insertion strip-needle guide. **b** Magnification of the end-tip of the 18G needle where is observed the Nitinol strip and the microdevice, in a semi-retracted position.

2.3.2 Assessing the translation from *in vitro* to *in vivo* cancer cell capture

The double-needle insertion assembly was first evaluated in vitro using a PDMS fluidic platform of 3 mm section, comparable to the one of the basilic vein in our model fluid. This adapted fluidic platform included a lateral port for the access of the double-needle insertion system as shown in **Figure 2.25a**. For this fluidic setup the rotation speed of the peristaltic pump was set to 28 rpm in order to reach v_{min}=0.072 m s^{-1} within the channel. As previously mentioned, we used DRAQ5-stained PC3-GFP cells in cell culture medium suspensions, this time at concentrations of 5000 cells per mL.

Early experiments using the proposed system evidenced the fragility of the microdevice. Despite having good mechanical adhesion onto the metallic strip, in most of the experiments the physical contact of it with the walls of the puncture needle, at the moment of retraction, damaged or detached the microdevice from the strip, **Figure 2.25b**. However, few successful experiments confirmed the cell-capture capability of this prototype. For example, in **Figure 2.25c** we identify a total of Cc=21 cells.

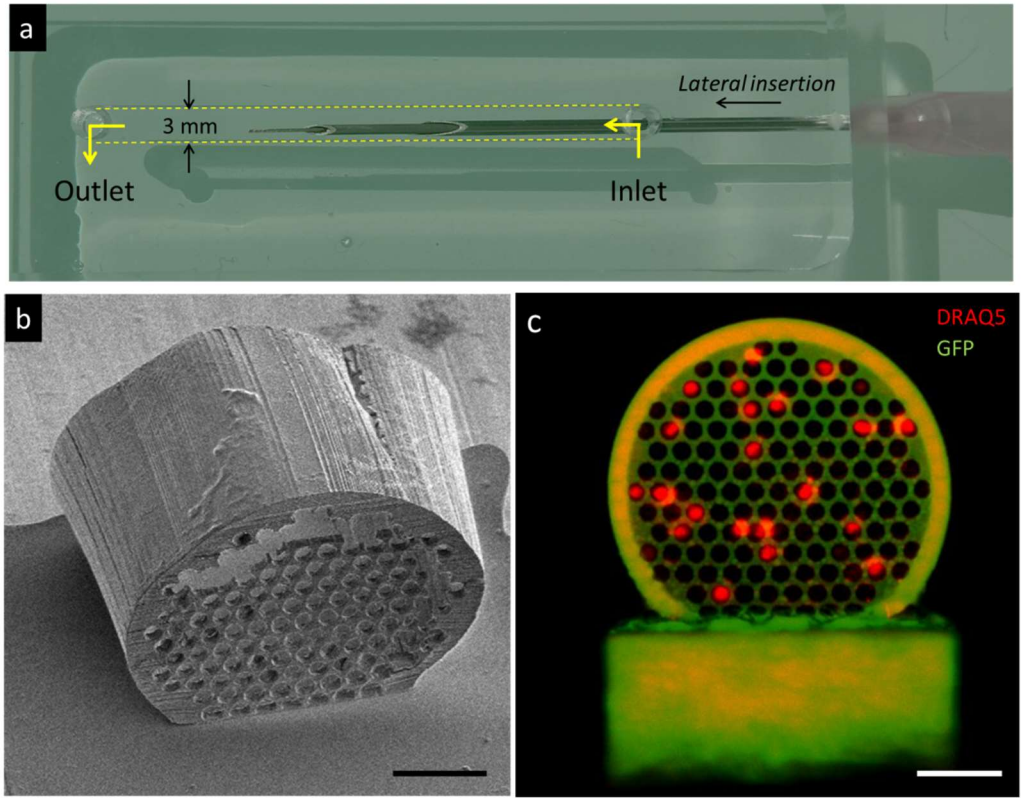

Figure 2.25 Fluidic platform for *in vitro* testing of the double-needle insertion system and experimental results. **a** Customized test-bench having a square cross section of 3 mm. The double-needle insertion system is inserted laterally through a pre-molded access. Dotted lines highlight walls of the channel. **b** SEM image of a damaged microdevice after fluidic experimentation. **c** Confocal image of trapped cells using this system and a suspension at 5000 cells per mL. Scale bars correspond to 50 µm.

Those few results evidenced a lower value of C_C when compared to the above-described 1 mm test-bench, section 2.2.2.8. The diminished capture performance of this prototype could be attributed to a lower flow velocity to which the microdevice is actually exposed, equivalent to $v_{freestream}$=0.0723 m s^{-1}, which is about half the one estimated in the 1 mm fluidic channel, **Figure 2.26**. This could result into a lower effective flow passing through the microdevice Q_{eff}. The disruption of the channel freestream velocity is caused by the double-needle system, which diverts the flow downstream towards the microdevice. However, the microdevice is still exposed to a constant flow and consequently cell capture is feasible, as demonstrated by our experimental results.

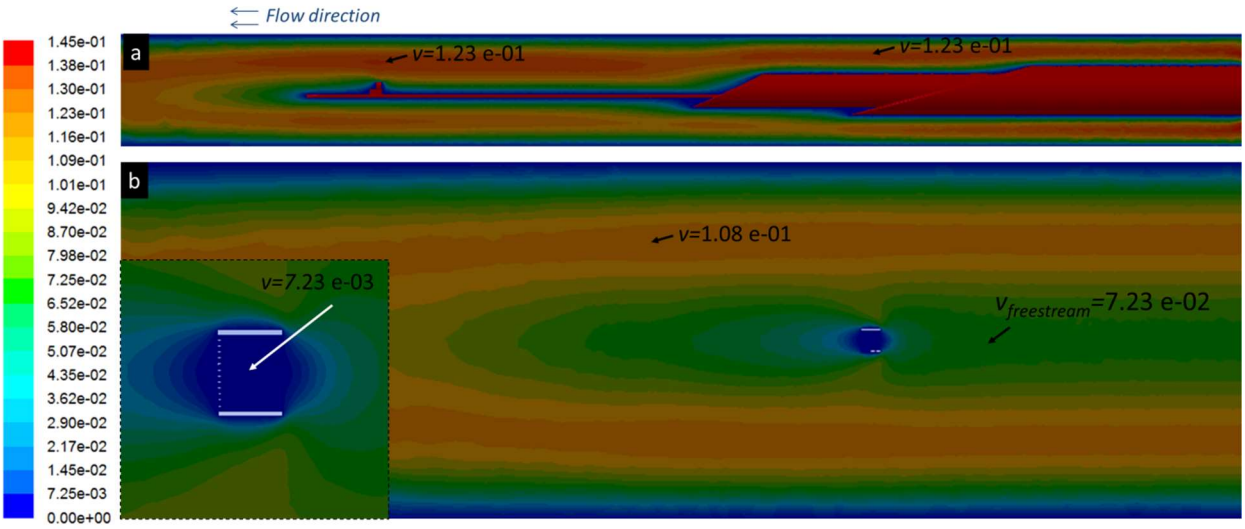

Figure 2.26 Fluid-dynamics within the 3 mm fluidic platform and having the double-needle insertion system placed into the channel. **a** Lateral view of the system placed within the channel evidencing the disruption of the flow field. **b** Sectional view and magnification around the microdevice. The colormap is in m s^{-1}.

We envisioned different strategies to overcome the mechanical fragility challenge and attain *in vivo* validation of the system. As an example, we proposed the use of a customized shielding catheter having openings which may allow the flow to pass through the microdevice, **Figure 2.27a**. However, the overall diameter of this set exceeded the one of medical routine venipuncture needles, hindering its insertion within the vein. Moreover, this design also decreases the velocity of the flow incoming in the microdevice. Thus, this solution was discarded.

A simpler solution consisting of a couple of semi-spheres, taller than the microdevice, was envisioned to protect it from mechanical contact, **Figure 2.27b**. The semi-spheres were fabricated after the microdevice by simple drop casting of a photosensitive resist and their subsequent UV polymerization. Those semi-spheres were placed at approximately 3 mm from the microdevice. This technical solution exhibited acceptable characteristics for *in vivo* experimentation, so we proceeded with its evaluation in animal models.

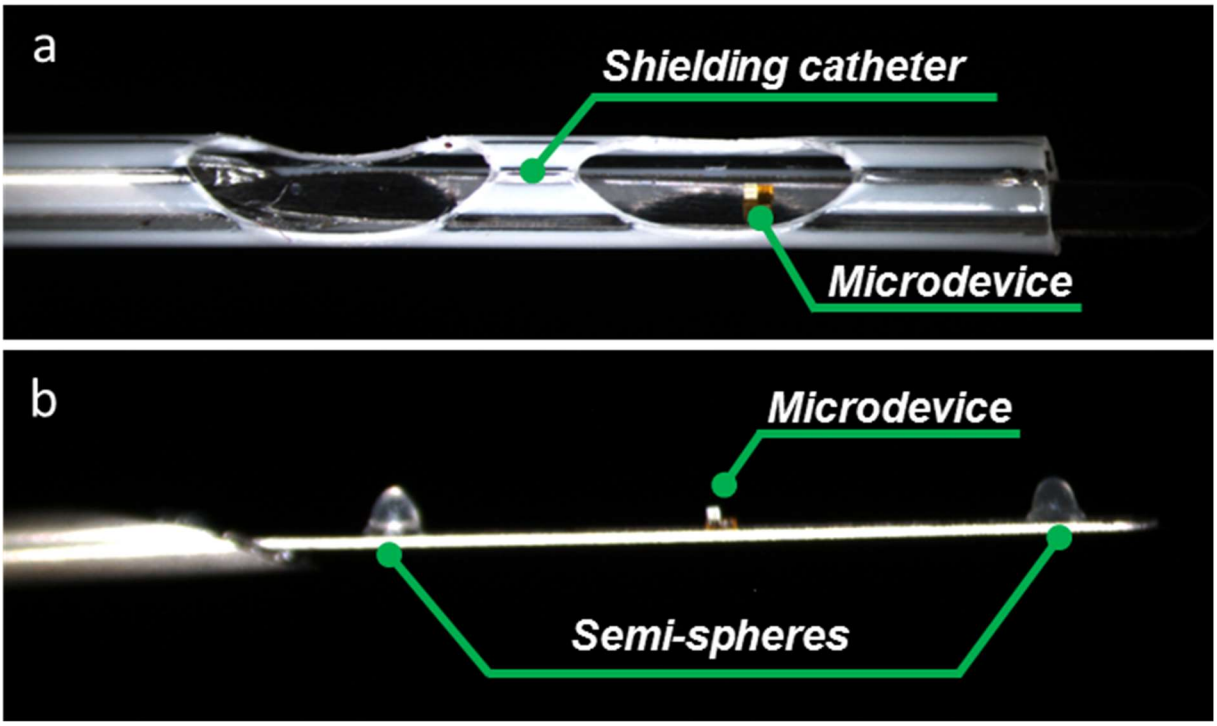

Figure 2.27 Proposed strategies to avoid the physical damage of the microdevice. **a** A customized catheter, containing two openings, shields the Nitinol strip. The microdevice and pillar are observed in one of the openings. **b** A couple of semi-spheres are fabricated at 3 mm from the microdevice, these are taller than the total height of the pillar and microdevice, thus prevent any direct mechanical contact on the microdevice.

In collaboration with Catherine Viguié from the École Nationale Vétérinaire de Toulouse (ENVT-INP, Toulouse, France), we established the required protocols for the use of miniature pigs as animal model. This model was chosen due to the physiological similarities in vein and blood cell sizes in humans. Two miniature pigs of approximately 20 kg were subjected to intervention. Accordingly with our *in vitro* experiments, we targeted a concentration of 25000 PC3-GFP cells per mL of blood in a total estimated volume of 2.0 L. The suspension of PC3-GFP cells was directly injected into superficial veins/arteries at the forearm and breast sites for each subject, and our prototype inserted within the same vein few centimeters after the cell injection site. The microdevice was exposed for a time span of 3-5 minutes, then retracted and removed from the vein. A rinsing step was performed *ex vivo* using the fluidic platform above introduced, with 40 mL of cell culture medium and the cellular material was then fixed. A total of four heparinized prototypes were tested.

The results were not satisfactory in terms of cell capture throughout this set of experiments, since no PC3 cells were identified by confocal inspection. However, these experiments allowed identifying several important factors for the improvement of the device and the experimental protocols. Those are enumerated as follows:

- ***Mechanically fragile microdevice*.** From the four prototypes tested *in vivo*, three of them were recovered with intact mechanical integrity, **Figure 2.28a**. The remaining one was too fragile to withstand the steps of insertion and recovery, and was detached during the procedure. This evidences that the proposed prototype based in a polymeric microdevice is not adapted to withstand inter-user handling since extreme precision and care was required at each step of the surgical procedure. Additionally, the characterization step, confocal and SEM, required the removal of the metallic strip from the 20G needle. This manual handling derived into the mechanical damage of one of the remaining microdevices, **Figure 2.28b**. Thus, great care must be also taken during the post-experimental steps. We concluded that polymeric devices are not suitable for *in vivo* PC3 capture trials.
- ***Non-conventional characterization*.** Similarly to the bottleneck faced using the 1 mm test bench, the overall observation of the holey membrane was challenging, since it required the vertical positioning of the strip, which implied an extra risk given the fragility of the microdevice. Therefore, confocal characterization was performed horizontally through the walls of the cylinder. This implied a loss in resolution and quality of the image, complicating the interpretation of the data. Despite this, there was no clear evidence of PC3 capture. From this experience, we concluded that the technology, apart from performing cell capture, must be compatible with conventional characterization methods.
- ***Appropriate selection of animal model and protocols for intervention***. The mini-pig animal model offers, in principle, physiological characteristics similar to those of humans, but given the relatively high blood volume of the model used and natural clearance of injected cells, it was difficult to ensure the circulation of cancer cells by means of intravenous injection. This is the reason injection and capture of cells was performed along the same venous pathway, although it was well known in advance that this methodology does not represent the actual conditions

found in patients. Thus, in order to ensure the real circulation of injected cancer cells into the body for a determined time span, smaller animal models might be more suited. Moreover, given that no cell capture events were registered in the microdevices, we proposed different aspects to be revised in the experimental protocols before, during and after the intervention. For example, we theorize the presence of an air bubble within the microdevice, sometimes observed during in vitro experiments, obstructing the blood flow.

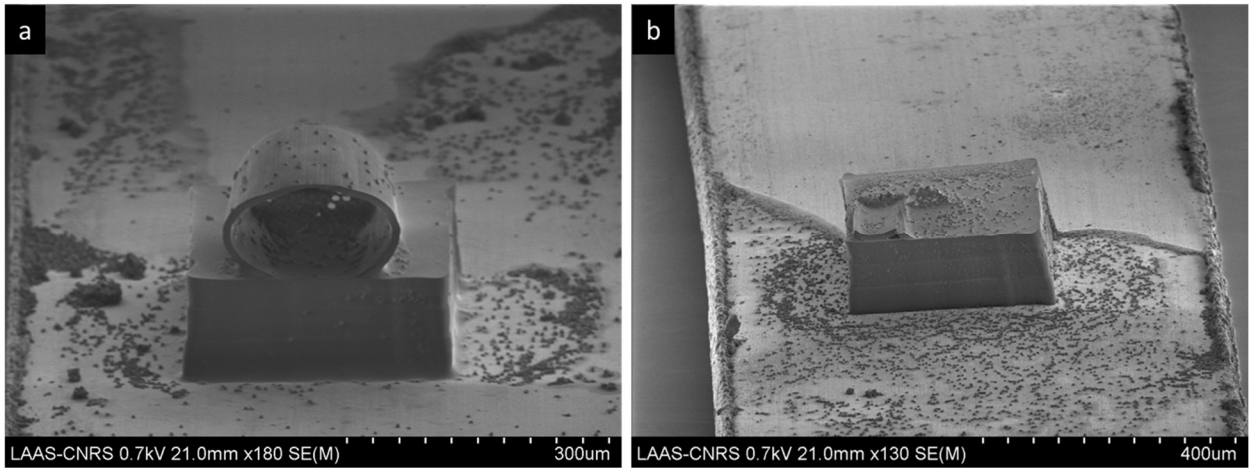

Figure 2.28 Scanning electron micrographs from 3D microdevices after being tested in mini-pig animal models. **a** Microdevice with intact mechanical integrity. **b** Microdevice damaged during the manual handling for post-experimental characterization.

2.4 Conclusions of Chapter II

In this chapter, we have introduced the field of blood microfiltration for CTC isolation which has been widely used in the field of Liquid Biopsy. On the basis of CTC being larger and less deformable, the scientific community has proposed a diversity of micropatterned filters, mainly supported by lithographic techniques developed in the microfabrication field. Among this diversity, the vast majority converge with the use of a dead-end configuration. Emphasis has been placed in the operating conditions of these platforms evidencing that CTC selectivity is not only determined by the size of targeted cells in relation with the one of pores, but also influenced by the pressure conditions of the filtering system and the sample processing time.

The bibliographic review, provided insights for the understanding of the physical mechanisms that would enable a successful *in vivo* capture of cancer cells present in human blood circulation. This premise set the basis for designing a 3D microdevice which was adapted to the medical requirements. We have fabricated the proposed microdevice using a high-resolution additive manufacturing technique and integrated it into a customized fluidic bench for the assessment of cancer cell capture.

The cancer cell capture concept under physiologically relevant flow conditions was successfully demonstrated in *in vitro* conditions using a prostate cancer cell line as model. We were able to obtain real-time monitoring of cell capture events, and to characterize the isolated biological material. Together with fluid dynamic simulations, we evaluated the associated issues of dead-end filtration systems such as pore clogging, evidencing that processing whole blood is possible. Furthermore, our results evidenced the preservation of cell morphology which in a preliminary study, suggest the viability of the captured biological material.

We have also provided first experimental clues of cancer-cell detection limit of our 3D microdevice, as conventionally established for different CTC isolation platforms. We believe the cell capture yield is closely related to the effective volume of flow screened by the 3D microdevice. Our preliminary results suggest a limited performance for the detection of extremely low cell suspensions for what we envision some technical strategies for the improvement of the capture microdevice and their implementation, which will be explained in detail in chapter III.

In the perspective of real *in vivo* cell capture, we developed an intravascular system integrating the capture microdevice. A first intravenous cell-capture trial was performed in animal models, and evidence that one of the main challenges for capture microdevices is robustness to withstand clinical routine handling and to be able to reach real clinical applications. This challenge is addressed in the first part of chapter III.

The techniques and protocols introduced along chapter II, will serve as a basis for the work presented in the subsequent chapter.

Bibliography of Chapter II

1. Bu, J. *et al.* Lab on a fabric: Mass producible and low-cost fabric filters for the high-throughput viable isolation of circulating tumor cells. *Biosens. Bioelectron.* **91,** 747–755 (2017).
2. VyCAP. CTC enumeration of whole blood (Circulating Tumor Cells, liquid biopsy). *VyCAP* Available at: https://www.vycap.com/technology/ctc-enumeration/. (Accessed: 5th July 2018)
3. Yeung, A. & Evans, E. Cortical shell-liquid core model for passive flow of liquid-like spherical cells into micropipets. *Biophys. J.* **56,** 139–149 (1989).
4. Lim, C. T., Zhou, E. H. & Quek, S. T. Mechanical models for living cells--a review. *J. Biomech.* **39,** 195–216 (2006).
5. Coumans, F. A. W., Dalum, G. van, Beck, M. & Terstappen, L. W. M. M. Filtration Parameters Influencing Circulating Tumor Cell Enrichment from Whole Blood. *PLOS ONE* **8,** e61774 (2013).
6. Evans, E. & Kukan, B. Passive material behavior of granulocytes based on large deformation and recovery after deformation tests. *Blood* **64,** 1028–1035 (1984).
7. Weiss, L. & Schmid-Schönbein, G. W. Biomechanical interactions of cancer cells with the microvasculature during metastasis. *Cell Biophys.* **14,** 187–215 (1989).
8. Zhang, Z., Xu, J., Hong, B. & Chen, X. The effects of 3D channel geometry on CTC passing pressure – towards deformability-based cancer cell separation. *Lab. Chip* **14,** 2576–2584 (2014).
9. Tsai, M. A., Frank, R. S. & Waugh, R. E. Passive mechanical behavior of human neutrophils: power-law fluid. *Biophys. J.* **65,** 2078–2088 (1993).
10. Adams, D. L. *et al.* The systematic study of circulating tumor cell isolation using lithographic microfilters. *RSC Adv.* **9,** 4334–4342 (2014).
11. Vona, G. *et al.* Isolation by Size of Epithelial Tumor Cells. *Am. J. Pathol.* **156,** 57–63 (2000).
12. Desitter, I. *et al.* A new device for rapid isolation by size and characterization of rare circulating tumor cells. *Anticancer Res.* **31,** 427–441 (2011).
13. Zheng, S. *et al.* Membrane microfilter device for selective capture, electrolysis and genomic analysis of human circulating tumor cells. *J. Chromatogr. A* **1162,** 154–161 (2007).
14. Zheng, S. *et al.* 3D microfilter device for viable circulating tumor cell (CTC) enrichment from blood. *Biomed. Microdevices* **13,** (2011).
15. Hosokawa, M. *et al.* Size-Selective Microcavity Array for Rapid and Efficient Detection of Circulating Tumor Cells. *Anal. Chem.* **82,** 6629–6635 (2010).
16. Hosokawa, M. *et al.* Size-Based Isolation of Circulating Tumor Cells in Lung Cancer Patients Using a Microcavity Array System. *PLOS ONE* **8,** e67466 (2013).
17. Yagi, S. *et al.* Development of an automated size-based filtration system for isolation of circulating tumor cells in lung cancer patients. *PLoS ONE* **12,** (2017).
18. Shi Lim, L. *et al.* Microsieve lab-chip device for rapid enumeration and fluorescence in situ hybridization of circulating tumor cells. *Lab. Chip* **12,** 4388–4396 (2012).
19. Wit, S. de *et al.* The detection of $EpCAM^+$ and $EpCAM^-$ circulating tumor cells. *Sci. Rep.* **5,** 12270 (2015).
20. Swennenhuis, J. F. *et al.* Self-seeding microwell chip for the isolation and characterization of single cells. *Lab. Chip* **15,** 3039–3046 (2015).

21. Evans, E. A. & Skalak, R. Mechanics and thermodynamics of biomembranes: part 1. *CRC Crit. Rev. Bioeng.* **3,** 181–330 (1979).
22. Dowgert, M. F., Wolfe, J. & Steponkus, P. L. The Mechanics of Injury to Isolated Protoplasts following Osmotic Contraction and Expansion. *Plant Physiol.* **83,** 1001–1007 (1987).
23. Harouaka, R. A. *et al.* Flexible Micro Spring Array Device for High-Throughput Enrichment of Viable Circulating Tumor Cells. *Clin. Chem.* **60,** 323–333 (2014).
24. ANATOMY OF THE BASILIC VEIN IN THE ARM AND ITS IMPORTANCE FOR SURGERY. *Periodikos* Available at: http://www.jms.periodikos.com.br/article/587cb4507f8c9d0d058b45da. (Accessed: 26th June 2018)
25. Purvis, E. S., Hyde, G. L. & Peck, D. Anatomy of arm veins: Significance for vein valve transplantation. *Clin. Anat.* **5,** 45–49 (2005).
26. Ooue, A. *et al.* Changes in blood flow in a conduit artery and superficial vein of the upper arm during passive heating in humans. *Eur. J. Appl. Physiol.* **101,** 97–103 (2007).
27. Ahn, W., Bahk, J.-H. & Lim, Y.-J. The 'Gauge' System for the Medical Use. *Anesth. Analg.* **95,** 1125 (2002).
28. Jensen, K. H. *et al.* Modeling the Hydrodynamics of Phloem Sieve Plates. *Front. Plant Sci.* **3,** (2012).
29. Selimis, A., Mironov, V. & Farsari, M. Direct laser writing: Principles and materials for scaffold 3D printing. *Microelectron. Eng.* **132,** 83–89 (2015).
30. Munis, J. R., Bhatia, S. & Lozada, L. J. Peripheral venous pressure as a hemodynamic variable in neurosurgical patients. *Anesth. Analg.* **92,** 172–179 (2001).
31. Baumann, U. A. *et al.* Estimation of central venous pressure by ultrasound. *Resuscitation* **64,** 193–199 (2005).
32. Chapter 5 Flow Around a Bluff Body: Obstacle Marks. in *Developments in Sedimentology* (ed. Allen, J. R. L.) **30,** 173–205 (Elsevier, 1982).
33. Accardo, A. *et al.* Multiphoton Direct Laser Writing and 3D Imaging of Polymeric Freestanding Architectures for Cell Colonization. *Small* **13,** 1700621
34. Yoon, Y. *et al.* Clogging-free microfluidics for continuous size-based separation of microparticles. *Sci. Rep.* **6,** 26531 (2016).
35. Wakeman, R. J. & Williams, C. J. Additional techniques to improve microfiltration. *Sep. Purif. Technol.* **26,** 3–18 (2002).
36. Chen, W. *et al.* Nanoroughened Surfaces for Efficient Capture of Circulating Tumor Cells without Using Capture Antibodies. *ACS Nano* **7,** 566–575 (2013).
37. Qiu, J. *et al.* A titanium dioxide nanorod array as a high-affinity nano-bio interface of a microfluidic device for efficient capture of circulating tumor cells. *Nano Res.* **10,** 776–784 (2017).
38. Shi, L., Wang, K. & Yang, Y. Adhesion-based tumor cell capture using nanotopography. *Colloids Surf. B Biointerfaces* **147,** 291–299 (2016).
39. Cayron, H. *Sélection et capture de biomarqueurs moléculaires et cellulaires à partir d'un fluide complexe*. (Toulouse, INSA, 2016).
40. Matthiasson, E. & Sivik, B. Concentration polarization and fouling. *Desalination* **35,** 59–103 (1980).

41. A. Crowley, T. & Pizziconi, V. Isolation of plasma from whole blood using planar microfilters for lab-on-a-chip applications. *Lab. Chip* **5,** 922–929 (2005).

Chapter III

Engineered metal-based microdevices for the isolation of CTCs

Chapter III

Engineered metal-based microdevices for the isolation of CTCs

3.1 Part I: *in vivo* cell capture using metal-based devices

3.1.1 Approaches to enhance the mechanical properties of the 3D microdevice

Altogether, *in vitro* and *in vivo* results from chapter II of this manuscript evidenced the need for microdevices with stronger mechanical performances than polymers. Even though several technologies have been recently developed in the field of additive manufacturing using materials as ceramics and metals,[1,2] those are still limited to ~20–50 µm in resolution, making them unsuitable for the fabrication of the holey membrane. More recently, a lithography-based process was proposed to create 3D nano-architectured metals with 100 nm in resolution,[3] which could potentially be adapted to our workflow. Another alternative could be the use of 3D printed glass,[4–6] an inert material which may offer advantages such as compatibility with the targeted medical needs.

At the stage of the project in which this technological need was identified, none of the above mentioned techniques was readily accessible in our lab facilities. However, another fabrication approach was suggested in collaboration with the electroplating specialists of our laboratory (David Bourrier, LAAS-CNRS). We proposed the implementation of a **multi-step electrochemical deposition of metal** to engineer **both the microdevice and the holding strip**.

Similarly to additive manufacturing techniques, the goal is the layer-by-layer addition of a metallic material onto an electrically conductive planar substrate. Metal ions can be deposited onto selected conductive regions of the substrate (cathode), immersed into an electrolytic bath, which are geometrically defined by a pre-patterned insulating material, i.e., photoresist, with a thickness determined by the deposition rate, **Figure 3.1a**.

A multi-step process was designed, **Figure 3.1b**, where the holey membrane first is fabricated onto a planar substrate with a thickness t_m. Subsequently, a second deposition forms the cylindrical architecture by growing a thick layer defined by the length of the cylinder L_C. In a final step, the resulting microdevice is released from the substrate. This engineered microdevice is then mechanically positioned onto the holding strip so that it can form a single 3D element where the holey membrane faces the upstream flow perpendicularly.

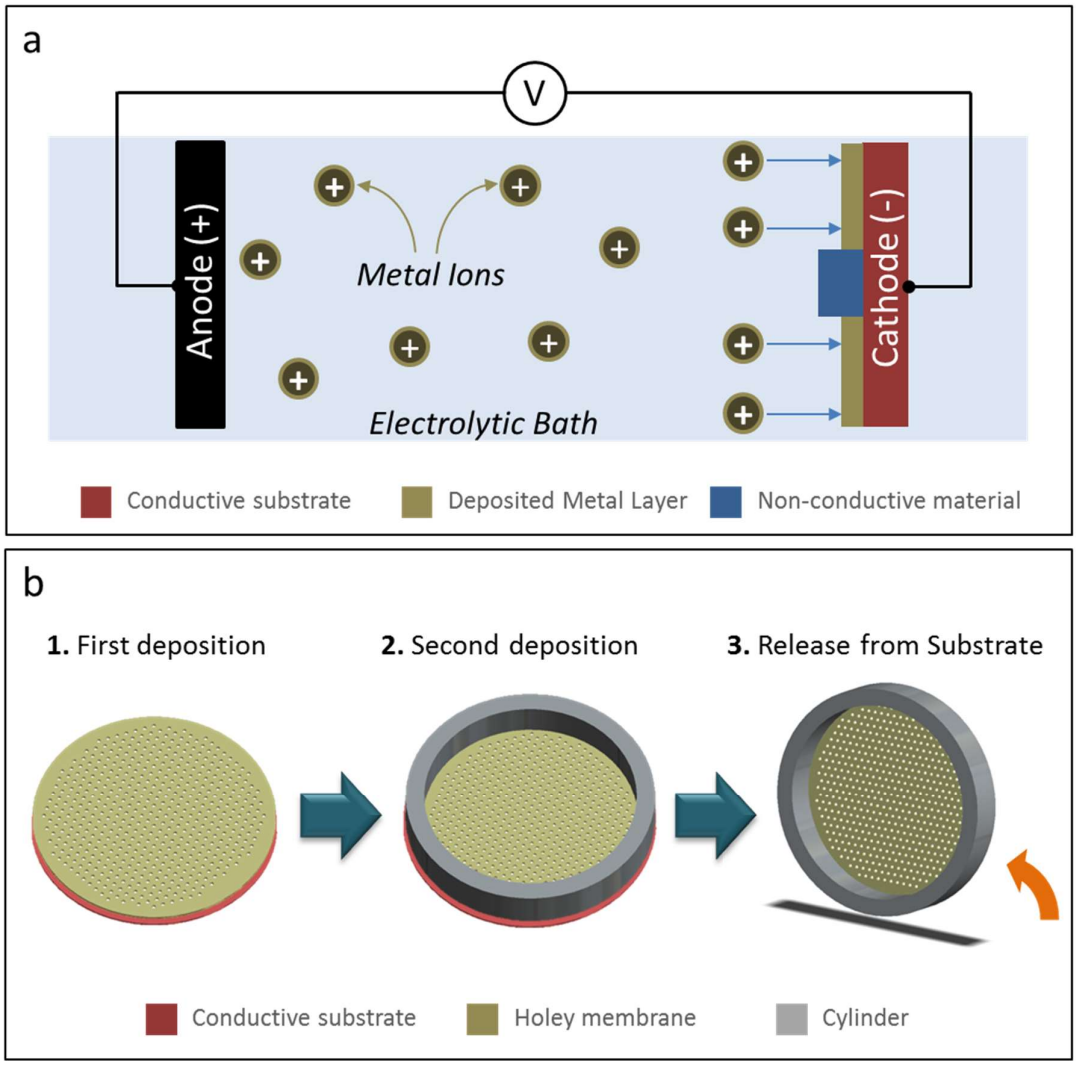

Figure 3.1 Schematic representation of the electrochemical deposition of metals. **a** The planar substrate is immersed into an electrolytic bath, acting as a cathode, and a voltage is applied in order to induce the electrochemical deposition of metal ions. **b** A simplified representation of the metallic microdevice's fabrication. A Three-step process is proposed, consisting of two independent depositions of metal, defining both the holey membrane and the cylinder, and the release of the microfabricated pieces from the substrate.

3.1.2 Strategies to form 3D-like devices

As above introduced, the electrochemical deposition allows conferring volume to planar architectures. Based on this, we imagined fabricating the microdevice and the strip during the same deposition process so that both pieces could adopt a 3D-like configuration similarly to the 3D microdevice fabricated in a polymeric material and thoroughly described in the previous section of this manuscript. Moreover, we also targeted designing this new generation of devices in a way that apart from performing cell capture, could be easily adapted to conventional microscopy techniques, thus enabling characterization of the captured biological material in depth, **Figure 3.2**.

We envisioned two strategies to reach a 3D-like configuration out from planar devices: a) A version allowing the mechanical assembly of up to six microdevices onto the metallic strip, **Figure 3.2a**. Both the microdevice and the strip were engineered with **complementary interlocking** joints, in a way that the microdevice could be mounted on the openings of the metal strip before cell capture, and then removed. Complementarily, b) A foldable version, **Figure 3.2b**, where both pieces, the strip and a single microdevice, were fabricated as a single planar substrate containing a **hinge-like joint** which allows the microdevice to be folded at 90° before cell capture, then folded back to its original position.

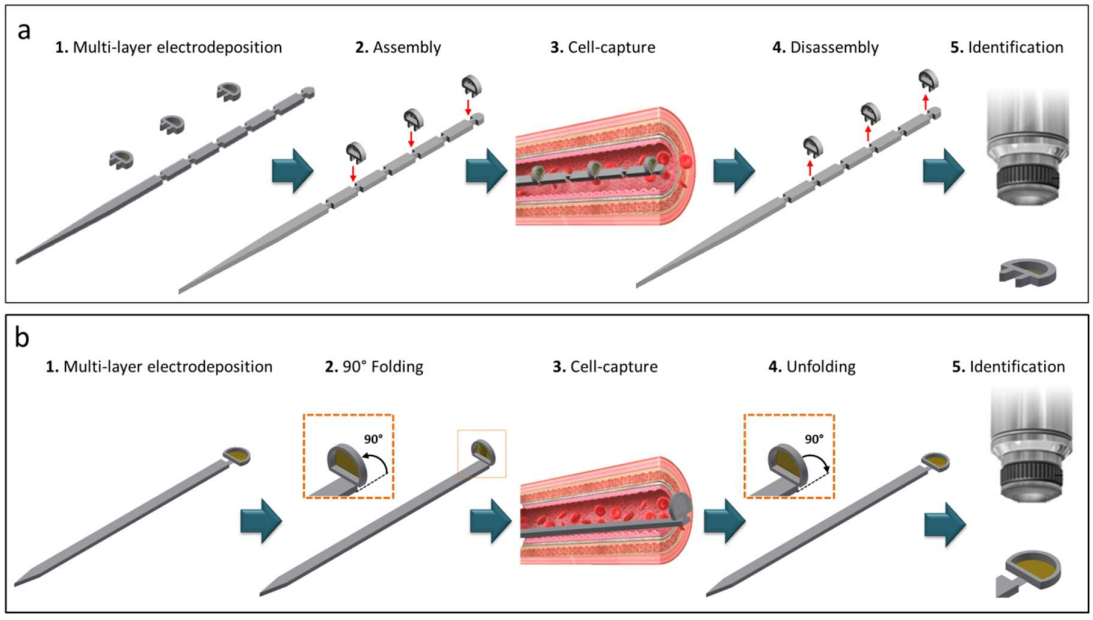

Figure 3.2 Proposed strategies to form 3D-like devices and their corresponding workflows. **a** Assembling version where independent microdevices are mechanically placed into the pre-fabricated openings of the strip. This design allows placing multiple microdevices onto a single strip. **b** Foldable version containing a single microdevice, which can be folded/unfolded thanks to a hinge-like joint.

3.1.3 Design constraints

The set composed by the metallic microdevice and the strip, for both the assembly and the foldable versions, was designed to fit into three different catheters sizes: 18G, 20G, or 22G (**Figure 3.3a**), foreseeing that larger devices would screen a larger amount of blood. We envisioned an ideal situation where the microdevice and the strip are fitting into the lumen of each of these catheters, and the whole set is positioned at the center of it, **Figure 3.3b**. The tolerance distance to avoid contact with the walls of the catheter was set to <60 µm. The geometry of the holey membrane was optimized to occupy the largest area of the lumen, possible so the coverage area of the holey membrane would be increased. Given this, the main constraint in terms of dimensions was given by the internal diameter of the targeted catheters.

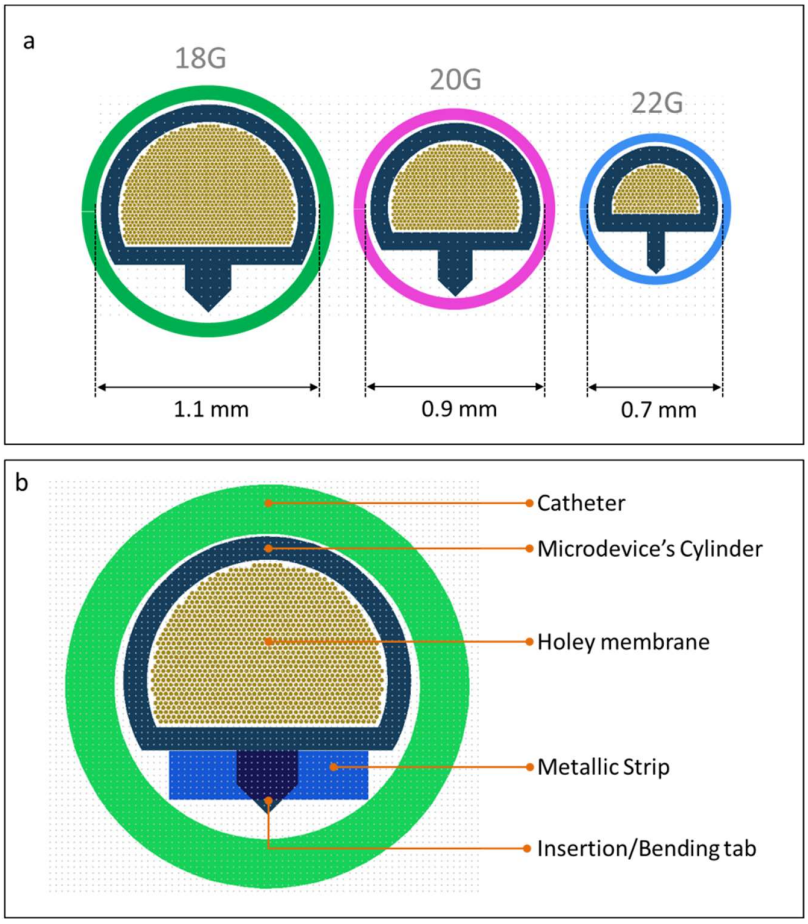

Figure 3.3 Inner diameter of targeted catheters and ideal positioning of the set composed by the microdevice and its holding strip. **a** The cross-sectional view of each catheter, where the microdevice is located within their lumen. **b** The microdevice and its holding strip must fit into the available lumen, while maximizing the coverage area of the holey membrane.

A second constraint was given by the technique used to define the deposition area, where the major challenge was established by the second deposition defining the microdevice's cylinder. The patterning of the insulating material was performed using UV photolithography, which limits obtaining high aspect ratio structures. For example, in order to obtain the expected length of the cylinder L_C=150 µm, it was required to have a minimum width of 75 µm, and an aspect ratio of 2:1, in order to ensure verticality of the walls and reproducibility. This dimension, in turn, defines the width of the walls constitutive of the cylinder t_C. Having thinner cylinder walls increases the effective area of the holey membrane, thus we targeted the minimum t_C=75 µm, which is approximately 7-fold the one of the polymeric microdevice. Other technological approaches, such as the LIGA process, could offer higher aspect ratios; unfortunately, this process was not available in our facilities.

In addition, and as a third constraint, we aimed at fabricating the microdevice and the strip using the same batch process. We deposited the layer corresponding to the cylinder along with the holding strip, so the thickness of the strips would be equal to the length of the cylinder, meaning 150 µm. Similarly to the polymeric microdevices, the size of the pores was also set to 12 µm.

For each of the proposed strategies, assembling and bending, we conceived designs composed by either a single tab or a double-tab, **Figure 3.4a**, in order to evaluate which of these options would offer improved mechanical properties and stability along different steps of the whole workflow. In addition to dimensions already fixed by the aforementioned constraints, some other parameters were established for the assembly version. The distance between each one of the microdevices was fixed to 1 mm, with a lateral margin of approximately 15 µm with respect to the strip openings, **Figure 3.4b**. Additionally, the total length of the strip was set to 11 mm. Given all these constraints, the geometrical dimensions for each catheter size were set as summarized in **Figure 3.4c**. Note that, for the bending version we tested two different bending tab lengths, denoted as H, 150 and 300 µm.

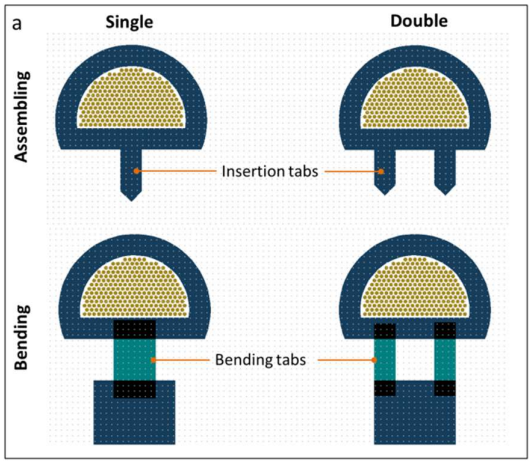

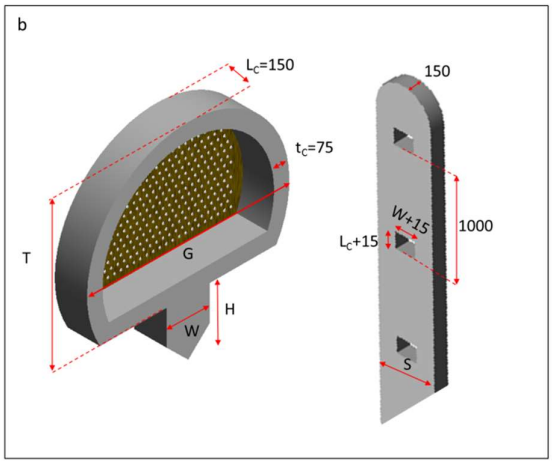

c

		18G						20G						22G					
		n	G	T	S	W	H	n	G	T	S	W	H	n	G	T	S	W	H
Assembling	Single	1303	940	700	600	200	180	693	740	554	400	150	180	247	540	374	290	75	180
	Double	1303	940	700	600	200	180	693	740	554	400	100	180	247	540	374	290	75	180
Bending	Single	1303	940	700	600	200	150/300	693	740	554	400	150	150/300	247	540	374	290	150	150/300
	Double	1303	940	700	600	200	150/300	693	740	554	400	100	150/300	247	540	374	290	75	150/300

Figure 3.4 Overview of design considerations. **a** Representative image evidencing the single and double tab version for each one of the designs. **b** Scheme depicting the overall dimensions of the microdevice and the holding strip. The image shows the design having a single tab, but it can be transposed to the double-tab version. **c** Table summarizing overall dimensions, in micrometers, for each catheter size. Schemes are not to scale.

3.1.4 Fabrication steps

Among different available materials for electrodeposition in our facilities, we selected Nickel. This metal is a widespread electrodeposited material and it has already been reported as a platform for isolation of CTCs and for cell culture of fibroblasts.[7,8] In practice, the microengineered devices were fabricated in a 5-step process, from which three steps correspond to UV photolithography and through-mask electrochemical deposition.

A three-layer mask was designed using CleWin software, **Figure 3.5**. The first layer (L1) defines the bendable tabs concerning the foldable design. In this layer, we also added identification labels in order to facilitate the recognition of the microfabricated devices once detached from the substrate. The second layer (L2) shapes the area corresponding to the holey membrane for both assembly and bending versions. An overlapping area, >20 μm, in between layers one and two was set to allow physical contact of these metal depositions; this only applies to the folding design, **Figure 3.5b**. The third layer (L3) defines the cylinder of the microdevice and the strip. Similarly, for the microdevice we established adhesion overlapping areas of a length >30μm between the second and the third layer. Regarding the bending version, an overlapping region was also defined to connect the bending tabs and the holding strip. Using this technique we were able to fabricate sets of >300 devices in a time span of 3 days.

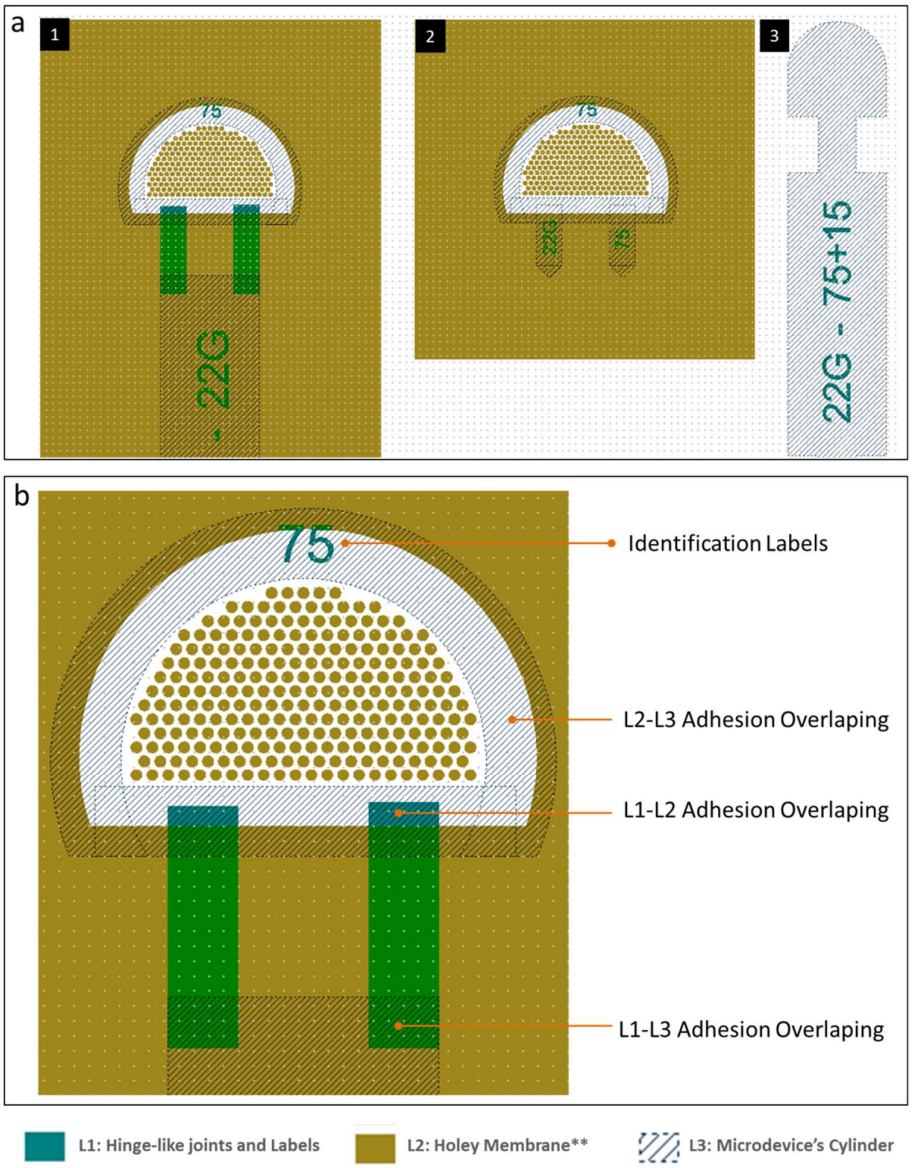

Figure 3.5 Representative images of the three-layer mask design. Layer color-code is shown at the bottom of the image, where L1 and L3 colors represent the area where Nickel is deposited. Conversely, L2 is represented by an inverted polarity**, where the colored area represents the insulating photoresist. The polarity of each layer shown here is only used as a visual example; the real polarity of each mask was selected according to the polarity of the used photoresist. **a** Particular examples of the bending version (1) and assembly version (2-3) for the 22G catheter design, evidencing the three-layer layout. The layout shown can be extrapolated to other catheter sizes, 20G and 18G. **b** Selected example, representing a 22G bending design, where identification labels and adhesion overlapping areas are shown.

The whole fabrication process was performed in a cleanroom environment and is summarized as follows:

1. ***Preparation of the substrate***. A 4 inches Silicon wafer was cleaned using O_2 plasma (800W, 5 min) and subsequently, 50 nm of Titanium followed by 200 nm of Copper were deposited as seed layer.
2. ***Deposition of hinge-like joints and identification labels (L1)***. A positive resist, AZ4562, was spin coated onto the wafer in order to obtain 10 µm thickness and then baked for 2 min at 105°C. UV-light was then exposed through the mask in order to define the L1 pattern, and was developed using MFCD26. A plasma cleaning step was performed to ensure the removal of the non-polymerized resist. The patterned wafer was then immersed into the electrolytic bath (NB SEMIPLATE NI 100) in order to perform the electrodeposition of 10 µm of Nickel (0.5 A dm^{-2}, RENA electroplating tool). The resist was then removed using acetone.
3. ***Deposition of the holey membrane (L2)***. A plasma cleaning step was further performed (CF_4+O_2) during two minutes at 200 W, in order to ensure both the removal of the photoresist used to define L1 layer, and a good adhesion of the new photoresist layer. In a similar fashion to L1, a new 10 µm layer of AZ4562 was deposited onto the wafer, patterned to define L2, and developed to clear non-polymerized regions. Given the importance of this layer, this step of the process required optimization of the UV-exposure dose, in order to reach an acceptable adhesion and verticality of the photoresist pillars defining the pores of the holey membrane, **Figure 3.6a**. Subsequently, 5 µm-thick Nickel was grown (NB SEMIPLATE NI 100 solution and 0.5 A dm^{-2}, RENA electroplating tool), and the remaining resist was then removed. An inspection at the end of this step was performed in order to verify the expected specifications were reached, **Figure 3.6b**. The mean diameter of the pores was measured at D_p=11.88±0.31 µm.
4. ***Deposition of the microdevice's cylinder (L3).*** We performed a plasma cleaning step (CF_4+O_2). We then laminated two layers of Dry Film photoresist (WBR-2100) in order to obtain a 200 µm-thick layer, which was UV patterned using L3 mask and developed with Na_2CO_3. Again, a plasma cleaning step (CF_4+O_2) was carried out to ensure the removal of the non-polymerized photoresist. This step was critical to remove residuals inhibiting the adhesion between L2 and L3 of Nickel, and propitiating detachment of the holey membrane, **Figure 3.6c**. Then, we deposited a 150 µm-thick layer of Nickel material (NB SEMIPLATE NI 100 solution and 2 A dm^{-2}, RENA electroplating tool), and the remaining photoresist was removed with NF52 at 1% heated to 90°C.
5. ***Release from substrate and etching of the seed layer***. Finally, the silicon wafer was chemically etched using KOH solution, so microfabricated devices were released. The seed layer was also removed, first using HF at 5% against Titanium and a mixture of 1% H_2O_2 + 1% H_2SO_4 + 98% H_20 to chemically etch the Copper layer.

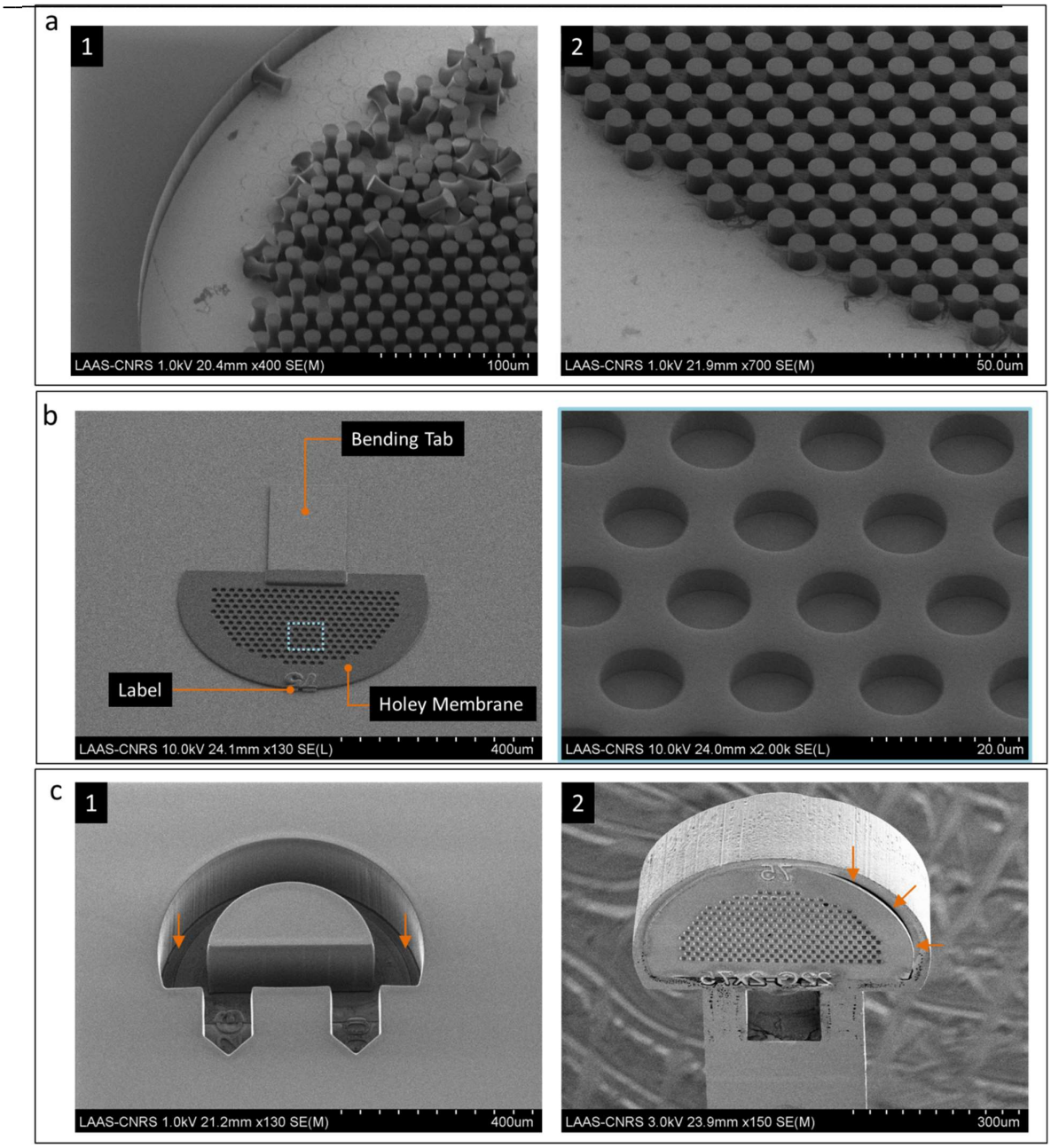

Figure 3.6 SEM micrographs of the patterned L2 photoresist and the corresponding electrodeposition of Nickel. **a** Image (1) depicts a case where both a poor adhesion and pillars with non-vertical walls are observed. We favored pillars having vertical walls (2), constant diameter along their thickness, so pores would have a well-defined dimension. **b** Magnification on a 22G microdevice, bending version, where L1 and L2 Nickel depositions are observed. The insert evidences the roundness of pores constitutive of the holey membrane. **c** After development of the non-polymerized resist, a thin layer of it was remaining on the surface (1) causing adhesion issues between L2 and L3 layers (2) of Nickel deposition. Representative images of a 22G microdevice, assembling version (1) and bending version (2).

3.1.5 Assembly and Bending of microfabricated devices

After releasing micropieces from the substrate, the latter were intensively rinsed with water and manually separated. Regarding the version to be assembled, capture microdevices were first manually placed into a customized holder under optical inspection. This holder allowed keeping the insertion tabs pointing up, **Figure 3.7a1**. In a second step, the openings of the strip were made to coincide with the insertion tabs, and by applying a gentle pressure on it, microdevices and strip were mechanically locked, **Figure 3.7a2**. In order to ensure fastening, a droplet of EP 630 glue (ratio 100:35) was deposited on the joint area, and cured at 80°C. At this step, controlling the size of the droplet was critical to avoid contamination of the holey membrane with the glue. The whole set was removed from the holder and inspected using SEM in order to verify the correct positioning of the microdevices and absence of glue contamination, **Figure 3.7c**. Note that, the handling of 22G microdevices was challenging given their reduced dimension and manual assembly, thus the procedure was time-consuming and required a lot of care. In a future, this procedure could be automatized to allow a more repeatable and systematic procedure.

Concerning the bending version, a single microdevice was first placed at the edge of a flat surface, **Figure 3.7b1**, in order to have it suspended and allow free vertical access. Second, under optical inspection and with the aid of tweezers, we manually applied a gentle pressure directly on the outer border of the microdevice in order to make it fold at 90° approximately, **Figure 3.7b2**. Given the mechanical properties of the 10-µm thick bending tabs, the microdevice kept a fixed position at an angle ranging from 70 to 85 degrees, showing a spring-like behavior. Pushing the microdevice beyond this angle induced high stress at the join regions resulting in fracture. This behavior was mainly observed in the design having 150 µm length tabs. Along these procedures, we were careful not to touch the holey membrane to avoid its damage. We also performed SEM inspection to verity the positioning and absence of microdevice degradation due to this procedure, **Figure 3.7d**. Similar to the assembly version, this manual procedure could be automatized in a future.

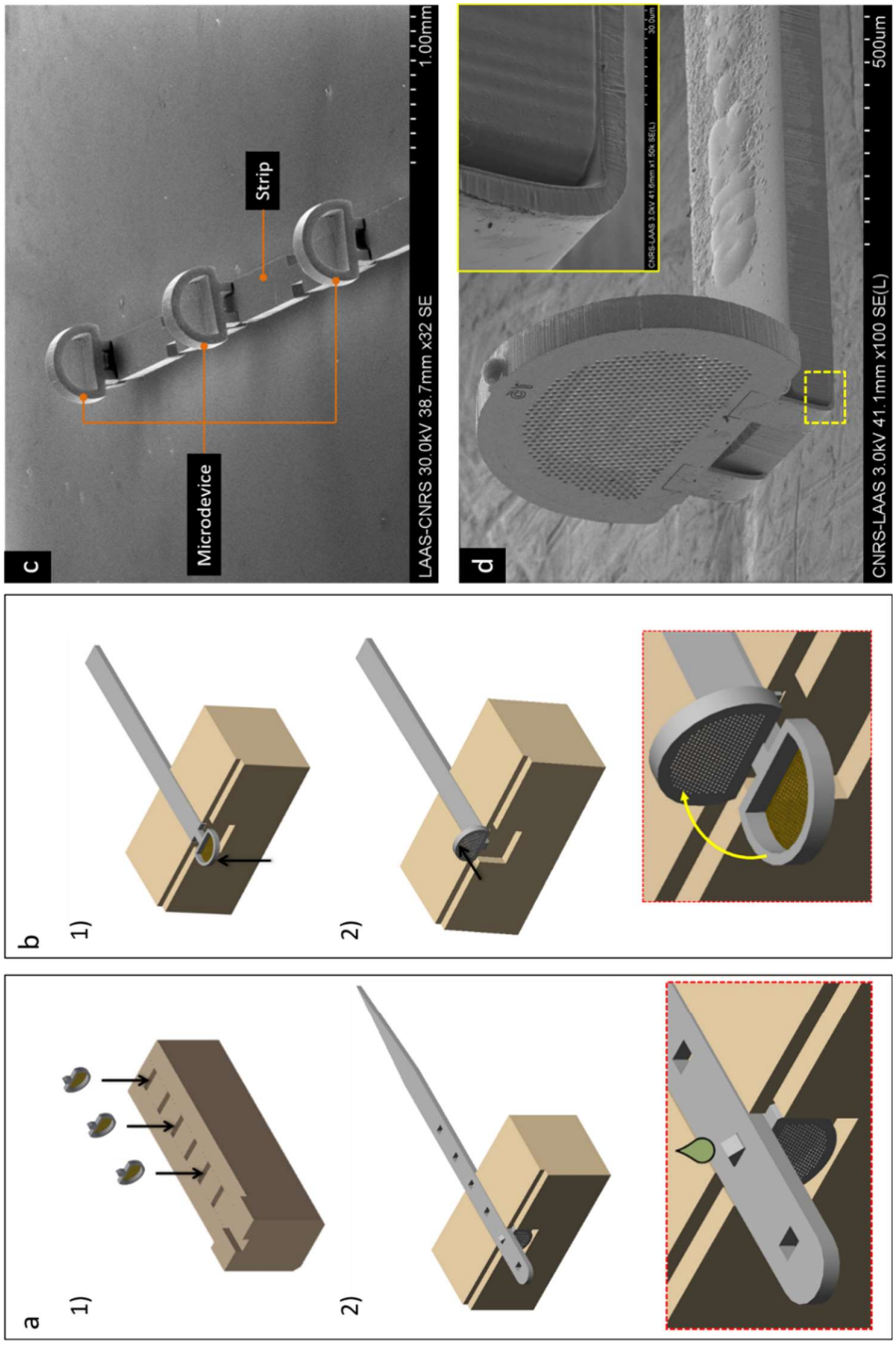

Figure 3.7 Assembling and bending of microdevices, in order to form 3D-like configurations. **a** Cross-sectional schematic representation of the manual assembly of devices, where first, microdevices are placed into the slots (1) and the strip is then aligned on top (2). **b** Schematic representation of the manual bending of a single microdevice. The microdevice is placed at the edge of a planar substrate (1) in order to allow its vertical access for bending (2). **c** Scanning electron micrograph of a strip containing three 22G microdevices after assembly. **d** Scanning electron micrograph showing the rear area of a 20G microdevice with bending tabs of 150µm. The insert shows a magnification of the tab-strip joint area.

3.1.6 Cell capture using Nickel microdevices: *in vitro* assessment

3.1.6.1 Cell capture from cell culture medium

In order to evaluate the cell capture capability of this new generation of microdevices, we first evaluated its integrability onto commercial medical consumables. As explained in section 3.1.3, Nickel microdevices were originally designed to be inserted through plastic catheters. However, given the restricted tolerances we established in the overall dimensions during the designing process, the microdevices did not easily fit into the corresponding catheter's lumen. Thus, we decided to continue using the double-needle insertion system early introduced in section 2.3.1, following the same assembling strategy. This setup allowed working directly with 20G and 22G designs and in a limited manner with 18G design using the fluidic platform introduced in section 2.3.2.

Given the abovementioned limitations, we particularly focused on using a small size design, i.e. 22G, for a first *in vitro* experimental set, mainly foreseeing its *in vivo* utilization in animal models. As a first step, we used PC3 suspensions in cell culture medium. Early experiments evidenced that Nickel material was auto-fluorescent, at low levels, in the emission range of DRAQ5. For this reason, in order to avoid a possible overlapping of signals during fluorescence characterization, we used Hoechst dye as a second label, which stains the nucleus of cells. Moreover, unlike the polymeric microdevice presented in section 2.2, the observation in real-time of capture events was not possible at the time of experiments due to the non-transparent properties of the metal.

For this set of experiments, we used a single metallic microdevice onto each strip keeping v_{min} as flow condition for 10 min, within the 3-mm PDMS channel, **Figure 3.8a**. At the time of experiments, we were careful of positioning the capture microdevices in the center region of the channel cross-section. Both versions, assembling and bending, having a single microdevice per strip, showed similar capture performances under similar experimental conditions. Results below presented encompass both designs.

We decided to prepare suspensions below 5000 per mL in cell concentration in order to be proximal to reported patient's CTC counts, section 1.6. As for the polymeric microdevice, we verified cell morphology after trapping at this cell concentration. As shown in **Figure 3.8b**, cell morphology is in agreement with the observations of captured cells using polymeric microdevices, section 2.2.2, cancer cells adhered to the holey membrane keeping a spherical shape and developing pseudopod protrusions. Moreover, cells also remained attached to the surface of the holey membrane during subsequent removal from the fluidic channel, cell fixation, and characterization steps after trapping. In agreement with previous observations, most of the trapped cells are located at the surface of the holey membrane and not within the pores. The number of captured cells was approximately C_c=60.

Although here and in following sections we just focus on results obtained using 22G design, some experiments were also performed using 20G and 18G. Those are summarized in Appendix B, and they seem to have an increase in the number of captured cells. However, further experiments would be required to conclude. Moreover, 20G and 18G microdevices, are larger in size which make them less compatible with routine venipuncture procedures.

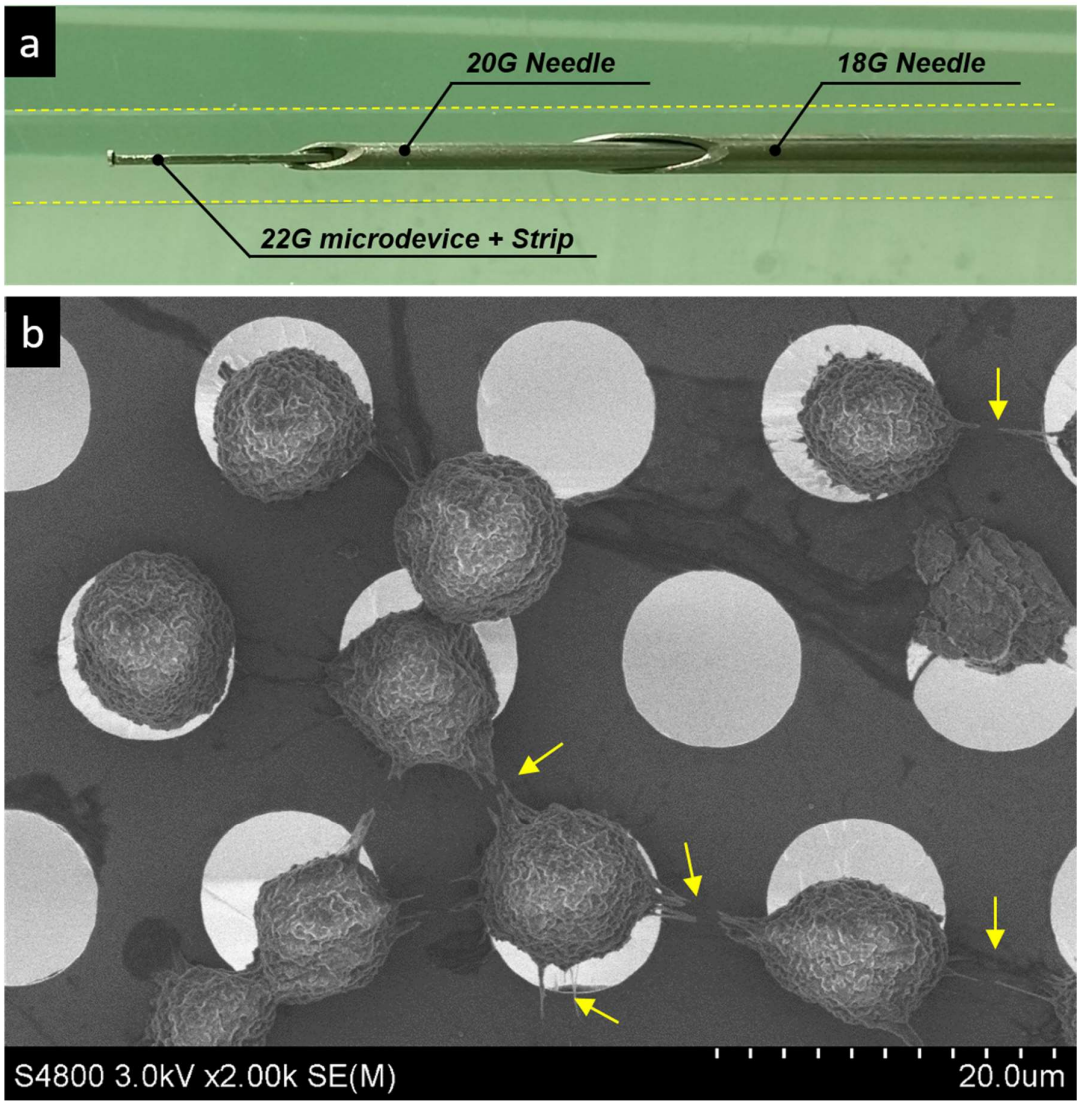

Figure 3.8 *In vitro* setup for cell capture assessment and cell morphology after capture. **a** Image of the double-needle insertion system having a 22G-bending device. The overall assembly is observed within a 3 mm PDMS channel. The microdevice is at the end-tip of the strip, and yellow dashed lines depict the walls of the 3 mm channel. **b** SEM image of typical cell morphology observed after trapping. Yellow arrows point to some of the cell protrusions observed.

For cells in suspension at a lower concentration, 1000 cells per mL, we found that the average number of captured cells was C_C=11.2 ± 6.38 (mean ± SD, n=5). We just considered those cells expressing both GFP and Hoechst staining, **Figure 3.9a**, and then further identified them by SEM. We were also able to isolate cells from a suspension at 100 cells per mL where the mean number was C_C=6 ± 1.73 (n=3), **Figure 3.9b**. Along this line, we also tried lower concentrations, in the range of 10 cells per mL, but none of the experiments clearly evidenced the trapping of PC3 cells.

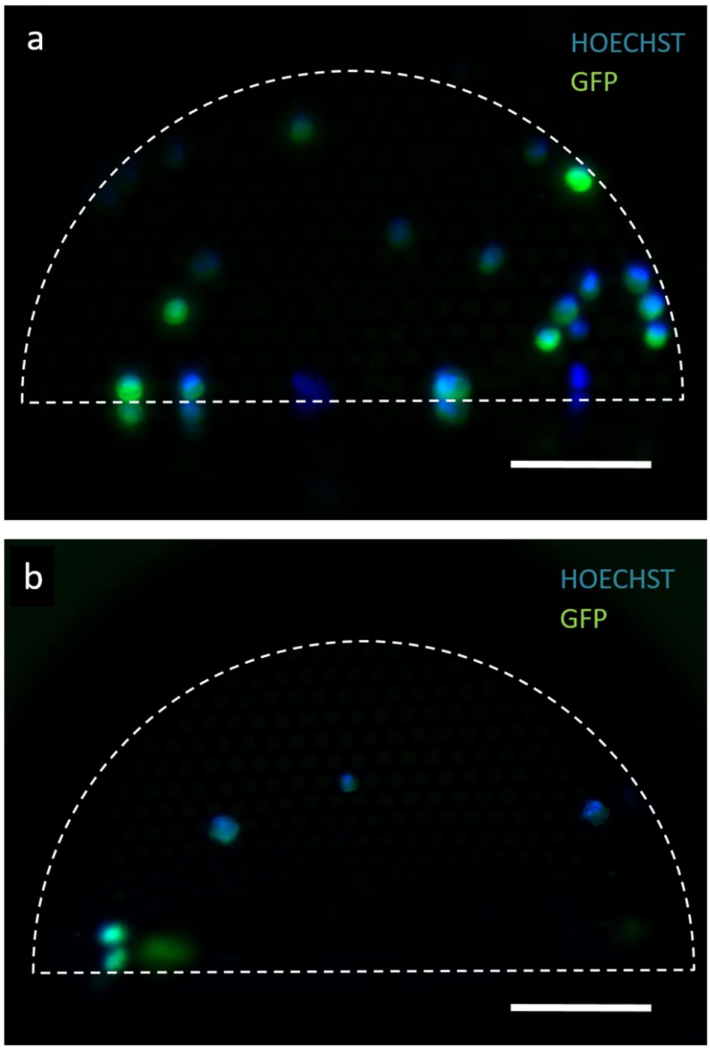

Figure 3.9 Fluorescence images of selected 22G devices evidencing the trapping of PC3 cells, expressing GFP and Hoechst, from cell culture medium suspensions. **a** A total of 22 cells are observed within the area corresponding to the holey membrane for a cell suspension containing 1000 cells per mL. **b** Five cells are observed in a sample processed containing 100 cells per mL. Dashed lines depict the holey membrane area. The fluorescent spots outside of the dashed lines are reflections due to the wall. Scale bars are 100 µm.

3.1.6.2 Cell capture from whole blood

Before evaluating cell capture, we first assessed the degree of contamination within the holey membrane when processing whole blood samples with no cancer cells. Microdevices were exposed *in vitro* to a whole blood flow at v_{min} during 10 min. Samples were then rinsed under the same flow conditions using 40-45 mL of cell culture media, as performed all along this manuscript.

Typical images of the holey membrane after whole blood exposure are observed in **Figure 3.10a-d**, where no clogging of pores was identified. We mostly observed platelets adhering to the holey membrane surface and a few blood cells accumulating in some pores, probably corresponding to WBCs. When the rinsing step was poorly performed, meaning using a lower volume of medium, a relatively higher degree of blood cell contamination was observed, **Figure 3.10e-f**. For the case of RBCs, we believe this is mainly resulting from residual accumulation and not from physical trapping. The degree of contamination with blood cells varied among experiments, mainly due to blood donor-dependent factors.

In a second set of experiments, we addressed the capture performance of a single 22G metallic microdevice from spiked cells in whole blood. Using a cell concentration of 1000 PC3 cells per mL in whole blood, we identified a mean value of C_C=2.83 ± 2.45 (n=5), where those cells were first identified by fluorescence microscopy, GFP and Hoechst emission, and second by SEM. In terms of fluorescence signal intensity, Hoechst had a higher intensity than GFP. These images were used as reference to identify their positioning within the holey membrane using SEM, **Figure 3.11a**.

We observed captured cells exhibited a similar morphology as the one from culture medium samples, **Figure 3.11**. Contrary to cell culture medium experiments, under blood flow conditions, trapped cells seem to be preferentially within pores. This observation could be associated to a higher transmembrane pressure. Additionally, in some cases, the isolated cells were found at the surface of the holey membrane with a high degree of platelet addition as observed in **Figure 3.11b**.

We also evaluated PC3 capture from whole blood at lower cell concentrations, i.e. 100 cells per mL. Those experiments did not reveal capture of cancer cells. We believe that at this range of concentrations, a longer screening time is required. Unfortunately, longer experiments were not performed, thus, further studies are still required.

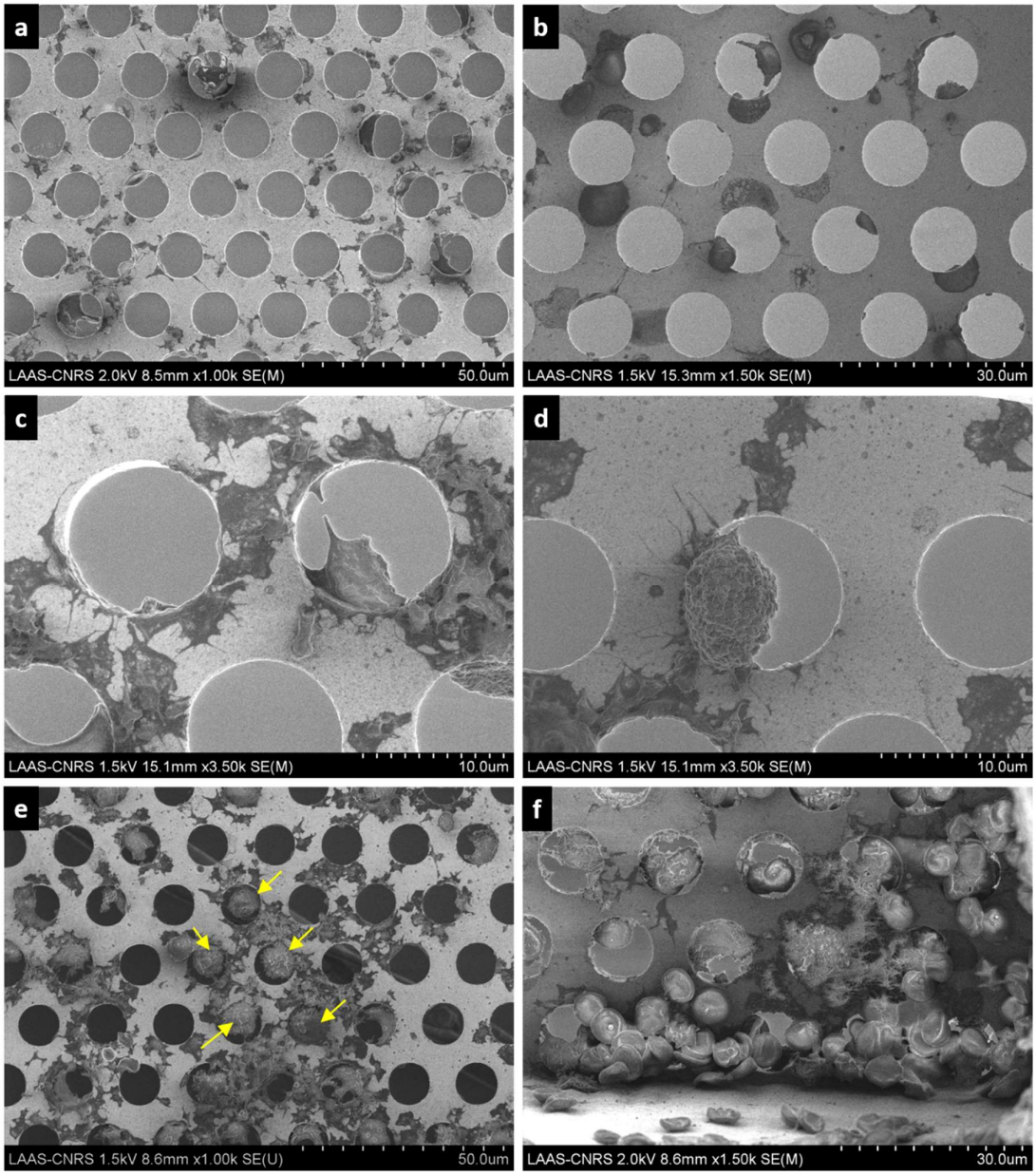

Figure 3.10 Scanning electron micrographs of different areas of the holey membrane after being exposed to a flow of whole blood. **a-b** Typical cases where no pore obstruction is observed. **c** Platelets adhering to the surface of the holey membrane are commonly found. **d-e** In some pores we found cells Hoechst- and GFP-negative alike WBCs, possibly trapped by their physical dimensions. **f** Accumulation of RBCs associated to a limited rinsing after blood exposure.

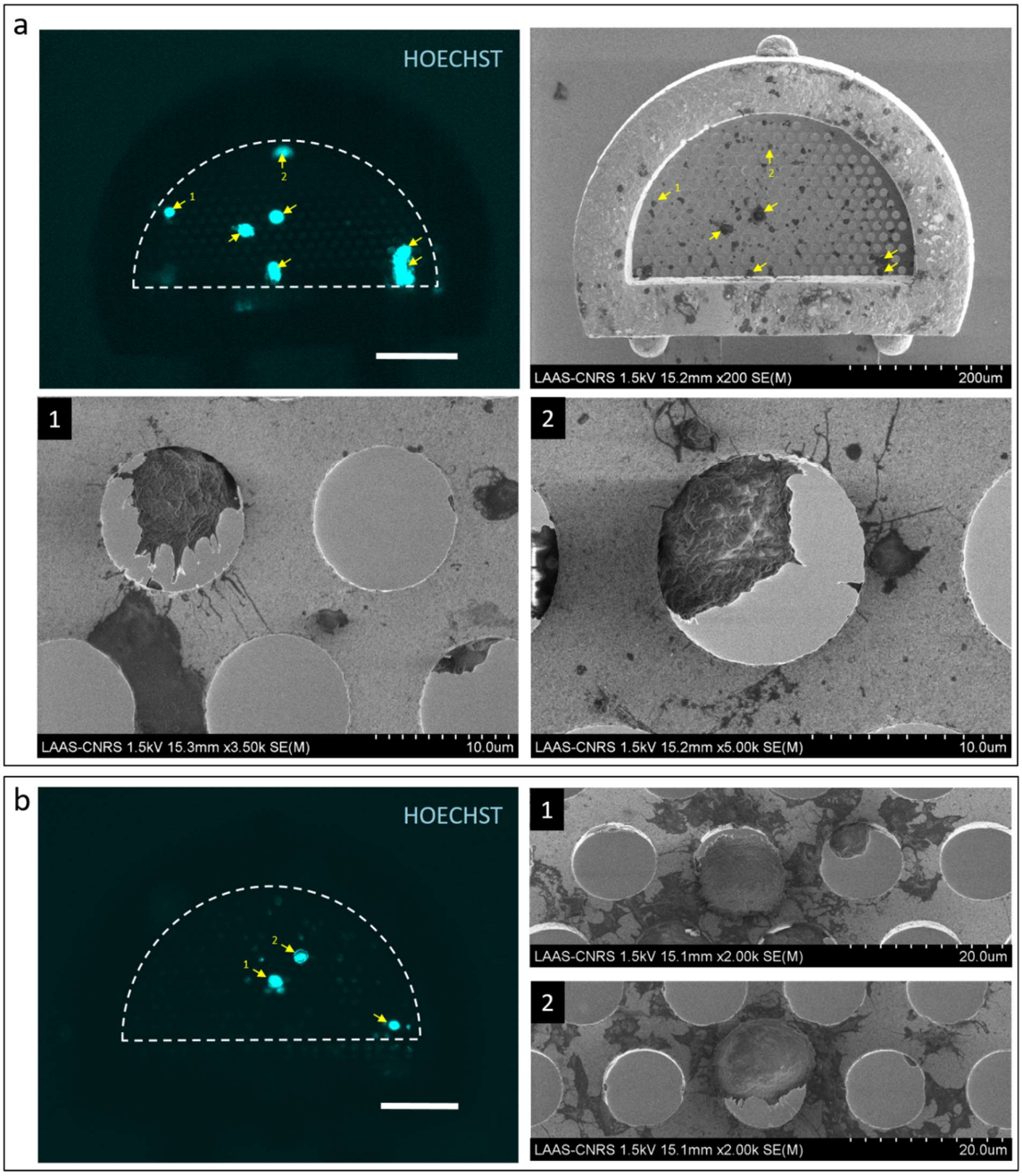

Figure 3.11 Fluorescence and SEM images of selected 22G samples evidencing the trapping of PC3 cells from whole blood. The PC3 concentration was 1000 cells per mL of blood. **a** Seven PC3 cells Hoechst stained were identified and confirmed by SEM inspection. The inserts (1) and (2) show two PC3 cells, whose morphology was recognized within the pores. **b** Three PC3 cells were identified in this sample, where insets (1) and (2) show cell morphology. A relatively high degree of platelet adhesion was observed at the surface of the holey membrane surrounding the cancer cells. Scale bars are 100 µm.

These results taken altogether, we concluded that the sensitivity threshold for a single 22G metallic microdevice is 1000 PC3 cells per mL of blood. This threshold is in the same range as the one obtained using polymeric microdevices, under same flow conditions and using the 1-mm fluidic platform. Considering that a 22G metallic microdevice has 1.8-fold more pores than the polymeric one, this conclusion was at first counterintuitive, since we were expecting that a greater number of pores will lead into a greater number of trapped cells.

We hypothesize this cell capture performance could be associated with the microdevice's geometry, particularly to L_C=150µm. Based on numerical models, in the case of polymeric devices the length of the cylinder allows the stabilization of the flow within the microdevice given the specific cross-sectional area of the holey membrane. Under these geometric and flow constraints, all velocity vectors point towards the holey membrane, as observed in **Figure 2.14b1** of chapter II. Conversely, for metallic microdevices, the equivalent numerical model reveals that velocity vectors do not point towards the holey membrane, at least along the first half of L_C, **Figure 3.12c**. Thus, we believe that enlarging L_C while keeping the current cross-sectional holey membrane area could result in flow stabilization. However, from a technological standpoint, the optimization of the corresponding photolithographic step would represent a bottleneck to overcome.

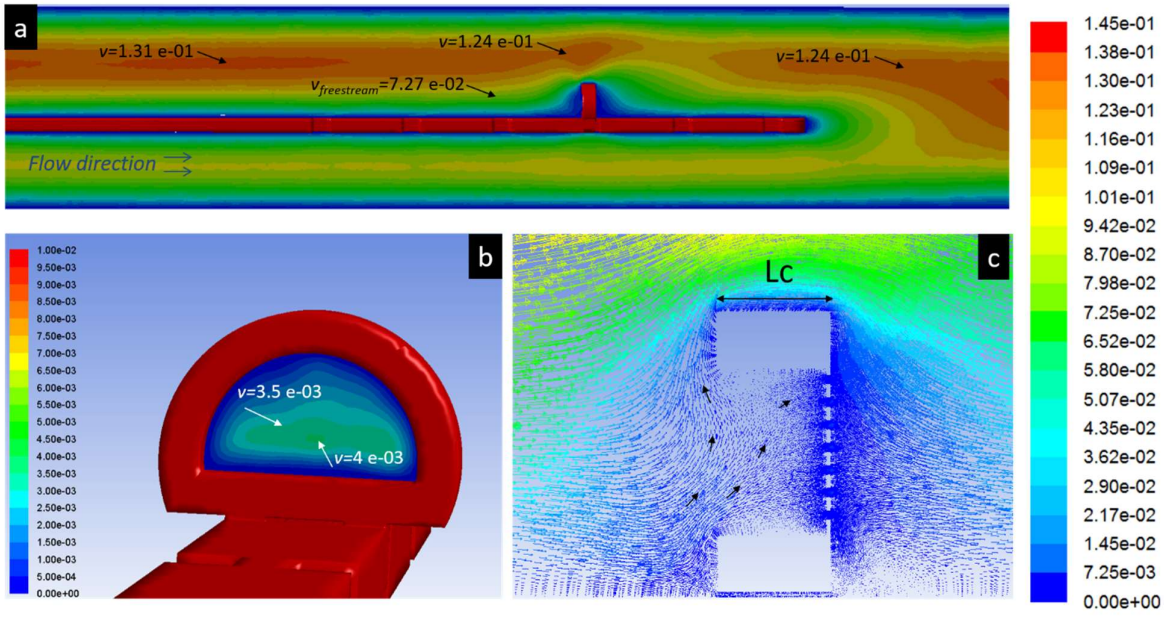

Figure 3.12 Fluid dynamics of a single 22G microdevice onto the strip and within a 3-mm channel. The velocity within the channel is v_{min} and the fluid model is water. However, the observations also apply for Newtonian blood as fluid, with even reduced velocities within the microdevice. **a** Longitudinal section of contours of velocity magnitude along the strip region. Representative velocities are shown. **b** Representative velocities found within the microdevice. **c** Vectors of velocity magnitude showing a longitudinal plane along the microdevice. Black arrows highlight some selected vectors to better visualize their direction. Color maps are in m s^{-1}.

If the patterns of velocity magnitude hold true in fluidic experiments, this phenomenon could mean that fluid streamlines did not follow straight paths, resulting in either an increase in the fluid transit time or fluid backflow, in the worst-case scenario. We believe this phenomenon could be in close relation with a reduced velocity at the freestream and within the microdevice, as observed in **Figure 3.12a-b**, and associated with an adverse pressure condition in the same region. However, our data is not conclusive enough to provide a comprehensive explanation of the fluid dynamics along the channel and within the microdevice. These observations can serve as a basis for future improvements in the geometric design of the device in order to increase the volume of liquid screened.

3.1.6.3 Cell capture from whole blood using multiple microdevices per single strip

From the conception stage, we envisioned placing multiple microdevices per strip in order to increase the probability of cell capture. The assembled version allows the assessment of this feature; consequently, we assembled strips having **three microdevices in series,** **Figure 3.13a**. Three 22G microdevices were placed onto the strip with 2-mm interdistance. A distance that would allow reducing the disturbances of the flow before the next microdevice. From a technical standpoint, the whole process of manual assembly, introduced in section 3.1.5, did not yield a numerous amount of usable devices, facing issues in handling, gluing and alignment. Despite this poor yield, we were able to perform *in vitro* evaluation of cell capture using this type of devices adapted to the double-needle insertion system.

We used a concentration of 1000 cancer cells per mL of blood, under the flow conditions used as a standard along this manuscript. From this experiment, we identified a total amount of C_C=7 PC3 cells distributed among the three microdevices, **Figure 3.13b**. According to our previously established protocols, we just considered as a PC3 cell that express both GFP and Hoechst, and confirmed by SEM inspection. The cell distribution among the three devices was one single cell for D1 and three cells for each one of the consecutive devices, D2 and D3.

A direct comparison in C_C between single and multiple microdevices, C_C=2.83 ± 2.45 and C_C=7 respectively, suggests that integrating several devices per strip could potentially result in the capture of a larger amount of cancer cells. However, the limited data here presented does not allow the possibility to quantitatively prove it, thus further experiments are required.

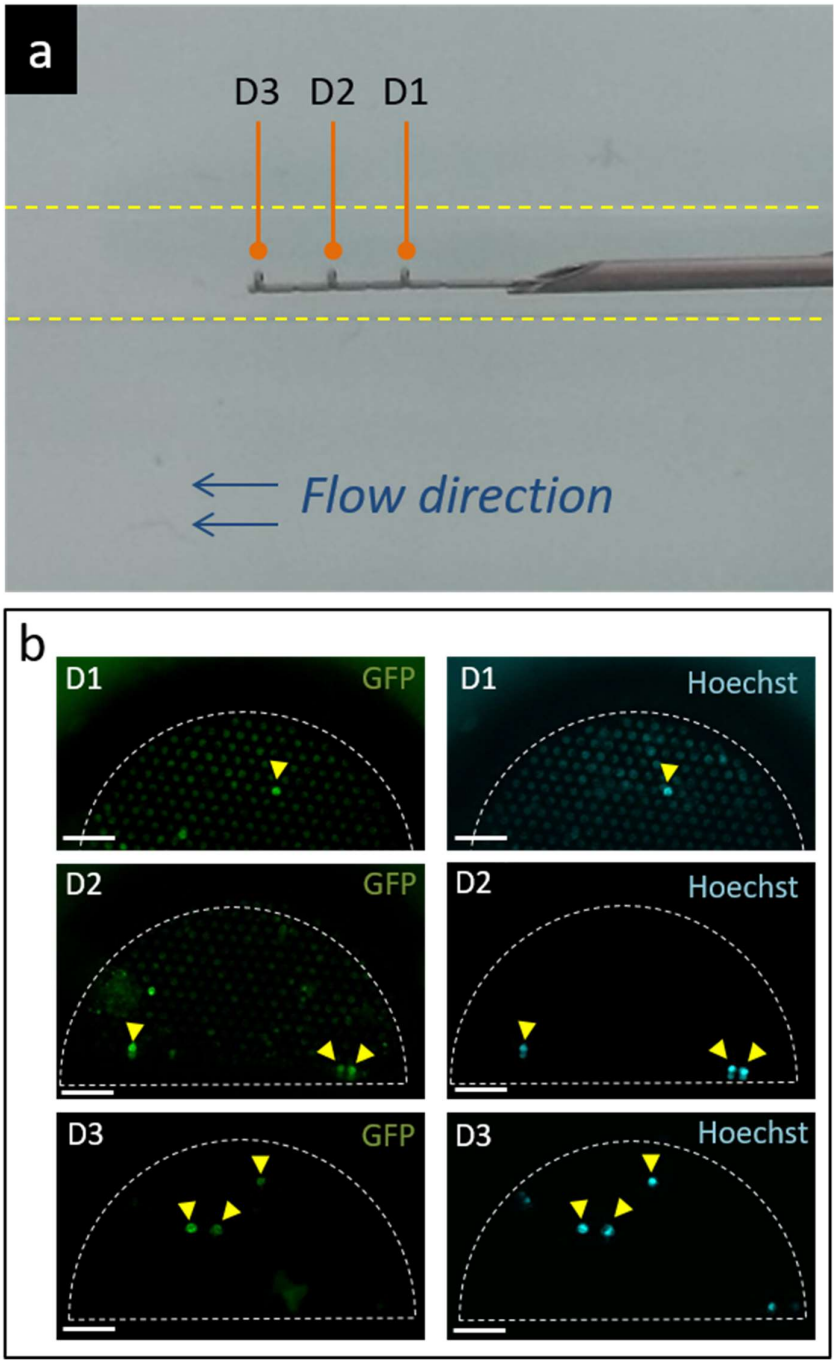

Figure 3.13 PC3 capture from whole blood using three microdevices per strip. The cell concentration used was 1000 cell per mL of blood. **a** Image showing the positioning of the micrcodevices with respect to the direction of the flow and with respect to the 3-mm channel. **b** Identification of captured cells by fluorescence imaging. Captured cells are indicated with arrows. The first device facing the flow, D1, evidenced the capture of a single cell, while the second (D2) and third (D3) devices captured three cells respectively. Scale bars correspond to 50 µm.

3.1.7 Cell capture using metal-based devices: in vivo assessment

As a last stage of this part of the project, we programmed a new set of in vivo experiments. Our main objective was to demonstrate the capture of true circulating cancer cells, driven in blood circulation by the heart. A second objective was to confirm the robustness of metal-based capture microdevices to withstand the whole procedure. A third one, was to determine whether our *in vitro* findings would be transposable to an *in vivo* setting, in terms of cell capture.

We decided to use rats as animal model, given our previous experience using animal models as explained in section 2.3.2. For this set, four male rats were subjected to surgical intervention ranging from 317 to 338 g in weight with an estimated blood volume summarized in **Table 3.1**, considering 64 mL per kg of body weight. The animals were intervened in the same order as shown in **Table 3.1** over two days. Animal experiments were conducted under the guidelines of animal care, at the zootechnics platform of the University-affiliated Hospital of Rangueil (CHU Rangueil) in Toulouse, and with the support of Denis Calise for the surgical intervention.

Capture microdevices used for this set were from the assembled version, placing three microdevices on each strip. The strips were adapted to the double-needle insertion system as performed *in vitro*. Hereinafter, this whole assembly will be referred as the intravascular device (IVD). Before surgical intervention, capture microdevices were pre-rinsed in counter flow using 3-mm channels, with 25 mL of ethanol followed by 25 ml of cell culture medium, this in order to avoid air bubbles in the microdevice region. Intravascular devices were maintained in culture media prior to being introduced into the animal's vein.

Initially, we aimed to inject PC3 cells in suspension within the animal's body in order to obtain an approximate concentration of 25 000 cells per mL of blood in circulation. In order to achieve so, we prepared cell suspensions of Hoechst-stained PC3-GFP cancer cells at ~$1x10^6$ cells per mL of culture medium in a total volume of 500 µL.

All animals were independently subjected to a pre-surgical preparation using O_2 with 4% Isoflurane and an injection of Buprenorphine (50 µg per kg), and they were kept under anesthesia (O_2 with 2% Isoflurane) during the whole intervention. We targeted performing cancer cell capture at the hepatic vena cava, with a mean diameter of 3.2±0.1 mm,[9] whereby a surgical procedure was required, **Figure 3.14**. A xyphopubic laparotomy was performed, which mainly consisted in an incision in the abdominal area. For rats 1 and 2, cells were injected intracardially through the left ventricle, while for animals 3 and 4, a rodent catheter (PE10) was pre-placed in the **carotid artery** (**Figure 3.14 inset 1**), through which the injection of cancer cells was performed at the required moment. Animals were heparinized (40 UI), except for rat 1, before exposing the capture microdevices through the inferior vena cava.

Once the surgical procedure was performed, the vena cava was punctured with the outer needle of the double-needle insertion system (**Figure 3.14 inset 2**) while capture microdevices were at the retracted position, meaning that they were not exposed to the bloodstream at this initial stage. Immediately after, the PC3 cell suspension was injected in the selected region as abovementioned. Approximately a minute after cell infusion, the capture microdevices were exposed to the blood flow using the plunger of the syringe, for a time span of 3 minutes. After this exposure time, microdevices were retracted into the puncture needle and the intravascular device was removed from the vena

cava. Immediately after retrieval, the intravascular device was inserted into an empty 3-mm fluidic channel where microdevices were exposed and rinsed with 50 mL of culture medium in order to remove the excess of blood. With respect to the animals, a volume of 500 µL of blood was extracted from the left femoral vein as control to verify the presence of PC3 cells within the circulation. Finally, animals were euthanized by a lethal injection with pentobarbital sodium.

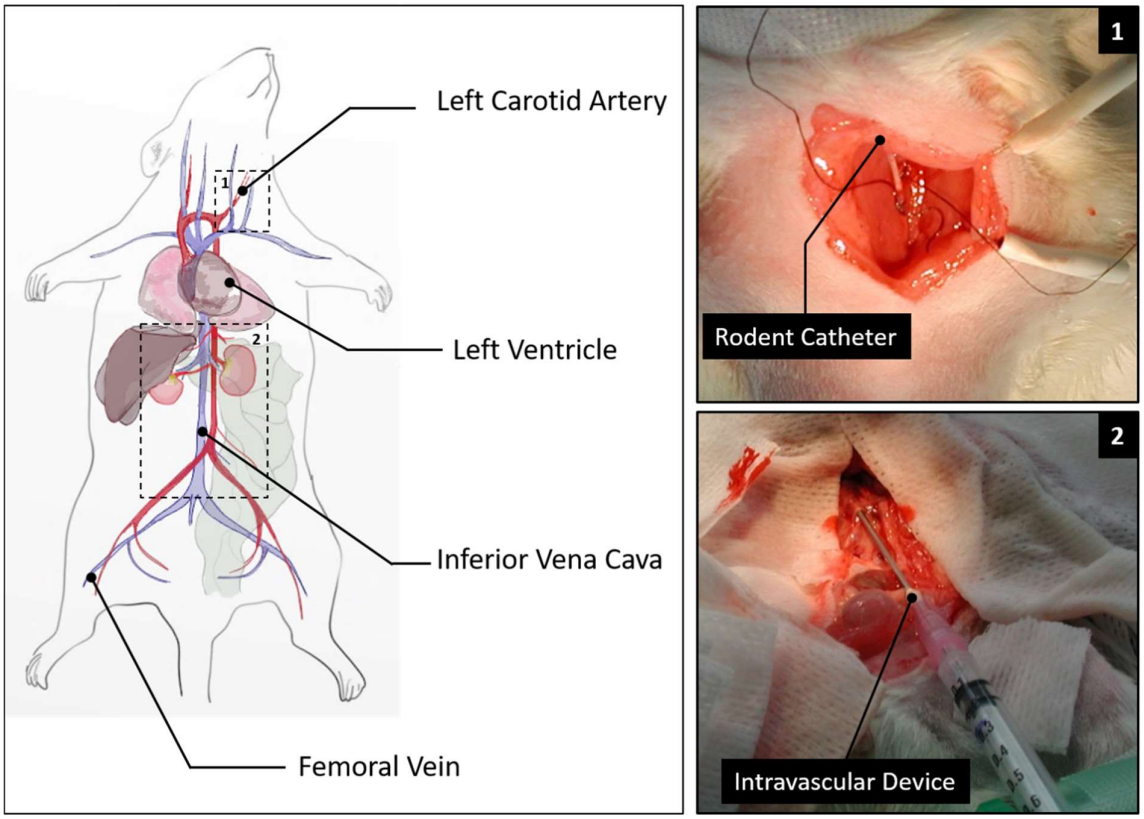

Figure 3.14 *In vivo* capture of PC3 cells using an intravascular device in a rat as animal model. The schematic diagram of the surgical intervention shows the intervention sites. Insert (1) corresponds to the left carotid artery where cancer cells where infused, and insert (2) shows the accessing of the intravascular prototype within the vena cava.

In a subsequent step, microdevices were fixed, dehydrated, and let dry in air conditions for a few hours. Afterwards, strips and microdevices were disassembled for characterization. At this step, one of the microdevices of IVD-2 was lost due to handling and IVD-3 was contaminated by blood residuals stagnating in the lumen of the puncture needle. Additionally, IVD-1 evidenced blood clotting due to the absence of heparin in the animal model. Thus, from the set of four intravascular devices used in animals, it was just possible to identify the capture of PC3 cells in IVD-4, while for the two remaining microdevices of IVD-2 no PC3 cells were evident. These results are summarized in **Table 3.1**.

Animal Model	Weight, g	Blood volume, mL	Heparinized model	Intravascular Device	Microdevices after vein insertion	PC3 identification
Rat-1	317	20.3	N	IVD-1	Intact	N*
Rat-2	327	20.9	Y	IVD-2	Intact	N
Rat-3	338	21.6	Y	IVD-3	Intact	N**
Rat-4	322	20.6	Y	IVD-4	Intact	Y

Table 3.1. Summary of animal models and intravascular devices used for *in vivo* PC3 capture trials. Y: Yes, N: Not, IVD: Intravascular Device. For N*, the no identification of PC3 cells was due to clotting, while for N**, the lack of identification of PC3 cells was due to blood contamination of stagnant blood.

For all animals, we confirmed the presence of PC3 cells within the circulatory system. From the total volume extracted, a few drops were analyzed on microscopy glass slides by conventional fluorescence microscopy, **Figure 3.15**. However, it was not possible to estimate the exact PC3 cell concentration in circulation as the quantification of dripping samples could not be extrapolated to a specific volume of blood. Other quantification approaches, such as flow cytometry, would be better suited for this goal.

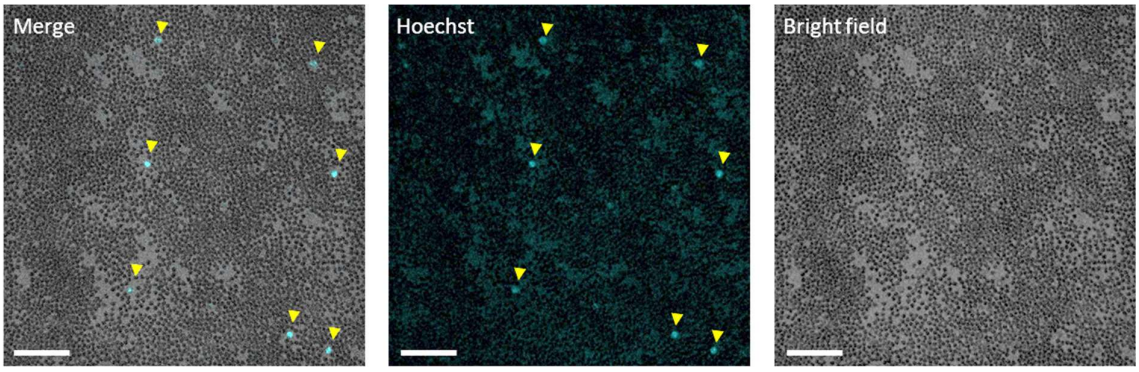

Figure 3.15 Hoechst-labeled PC3 cells were identified among the different droplets of blood. Images corresponding to the blood sample taken from Rat-4. Cancer cells are pointed with yellow arrows.

As mentioned above, IVD-4 was the only device clearly evidencing the trapping of injected cancer cells. Using fluorescence microscopy, we quantified a total of Cc=4 PC3 cells from which one was found in D1, two in D2, and one in D3. These cells were Hoechst and GFP positive and their presence was confirmed by SEM inspection, **Figure 3.16**. D1 corresponds to the microdevice first exposed to the bloodstream, and we observed a homogeneous distribution of the total captured cells among the three microdevices.

SEM imaging evidenced the accumulation of blood debris and other residuals all over the holey membrane surface. However, neither full obstruction of the holey membrane nor RBCs clogging was observed. The morphology of identified cancer cells seems to be preserved, and half of those cells were found within the pores.

Given the theoretical PC3 cell concentration, 25 000 cells per mL of blood, within the circulatory system of rat 4, the number of captured cells is in principle lower than expected. We speculate this is due to the association of different factors. First, it is possible that the real injected volume of PC3 cells was ranging from 410 to 430 µL, due to dead-volume losses in the needle used during injection.[10] Second, after the infusion of cancer cells, a considerable amount of them, 55-60 percent,[11,12] would eventually home, probably within a few minutes, in the liver, lungs and kidney owing to the small size of capillaries. Thus, given the estimated blood volume of the animal model used, we calculated that the real concentration of PC3 cells circulating in large veins would range from 8000 to 9000 cells per mL.

Additionally, the flow conditions within the cava vein at the moment of capture were unknown. Given the surgical procedure the rat was exposed to, it is likely that the blood velocity and pressure were below the reference values used as minima across the *in vitro* experiments carried out. Moreover, the position of the intravascular device within the vein is also unknown which can also affect its capture performance. In the same order of ideas, it is also possible that exposing the capture microdevices for three minutes to the bloodstream is a limited time span, which has a significant impact on the number of collected cells. However, the present animal model does not ensure cancer cell circulation for prolonged times.

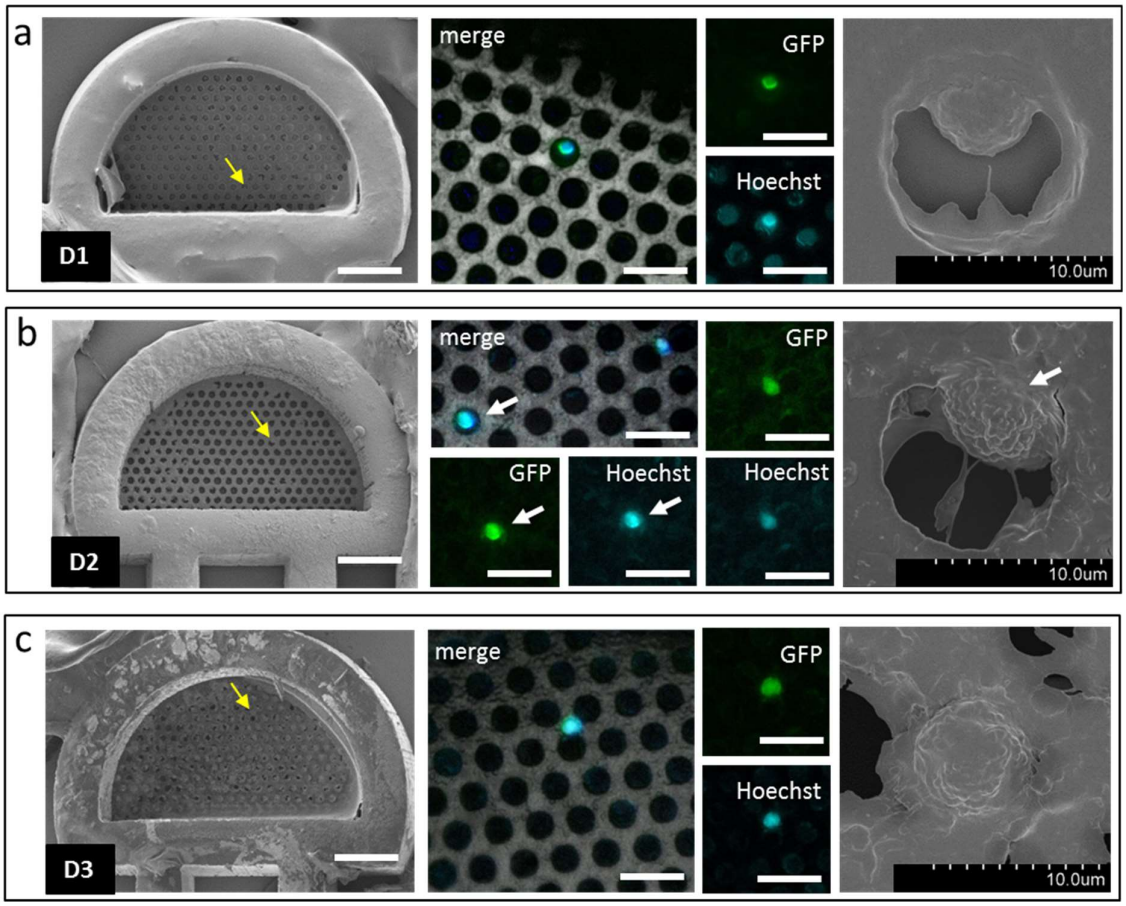

Figure 3.16 Fluorescence and SEM characterization of IVD-4. From left to right and for each microdevice: (left panel) SEM image of the whole microdevice. Arrow points PC3 cell position and scale bar is 100 µm; (middle panel) Fluorescence image magnification of identified PC3 cells, (GFP and Hoechst emission). Scale bar is 20 µm; (right panel) SEM image of the captured PC3 cell. **a** Microdevice number 1 (D1). **b** Microdevice number 2 (D2) **c** Microdevice number 3 (D3).

3.1.8 Conclusions of Part I

The first part of this chapter presents the main strategy followed in order to provide a robust and mechanically resistant 3D cell-capture microdevice, to address the challenges highlighted in chapter II. We conceived microdevices having a maximized number of pores to increase the likelihood of cell capture. We have also described two simple strategies to form metallic 3D-like capture microdevices from planar fabrication techniques, which similarly to the design introduced in chapter II, were engineered to meet medical requirements of intravenous access. In this first section, we have detailed the technical design and fabrication process as well as the challenges encountered.

We evaluated the cell capture performance of those metallic microdevices, mounted into the customized vein insertion system presented in chapter II, in both an ideal fluid and whole blood. Interestingly, the detection limit of cancer cells in whole blood is at a similar cell concentration range as the 3D microdevice introduced in chapter II. Given those results and in combination with computational simulations, we identified geometrical variables of the microdevice that would potentially improve the stabilization of the flow within the area of interest. However, we believe that further understanding of the fluid dynamics, based on both numerical and experimental data, would provide pathways for the improvement of the intravascular device.

We suggested the use of multiple capture microdevices per single strip, which experimentally set the first evidence of an improved overall cell capture performance. Following this multiple-microdevice strategy, we successfully demonstrated, for the first time, the capture of cancer cells from the bloodstream of an animal model. Taken together, these results provide strong evidence for the potential use of 3D engineered microdevices for CTC isolation from the bloodstream. We are aware that a much more systematic and detailed investigation of cell-capture performance is still needed, particularly in the range of concentrations reported in the literature in the blood from patients with cancer disease. Therefore, the technological development, protocols, and preliminary results here introduced, could serve as a starting point for future clinical trials.

Since the application of the concept of *in vivo* filtration represents a major challenge, we proposed an alternative *ex vivo* concept, which is also based on microfiltration of blood for the isolation of cancer cells based on their intrinsic physical properties at physiologically relevant flow conditions. This alternative concept could potentially be readily integrated by the medical community in a point-of-care fashion. Therefore, the second part of this chapter is dedicated to introduce it.

3.2 Part II: Portable metal-based filters for high-throughput *ex vivo* blood screening

3.2.1 General concept: the transcendence of a portable filter

As presented in chapter II, using the test-bench, the partial occlusion of a fluidic channel by a filtering microdevice allows cancer cell capture at a relatively low ΔP in a closed-loop fluidic system. Following the principle of cancer cell isolation from whole blood under physiologically relevant flow conditions, we envisioned an innovative *ex vivo* approach in which an engineered filter, having dimensions in the range of millimeters, could perform cancer cell capture with an improved performance while keeping low-pressure operating conditions. Contrary to the *in vivo* approach in which the overall dimensions were limited to a few hundreds of micrometers, by the size of the vein and the venipuncture strategy, this ex vivo approach does not have any dimensional constrictions.

We also conceived this filter as portable, meaning that it could be integrated into commercially available blood-contact consumables used in clinical routine, or any other similar platform, in order to perform cancer cell capture, and then removed from the consumable for cytomorphological characterization, **Figure 3.17c**. Additionally, the portability of this filter could potentially allow performing in situ functional analysis of the captured biological material, **Figure 3.17d**. The integrability concept has been added as an innovative perspective, foreseeing, for example, a filter performing continuous blood screening in an *ex vivo* derivation manner similar to hemodialysis systems, **Figure 3.17a**, but more importantly, without the use of external pumping. Another alternative application of the integrability concept may be performing cancer cell capture simultaneously with the routine blood draw, **Figure 3.17b**, taking advantage of the vacuum of evacuated tubes as the pumping system.

In general, this approach could enable a more systematic monitoring of cancer disease progression in clinical routine. Moreover, it could potentially meet the requirements of a point-of-care system. The work presented in the following subsections is preliminary and was mainly intended to demonstrate the technological feasibility rather than offering a quantitative proof of the aforementioned concepts.

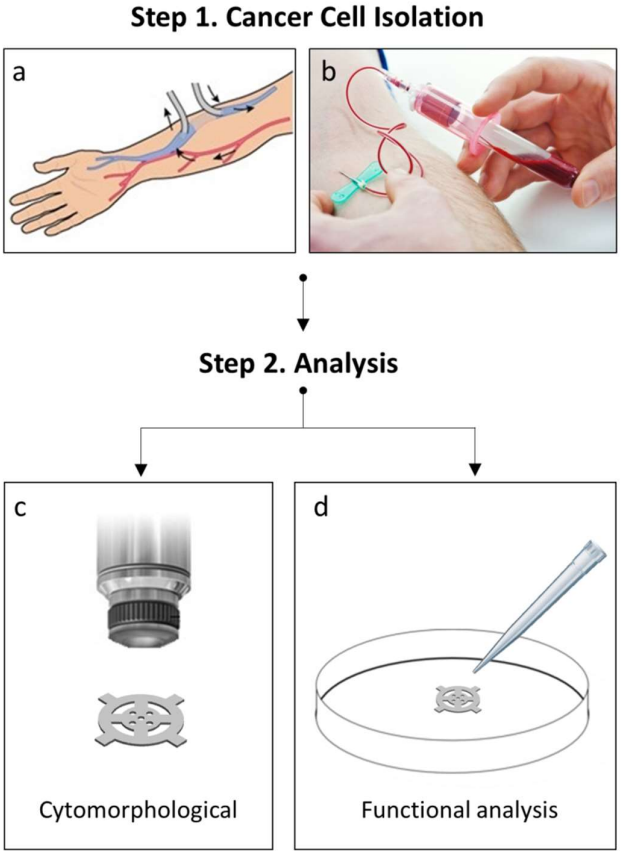

Figure 3.17 The concept of ex vivo isolation of cancer cells using a filter easily integrable to medical consumables. **a** The portable filter could be integrated in external vein derivations, to perform continuous blood screening. **b** The filter may be suited to be also adapted to conventional blood collection sets. **c** The portability of this approach may render the filter compatible with conventional cytomorphologial analysis. **d** The filter could potentially be used as a platform to perform functional analysis of the captured cancer cells, with no need of cell removal.

3.2.2 Design of the portable filter

We used a double-ended-needle tubing (BD Vacutainer), **Figure 3.18**, as a holder for the portable filter. This holder setup is a commercially available consumable and used as a standard in clinical routine for blood collection in evacuated tubes. Sizes of this blood collection set are standardized under the Luer taper system (ISO 594, ISO 80369) for medical use. We envisioned placing the portable device into the lumen of a male Luer Slip connection fitting, as shown in **Figure 3.18**. In order to allow the right placement of the filter, we machined four grooves to the original connection fitting.

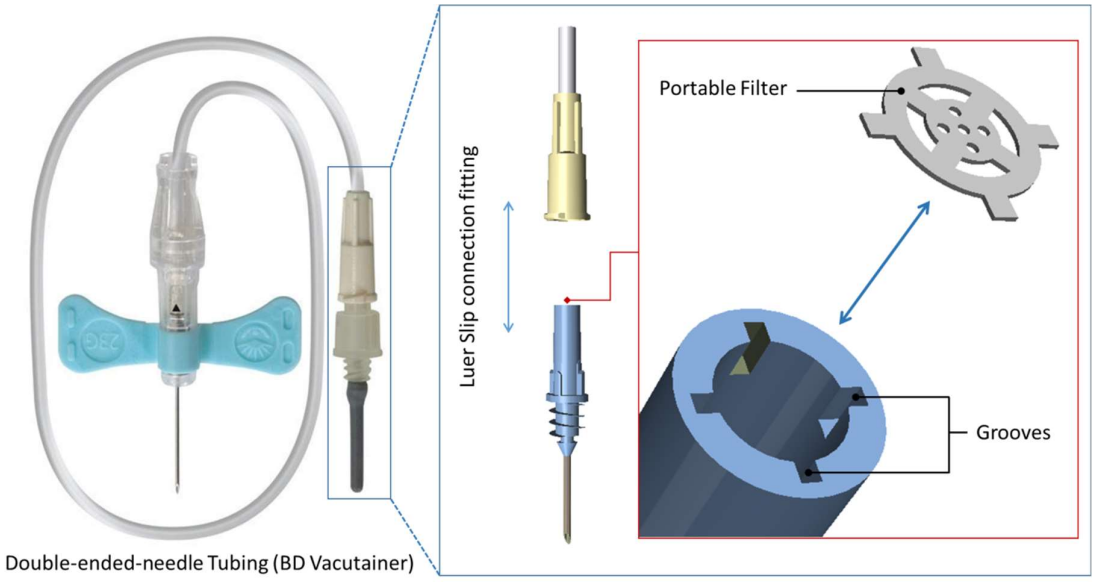

Figure 3.18 The double-ended-needle set used for blood collection. The portable filter was adapted to the male Luer Slip connection fitting, which was slightly modified to host the filter.

The lumen of the male Luer slip connector has a diameter of ~2.3 mm, thus we set as the main diameter of the portable filter D=2.2mm, **Figure 3.19.** We also set four symmetrical clamping tabs having a length of L_{tab}=370 µm which would enable the right placement of the portable filter into the grooves. The isolation of CTCs at low pressure conditions from whole blood, is hindered by clogging of pores, since cells are not able to pass through the pores below a determined ΔP. In order to avoid clogging, we conceived a filter having large openings that would allow a continuous circulation of a portion of the fluid, while the remaining stream would be filtered. We placed four symmetrical openings representing approximately 25% of the lumen's cross-section.

Pores were placed at the center of the portable device having a uniform and symmetrical distribution, **Figure 3.19**. The filtering area is defined by 200-µm wells, giving to the filter a 3D-like topography. At an early stage of this project, two designs were proposed: a) A filter containing five independent wells, **Figure 3.19a**, and b) a filter containing five interconnected wells, **Figure 3.19b**. At this initial stage, we set the diameter of the pore as 10 µm for both designs. Given this, the total number of pores for the five-well design was 635, while for the five-interconnected-well the total number of pores was 821. The total area for the filtering region represents less than 2% of the lumen's cross-section.

The idea of creating filtering wells is justified by two reasons; firstly it may facilitate the characterization by conventional fluorescence microscopy since the positioning of each well is easily recognized. Secondly, we believe that in order to favor the *in situ* culturing of the isolated cells, having small wells is better suited, as cells should be concentrated in confined regions.

The conception and development of this concept was concurrent with the one of metal-based microdevices for the *in vivo* cancer cell capture, presented in Part I of this chapter. Thus, the technological approach used for their fabrication was also implemented using multilayer electrodeposition of metal, introduced in section 3.1.4.

Two depositions of Nickel were implemented and the mask layout for this design is shown in **Figure 3.19**. The thickness of L1 was set as 5 µm while the thickness of L2 corresponding to the support was set at 150 µm. Both thicknesses were defined in order to be compatible with the process established in section 3.1.4, where similar challenges were encountered along the fabrication process. Similarly as to *in vivo* metallic microdevices, we set an overlapping region between L1 and L2, aiming to ensure adhesion. The minimum overlapping distance was 50 µm.

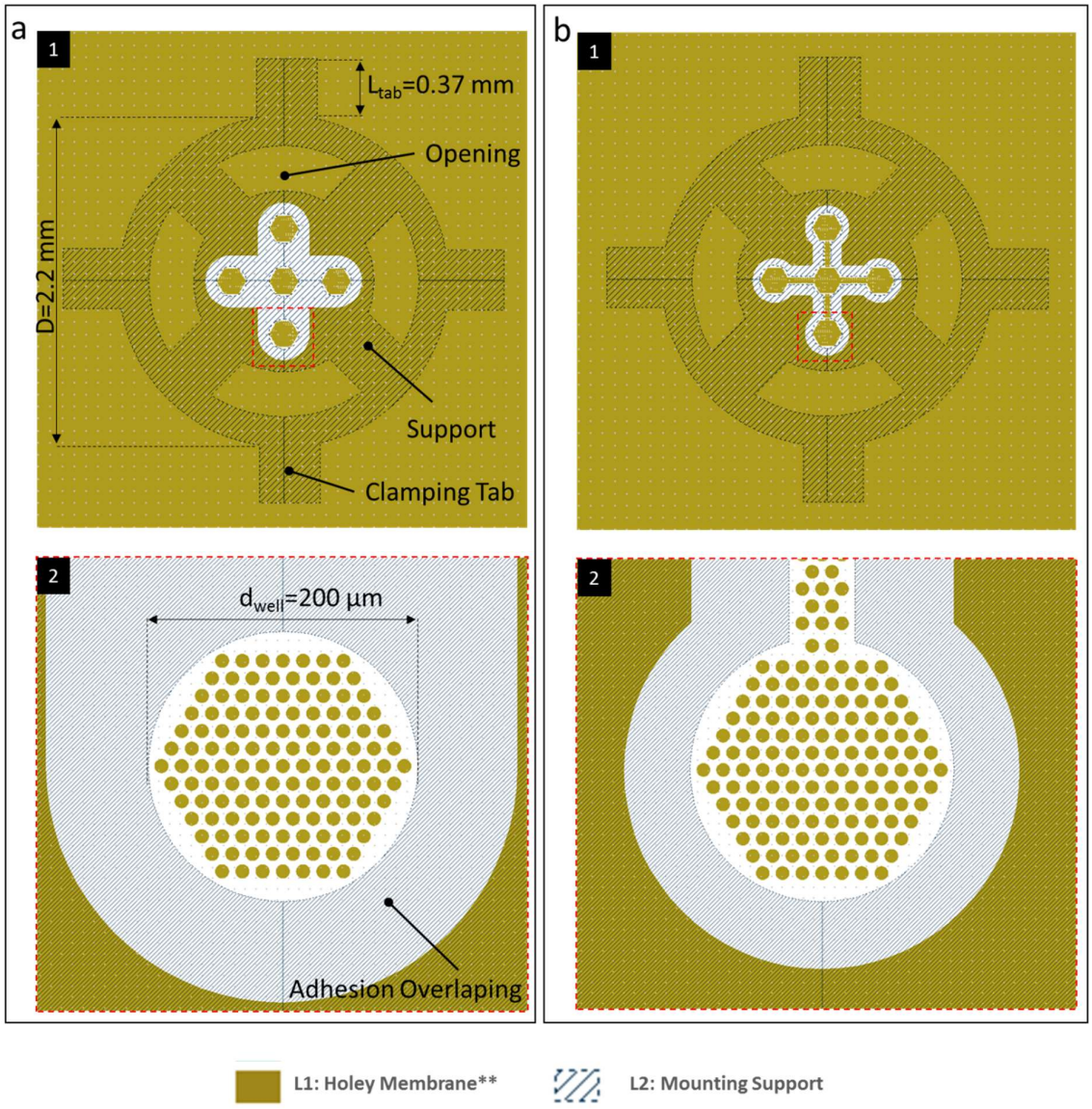

Figure 3.19 Layout and characteristic dimensions of the portable filter. Layer color-code is shown at the bottom of the image. L1, corresponding to the pores, is represented by an inverted polarity**, where the colored area represents the insulating photoresist. L2 represents the area where Nickel is deposited. **a** Layout of a portable filter containing five independent wells (1), the insert (2) shows a magnification of a single 200-µm well containing 127 pores of 10 µm. **b** Layout of a filter having five interconnected wells (1), the characteristic dimensions are the same as the aforementioned design. The insert (2) shows a magnification of a single well.

3.2.3 PC3 capture from whole blood using the portable filter

The designed devices were fabricated in Nickel, **Figure 3.20a**, and they offered important ease-of-use for their manipulation without damaging the filtering area. The diameter of pores was 9.30±0.47 µm. We evaluated the cancer cell capture capabilities of these designs using suspensions of Hoechst stained PC3-GFP cancer cells in whole blood. Similarly to the test-bench of chapter II, the fluidic setup was pumped using a peristaltic pump in closed-loop configuration for a time span of 10min. The rotation was adapted in order to have a velocity within the holder similar to the minimal velocity found in vivo, v_{min}=0.072 m s^{-1}. Given the non-uniform cross section of the Luer adapter, having a conical shape along the longitudinal section, we estimated that the rotation speed should range from 20 to 40 rpm.

Early experimentation evidenced that the five-interconnected-well design yielded a larger number of captured cells. We believe this is related to the high number of pores. Given this, we continued using the interconnected-well design for consecutive experiments. Using this design, we succeeded in detecting PC3 cells using cell suspensions as low as 10 PC3 cells per mL of whole blood, **Figure 3.20b**, where we identified a couple of cancer cells. However, this single set of experiments does not allow us to truly conclude about the capture sensitivity of these devices.

As expected, using more concentrated suspensions resulted in a larger amount of captured cells. Interestingly, captured cells were uniformly distributed over the whole filtering area, **Figure 3.20c**. This preliminary set of results suggested that in order to capture more cancer cells, the filtering area needs to be maximized all over the available support surface. Based on this premise, we designed a new generation of portable devices.

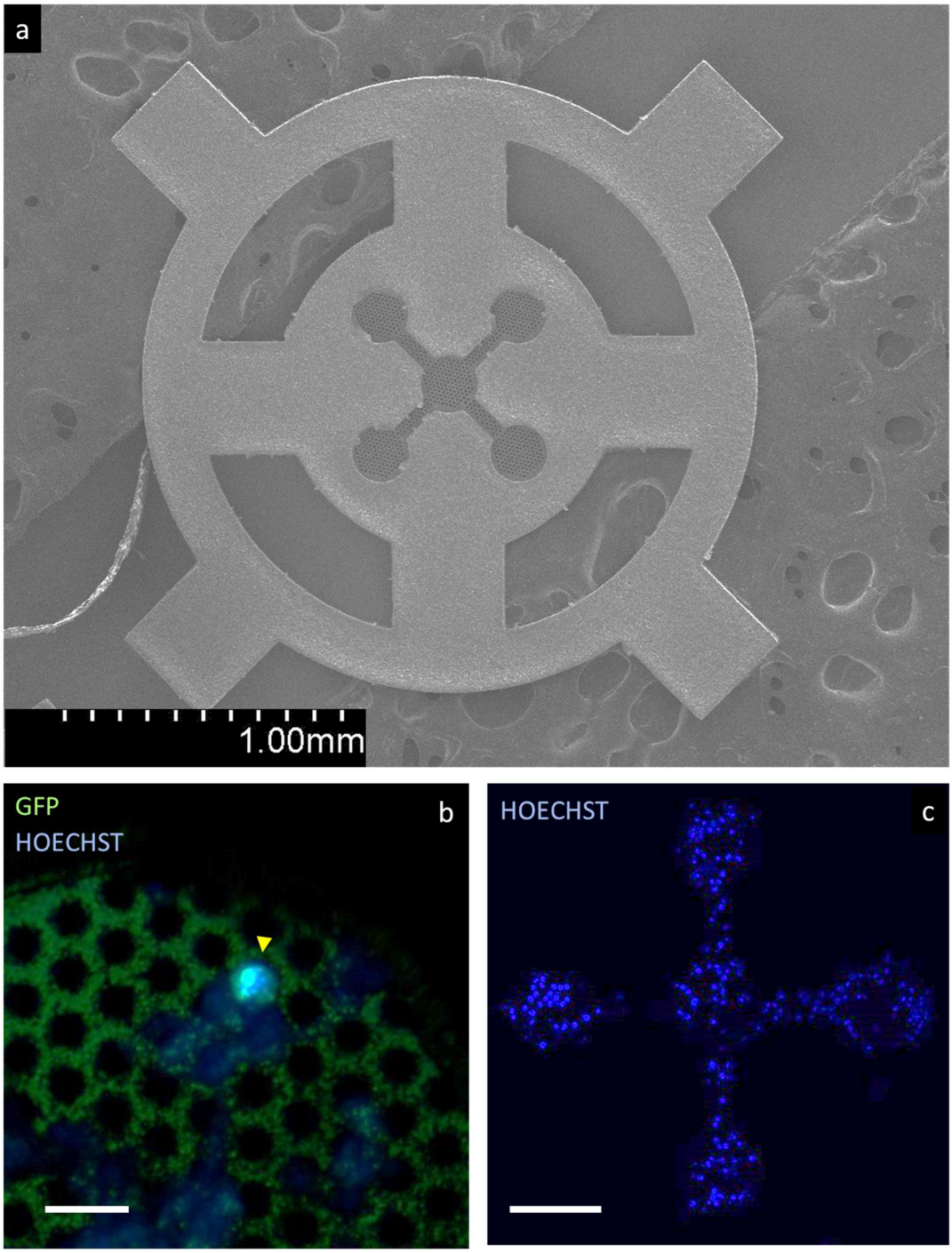

Figure 3.20 SEM macrograph and fluorescence images of captured PC3 cells from whole blood using the five-interconnected-well design. **a** Scanning electron micrograph of the portable filter. **b** The fluorescence image shows one of two cells detected when a concentration of 10 PC3 cell per mL of whole blood was flowed. The green background evidences the pores of the filter. Cells were identified by GFP and Hoechst emission. Scale bar is 20 µm. **c** Approximately 160 PC3 cells were identified when a suspension of 5000 PC3 cells per mL of blood was processed. Cells are uniformly distributed over the filter. Scale bar is 200 µm.

3.2.4 Portable filters with maximized filtering area

As mentioned above, we envisioned fabricating portable filters with a maximized coverage of pores. Keeping the same overall dimensions, we reduced the opening to the half value of previous designs, resulting in approximately 12% of the lumen's cross-section, **Figure 3.21**. For this batch of filters, we proposed two designs. First, one keeping interconnected wells, **Figure 3.21a**, and a second design being a single well at the center of the device **Figure 3.21a**. We increased the number of 10-µm pores for both designs (interconnected-well design has a total of 2155 pores, while single-well design has 2176). The filtering area represents approximately 5% of the lumen's cross-section.

Preliminary results, using Hoechst stained PC3-GFP cells suspended in cell culture medium at a concentration of 2000 cell per mL, evidenced that those designs were able to isolate over 400 cells in a 10-minute experiment, **Figure 3.21 insets 1**. Interestingly, captured cells are mainly found at the surface of the filter and their morphology seems to be preserved, **Figure 3.21 insets 2**. Given this promising data, experiments using whole blood are currently ongoing in order to determine the capture sensitivity.

Data obtained so far does not allow concluding what the optimal surface ratio between open and filter areas is. We believe there is a threshold in which cancer cell capture can be maximized without the filter representing a significant resistance to the flow, at the present flow conditions. Further understanding of the fluid dynamics is required for which computational simulations are currently been conducted.

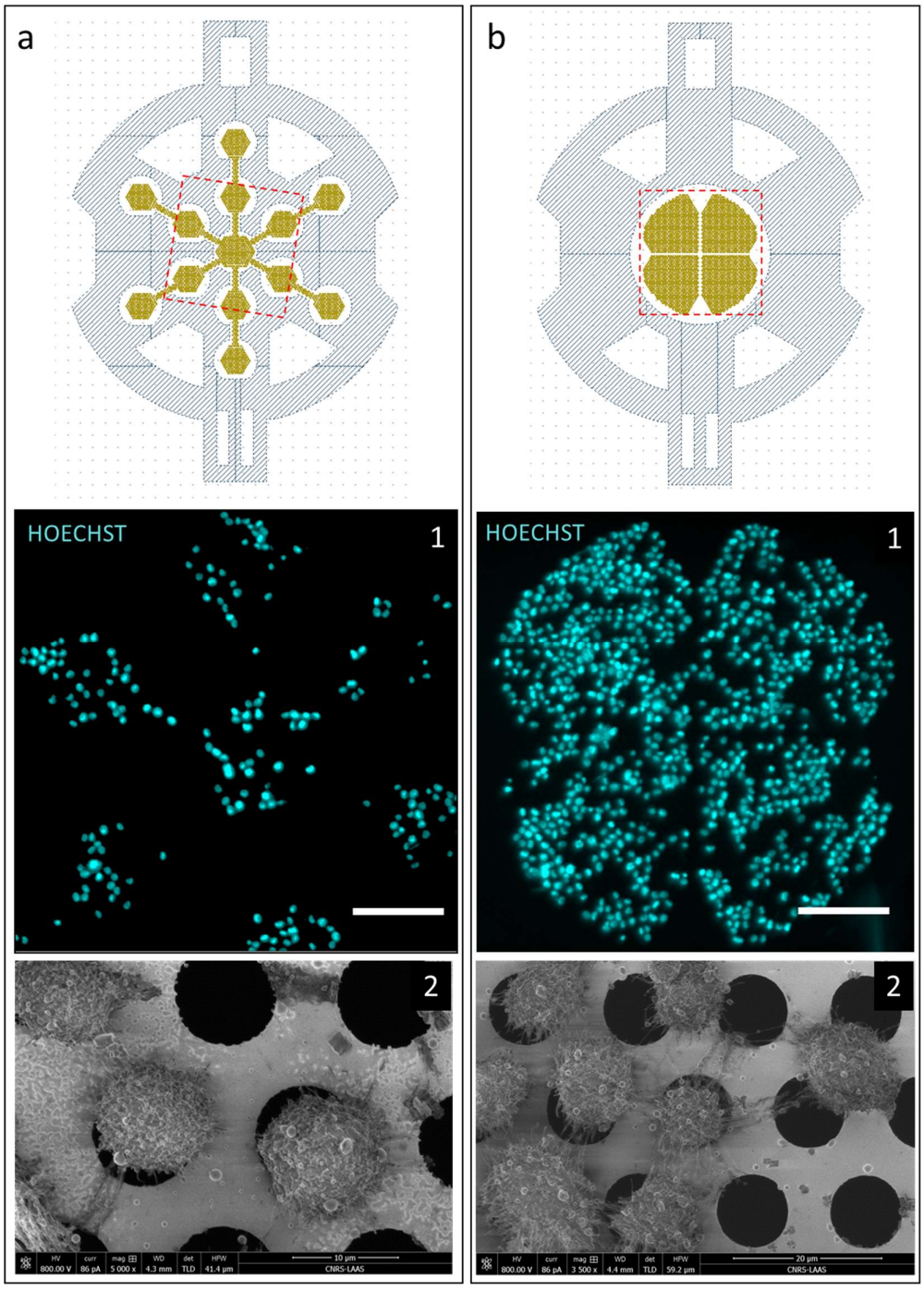

Figure 3.21 Portable filters having a maximized filtering area. Cell capture was evaluated using culture media suspensions at a PC3 concentration of 2000 cells per mL. **a** Interconnected-well design having a total of 13 wells. The total number of captured cells for this sample was 422, a partial view of captured cells at the middle region, dashed square, is shown in inset (1). Scale bar is 200 µm. Inset (2) shows the typical cell morphology found over the filter. **b** Single-well design captures a total of 477 PC3 cells where the whole view, dashed square, of the filtering region is shown in inset (1). Scale bar is 20 µm. Similarly, inset (2) shows the cell morphology of isolated cells.

3.2.5 Cell viability of PC3 in Nickel substrates

We used a colorimetric assay, MTT assay, to evaluate the viability of PC3 cells cultured directly in contact with Nickel substrates. In this experiment, we assessed determining the cell viability with respect to different Ni substrates and surface coating materials. To this aim, we used portable filters fabricated in Nickel and subsequently coated with heparin and/or Gold (<50 nm). Additionally, and for comparison purposes, we also fabricated portable filters made of a photosensitive polymer (DryFilms Resist). All portables filters had the same surface area. Experiments were performed in a 96-well plate and using PC3-GFP cells. The experimental set of filters was defined as follows: Control (well only), pure Nickel, Nickel and heparin coating, Nickel and Gold coating, Nickel and both Gold and heparin coating, and pure dry film resist. Experiments were carried out in three replicates, and followed along 72 hours.

Results obtained from this viability test are summarized in **Figure 3.22a**, and percentage values are given with respect the control experiments at three time spots. From this set, we observed that pure Nickel exhibit higher viability levels that other evaluated conditions. Surprisingly, Gold coating shows the lowest viability levels, we believe this is a result from the deposition process followed, since the electrodeposition bath used contains cyanide complex, which is known to be cytotoxic. In addition, in pure Nickel samples we observed high adhesion of cells onto the overall surface, **Figure 3.22b**, suggesting cell compatibility of this material. Further experiments are required to confirm this preliminary data.

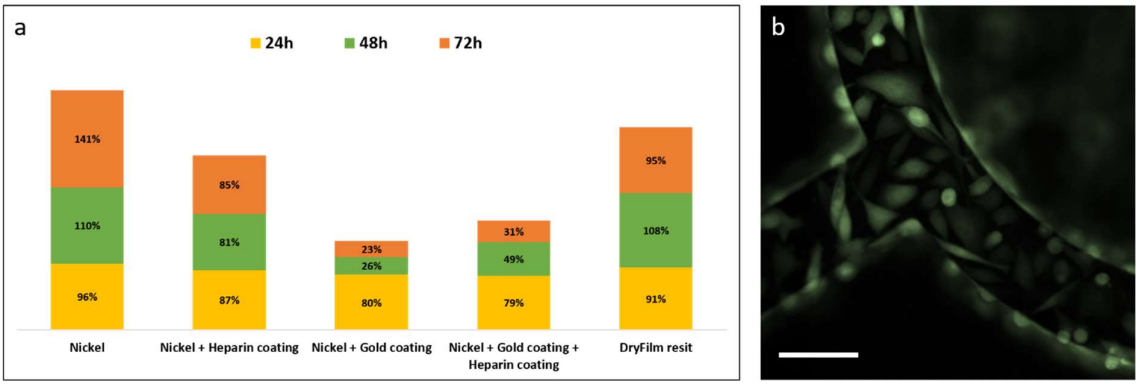

Figure 3.22 Cell viability of PC3 cells cultured onto different substrates. **a** Relative percentage of cell viability with respect to control experiments at 24, 48 and 72 hours. **b** Fluorescence image (GFP emission) of PC3 cells adhered to the surface of a Nickel substrate at 72 hours of culturing.

3.2.5 Conclusions of Part II

In the second part of this chapter, we introduced a portable filter which given its dimension and design could be readily integrated into blood-contact medical consumables used as a standard in clinical routine. The filter was conceived and envisioned as a potential platform for in situ studies of the captured biological material.

Having as a basis the technological optimization performed for the fabrication of metallic 3D-like microdevices presented in the first part of this chapter, we similarly fabricated the proposed portable filters. Remarkably, those filters detected cancer cell concentrations as low as 10 cancer cells per mL of whole blood. Based on this set of results, we are currently exploring the cell-capture performance of the second generation of portable filters, where the filtering area is maximized. Further ongoing experiments and perspectives regarding this cell capture approach are presented in the section corresponding to the conclusions and perspectives of this manuscript.

Bibliography of Chapter III

1. Zocca, A., Colombo, P., Gomes, C. M. & Günster, J. Additive Manufacturing of Ceramics: Issues, Potentialities, and Opportunities. *J. Am. Ceram. Soc.* **98,** 1983–2001
2. Frazier, W. E. Metal Additive Manufacturing: A Review. *J. Mater. Eng. Perform.* **23,** 1917–1928 (2014).
3. Vyatskikh, A. *et al.* Additive manufacturing of 3D nano-architected metals. *Nat. Commun.* **9,** 593 (2018).
4. Kotz, F. *et al.* Three-dimensional printing of transparent fused silica glass. *Nature* **544,** 337–339 (2017).
5. FEMTOprint | 3D printing for glass microdevices. *FEMTOprint | 3D printing for glass microdevices* Available at: https://www.femtoprint.ch. (Accessed: 28th July 2018)
6. 3d-Laserprint - LightFab. Available at: https://www.lightfab.de/. (Accessed: 28th July 2018)
7. Hosokawa, M. *et al.* Size-Selective Microcavity Array for Rapid and Efficient Detection of Circulating Tumor Cells. *Anal. Chem.* **82,** 6629–6635 (2010).
8. Sun, T., Smallwood, R. & MacNeil, S. Development of a mini 3D cell culture system using well defined nickel grids for the investigation of cell scaffold interactions. *J. Mater. Sci. Mater. Med.* **20,** 1483–1493 (2009).
9. Seitz, B. M., Krieger-Burke, T., Fink, G. D. & Watts, S. W. Serial Measurements of Splanchnic Vein Diameters in Rats Using High-Frequency Ultrasound. *Front. Pharmacol.* **7,** 116 (2016).
10. Küme, T. *et al.* The effects of different syringe volume, needle size and sample volume on blood gas analysis in syringes washed with heparin. *Biochem. Medica* **22,** 189–201 (2012).
11. Gao, J., Dennis, J. E., Muzic, R. F., Lundberg, M. & Caplan, A. I. The dynamic in vivo distribution of bone marrow-derived mesenchymal stem cells after infusion. *Cells Tissues Organs* **169,** 12–20 (2001).
12. Madden, R. E. & Malmgren, R. A. Quantitative studies on circulating cancer cells in the mouse. *Cancer Res.* **22,** 62–66 (1962).

Conclusions and Perspectives

Conclusions and perspectives

Liquid biopsy has the potential to revolutionize the management of cancer patients and improve their quality-of-life. In this framework, CTCs could increase the temporal and spatial representativeness of heterogeneous solid tumors, both in primary and metastatic sites. In addition, minimally invasive techniques could offer frequent sampling, and consequently, enable real-time treatment adaptation and monitoring of the disease.

In this thesis work, we have focused our efforts in developing engineered devices for the capture of circulating tumor cells, based on their intrinsic physical properties, under physiologically relevant flow conditions. The proposed technologies were designed as medical tools for the isolation of CTCs in clinical routine. The results here presented are the first proof-of-concept demonstrating the feasibility of this approach.

In Chapter II we described the implementation of a customized fluidic platform in which we integrated an engineered 3D microdevice fully designed to perform cancer cell capture and fabricated using rapid prototyping. This platform elucidated, for the first time, the feasibility of cancer cell detection from whole blood samples under physiologically relevant flow conditions. As a hallmark, RBCs lysis, the addition of cell fixatives, or the dilution of blood as one could find in many commercial CTC-isolation platforms were not required here. In the perspective of *in vivo* CTC capture, we also developed an intravascular system, adapted to clinical needs, which allows the simple exposure to the blood flow and retrieval of the capture 3D microdevices.

Those results were the basis for the development of two other alternative micro-engineered devices fabricated in Nickel using electrochemical deposition, thoroughly described in Chapter III. In the first part of the chapter, we introduced novel low-cost and high-throughput strategies to form metallic 3D-like configurations starting from planar ones, intended for *in vivo* CTC capture. In order to demonstrate their functionality, this second generation of devices was evaluated *in vitro* and, more importantly, *in vivo,* using murine animal models. For the first time, truly circulating CTCs were captured within three minutes, in native conditions, with no external pumping but the heart. These results are the accomplishment of this thesis work, as it embodies the proof of concept demonstrating that direct and physical isolation of tumor cells circulating within the bloodstream could be possible, preserving them in a native state so preserving the information they carry intact.

The purpose of this thesis work was also to bridge the gap between cutting-edge technologies developed in cleanrooms and research labs, and medical needs. Our motivation was to offer new deep-tech tools and alternatives compatible with clinical practice. Along the same perspective of CTC capture under physiologically relevant flow, in the second part of this chapter we presented an affordable technology that could be used as a point-of-care device. A portable filter was engineered to be adapted to blood-contact medical consumables. These first generations of devices showed great promise to screen larger amounts of blood and to maximize the number of CTCs captured, an important step as well towards the use of CTCs as biomarkers in clinical routine. The promising results obtained enabled us to gain deeper insights into the mechanisms and key-players involved in this complex CTC capture process. We identified several possible optimization and development routes to pursue the improvement of the devices performances.

Enumeration of CTCs isolated with Ni-based technologies

From the *in vivo* 3D microdevice standpoint, geometrical variables as the size of pores, overall dimensions, and number of capture microdevices per intravascular device still have room for optimization. To this end, at the time of writing this dissertation, we fabricated a new generation of intravascular devices composed with up to six microdevices per strip, and based on the bending strategy to minimize handling. We expect these devices could demonstrate a higher cancer cell capture yield.

Given that in clinical practice the concentration of CTCs per specific volume of blood is unknown, we envision developing a device able to perform real-time monitoring of cell capture events in *in vivo* settings. This configuration could provide experimental data to correlate blood flow conditions with the number of captured cells per device at a determined timespan. In the same perspective, we also envision a real estimation of the total volume of blood screened per microdevice. This data could contribute to the generation of statistical analyses and a numerical model to predict CTC enumeration in patients.

Similar perspectives need to be implemented in the proposed portable filters for ex vivo CTC capture. Given the overall dimensions of the filter, this second technology is more suitable for integrating the required sensor together with the filtering surface. The design and implementation of it, is currently the main project topic of Elise Bou, PhD student at LAAS-CNRS.

Along the line of maximizing CTC capture, we also envision complementing our physical-based CTC capture approach with the immunoaffinity-based one. Given the large surface area available in our micro-engineered devices, it may be possible to functionalize it with antibodies against EpCAM, in a similar fashion as some of the technologies introduced in Chapter I. However, a better understanding of flow dynamics may be required to maximize antibody-antigen interactions.

Cell capture from blood samples with cancer disease

For both the intravascular device and the portable filter, the assessment of CTC capture from blood samples from cancer patients, is of utmost importance. Given that CTCs, aside from their low frequency, exhibit a higher degree of pleomorphism, cell variations in size and shape are expected, compared to model cell lines. To this end, the implementation of conventional CTC-identification protocols adapted to our customized workflow will be required. Additionally, it will be important to quantify the degree of blood-cell contamination at the filter level, as even though our results have shown low levels of contamination, a deeper analysis would provide better clues to improve the size of pores.

Based on the capture sensitivity result presented in this manuscript, we believe our CTC-capture devices, at the current state, would be suited to analyze blood from metastatic patients. Given the fact that cell capture is performed at low-pressure conditions, we believe it could broaden the spectral heterogeneity of captured CTCs. Additionally, we would expect the direct isolation of CTC clusters.

The intravenous CTC isolation in cancer patients

In addition to the abovementioned, the intravenous capture of cancer cells in cancer patients can become much more complex. For example, the viscosity of whole blood from cancer patients may differ from that of healthy donors due to diverse medical conditions such as chronic inflammation, or response to chemotherapy. Moreover, thrombosis is a frequent complication of cancer patients. Thus, these patient-depended factors also need to be considered for future optimization.

Nickel as a constitutive material of CTC-capture devices is probably not the ideal material. Even if from a mechanical standpoint it offers attractive properties in the field of medical devices, certain levels of toxicity and allergic reaction have been reported. However, these can be overcome by the deposition of biocompatible materials, such as Parylene-c onto the surface in a conformal manner.

At the same level of importance, the use of anticoagulant surface coatings, such as heparin, would be required to avoid the formation of blood clots on the filtering area as demonstrated by our experiments in animal models. Another alternative could be the use of other types of materials that could fulfill medical requirements such as gold or biodegradable materials.

Beyond CTC enumeration: CTC manipulation and *in situ* culture

In addition to the isolation of CTCs from the vast blood cell population and their enumeration, performing systematic functional analyses could provide complementary information, since they provide the unique opportunity to study the whole cell, allowing DNA, RNA and protein-based molecular profiling.

In Chapter II, we suggested the viability of isolated cells based on the preservation of cell morphology. However, the biochemical detachment of captured cells from the filtering surface is not convenient. For example, the use trypsin to dissociate the adherent cells from the filtering surface could induce proteome alterations in mammalian cells. We have envisioned integrating more gentle strategies to detach captured cells, such as the use of sacrificial layers or externally-controlled tunable surfaces, from which cells could be released thanks to an external stimulus (heat, electrical impulse, etc.).

However, we think that an easy and accessible way to perform functional studies on captured cells is performing them *in situ*. Functional on-filter analyses would not require the detachment of cells and would allow their real-time monitoring. To this end, we are currently implementing cytotoxicity and viability assays using Ni-based devices coated with different materials in order to determine those favoring the proliferation of captured cells.

Finally, this thesis work opens up new possibilities for the capture of CTCs, their enumeration and analysis in the framework of cancerous pathology. Being minimally invasive, stealthy and compatible with common medical consumables used in clinical trials, our microengineered devices could be used for the repeated and systematic monitoring of cancer progression in clinical routine.

Appendix

Appendix A
Hydraulic resistance of the microdevice

Considering that the hydraulic resistance $R_H = \Delta P/Q$ is defined as the ratio of the pressure drop ΔP over the volumetric flow rate Q, and that it has a direct impact on the volume of liquid passing through the microdevice, we aimed at minimizing this value. The overall hydraulic resistance of the microdevice is defined as the sum of two contributions: the hollow cylinder resistance R_C and the holey membrane resistance R_M, as $R_H = R_C + R_M$. We performed the following analysis assuming an incompressible Stokes flow, where viscous forces dominate inertia forces, and a constant viscosity η.

For a circular cylinder, the associated resistance, $R_C = 8\eta L/\pi r_c^4$, is dominated by the length of the cylinder L and its radius r_c, as shorter in length and larger in radius, smaller the cylinder resistance. However, variations in cylinder radius contribute more significantly.

The holey membrane was conceived as a uniformly distributed arrangement of pores, where the hydraulic resistance of a single pore, $R_P = (8\eta t/\pi r p^4) + (3\eta/r_p^3)$, of radius r_p and thickness t was first proposed by Weissberg.[1] The model can be simplified removing the second term accounting for a numerical error of less than 1% as shown by Degan et al.[2] Similarly to the cylinder resistance discussed above, the resistance R_P is dominated by the pore radius r_p. The total membrane resistance $R_M = 8\eta t/\pi n r_p^4$ results from coupling in parallel the individual pore resistances under the consideration that all pores have the same radius,[3] being n the total number of pores. This model does not take into consideration the hydrodynamic interactions of the pore-to-pore distribution, which can increase the flow up to 10%.[4]

Based on the aforementioned, the intrinsic hydraulic resistance of the microdevice is given by $R_H = 8\eta/\pi\ (L/r_c^4 + t/n r_p^4)$, where the design variables are: length and radius of the cylinder (L, r_c) and thickness, pore radius and, pore number (t, r_p, n_p) of the membrane. From the hydraulic resistance model, we observed that the holey membrane contributes the most to the overall resistance of the microdevice.

References

1. Weissberg, H. L. End Correction for Slow Viscous Flow through Long Tubes. *Phys. Fluids* **5,** 1033–1036 (1962).
2. Dagan, Z., Weinbaum, S. & Pfeffer, R. An infinite-series solution for the creeping motion through an orifice of finite length. *J. Fluid Mech.* **115,** 505–523 (1982).
3. Jensen, K. H. *et al.* Modeling the Hydrodynamics of Phloem Sieve Plates. *Front. Plant Sci.* **3,** (2012).
4. Jensen, K. H., Valente, A. X. C. N. & Stone, H. A. Flow rate through microfilters: Influence of the pore size distribution, hydrodynamic interactions, wall slip, and inertia. *Phys. Fluids* **26,** 52004 (2014).

Appendix B
PC3 capture using 20G and 18G designs

Fluidic experiments for the capture of PC3 cells in suspension using 20G and 18G designs. The most significant results are summarized in **Table A-1**. For instance, a cell capture experiment using an 18G device and a cell suspension of 5000 cell per mL of culture medium evidences the trapping of 433 cells (**Figure A-1**). The amount of cells trapped is the largest found throughout this project and it could be correlated to the larger filtration area available. We also observed that the vast majority of cells are found in the lower region of the filter.

Cell Supension	Number of captured cells using 20G	Number of captured cells using 18G
1000 cell mL	41	---
5000 cell mL	---	433
10 000 cell mL (Blood)	33	---
10 000 cell mL (Blood)	(1): 81 (2): 138 (3): 46	---

Table A-1 Representative results of PC3 trapping using 20G and 18G. The number of captured cells is shown for each cells concentration either in cell culture medium.

Even more interestingly, experiments using 20G design and PC3 cells spiked in blood at a cell concentration of 10 000 cell per mL resulted in 33 and 265 trapped cells in a single and multiple (3x) configuration respectively (**Figure A-2**). Remarkably the use of a multiple cell capture microdevices per single strip evidenced as the first time an improved performance in cell capture.

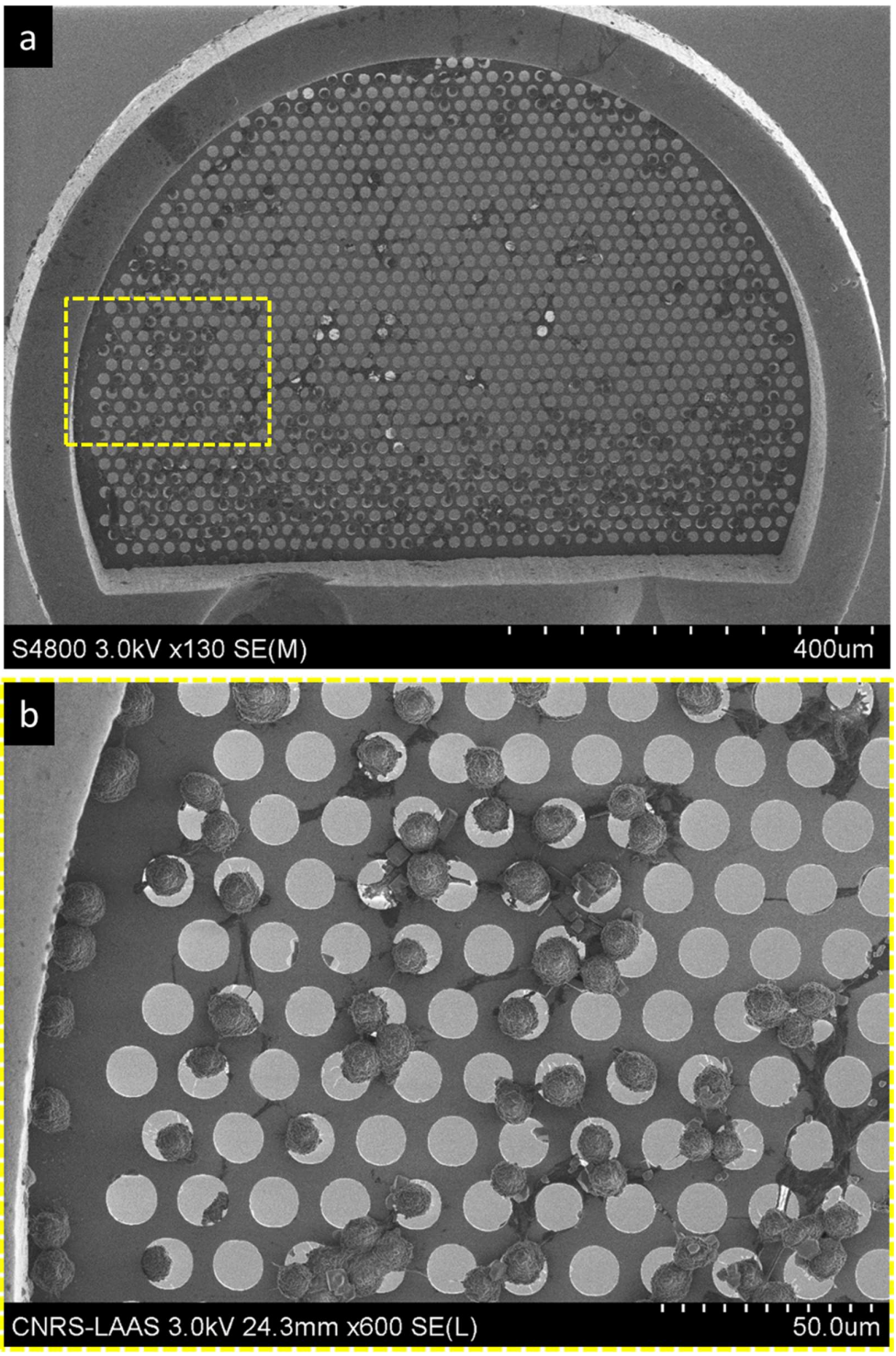

Figure A-1 Scanning electron micrograph of captured cells using an 18G and a cell concentration of 5000 cell per mL in cell culture media. A total of 433 PC3 cells were identified.

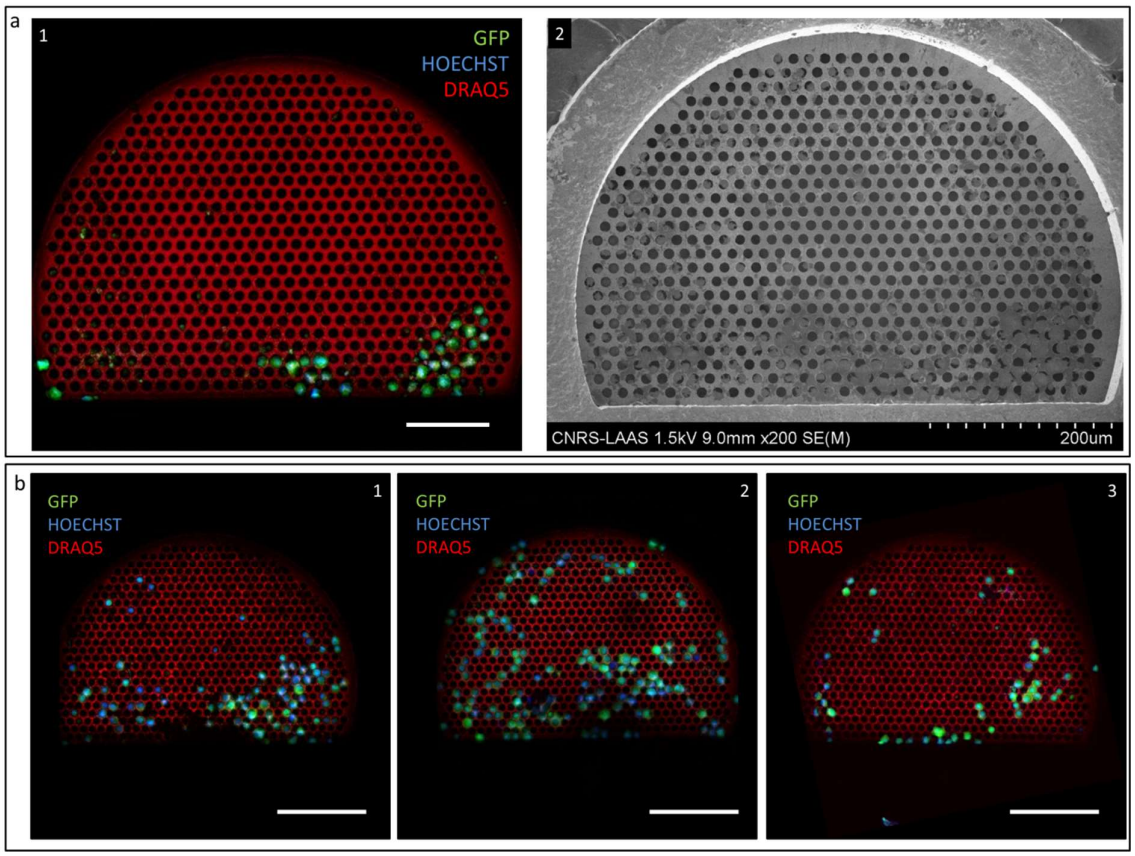

Figure A-2 Scanning electron micrographs and fluorescence images of 20G microdevices after trapping of PC3 cells from blood. **a** A single microdevice captured 41 cells from a cell suspension of 5000 cell per mL in whole blood. **b** The use of multiple cell capture microdevices in a single strip results in the isolation of 81 cells (1) by the first device facing the flow , 138 cells (2) by the second one, and 46 cells by the third one.

Résumé en Français

Chapitre I

Biopsie liquide : un concept émergent vers une médecine de précision

1.1 Le cancer

Le cancer est un terme générique pour un grand groupe de maladies apparentées caractérisées par la prolifération continue et non régulée des cellules. On croit que l'apparition du cancer est le résultat d'une série de changements génétiques directement liés à la division cellulaire et à la dérégulation de la croissance. Les cellules qui se développent de manière incontrôlée envahissent les tissus et organes normaux, ce qui entraîne une formation anormale de néoplasie, communément appelée tumeur. En oncologie, les tumeurs sont classées selon le type de cellule d'où provient le cancer et sont regroupées en trois grandes catégories : carcinomes, leucémies/lymphomes et sarcomes. Les carcinomes représentent 80 à 90 % de tous les cancers et proviennent de cellules épithéliales. Ci-après et le long de ce manuscrit, le terme tumeur ne fera référence qu'à la catégorie des carcinomes.

Bien que la formation d'une tumeur dans un site primaire implique un risque pour la santé des patients, la formation de métastases distantes est la phase la plus mortelle de la progression du cancer car il n'est pas encore possible de la prévenir et les traitements sont beaucoup moins efficaces. Les patients atteints d'une maladie métastatique ont souvent un ou plusieurs foyers micrométastatiques/macrométastatiques détectables cliniquement, mais il est probable que beaucoup d'autres puissent être présents sans pouvoir être détectés. L'une des raisons du mauvais résultat des traitements est que les stratégies de traitement actuelles sont généralement basées sur la caractérisation pathologique et moléculaire de la tumeur primaire et non sur l'ensemble de l'environnement, y compris les lésions métastatiques. Il y a donc un besoin en clinique d'obtenir des informations sur les métastases difficilement accessibles et/ou indétectables afin de fournir des thérapies plus efficaces chez les patients.

1.2 Progression tumorale et voie de dissémination du cancer

Le développement d'une tumeur est un processus en plusieurs étapes, conséquence de multiples anomalies qui s'accumulent au fil du temps. On pense que l'apparition d'une tumeur est le résultat d'une altération génétique au niveau cellulaire. D'une manière générale, les cellules malignes prolifèrent et interagissent avec de nombreuses autres cellules environnantes formant ce que l'on appelle un microenvironnement tumoral. Aux stades précoces, le microenvironnement tend à exercer des fonctions anti-malignes, alors qu'aux stades avancés, il exerce des fonctions pro-malignes. Selon le modèle darwinien, les tumeurs évoluent vers une plus grande malignité au fil du temps, favorisant un comportement invasif et une dissémination dans les stades ultérieurs de l'évolution tumorale, de sorte que le développement de métastases distantes est l'étape finale de la progression tumorale. Ce modèle explique avec succès les étapes de la progression tumorale en tenant compte des métastases cancéreuses, mais il fait face à des problèmes conceptuels pour expliquer les observations cliniques suggérant que l'ensemencement métastatique se produit avant la formation d'une tumeur primaire identifiable. Ces observations cliniques sont à la base d'un nouveau modèle de propagation du cancer. Actuellement, les deux hypothèses sont largement étudiées, mais la seconde est confrontée à des défis plus importants en raison de sa nature clinique.

La cascade métastatique comprend principalement la translocation physique d'une cellule cancéreuse de la tumeur primaire vers le microenvironnement d'un tissu distant, et ayant comme stade final sa colonisation. Ce processus consiste en une série d'étapes complexes, impliquant:

b) l'angiogenèse, formant de nouveaux vaisseaux sanguins,
c) l'intravasation, où les cellules tumorales se détachent et quittent la tumeur primaire par la circulation sanguine ou le système lymphatique,
d) la survie des cellules tumorales dans la circulation sanguine et l'arrêt dans les capillaires d'organes distants,
e) l'extravasation des cellules tumorales,
f) la colonisation et la formation d'une tumeur secondaire.

Lorsque la tumeur atteint une taille spécifique, 1-2 mm, la vascularisation est nécessaire pour que la tumeur se développe. Ainsi, l'angiogenèse est une condition préalable à une croissance tumorale massive et à une progression métastatique. Cette néo-vasculature peut également fournir une voie d'échappement grâce à laquelle les cellules peuvent quitter la tumeur et entrer dans le système sanguin circulatoire du corps. Selon l'environnement tumoral, la migration des cellules cancéreuses peut se produire individuellement, lorsque les jonctions cellule-cellule sont absentes, ou collectivement en tant que groupes multicellulaires, lorsque les adhérences cellule-cellule sont maintenues. Le processus d'individualisation des cellules cancéreuses et d'acquisition d'un phénotype migratoire invasif est associé à l'activation du programme de transition épithélio-mésenchymateuse (EMT), qui permet une migration active des cellules cancéreuses. Les cellules tumorales en transition entre les phénotypes épithélial et mésenchymateux (c.-à-d., EMT partielle) ont des propriétés épithéliales (p. ex., adhésion) et mésenchymateuses (p. ex., migration) mixtes, ce qui leur permet de se déplacer collectivement sous forme de grappes.

Les cellules migratrices qui se sont détachées de la tumeur primaire et s'infiltrent avec succès dans les vaisseaux sanguins sont susceptibles de suivre la voie hématogène pour se propager dans le corps. Bien que le système circulatoire soit souvent considéré comme la principale voie de dissémination du cancer, les données suggèrent que le système lymphatique y joue également un rôle. Gagner l'accès au système circulatoire fournir des cellules tumorales, dans cette étape de la propagation du cancer également connu sous le nom de cellules tumorales circulantes (CTC), l'accès direct à pratiquement tous les organes du corps.

Une fois dans la circulation sanguine, une apoptose massive des CTCs se produit en raison de l'anoikis, une mort cellulaire programmée qui se produit lorsqu'elles se détachent de la matrice extracellulaire. Les CTCs sont généralement piégées dans le premier (ou deuxième) lit capillaire qu'elles rencontrent lors de leur premier passage à travers le cœur, ceci en raison de la restriction en taille puisqu'elles sont généralement 2 à 4 fois plus grandes en diamètre que les capillaires (~8-µm de diamètre). D'autres facteurs physiques tels que les forces hémodynamiques et la déformabilité des cellules cancéreuses détermineront leur arrêt dans la microvasculature. On pense que le piégeage physique dans les capillaires est l'un des mécanismes exploités par les cellules tumorales pour l'extravasation.

Les cellules cancéreuses infiltrées peuvent envahir la matrice extracellulaire locale et coloniser le tissu distant ciblé. Ce stade de la cascade métastatique est considéré comme le moins efficace, seul

un petit sous-ensemble (<0,01%) de cellules cancéreuses infiltrées est capable d'initier la division cellulaire et de proliférer, et la grande majorité subira une apoptose dans les 24 heures suivant l'extravasation. Par conséquent, les cellules qui survivent au nouveau microenvironnement formeront des micrométastases et une portion encore plus petite d'entre elles continuera sa croissance pour former des métastases macroscopiques. On pense que les CTCs avec un phénotype de type épithélial sont plus adaptées pour coloniser, ce qui signifie que les métastases peuvent provenir de CTCs avec des caractéristiques épithéliales préservées/conservées ou de cellules qui ont subi une TEM et, lorsqu'elles atteignent un organe secondaire, subissent le processus inverse, la transition mésenchymateuse à épithéliale (MET).

1.3 Biopsie liquide : biomarqueurs du cancer dans le sang

La biopsie solide comprend un groupe de procédures médicales basées sur l'obtention de tissus corporels par biopsie à l'aiguille, des procédures endoscopiques ou une intervention chirurgicale pour l'examen et le diagnostic du cancer. L'analyse pathologique des biopsies tissulaires n'est pas toujours précise car elle ne reflète qu'un seul point dans le temps de toute l'hétérogénéité intratumorale. Il existe un besoin clinique d'accéder à l'information biologique du cancer d'une manière cohérente, moins invasive et répétée afin d'améliorer la prise en charge clinique des patients.

Les biomarqueurs sont définis comme une caractéristique mesurée qui est en corrélation avec un état biologique normal ou anormal dans un organisme vivant. La quantification du biomarqueur approprié peut être utilisée pour différencier un patient affecté d'un sujet sain. En oncologie, les biomarqueurs pourraient fournir des informations pertinentes pour le diagnostic des patients et le pronostic du cancer. De plus, ils pourraient également prédire la réponse au traitement et permettre de surveiller la progression de la maladie. Comme les biomarqueurs jouent un rôle crucial à tous les stades de la pathologie cancéreuse, il y a donc une recherche continue de biomarqueurs fiables qui puissent être facilement mis en œuvre en clinique et qui puissent améliorer l'issue de la maladie et la survie des patients. À cette fin, les efforts se sont concentrés sur l'étude du matériel biologique de divers fluides corporels biologiques tels que le sang, l'urine, la salive, le plasma séminal, le liquide céphalorachidien, pour n'en nommer que quelques-uns.

Dans ce contexte, l'analyse des biomarqueurs du cancer, au niveau cellulaire et moléculaire, portés par la circulation sanguine, a donné naissance au concept émergent de biopsie liquide. La biopsie liquide apparaît comme une approche peu invasive s'intégrant dans la pratique clinique actuelle et offrant des avantages par rapport aux biopsies tissulaires traditionnelles telles qu'une représentativité temporelle et spatiale accrue de l'hétérogénéité des tumeurs solides, et des prélèvements plus fréquents. Ces caractéristiques supplémentaires permettraient principalement de surveiller en temps réel la maladie et d'étudier le comportement biologique de la tumeur, particulièrement utile lors du suivi de la maladie pour l'application d'un plan de traitement adapté à l'échelle du patient que la communauté appelle désormais **médecine de précision**. La biopsie liquide est devenue une nouvelle source reconnue de biomarqueurs du cancer, et ces signatures sanguines peuvent être traitées en analysant des matériaux dérivés de tumeurs comme les CTCs, des fragments d'acides nucléiques exempts de cellules (ADN, ARNm, ARNm, miARN et ARNl), des protéines, des peptides ou des vésicules extracellulaires. Plus récemment, les plaquettes tumorales ont également été signalées comme une autre source de signature tumorale dans le sang.

Parmi la vaste gamme de matériel dérivé d'une tumeur dans la circulation sanguine, les cellules tumorales circulantes, l'ADN libre circulant (cfDNA) et les vésicules extracellulaires dominent le champ de recherche de la biopsie liquide. La facilité relative d'isolement de l'ADN sans cellules à partir d'échantillons de plasma et l'avènement de la PCR numérique et des technologies de séquençage de nouvelle génération ont accéléré les activités de recherche dans ce domaine. Dans les paragraphes suivants, les CTCs seront présentées plus en détail puisqu'elles sont la cible biologique principale de ce manuscrit. La version anglaise de ce manuscrit contient plus d'informations sur les autres biomarqueurs sanguins pour la biopsie liquide.

1.3.1 Cellules tumorales circulantes (CTCs)

1.3.1.1 Transit intravasculaire des CTCs

La survie des rares CTCs trouvées dans la circulation sanguine dépend principalement des interactions favorables qu'elles pourraient avoir avec le bruit de fond important de cellules sanguines normales. Cette interaction se produit principalement avec les leucocytes et les plaquettes, cellules liées respectivement à la surveillance immunitaire et à la coagulation. Afin d'échapper à la surveillance immunitaire, les cellules tumorales peuvent perdre/limiter la présentation/l'exposition des ligands impliqués dans leur reconnaissance et leur interrogation par les cellules du système immunitaire, principalement les cellules NK (Natural Killer) et les lymphocytes T cytotoxiques, ce qui représente un avantage pour contourner leur élimination. Récemment, des études ont également suggéré l'adhésion directe des CTCs sur les neutrophiles, indiquant que les CTCs pourraient potentiellement utiliser les cellules immunitaires comme intermédiaire pour faciliter l'extravasation, ainsi que la présence de macrophages géants circulants capables de lier les CTCs dans le sang périphérique, indiquant que les CTCs interagissent avec presque tous les leucocytes.

L'association entre les plaquettes et les CTCs lors de la translocation, appelée agrégation plaquettaire induite par les cellules tumorales, confère plusieurs avantages à l'immunoévasion. Il a été rapporté que l'agrégation/adhésion des plaquettes autour des cellules tumorales peut former un " manteau " protecteur qui pourrait protéger les CTCs contre la cytotoxicité médiée par les cellules NK et la cytolyse médiée par le TNF-α. Les plaquettes adhérentes peuvent également protéger les cellules cancéreuses du cisaillement hémodynamique exercé par le flux sanguin. De plus, l'agrégation plaquettaire peut également contribuer à l'activation du programme EMT sur les CTCs et favoriser l'extravasation des CTC en améliorant leur adhésion à l'endothélium.

En plus des interactions physico-chimiques entre les cellules sanguines et les CTCs, les cellules cancéreuses subissent un stress de cisaillement généré principalement par le flux sanguin mais aussi par les collisions entre les CTCs, les cellules sanguines et les cellules endothéliales qui tapissent/recouvrent la paroi des vaisseaux. Il a récemment été démontré que les lignées de cellules cancéreuses ayant un potentiel métastatique plus élevé sont plus résistantes au stress de cisaillement. Cependant, il n'est pas clair si le cisaillement hémodynamique peut moduler les propriétés biophysiques et les fonctions des CTCs, et leur conférer une capacité d'initiation de métastases.

Outre les mécanismes de survie susmentionnés, la survie des cellules tumorales disséminées dans la circulation sanguine pourrait être améliorée lorsque les cellules cancéreuses se déplacent en grappes. Les grappes sont rares dans la circulation, 2 à 5 % de la population totale de CTCs, et on

pense qu'elles proviennent de la tumeur solide et non d'événements d'agrégation intravasculaire. Les groupes de CTCs présentent une résistance accrue à l'anoikis en raison d'une combinaison de propriétés mésenchymateuses par rapport à la CTC individuelle, et de jonctions épithéliales persistantes entre cellules épithéliales et cellules. De plus, la coopération entre les cellules au sein des groupes de CTCs peut conférer une résistance aux forces hémodynamiques au sein de la circulation. En plus de sa capacité à survivre dans la circulation sanguine, les groupes de CTCs sont également suggérés comme ayant un potentiel métastatique accru.

1.3.1.2 Différences biophysiques entre les CTCs et les cellules sanguines

La présence de cellules cancéreuses dans le sang des patients métastatiques a été quantifiée depuis le début des années 50, ce qui met en évidence sa faible fréquence, une cellule cancéreuse parmi 10^5-10^6 cellules mononucléaires du sang périphérique. Leur identification par analyse pathologique microscopique a indiqué que les CTCs préservent les caractéristiques cytomorphologiques des cellules tumorales dans les tissus, caractérisées par un rapport noyau/cytoplasme élevé, ainsi qu'une taille et une forme irrégulières par rapport aux cellules épithéliales normales. Les cellules cancéreuses ont souvent des noyaux importants et sont multinucléées. Il convient de noter que les CTCs présentent un degré élevé de pléomorphisme, des variations de taille et de forme des cellules, semblables à celles observées dans les tissus tumoraux primaires et métastatiques. Compte tenu de ces caractéristiques, les cellules cancéreuses sont normalement plus larges que les cellules sanguines normales. Il est généralement admis que la grande majorité des cellules tumorales, ont des propriétés biophysiques distinctes par rapport aux cellules sanguines normales. En termes de taille, les CTCs varient de <4 à >30 µm de diamètre, et cette dimension varie selon le tissu d'origine ainsi que selon les patients.

La déformabilité des cellules cancéreuses a également été étudiée puisque cette propriété est associée à un phénotype invasif et migratoire. Un degré élevé de déformabilité du cytosquelette semble être un trait prédominant des cellules cancéreuses malignes au niveau de la tumeur puisqu'il peut conférer aux cellules cancéreuses la capacité d'envahir les tissus environnants et d'obtenir un accès vasculaire, tandis qu'un cytosquelette plus rigide peut être capable de développer les contraintes internes nécessaires pour contrer les forces hématologiques et résister aux déformations létales.

En ce qui concerne les CTCs et les différences de déformabilité des cellules sanguines, le fait qu'une fraction significative des CTCs soit physiquement retenue dans la microvasculature est peut-être la preuve la plus évidente que les cellules cancéreuses ont des caractéristiques mécaniques plus rigides que les cellules sanguines normales. Certains efforts ont été faits pour comparer directement la déformabilité cellulaire intrinsèque des cellules tumorales tissulaires et des leucocytes, mettant en évidence que les cellules cancéreuses sont significativement plus rigides, même si la déformabilité des CTCs issues de patients reste encore incertaine. En effet, la caractéristique de déformabilité permettrait aux CTCs d'échapper au piégeage mécanique des capillaires, similaire à celui des globules rouges, et de se propager à tous les tissus et organes.

1.3.1.3 Marqueurs de surface membranaires des CTCs

En termes de propriétés biochimiques, les CTCs diffèrent également du sang et des cellules épithéliales normales. De vastes efforts ont ciblé les récepteurs de surface cellulaire accessibles au niveau de la membrane, car il s'agit de la structure principale par laquelle les cellules communiquent et interagissent avec d'autres cellules et leur microenvironnement. Les molécules extracellulaires présentes dans les cellules cancéreuses peuvent être des molécules d'adhésion cellulaire, des cytokines/facteurs de croissance, des récepteurs hormonaux et des récepteurs de neurotransmetteurs.

Au niveau cellulaire, l'identification des marqueurs de surface cellulaire, également appelés antigènes de surface, a été utilisée pour classer les CTCs selon le niveau d'expression de molécules spécifiques. Les trois familles de signatures antigéniques les plus reconnues, présentes seules ou en différentes combinaisons à la surface des CTC, sont les marqueurs épithéliaux, mésenchymateux et les marqueurs de type cellule souche.

En raison de la nature épithéliale des carcinomes, certaines CTCs pourraient exprimer la molécule d'adhésion des cellules épithéliales (EpCAM), une glycoprotéine de surface cellulaire que l'on trouve généralement dans les cellules épithéliales néoplasiques et à des niveaux inférieurs dans l'épithélium normal. Cependant, la sous-régulation d'EpCAM se produit généralement au cours de la transition épithélio-mésenchymateuse, un processus largement associé à la capacité accrue des cellules à pénétrer dans la circulation sanguine, à survivre dans la circulation sanguine et à développer une résistance au traitement.

Dans l'ensemble de la population des CTCs, il a été suggéré que seule une sous-population spécifique d'entre elles peut avoir la capacité de s'auto-renouveler et de se différencier afin de créer de nouvelles tumeurs à des sites distants du site primaire. Dans ce contexte, les cellules souches cancéreuses (CSC) possèdent toutes ces conditions fondamentales pour l'invasion et la métastase des cellules cancéreuses ; il y a donc un intérêt particulier à reconnaître cette sous-population de CTC. La population de CTCs identifiée comme SCC a généralement des propriétés épithéliales, mésenchymateuses et pédiculaires mixtes et la diversité des marqueurs de surface peut être augmentée en fonction de l'organe/tissu d'origine. Toutefois, les marqueurs de pédonculature sur les CTCs font encore l'objet d'études et de discussions approfondies.

Globalement, ces résultats prouvent que notre connaissance des caractéristiques biophysiques, biochimiques et phénotypiques des CTCs contraste avec notre compréhension des constituants normaux du sang périphérique. Des études plus approfondies utilisant une variété de plateformes et de CTCs issues de patients sont nécessaires pour révéler pleinement leurs propriétés, puisque les CTCs offrent l'occasion unique d'étudier la cellule entière, ce qui permet un profilage moléculaire à base d'ADN, d'ARN et de protéines, qui peuvent être utilisés comme biomarqueurs du cancer et aussi pour identifier les cellules ayant une capacité accrue d'initiation d'une tumeur. Cependant, l'un des principaux défis consiste à isoler ce type de cellules anormales de la vaste population de cellules sanguines et, peut-être, avec le même degré d'importance, à les maintenir vivantes pour effectuer une caractérisation protéomique fine et systématique, ainsi qu'une analyse fonctionnelle. Dans cette optique, un aperçu des efforts technologiques qui ont été récemment mis au point pour relever ces défis est présenté ci-dessous.

1.4 Méthodes et technologies de séparation de CTCs à partir d'échantillons de sang

Actuellement, les CTCs doivent d'abord être isolées avant toute analyse phénotypique ou génotypique pour confirmer leur nature. L'isolement des CTCs, extrêmement rares, des échantillons de sang est l'étape initiale du flux opérationnel, et l'avènement de techniques et de processus pour y parvenir a été favorisé par l'accès relativement facile aux échantillons de sang directement des patients cancéreux.

Le principe de base de la séparation des CTCs des cellules sanguines est d'utiliser une ou plusieurs propriétés, biochimiques ou biophysiques, qui sont uniques à ce type de cellules. Deux groupes principaux sont couramment proposés pour classer les technologies dédiées à la séparation des CTCs. Les plateformes qui tirent partie des marqueurs de surface des cellules cancéreuses constituent l'approche par immunoaffinité. Le second, bénéficie des différences biophysiques des CTCs en ce qui concerne les cellules sanguines. De plus, la séparation des cellules peut également être classée en sélection positive et négative. La sélection positive vise à isoler le type de cellule cible (c.-à-d. la CTC) de l'ensemble de la population (c.-à-d. les cellules sanguines), tandis qu'une sélection négative est une méthode indirecte de séparation des CTCs basée sur l'élimination/déplétion des types de cellules indésirables. Certaines plateformes combinent également des approches de sélection positive et négative afin de réduire le bruit de fond des cellules sanguines et d'améliorer la pureté des cellules isolées.

1.4.1 Technologies fondées sur l'immunoaffinité

La stratégie d'isolement fondée sur l'immunoaffinité est l'approche la plus utilisée pour isoler les CTCs des échantillons de sang. Cette méthode utilise des anticorps modifiés dirigés contre les antigènes exprimés par les cellules ciblées. Un anticorps ou un cocktail d'anticorps spécifique peut être déposé sur une surface et placé directement en contact avec l'échantillon de sang, pour une interaction antigène-anticorps. Cette interaction lie la cellule ciblée à la surface fonctionnalisée et permet la séparation cellulaire. Il est important de souligner qu'il n'existe actuellement aucun antigène spécifique de la CTC, ce qui rend difficile leur séparation des cellules sanguines.

Lorsqu'une sélection positive de CTCs est effectuée, les anticorps contre les cellules cancéreuses sont généralement liés à la surface fonctionnalisée de micro/nano perles magnétiques ou de dispositifs spécifiques. Comme précédemment explicité, l'antigène EpCAM est exprimé par les cellules cancéreuses d'origine épithéliale et non par les cellules sanguines normales, cet antigène est donc amplement utilisé comme cible pour l'enrichissement des CTCs par affinité, en gardant à l'esprit qu'aucun antigène spécifique des CTCs n'a été mis en évidence jusqu'à présent. Basé sur des nanoparticules ferrofluidiques recouvertes d'anticorps anti-EpCAM, le système CellSearch (Menarini Silicon Biosystems) est le premier et le seul test sanguin cliniquement validé par la Food and Drug Administration (FDA) des États-Unis pour la détection et le dénombrement des CTCs. Les CTCs sont séparées magnétiquement des échantillons de sang centrifugés dans un système entièrement automatisé, qui peut également effectuer leur reconnaissance. Actuellement, ce système est considéré comme la référence dans le domaine, puisque les technologies émergentes pour l'isolement des CTCs y sont généralement comparées. D'autres technologies émergentes basées sur ce principe de séparation cellulaire sont présentées dans la version anglaise de ce manuscrit.

1.4.2 Technologies basées sur les propriétés physiques

Certaines plateformes d'isolement ont profité des caractéristiques communes observées sur les CTCs, telles que la densité, la taille, la déformabilité et la charge électrique pour les isoler des cellules sanguines normales. Ces méthodes sans l'utilisation d'anticorps sont présentées dans les paragraphes suivants.

1.4.2.1 Centrifugation

Les plateformes basées sur la centrifugation sont généralement une étape de pré-enrichissement pour les plateformes d'isolement de CTCs spécifiques ultérieures. Bien qu'il n'ait pas été conçu à l'origine pour l'isolement des CTCs, les premières études ont fait état de l'utilisation de milieux de gradient de densité Ficoll-Paque (GE Healthcare) pour améliorer le fractionnement du sang. Plus récemment, OncoQuick (Greiner Bio-One) a développé un tube de séparation spécialisé pour permettre une déplétion des érythrocytes, granulocytes, lymphocytes et cellules mononucléaires vers la couche inférieure. RosetteSep™ (STEMCELLL Technologies), combine la centrifugation avec l'enrichissement par immunoaffinité et la suppression des cellules indésirables vers les globules rouges, afin d'augmenter la pureté des CTCs ciblées. Basé sur le principe de la centrifugation, Accucyte® (RareCyte) est une autre plateforme disponible pour le fractionnement du sang.

1.4.2.2 Microfiltration

La microfiltration du sang est utilisée depuis que S. H. Seal a observé que certaines des propriétés intrinsèques des cellules cancéreuses sont qu'elles exhibent une taille relativement plus grande que les globules blancs et une moindre déformabilité que les cellules sanguines. Ces caractéristiques permettent aux cellules sanguines de s'écouler à travers des rétrécissements micrométriques conçus pour ne retenir que la population de CTCs. Grâce à cette approche, aucune modification fonctionnelle de la surface n'est requise puisque les cellules sont piégées par leur taille intrinsèque et leur déformabilité.

Sur la base de ce principe, ISET® (Rarecells Diagnostics) et ScreenCell® (ScreenCell) utilisent des membranes perforées par gravure contenant des pores de 8 µm placés de manière aléatoire pour isoler les CTCs des échantillons de sang dilués dans un tampon. Des membranes microstructurées basées sur une technique de photolithographie ont également été proposées pour contrôler la taille, la forme/géométrie et la distribution des pores sur différents matériaux tels que le silicium, le silicium/nitrure de silicium (VyCAP microsieve, VyCAP), le nickel, et les polymères comme la SU-8 (CellSieveTM, Creatv MicroTech), et le parylène-C. De plus amples informations peuvent être consultées dans la version anglaise de ce manuscrit.

1.4.2.3 Tri hydrodynamique des cellules

Les canaux microfluidiques ayant des dimensions géométriques spécifiques et un débit contrôlé génèrent des forces hydrodynamiques (forces inertielles) qui permettent de trier les cellules selon leur taille. Par exemple, Vortex HT Chip (Vortex Biosciences) utilise la focalisation inertielle pour positionner les CTCs le long du microcanal et les piéger dans les tourbillons générés par l'expansion soudaine du canal. De même, le CTChip® FR (Clearbridge Biomedics) utilise des microcanaux en forme de spirale pour exploiter les forces centrifuges (Dean drag force) en combinaison avec la focalisation inertielle pour séparer les CTCs du reste des éléments sanguins. Dans ce contexte, certaines plateformes ont utilisé le déplacement latéral déterministe (DLD) pour séparer les grandes

cellules des échantillons de sang. Cette technologie utilise une disposition spécifique de micropilliers le long du canal pour contrôler la trajectoire des cellules.

1.4.2.4 Diélectrophorèse (DEP)

Cette approche utilise les propriétés électriques des cellules pour exercer des forces sur elles par l'intermédiaire d'un champ électrique externe. Ces forces peuvent être répulsives ou attractives par rapport à la position de la source de champ électrique et dépendent à la fois des caractéristiques diélectriques des cellules (diamètre, membrane, densité, conductivité, volume) et de leur environnement. Par exemple, ApoStream® (ApoCell) utilise les forces diélectrophorétiques pour attirer les CTCs près du champ électrique et repousser les globules blancs en flux continu. Utilisant un principe similaire, DEPArray™ (Menarini Silicon Biosystems) est une plateforme basée sur des forces répulsives pour manipuler et récupérer des cellules individuelles au sein d'un réseau d'électrodes.

1.5 Méthodes et technologies d'identification des cellules

L'isolement des CTCs à partir d'échantillons de sang à l'aide des technologies décrites ci-dessus est l'étape initiale du flux opérationnel pour une biopsie liquide exploitant les CTCs. Pour pouvoir utiliser ces cellules et les informations biologiques qu'elles contiennent, il est nécessaire de les interroger et de les identifier comme étant des cellules cancéreuses. Les méthodes conventionnelles actuellement utilisées pour l'identification des CTCs sont basées sur les techniques de cytométrie et de réaction en chaîne par polymérase (PCR).

Il n'existe actuellement aucune méthode de détection normalisée pour les CTCs ; néanmoins, l'analyse cytomorphologique combinée à des protocoles d'immunocytochimie est la stratégie la plus fréquemment utilisée puisqu'elle permet l'inspection visuelle et le dénombrement des cellules. Dans cette optique et compte-tenu de l'absence de marqueurs spécifiques des CTCs, les CTCs ont été couramment discriminées des cellules sanguines par l'expression positive de la molécule d'adhésion des cellules épithéliales (EpCAM+), les cytokératines (CK+) qui sont des protéines de structure intracellulaire trouvées dans les cellules épithéliales, et l'expression négative de CD45 (CD45-) qui est spécifique des leucocytes et utilisée pour éliminer la contamination des cellules sanguines ayant une morphologie similaire à celle des CTCs. En complément, le noyau cellulaire est coloré avec du DAPI (DAPI+) pour exclure les fragments cellulaires et une analyse cytomorphologique est également effectuée.

L'expression de ces anticorps conjugués à un fluorochrome est vérifiée en mesurant l'intensité du fluorophore avec des systèmes optiques à haute définition (HD) basés sur la fluorescence tels que la microscopie par fluorescence (statique) et la cytométrie de flux (en flux). Les plateformes comme CellSearch et DEPArray ont incorporé des systèmes d'imagerie par fluorescence semi-automatique dans leur flux opérationnel.

Les cellules isolées sont habituellement caractérisées de manière plus poussée pour évaluer leur nature d'origine tumorale. Des techniques telles que l'hybridation in situ en fluorescence (FISH) sont fréquemment appliquées pour la localisation d'un segment spécifique d'un acide nucléique. Dans la même manière, l'hybridation in situ de l'ARN (ARN-ISH) a également été utilisée pour confirmer l'expression différentielle du phénotype épithélial par rapport au phénotype mésenchymateux.

En plus de l'identification visuelle des CTCs par des techniques basées sur l'expression des protéines, certaines techniques basées sur les acides nucléiques ont également été utilisées pour identifier les CTCs, en particulier les tests basés sur la PCR. Suite à l'extraction des acides nucléiques, l'analyse de l'ARNm fournit des informations en temps réel sur l'activité intracellulaire puisqu'ils sont les produits directs de transcription, synthèse de l'ARNm. L'amplification en chaîne par polymérase et transcription inverse quantitative (qRT-PCR) a été utilisée pour trouver des modèles d'expression associés à la tumeur en utilisant des brins d'ARNm transcrits en ADNc. Cette technique s'est révélée très sensible et spécifique pour quantifier des mutations CTC-spécifiques au niveau de l'ARNm.

1.6 Relevance clinique des CTCs : énumération en tant que biomarqueur pronostique

On croit que les CTCs sont représentatives de la tumeur, à la fois primaire et métastatique, et leur présence dans la circulation sanguine est donc associée à un risque accru de tumeur maligne. Leur isolement, leur détection et leur dénombrement sur la base d'un volume déterminé de sang à plusieurs temps ont été définis comme le procotole à suivre pour offrir des informations quantitatives pendant l'évolution de la maladie. L'énumération des CTCs a été amplement réalisée à l'aide du système CellSearch, qui est devenu la technique de référence dans l'énumération des CTCs. Dans l'ensemble, les études conduites ont porté sur la surveillance de l'évolution du nombre de CTCs dans le sang périphérique avant et après un nouveau traitement, en observant qu'une augmentation du nombre de CTCs, au-delà d'un seuil spécifique, est associée à la progression du cancer. Dans les études cliniques, les données obtenues ont été utilisées comme biomarqueur pronostique pour estimer la survie globale et la survie sans progression.

Des études multicentriques ont prouvé la valeur pronostique de la numération de CTCs chez les patients métastatiques (M1) atteints d'un cancer du sein, de la prostate et colorectal. Les résultats de patients atteints d'un cancer du sein et de la prostate ont montré que les taux de cellules tumorales circulantes ≥ 5 par 7,5 ml de sang total, par rapport au groupe ayant <5 cellules tumorales circulantes par 7,5 ml de sang, avaient une progression médiane plus courte et une survie globale plus courte. Sur la base de ce critère, les patients sont stratifiés en groupes favorables ou défavorables selon les niveaux de CTCs, où 5 CTCs dans 7,5 mL est la valeur seuil. Différentes valeurs seuils ont été établies pour chaque carcinome ; par exemple, le cancer colorectal a une valeur seuil de 3 CTCs dans 7,5 mL de sang.

L'utilisation de la CTC comme biomarqueur prédictif, évaluant la probabilité que la maladie réponde à une intervention thérapeutique, est incertaine et encore à l'étude. Parallèlement, peu d'essais interventionnels, également appelés essais cliniques, sont actuellement menés par différents groupes, dans le but de démontrer que l'utilisation de l'énumération et de la surveillance des CTCs pourrait orienter les décisions cliniques et améliorer les résultats cliniques des patients atteints d'un cancer métastatique.

1.7 Perspectives actuelles des CTCs en biopsie liquide

Comme nous l'avons vu, il existe un besoin clinique évident d'obtenir de façon répétée des informations biologiques liées à la fois à la tumeur primaire et à la lésion métastatique afin de fournir des traitements plus efficaces aux patients. Les biomarqueurs cancéreux circulants offrent l'occasion de répondre à ce besoin. Dans le spectre de la biopsie liquide, les CTCs sont les seules à pouvoir fournir des informations aussi bien génomiques, protéomiques que fonctionnelles liées à la maladie.

D'un point de vue thérapeutique, chez les patients atteints de lésions cancéreuses précoces, l'isolement répété du plus grand nombre possible de CTCs dans le sang et l'identification de leurs signatures moléculaires et fonctionnelles permettraient leur translocation physique. Ainsi, la caractérisation approfondie de ces cellules cancéreuses ayant une capacité d'initiation des métastases fournirait des connaissances et de nouvelles stratégies thérapeutiques pour prévenir les métastases. De même, chez les patients atteints de métastases déjà établies, la caractérisation des cellules isolées pourrait permettre d'identifier des cibles thérapeutiques spécifiques du patient qui pourraient mener à des thérapies plus efficaces.

1.7.1 Isolement d'une population de CTCs hétérogène

Malgré le développement considérable des technologies d'isolement des CTC à partir du sang, il n'existe à ce jour aucune technologie ou méthode capable d'identifier et/ou d'isoler tous les types de cellules tumorales présentes dans la circulation sanguine humaine. Comme nous l'avons vu tout au long de ce chapitre, bon nombre des méthodes d'isolement de CTCs reposent sur la détection de cellules qui expriment des marqueurs épithéliaux dans le sang. De plus, les essais cliniques les plus récents énumèrent les CTCs en utilisant des plateformes basées sur cette approche (CellSearch), ciblant la population de cellules exprimant la glycoprotéine de surface EpCAM.

L'expression transitoire et variable d'EpCAM à la surface des CTCs indique une population dynamique et hétérogène où les mécanismes qui sous-tendent l'EpCAM et d'autres expressions moléculaires différentes ne sont pas bien compris. Cela ouvre de nouvelles possibilités pour les méthodes basées sur des marqueurs multiples et indépendantes de l'antigène dans la voie de la capture d'un plus grand nombre de cellules dérivées de tumeurs et d'une spectre phénotypiquement plus large de cellules dérivées de tumeurs.

1.7.2 Traitement de volumes de sang plus importants

Intrinsèquement, une faible numération de CTCs est étroitement liée à la quantité de sang soumis à un dépistage. L'énumération de CTCs à partir du traitement de volumes sanguins cliniquement pertinents de 7,5 mL souffre d'une faible puissance statistique, principalement parce-que ce volume représente moins de 0,2 % du volume sanguin total. Différentes études ont souligné le besoin d'un plus grand volume de sang en combinaison avec des tests de sensibilité élevée afin d'augmenter le nombre de CTCs et les taux de détection.

Pour répondre à ce besoin, CellCollector (GILUPI Nanomedizin) est une technologie qui prétend avoir accès à de grandes quantités de sang en la plaçant par voie intraveineuse. Ce dispositif est un guide médical structuré recouvert d'une couche d'hydrogel qui, à son tour, est couplée de manière covalente avec des anticorps anti-EpCAM. L'équipe estime que le dispositif est exposé à environ 1 L de sang pendant 30 minutes dans la veine. Dans une étude avec une petite cohorte de patients, cette technologie a montré un plus grand nombre de CTCs chez un plus grand nombre de patients que le système CellSearch. En complément, une stratégie indépendante de l'utilisation d'EpCAM, la leucaphérèse diagnostique, a récemment été proposée pour augmenter le volume de sang prélevé. Cette méthode basée sur la densité traite jusqu'à 62% du sang total par centrifugation continue et recueille des cellules mononucléaires avec des niveaux élevés de CTCs. L'approche combinée à la technologie CellSearch a révélé un taux de détection significativement plus élevé, de 28% à 72%, en comparaison directe.

En plus du traitement en un seul site de prélèvement de grands volumes sanguins, des stratégies de prélèvement sanguin sont également nécessaires à de multiples moments et à différents sites de ponction veineuse afin d'élucider la cinétique réelle de la dissémination des CTCs et les changements phénotypiques et moléculaires dans le sang des patients cancéreux. En général, en milieu clinique, les échantillons de sang des patients cancéreux sont prélevés à intervalles mensuels. Cependant, une étude récente basée sur des cas et des modèles de simulation hypothétiques, a suggéré que l'échantillonnage hebdomadaire, ou même plus fréquent, pourrait améliorer le diagnostic et la prise en charge des patients.

1.7.3 Traitement du sang : prélèvement et préparation des échantillons sanguins

La biopsie liquide, comme toute autre procédure clinique impliquant la manipulation d'échantillons biologiques, comme le sang, doit être traitée immédiatement (<24 heures) ou stabilisée avec des fixatifs. En plus de leur rareté, les CTCs sont soumises à différents facteurs de stress pendant leur transit dans la circulation sanguine humaine, mais peut-être à une altération encore plus importante pendant la prise de sang. En fait, un nombre relativement élevé de CTCs apoptotiques a été signalé dans des échantillons de sang périphérique, ce qui témoigne de leur fragilité.

Il a été rapporté que le nombre de cellules cancéreuses dans les échantillons de sang diminue rapidement sur une période de 5 heures, révélant que le temps entre la prise de sang et la récolte des cellules est critique. D'autres travaux ont montré qu'une dégradation significative de l'ARN se produit dans un délai de 2 à 4 heures. Ces études soulignent la nécessité d'une préservation adéquate de l'échantillon pour le profilage ultérieur de l'expression génétique. Parallèlement, diverses stratégies ont été proposées pour stabiliser les CTCs dans les échantillons de sang, comme les tubes CellSave (CellSearch System, Menarini Silicon Biosystems), l'approche la plus utilisée permettant jusqu'à 96 heures de conservation du sang à température ambiante.

En plus des questions de recueil et de préservation du sang, un caractéristique commune des plateformes d'isolement des CTCs est l'utilisation de fixatifs cellulaires. Cependant, l'utilisation d'une solution de fixation sacrifie la viabilité cellulaire et dégrade l'ARN. Une autre caractéristique prédominante des plateformes d'isolement des CTCs est l'exigence d'une préparation lourde des échantillons, comme la lyse des RBC, la centrifugation, la coloration, le lavage en plusieurs étapes, etc. pour n'en citer que quelques-uns. Ainsi, ces plateformes sont sujettes à la perte de CTCs pendant le processus d'isolement. Par exemple, dans une comparaison directe entre CellSearch et les plateformes de cytométrie en flux, une perte de CTCs 3,3 fois plus importante a été rapportée en raison des procédures d'isolement et de coloration où la cytométrie en flux a donné de meilleurs résultats.

1.7.4 Études fonctionnelles sur les CTCs

Au-delà de l'énumération des CTCs à partir d'échantillons de sang, il n'existe pas à ce jour de données unanimes démontrant leur utilité clinique pour guider les décisions thérapeutiques. Ce dernier est peut-être le principal obstacle à leur mise en œuvre en tant que biomarqueur du cancer en routine clinique. La culture à long terme des CTCs et l'établissement de lignées de CTCs sont la première étape permettant l'acquisition d'informations qualitatives et quantitatives liées à l'activité biologique des CTCs. Les données obtenues à partir de ce type d'études pourraient offrir, par exemple, la possibilité d'identifier les propriétés biologiques des cellules métastatiques, de développer de

nouveaux médicaments anticancéreux ou de comprendre les mécanismes de résistance aux médicaments.

Dans ce contexte, l'isolement de CTCs viables est une condition préalable nécessaire. Une plateforme dédiée à la détection de CTCs viables et à la culture ultérieure des CTCs a été récemment introduite, la technologie EPISPOT. Cette technologie est basée sur la libération du marqueur CK19 à partir des cellules tumorales. Cette plateforme a permis l'établissement de lignées cellulaires dérivées des CTCs à partir d'échantillons de sang présentant différentes pathologies cancéreuses. Une autre alternative est l'utilisation de modèles in vivo, la xénogreffe, pour créer des pathologies cancéreuses cliniquement pertinentes à partir de CTCs. Cette technique a également permis d'identifier un sous-ensemble de la population de CTCs avec un potentiel métastatique accru et d'évaluer certains médicaments anticancéreux.

Cependant, la mise en œuvre courante de ces techniques est actuellement entravée par la difficulté d'isoler systématiquement et fréquemment des CTCs viables en grand nombre, ainsi que par les difficultés techniques rencontrées par la culture de CTCs.

1.8 Objectifs de la thèse

Les objectifs de ce travail de doctorat sont le développement, allant de la conception à la validation, de nouvelles technologies micro-ingénierées pour l'isolement physique des cellules tumorales circulantes à partir de sang total. D'une manière générale, notre objectif principal est de concevoir des dispositifs de capture de CTCs adaptés aux spécifications suivantes :

- Capture des CTCs dans des conditions d'écoulement physiologiquement pertinentes, similaires à celles que l'on trouve dans les veines superficielles humaines, en termes de vitesse d'écoulement et de pression.
- Traitement du sang total, ne nécessitant aucune préparation/traitement préalable.
- Utilisation de techniques conventionnelles pour la fabrication des dispositifs.
- Respect des exigences médicales et mise en œuvre facile des dispositifs en routine clinique.

Sur la base des spécifications générales ci-dessus, notre stratégie a consisté à mettre en œuvre deux approches de capture de CTCs :

1) Directement à partir de la circulation sanguine en utilisant des dispositifs de capture de CTCs qui pourraient être introduits directement dans les veines superficielles humaines pendant une période de temps limitée.
2) En tant que dispositif médical à utiliser au chevet du patient, en utilisant des dispositifs de capture de CTCs adaptés aux consommables médicaux conventionnels en contact avec le sang et aux protocoles cliniques.

Ces nouveaux concepts et dispositifs ont été conçus dans le contexte de la micro-ingénierie, pour répondre aux besoins médicaux et biologiques de la communauté des biopsies liquides.

Chapitre II

Microdispositifs à base de polymères pour l'isolement des CTCs

2.1 Cadre conceptuel et théorique

2.1.1 Concept : microfiltration in vivo du sang pour le piégeage de CTCs

Comme nous l'avons présenté au chapitre I, il existe un besoin clinique pour un accès répété aux CTCs présentes dans le sang des patients atteints de cancer. Outre les technologies hautement sensibles, il a été largement suggéré que l'interrogation d'un grand volume de sang pourrait potentiellement augmenter le nombre de CTCs et les taux de détection. Au moment de la rédaction de cette thèse, la seule technologie d'isolement in vivo de CTCs directement dans le sang, CellCollector®, repose sur l'expression de l'antigène EpCAM à la surface des CTCs. Selon différentes études, les technologies immunologiques basées uniquement sur EpCAM sont sujettes à des biais de sélection, en raison de l'expression hétérogène et dynamique de cet antigène et d'autres antigènes des CTC.

Dans ce chapitre, nous présentons un dispositif médical intravasculaire innovant pour le piégeage physique des CTCs à partir du sang humain, dans des conditions physiologiques de flux veineux. Conceptuellement, le dispositif peut être inséré via un cathéter médical dans une veine superficielle de l'avant-bras d'un patient, une procédure standard en routine clinique, puis exposé à la circulation sanguine pendant une courte période de temps. Les cellules cancéreuses sont distinguées des cellules sanguines normales uniquement sur la base de leurs propriétés physiques intrinsèques.

Nous émettons l'hypothèse que cette nouvelle approche pourrait offrir plusieurs avantages par rapport aux plateformes d'isolement de CTCs conventionnelles actuelles. Premièrement, cette technologie pourrait potentiellement donner accès à des volumes élevés de sang non traité et isoler un large éventail de phénotypes de CTCs préservant l'intégrité cellulaire, puisque l'isolement est effectué dans des conditions physiologiques natives et ne dépend pas de l'expression cellulaire d'un antigène spécifique. Deuxièmement, en raison de son adaptabilité potentielle aux contraintes cliniques, cette technologie pourrait permettre d'effectuer des analyses sanguines plus fréquentes pour suivre avec précision l'évolution du cancer à différents temps. Troisièmement, les cellules isolées sont concentrées dans une petite zone permettant une identification rapide et pourraient servir de plateforme pour des études fonctionnelles. Ainsi, le dispositif de piégeage profite des conditions hémodynamiques des veines superficielles humaines, en tant que source continue de sang, pour effectuer la séparation physique des cellules à travers un réseau de pores micrométriques. En plus de la séparation des cellules, le dispositif de piégeage permet la rétention de ces cellules piégées pour ensuite les récupérer avec le dispositif, afin de les identifier et de les caractériser de manière approfondie.

2.1.2 Microfiltration du sang pour la capture de CTCs : leçons tirées des plateformes ex vivo

La microfiltration du sang a été largement utilisée pour l'isolement ex vivo des CTC. Les configurations conventionnelles utilisent généralement une surface perforée, ou filtre, de quelques millimètres carrés contenant des pores micrométriques placés dans une configuration appelée cul-de-sac, qui permet la filtration cellulaire lorsqu'un flux sous pression pénètre perpendiculairement à

la surface perforée, de sorte que des cellules plus grandes et moins déformables, sont naturellement capturées à l'intérieur des pores. La surface trouée occulte complètement la lumière du système, forçant ainsi le transit du volume total de l'échantillon en un seul passage. Dans des configurations plus conventionnelles, le filtre est placé en sandwich dans des supports à façon et l'échantillon de sang est traité par gravité, à l'aide de seringues, de pompes péristaltiques ou de systèmes à vide. Cependant, la présence du filtre représente une augmentation substantielle de la résistance hydraulique du système, de sorte qu'un système de pompage contrôlé est habituellement préféré pour assurer un débit constant et contrôlé pendant le processus de filtration.

L'interaction de n'importe quel type de cellule avec un pore du filtre dépend des propriétés mécaniques intrinsèques de chaque cellule, et sa capture pendant le processus de filtration est principalement déterminée par le degré de déformation et la pression externe exercée sur elles (différence de pression dans le filtre, ΔP). Les cellules plus larges, à savoir les leucocytes et les CTCs, auront tendance à se déformer afin de se déplacer dans le pore, cette propriété de déformation est déterminée par la viscosité globale apparente de la cellule, qui dépend des caractéristiques cellulaires telles que la membrane cellulaire, le cytoplasme et le noyau.

Les cellules ayant une viscosité apparente plus élevée auront un transit plus lent à travers la constriction à une pression spécifique ΔP, connue sous le nom de pression critique, le piégeage complet d'une cellule dans le pore est ainsi assuré. En dessous d'une pression critique, la tension superficielle de la membrane cellulaire équilibrera la force qui pousse la cellule dans le pore du filtre. Inversement, à des pressions supérieures à cette pression critique, la cellule se déplacera dans le pore à un taux déterminé par la viscosité apparente. La pression critique de certaines lignées cellulaires cancéreuses est de 160-800 Pa.

Par conséquent, la plage de ΔP dans laquelle la filtration CTC est plus efficace doit être légèrement supérieure à la pression critique des CTC (Coumans et al). Dans ces conditions, et en supposant que la pression critique des CTCs est plus élevée que celle des cellules sanguines, toutes les cellules sanguines passeront à travers les pores et les CTCs seront retenues en raison de leur tension superficielle intrinsèque. Dans la pratique, la filtration du sang pour la capture de CTCs est généralement effectuée à des valeurs plus élevées que la pression critique de tous les types cellulaires, allant de 0,1 psi à ΔP psi (700 Pa à 100 kPa). L'exécution du traitement du sang total à l'aide de ces filtres et dans des conditions de pression plus basse peut conduire à l'obstruction des pores étant donné la complexité du sang. Par conséquent, la plupart des technologies utilisent des échantillons de sang dilué ou préparent des échantillons par exemple en lysant les globules rouges.

Le traitement d'importants volumes de sang ou leur traitement pendant une période prolongée entraînera une réduction du taux de récupération des CTCs. C'est probablement l'une des raisons pour lesquelles certaines des plateformes actuelles ne traitent que quelques ml de sang total. Par conséquent, en termes pratiques, la sélection d'une pression de travail/débit adéquate pour un type de filtre spécifique, défini par sa porosité et la taille des pores, et un volume déterminé de sang, semble être un facteur déterminant pour maximiser la capture de CTCs. Compte-tenu de ce qui vient d'être mentionné, la sélectivité des systèmes de filtration n'est pas seulement déterminée par la taille des cellules ciblées par rapport à celle des pores, mais aussi par les conditions de fonctionnement du système de filtration et le temps de traitement de l'échantillon.

Un effet associé aux systèmes de filtration est l'endommagement des cellules. Des expériences utilisant l'aspiration par micropipette ont montré qu'une augmentation supérieure à 3 % de la surface de la membrane cellulaire entraînera des dommages permanents. Les contraintes mécaniques induites sur les cellules pendant le processus de filtration sont directement liées aux conditions de pression expérimentale et à la taille/géométrie de la constriction. Lors du processus de capture des cellules, la principale source de stress mécanique provient de la pression statique du système de filtration.

A notre connaissance, il n'existe actuellement aucun système de filtration conçu pour la capture de CTCs dans lequel les conditions d'écoulement sont adaptées pour fonctionner dans la plage de pression critique théorique des CTCs. Ayant ceci comme prémisse, nous envisageons ici de fournir, pour la première fois, des preuves expérimentales de la capture de cellules cancéreuses à partir d'échantillons de sang dans des conditions d'écoulement physiologiquement pertinentes, répondant aux exigences susmentionnées de pression critique.

2.1.3 Spécifications ciblées et paramètres de conception

Comme nous l'avons présenté au début de ce chapitre, notre principal objectif est d'évaluer le piégeage physique des CTCs directement à partir du sang humain à l'aide d'un dispositif technique contenant un réseau de pores micrométriques. Il est utile d'établir clairement le cadre et les contraintes de ce développement.

La première contrainte est liée aux dimensions physiques. Notre objectif est de réaliser la procédure de capture de CTCs in vivo au niveau de la veine basilique superficielle, l'un des sites de ponction veineuse les plus courants dans l'avant-bras humain, avec un diamètre allant de 2 à 7 mm. Dans le cadre d'une première étape de prototypage rapide, nous avons utilisé des aiguilles de ponction veineuse comme canule d'insertion, en sélectionnant une aiguille hypodermique 18G (diamètre intérieur 860-920 µm). En prévision de son application future en tant que consommable médical potentiel et compte-tenu de son utilisation pratique en routine clinique, nous avons limité les dimensions globales du dispositif à <500 µm.

Notre approche de filtrage du sang ne vise pas à interroger le volume sanguin total circulant dans la veine basilique car il impliquerait l'occlusion totale de la section veineuse, et par conséquent représenterait un risque pour le patient. Cependant, nous cherchons à maximiser la quantité de sang interrogé par le dispositif de capture sans avoir d'effets secondaires liés à la perturbation du flux sanguin. Par conséquent, la raison d'être de la conception géométrique du dispositif de capture est basée sur la création d'une dérivation du flux principal, dans lequel la filtration du sang et le piégeage des CTCs seront effectués. Sur la base de cette prémisse, nous avons envisagé une géométrie tubulaire 3D. Le cylindre est aligné longitudinalement le long de la direction du courant où le flux sanguin entrant est dévié, créant une zone confinée caractérisée par une vitesse plus faible. Ce flux d'écoulement secondaire passera à son tour à travers une membrane trouée placée à l'extrémité de la géométrie tubulaire. Ci-après, l'ensemble formé par la géométrie tubulaire et la membrane trouée sera appelé microdispositif.

Le diamètre du cylindre constitutif du microdispositif a été fixé à D_C= 200 µm et sa longueur à L_C= 150 µm. La membrane trouée contient 137 pores de d_p=12 µm de diamètre chacun. Le raisonnement

détaillé sur la façon dont les dimensions physiques du microdispositif ont été sélectionnées peut être consulté dans la version anglaise de ce manuscrit.

2.2 Preuve de concept à l'aide d'une technique de prototypage rapide

2.2.1 Technique d'écriture directe par laser pour la fabrication en 3D du microdispositif

Compte-tenu des caractéristiques spécifiques de notre concept et de la disponibilité de l'équipement dans les infrastructures de notre laboratoire, nous avons évalué la faisabilité de la fabrication du microdispositif à l'aide de techniques de prototypage rapide. L'écriture directe par laser (DLW) basée sur une polymérisation à deux photons est une technique unique offrant une structuration tridimensionnelle (3D) de haute précision. Nous avons utilisé l'équipement disponible commercialement (système Photonic Professional, Nanoscribe® GmbH) au début de ce projet, et plus tard, la version GT mise à jour du Photonic Professional a été utilisée.

Nos microdispositifs 3D sur-mesure ont été conçus à l'aide d'un logiciel de conception assistée par ordinateur (CAO) (Autodesk Inventor® 2015) et paramétrés à l'aide du logiciel DeScribe® (Nanoscribe® GmbH). Des paramètres tels que la puissance laser et la vitesse d'écriture ont été optimisés à l'aide d'une résine photosensible négative (IP-Dip, Nanoscribe® GmbH). Les microstructures fabriquées ont été développées en suivant le processus suggéré par le fournisseur. Ainsi, la puissance laser optimale a été fixée à 65 % et la vitesse de balayage à 50 mm s^{-1}, tandis que les distances de sectionnement/hachure ont été fixées à 200 nm. Parallèlement à l'optimisation de l'exposition (dose), les variables géométriques correspondant à l'épaisseur de la membrane trouée et à l'épaisseur de paroi du cylindre ont été fixées à t_m = 6 µm et t_c = 10 µm respectivement. Le diamètre des pores a été mesuré avec un diamètre moyen Dp=11,5±0,08 µm.

2.2.2 Validation de la capture des cellules à l'aide d'un microdispositif intégré à une plateforme fluidique.

2.2.2.1 Fabrication de la plateforme fluidique

Tout d'abord, nous avons voulu valider notre concept dans des conditions d'écoulement similaires à celles que l'on trouve dans les veines humaines. Nous avons conçu la fabrication d'une plateforme fluidique dans laquelle les conditions géométriques et d'écoulement reproduisent celles de la veine basilique de l'avant-bras humain. La vitesse moyenne rapportée varie d'une valeur minimale de 0,072 ± 0,007 ms^{-1} à une valeur maximale de 0,24 ± 0,027 ms^{-1}. De plus, la pression moyenne est d'environ 10 mmHg, ce qui équivaut à 1333,22 Pa. Ce banc fluidique a été conçu pour permettre des conditions expérimentales contrôlées, l'observation en temps réel des événements de capture et la caractérisation par microscopie in situ.

La plateforme fluidique a été adaptée aux techniques de moulage disponibles dans notre laboratoire (moulage par utilisation du polydimethylsiloxane ou PDMS), ce qui nous a permis d'obtenir un canal de 1 mm de haut de section carrée et une longueur totale de 12 mm. Nous avons proposé l'utilisation d'une base élévatrice pour placer le microdispositif au milieu de la section transversale du canal (pilier en SU-8), afin d'améliorer l'efficacité de capture des cellules. Les détails sur les étapes de fabrication peuvent être consultés dans la version anglaise.

2.2.2.2 Dynamique des fluides dans la plateforme fluidique

Avant d'évaluer les performances de capture du concept proposé dans des conditions réelles d'écoulement, une évaluation in silico a été effectuée dans le but de prédire le champ d'écoulement et la dynamique à l'intérieur et autour du microdispositif 3D. Des simulations de la dynamique des fluides à l'état d'équilibre ont été réalisées avec ANSYS Fluent (ANSYS Fluent® v15). Au début, le fluide a été modélisé en tant que fluide simple (eau, ρ=997.13 kg m^{-3}, μ=0.000891 kg m^{-1} s^{-1}), la pression en entrée fixée à P=1333.33 Pa, et les vitesses de référence, v_{min}=0.072 m s^{-1} et v_{max}=0.275 m s^{-1}, ont été ciblées.

Nous avons d'abord observé que le banc d'essai proposé permettrait d'obtenir un champ de vitesse ayant un profil parabolique pleinement développé, comme on peut s'y attendre dans des conditions expérimentales réelles. D'une manière générale, l'ensemble formé par le microdispositif et le pilier modifie, en amont et en aval, le champ d'écoulement. En prenant comme référence la position de cet ensemble, en amont, le champ de vitesse est perturbé à une distance 3 fois la longueur L_c du microdispositif ($L_{upstream}$) approximativement. Le profil initial est récupéré après 12 à 15 fois la même distance caractéristique ($L_{downstream}$).

Nous nous attendions à ce que le microdispositif 3D favorise une redistribution du flux et qu'une partie du flux passe en son sein. La vitesse globale à l'intérieur du microdispositif varie de 10 mm s^{-1} à 60 mm s^{-1}, lorsque v_{min}=0,072 m s^{-1}, et de 100 mm s^{-1} à 180 mm s^{-1} lorsque v_{max}=0,275 m s^{-1}. De plus, nous avons estimé le volume total de liquide traversant le microdispositif par unité de temps (débit effectif Q_{eff}). Le modèle numérique révèle que Q_{eff} varie de 45 à 145 µl par minute à v_{min} et v_{max} respectivement. Nous n'avons observé aucun tourbillon en aval du microdispositif dans la plage de vitesses d'intérêt.

Nous avons également analysé la distribution de pression dans le microdispositif à v_{min} et v_{max}. Nous avons estimé la différence de pression à travers le filtre ΔP en trouvant des valeurs de 40 à 200 Pa lorsqu'on considère l'eau et de 200 à 700 Pa dans le cas du sang.

2.2.2.3 Capture de cellules à l'aide du microdispositif intégré à la plateforme fluidique

Les performances de capture du microdispositif 3D sous flux ont été analysées dans la plateforme fluidique décrite ci-dessus, adaptée à un système de pompage péristaltique externe. Afin d'observer les événements de capture, nous avons eu besoin d'un fluide optiquement transparent, c'est pourquoi nous avons utilisé un milieu de culture cellulaire comme liquide modèle. Nous avons d'abord préparé des suspensions contrôlées de cellules cancéreuses de la prostate humaine (PC3), génétiquement modifiées pour exprimer la protéine fluorescente verte (GFP). De plus, nous avons marqué l'ADN des cellules cancéreuses au DRAQ5 (rouge lointain) afin de pouvoir facilement les identifier par rapport au fond fluorescent émis par le microdispositif.

Au système de pompage (FH100®, Thermo Scientific) a été réglé pour atteindre soit v_{min} ou v_{max} à travers le canal en ajustant la vitesse de rotation à 10 rpm et 40 rpm respectivement. La plateforme fluidique a été pré-rincée en sens inverse, avec 30 mL d'éthanol suivi de 30 mL de milieu de culture cellulaire RPMI-1640. Les suspensions cellulaires ont été préparées en volumes de 10 mL et ont circulé en boucle fermée c'est-à-dire que les tubulures d'entrée et de sortie ont été placées dans le même contenant. Après écoulement des cellules, une étape de rinçage a été effectuée avec 30 mL de milieu de culture cellulaire RPMI-1640, puis les cellules capturées ont été fixées à l'aide de formaldéhyde à 4% (solution de formol, tampon neutre, 10%, SIGMA-ALDRICH®).

2.2.2.4 Évaluation de la contamination de la membrane trouée

Selon le principe de filtration "tronquée" (*dead-end filtration*), l'obstruction progressive des pores, au fur et à mesure que les cellules sont capturées, devrait entraîner une diminution du débit efficace passant à travers le microdispositif au fil du temps avant d'atteindre l'obstruction totale de la membrane trouée. Ce mécanisme a été évalué afin d'estimer un délai raisonnable qui permettrait de capturer les CTCs sans atteindre le stade d'obstruction. Pour ce faire, on a utilisé des suspensions hautement concentrées, contenant 25 000 cellules mL^{-1} et 1000 cellules mL^{-1}.

Nos observations expérimentales suggèrent que la performance de capture du microdispositif 3D est diminuée d'environ 60% de sa capacité potentielle de capture cellulaire. Cette caractéristique a été observée à t ≈ 8 min et t ≈ 2 min pour la vitesse = v_{min} et la vitesse = v_{max} respectivement. Nous avons suggéré qu'une durée acceptable de 10 minutes permettrait de capturer les cellules à une plage de concentration relativement faible, évitant à la fois la saturation de la membrane trouée et la surexposition du microdispositif à l'écoulement.

Nous avons ensuite inspecté ces échantillons par microscopie confocale à fluorescence (Upright Leica SP8). L'inspection de la membrane trouée a révélé que les cellules sont uniformément réparties sur toute la surface et que les cellules bloquant les pores sont la cause de la diminution observée de la perméabilité. De plus, les cellules piégées semblent aussi fortement adhérer à la surface trouée de la membrane.

2.2.2.5 Effets hydrodynamiques dus à l'obstruction de la membrane trouée

Nous avons évalué numériquement les effets hydrodynamiques possibles à l'intérieur du microdispositif en raison de l'obstruction de la membrane trouée. Nos résultats montrent une diminution graduelle de Q_{eff} à mesure que le nombre de pores bloqués augmente, et diminue à 50% lorsque 80/137 pores sont bloqués. Dans ces conditions, on observe une région de stagnation près de l'entrée du microdispositif et les vecteurs de vitesse présentent un profil similaire aux tourbillons symétriques.

Nos données expérimentales suggèrent que le plateau de saturation se produit à C_C=90-100, alors que les simulations montrent une baisse significative de Q_{eff} et une région de stagnation lorsque >80 pores sont bloqués. De plus, nous considérons que la configuration symétrique des tourbillons, comme le montrent les vecteurs de vitesse, n'induit aucun reflux des cellules piégées. Ceci est renforcé par nos preuves expérimentales, où nous n'avons pas observé le détachement et le reflux des cellules piégées. Toutefois, il n'est pas écarté que cette région de stagnation puisse induire des instabilités de débit.

2.2.2.6 Évaluation des changements de morphologie cellulaire dus à l'amplitude de vitesse

Nous avons évalué si des changements dans l'amplitude de vitesse pourraient avoir un impact sur la morphologie des cellules piégées. Nous avons traité 40 mL d'une suspension à 5000 cellules mL-1, à la fois à vmin=0,072 m s-1 et vmax=0,275 m s-1. La caractérisation par microscopie électronique a montré que la plupart des cellules capturées conservent une forme sphérique et restent adhérentes à la surface de la membrane trouée dans les deux conditions de vitesse testées. Une morphologie plus arrondie a été observée à vmin, ce qui est probablement associé à la différence de pression plus

faible à travers le filtre ΔP. Certaines cellules de forme aplatie ont rarement été identifiées, ce qui pourrait être un artefact résultant de l'étape de déshydratation.

2.2.2.7 Évaluation de la viabilité cellulaire des cellules capturées

Comme le suggère l'imagerie morphologique, les cellules piégées semblent préserver leur intégrité et leur viabilité. Pour vérifier cette hypothèse, nous avons procédé à la culture des cellules piégées. Après piégeage cellulaire, nous avons introduit 500 µL de trypsine dans le canal fluidique, afin de favoriser le détachement des cellules de la membrane trouée, puis les cellules ont été récupérées par flux inverse. Le volume recueilli a été réparti entre trois puits différents d'une plaque de 96 puits et monitoré pendant deux semaines.

Nous avons observé la prolifération des cellules, à partir de <10 cellules par puits jusqu'à atteindre confluence, avec un taux de duplication de 44h. Ce résultat suggère que les cellules capturées sont représentatives en termes de caractéristiques phénotypiques et génotypiques de la population initiale de cellules.

2.2.2.8 Évaluation de la limite de détection

Nous avons réalisé une série d'expériences afin d'étudier la limite de détection du microdispositif 3D. Nous avons traité des suspensions cellulaires à des concentrations allant de 10 à 25 000 cellules par mL de cellules modèles (PC3-GFP marquées au DRAQ5) pendant 10 minutes à v_{min}. Nous avons observé une relation directe entre le nombre de cellules C_C capturées et la concentration cellulaire de la suspension traitée. Les cellules ont été détectées jusqu'à une concentration de 10 cellules mL^{-1}, où le nombre de cellules récupérées était d'une cellule. En dessous d'une concentration de 500 cellules mL^{-1}, le nombre de C_C n'était pas plus élevé qu'une seule cellule. Nous croyons que ce nombre de cellules capturées est la conséquence de la quantité relativement faible de liquide filtré par un seul microdispositif (débit effectif $Q_{eff} \approx$ µL) pendant une expérience de 10 minutes, imposée par le temps de filtration établi et la vitesse du fluide dans le canal.

2.2.2.9 Évaluation de la contamination des pores par les cellules sanguines

Il existe des différences significatives entre le fluide de notre modèle (c'est-à-dire le milieu de culture cellulaire) et le sang total. En particulier, le sang est considéré comme un fluide complexe en raison de l'hétérogénéité de sa composition cellulaire, du nombre de cellules (~10^9 cellules par mL) et de ses propriétés rhéologiques.

Nous avons d'abord évalué la contamination possible de la membrane trouée et l'adhérence non spécifique des éléments sanguins sur le microdispositif. Le sang a circulé à travers la plateforme fluidique pendant 10 minutes à v_{min} et a ensuite été rincé avec un milieu de culture cellulaire. L'inspection globale des échantillons n'a pas révélé d'accumulation massive de cellules sanguines, que ce soit dans l'environnement ou à l'intérieur du microdispositif. Nous avons observé des agrégats plaquettaires mineurs et des débris non identifiés à la surface ou à l'intérieur des pores de la membrane.

De plus, nous avons évalué l'utilisation d'héparine pour inhiber l'adhésion des plaquettes et la formation potentielle de caillots sanguins. Cependant, nous n'avons pas observé d'amélioration significative du nombre d'agrégats plaquettaires, puisque le sang traité à l'EDTA utilisé permet déjà

d'éviter ces effets. Ainsi, nous avons continué à utiliser des microdispositifs sans traitement de surface.

2.2.2.10 Évaluation de la capture de cellules PC3 à partir d'échantillons de sang

Après avoir établi la faisabilité de l'utilisation de sang total dans notre plateforme fluidique sans contamination considérable de la membrane trouée, nous avons ensuite évalué si nos résultats dans la capture de PC3 à partir de milieu de culture cellulaire étaient transposables aux échantillons de sang. Comme dans le cas des expériences à partir de milieu de culture cellulaire, nous avons ajouté des concentrations contrôlées de cellules PC3-GFP marquées au DRAQ5 dans le sang total de donneurs sains. Nous avons réglé la vitesse dans le canal à v_{min} et le temps expérimental a été fixé à 10 minutes, comme pour les expériences précédentes.

Le piégeage des cellules indésirables, comme les globules blancs, est un paramètre couramment étudié dans ce domaine. Nous avons trouvé une contamination négligeable de globules rouges ou de leucocytes, résultant en une très large majorité de pores libres. Toutefois, comme nous l'avons déjà mentionné, des agrégats plaquettaires sont occasionnellement observés. Dans la plupart des échantillons, nous avons pu reconnaître la morphologie arrondie des cellules cancéreuses piégées, semblable à celle que l'on trouve dans les milieux de culture. Par conséquent et ci-après, nous avons défini comme C_C ces cellules exprimant la double coloration dans la caractérisation confocale, et également trouvé par imagerie électronique ayant >5µm comme diamètre caractéristique.

Nous avons comparé le nombre de cellules piégées en utilisant les valeurs C_C obtenues à partir d'expériences avec du milieu de culture comme base de référence. Dans le cas des expériences sanguines, à 25 000 mL^{-1}, la C_C variait de 13 à 36 cellules dans les quatre expériences réalisées. Notez que moins de cellules PC3 ont été capturées dans le sang total que dans les suspensions de milieu de culture cellulaire (moins 60 à 70 %). Nous croyons que cette réduction du nombre de cellules capturées est due à la combinaison de deux facteurs provoqués/induits par les cellules sanguines : la polarisation de la concentration et le temps de transit cellulaire. Voir la version anglaise pour une explication plus détaillée.

Étant donné les observations du nombre de capture de cellules à des concentrations élevées de PC3, nous avons également évalué la performance du microdispositif à des concentrations relativement faibles. De même, nous avons traité 8 mL de sang total enrichi avec des PC3-GFP marquées au DRAQ5 afin d'obtenir une concentration de 1000 cellules mL^{-1}. Sur les cinq expériences, aucune cellule n'a été trouvée dans trois échantillons, et le nombre de cellules capturées était de C_C=2 et C_C=4 respectivement dans les deux autres échantillons.

2.3 Conception du prototype intravasculaire

2.3.1 La stratégie de ponction veineuse et d'insertion

Le banc d'essai fluidique a permis de démontrer la faisabilité de la capture de cellules cancéreuses dans différentes conditions d'écoulement. Cependant, notre objectif final est l'intégration du microdispositif 3D sur des substrats à-façon qui permettrait son insertion dans la veine par le biais d'aiguilles de ponction veineuse. Pour ce faire, nous avons proposé un système d'insertion à double aiguille, qui se compose d'une aiguille de ponction, d'une languette adaptée à une aiguille d'insertion et du microdispositif de capture.

En pratique, nous avons fabriqué le microdispositif sur une languette en alliage Nickel-Titane, et cet ensemble a ensuite été intégré à une aiguille 20G. Par la suite, ce guide a été fixé au piston d'une seringue de 1 mL munie d'une aiguille à ponction veineuse de 18G. Ce montage pourrait permettre de protéger le microdispositif pendant la pénétration de la peau/veine par l'aiguille de ponction et, une fois à l'intérieur de la veine, son exposition à la circulation sanguine. De plus amples détails sont fournis dans la version anglaise de ce manuscrit.

2.3.2 Évaluation de la transposition de la capture de cellules cancéreuses in vitro à la capture des cellules cancéreuses in vivo

L'ensemble à double aiguille a d'abord été évalué in vitro à l'aide d'une plateforme fluidique en PDMS de 3 mm de section, comparable à celle mimant la veine basilique et en utilisant notre fluide modèle. Pour cette configuration, la vitesse de rotation de la pompe péristaltique a été réglée à 28 rpm afin d'atteindre v_{min}=0.072 m s^{-1} dans le canal. Comme nous l'avons déjà mentionné, nous avons utilisé des cellules PC3-GFP marquées au DRAQ5 dans des suspensions de milieu de culture cellulaire, cette fois à des concentrations de 5000 cellules par mL.

Les premières expériences utilisant le système proposé ont mis en évidence la fragilité du microdispositif. Malgré une bonne adhérence mécanique sur la languette métallique, dans la plupart des expériences, le contact physique de celle-ci avec les parois de l'aiguille de ponction, au moment de la rétraction, ont endommagé ou détaché le microdispositif de la languette. Cependant, les quelques expériences réussies ont confirmé la capacité de capture cellulaire de ce prototype. Ces quelques résultats ont mis en évidence une valeur inférieure de Cc par rapport au banc d'essai de 1 mm décrit ci-dessus. La diminution de la performance de capture de ce prototype pourrait être attribuée à la perturbation de la vitesse du flux dans le canal, causée par le système à double aiguille, qui détourne le flux en aval vers le microdispositif, ce qui entraîne un flux effectif plus faible passant à travers le microdispositif Q_{eff}.

Nous avons envisagé différentes stratégies pour surmonter le défi de la fragilité mécanique et obtenir la validation in vivo du système. Nous avons envisagé de protéger le microdispositif d'un contact mécanique en adaptant un couple de demi-sphères avec une dimension plus grande que le microdispositif. Cette solution technique présentait des caractéristiques acceptables pour l'expérimentation in vivo, nous avons donc procédé à son évaluation dans des modèles animaux.

En collaboration avec Catherine Viguié de l'École Nationale Vétérinaire de Toulouse (ENVT-INP, Toulouse, France), nous avons établi les protocoles requis pour l'utilisation de mini-porcs comme modèle animal. Ce modèle a été choisi en raison des similitudes physiologiques dans la taille des veines et des cellules sanguines chez l'homme. Une suspension de cellules PC3-GFP a été injectée directement dans les veines superficielles au niveau de l'avant-bras et du sein, et notre prototype a été inséré dans la même veine quelques centimètres après le site d'injection cellulaire.

Les résultats n'ont pas été satisfaisants en termes de capture de cellules tout au long de cet ensemble d'expériences, puisqu'aucune cellule PC3 n'a été identifiée par inspection confocale. Cependant, ces expériences ont permis d'identifier plusieurs facteurs importants pour l'amélioration du dispositif et des protocoles expérimentaux. Celles-ci sont énumérées ci-dessous :

- Microdispositif mécaniquement fragile. Sur les quatre prototypes testés in vivo, trois d'entre eux ont été récupérés avec une intégrité mécanique intacte. L'autre était trop fragile pour résister aux étapes d'insertion et de récupération, et s'est détaché pendant l'intervention. Cela prouve que le prototype proposé, basé sur un microdispositif polymère, n'est pas adapté pour résister à la manipulation entre utilisateurs, puisque la précision et le soin extrêmes étaient nécessaires à chaque étape de la procédure chirurgicale. Nous avons conclu que les dispositifs polymères ne conviennent pas aux essais de capture de PC3 in vivo.
- Caractérisation non conventionnelle. L'observation globale de la membrane trouée a été difficile, car elle exige le positionnement vertical de la languette, ce qui implique un risque supplémentaire étant donné la fragilité du microdispositif. À partir de cette expérience, nous avons conclu que la technologie, en plus d'effectuer la capture des cellules, doit être compatible avec les méthodes de caractérisation conventionnelles.
- Sélection appropriée du modèle animal et des protocoles d'intervention. Le mini-porc comme modèle animal offre, en principe, des caractéristiques physiologiques similaires à celles de l'homme, mais étant donné le volume sanguin relativement élevé du modèle utilisé et l'évacuation naturelle des cellules injectées, il était difficile d'assurer la circulation des cellules cancéreuses par injection intraveineuse. C'est la raison pour laquelle l'injection et la capture des cellules ont été effectuées le long de la même voie veineuse, bien qu'il ait été bien connu à l'avance que cette méthodologie ne représente pas les conditions réelles trouvées chez les patients. Ainsi, afin d'assurer la circulation réelle des cellules cancéreuses injectées dans l'organisme pendant une durée déterminée, il a été défini que des modèles animaux plus petits pouvaient être plus appropriés.

2.4 Conclusions du chapitre II

Dans ce chapitre, nous avons introduit la microfiltration sanguine pour l'isolement de CTCs, une approche technologique largement utilisée dans le domaine de la biopsie liquide. Partant du principe que les CTCs sont plus larges et moins déformables, la communauté scientifique a proposé une diversité de filtres microstructurés, fabriqués principalement par des techniques de lithographie développées dans le domaine de la microfabrication. Parmi ces dernières, la grande majorité converge vers l'utilisation d'une configuration "tronquée". L'accent a été mis sur les conditions d'exploitation de ces plateformes, ce qui prouve que la sélectivité des CTCs n'est pas seulement déterminée par la taille des cellules ciblées par rapport à celle des pores, mais aussi par les conditions de pression du système de filtration et le temps de traitement de l'échantillon.

La revue bibliographique a permis de mieux comprendre les mécanismes physiques qui permettraient une capture in vivo des cellules cancéreuses présentes dans la circulation sanguine humaine. Cette prémisse a jeté les bases de la conception d'un microdispositif 3D adapté aux exigences médicales. Nous avons fabriqué le microdispositif proposé en utilisant une technique de fabrication additive à haute résolution et l'avons intégré dans un banc fluidique à façon pour l'évaluation de la capture des cellules cancéreuses.

Le concept de capture des cellules cancéreuses dans des conditions d'écoulement physiologiquement pertinentes a été démontré avec succès dans des conditions in vitro en utilisant une lignée de cellules cancéreuses prostatiques comme modèle. Nous avons pu obtenir

un suivi en temps réel des événements de capture de cellules et avons pu caractériser le matériel biologique isolé. En combinaison avec des simulations en dynamique des fluides, nous avons évalué les problèmes associés aux systèmes de filtration "tronquée", comme l'obstruction des pores, ce qui prouve qu'il est possible de traiter du sang total. De plus, nos résultats ont mis en évidence la préservation de la morphologie cellulaire qui, dans une étude préliminaire, suggère la viabilité du matériel biologique capturé.

Nous avons également fourni une première évaluation expérimentale de la limite de détection de notre microdispositif 3D, tel qu'établi pour différentes plateformes d'isolement de CTCs. Nous pensons que l'efficacité de capture de cellules est étroitement lié au volume effectif de flux sondé par le microdispositif 3D. Nos résultats préliminaires suggèrent une performance limitée pour la détection de suspensions cellulaires très faiblement concentrées mais nous envisageons quelques stratégies techniques pour l'amélioration du microdispositif de capture et leur mise en œuvre, qui seront expliquées en détail au chapitre III.

Dans la perspective d'une véritable capture cellulaire in vivo, nous avons développé un système intravasculaire intégrant le microdispositif de capture. Un premier essai de capture de cellules par voie intraveineuse a été réalisé sur des modèles animaux, et nous avons prouvé que l'un des principaux défis pour une utilisation des microdispositifs de capture est leur robustesse pour résister aux manipulations en routine clinique et pour pouvoir atteindre des applications cliniques réelles. Ce problème est abordé dans la première partie du chapitre III.

Les techniques et protocoles présentés dans le chapitre II serviront de base aux travaux présentés dans le chapitre suivant.

Chapitre III

Microdispositifs métalliques pour l'isolement de CTCs

3.1 Partie I : Capture de cellules in vivo à l'aide de dispositifs métalliques

3.1.1.1 Approches visant à améliorer les propriétés mécaniques du microdispositif 3D

Dans l'ensemble, les résultats in vitro et in vivo du chapitre II de ce manuscrit ont mis en évidence la nécessité de microdispositifs aux performances mécaniques supérieures comparées à celles des microdispositifs en polymère. Bien que plusieurs technologies aient été récemment développées dans le domaine de la fabrication additive utilisant des matériaux tels que la céramique et les métaux, celles-ci sont encore limitées à ~20-50 µm en résolution, ce qui les rend impropres à la fabrication de la membrane trouée. Afin de répondre à ce besoin technologique, nous avons proposé la mise en œuvre d'un dépôt électrochimique de métal en plusieurs étapes afin de concevoir à la fois le microdispositif et la languette de maintien.

Comme pour les techniques de fabrication additive, l'objectif est l'addition couche par couche d'un matériau métallique sur un substrat plan électriquement conducteur. Les ions métalliques peuvent être déposés sur des zones conductrices pré-définies du substrat (cathode), immergées dans un bain électrolytique, qui sont définies géométriquement par un matériau isolant prédéfini, dont l'épaisseur est déterminée par la vitesse de dépôt.

Un procédé en plusieurs étapes a été conçu, où la membrane trouée est d'abord fabriquée sur un substrat plan d'une épaisseur t_m. Par la suite, un second dépôt forme l'architecture cylindrique en faisant croître une couche épaisse définie par la longueur du cylindre L_C. Dans une dernière étape, le microdispositif résultant est libéré du substrat. Ce microdispositif est ensuite positionné mécaniquement sur la languette de maintien de sorte qu'il peut former un seul élément 3D où la membrane perforée fait face à l'écoulement perpendiculairement.

3.1.2 Stratégies pour former des dispositifs de type 3D

Nous avons imaginé la fabrication du microdispositif et de la languette au cours du même processus de dépôt afin que les deux pièces puissent adopter une configuration de type 3D similaire à celle du microdispositif 3D fabriqué dans un matériau polymère et décrit en détail dans la section précédente de ce manuscrit. De plus, nous avons également ciblé la conception de cette nouvelle génération de dispositifs d'une manière qui, en plus de la capture cellulaire, pourrait être facilement adaptée aux techniques de microscopie conventionnelles.

Nous avons envisagé deux stratégies pour atteindre une configuration de type 3D à partir de dispositifs planaires : a) une version permettant l'assemblage mécanique de jusqu'à six microdispositifs sur la languette métallique et b) une version pliable, où les deux pièces, la languette et un seul microdispositif, ont été fabriqués comme un seul substrat plan contenant un joint en forme de charnière qui permet au microdispositif d'être plié/déplié à 90°.

3.1.3 Contraintes de conception

L'ensemble composé du microdispositif métallique et de la languette, tant pour l'assemblage que pour la version pliable, a été conçu pour s'adapter à trois tailles différentes de cathéters : 18G, 20G ou 22G. La géométrie de la membrane trouée a été optimisée pour occuper la plus grande surface possible, afin d'augmenter la surface d'occupation de la membrane trouée.

Une deuxième contrainte a été donnée par la technique utilisée pour définir la zone de dépôt correspondant au cylindre du microdispositif. La structuration du matériau isolant a été réalisée par photolithographie UV, ce qui limite l'obtention de structures à rapport d'aspect élevé. Par exemple, pour obtenir la longueur attendue du cylindre L_C=150 µm, il fallait avoir une largeur minimale de 75 µm et un rapport d'aspect de 2:1. D'autres approches technologiques, comme le procédé LIGA, pouvaient offrir des rapports d'aspect plus élevés ; malheureusement, ce procédé n'était pas disponible dans notre infrastructure.

De plus, et comme troisième contrainte, nous voulions fabriquer le microdispositif et la languette en utilisant le même procédé. Nous avons déposé la couche correspondant au cylindre avec la languette de maintien, de sorte que l'épaisseur des languettes serait égale à la longueur du cylindre, soit 150 µm. Comme pour les microdispositifs en polymère, la taille des pores a également été fixée à 12 µm. De plus amples détails peuvent être trouvés dans la version anglaise de ce manuscrit.

3.1.4 Étapes de fabrication

Parmi les différents matériaux disponibles pour l'électrodéposition dans notre centrale technologique, nous avons choisi le Nickel. Ce métal est un matériau électrodéposé très répandu et il a déjà été utilisé comme plateforme pour l'isolement de CTCs et pour la culture cellulaire de fibroblastes. Dans la pratique, les dispositifs micro-ingénierés ont été fabriqués selon un procédé en 5 étapes, pour lequel trois étapes correspondent à la photolithographie UV et au dépôt électrochimique à travers le masque.

Un masque à trois niveaux a été conçu à l'aide du logiciel CleWin. Le premier niveau (L1) définit les rabats pliables pour le concept pliable. Dans ce niveau, nous avons également ajouté du texte afin de faciliter la reconnaissance des dispositifs microfabriqués une fois détachés du substrat. Le deuxième niveau (L2) forme la zone correspondant à la membrane perforée pour la version assemblée et pliable. Une zone de chevauchement, >20 µm, entre les niveaux un et deux, a été définie pour permettre le contact physique de ces dépôts métalliques ; ceci ne s'applique qu'à la version pliable. Le troisième niveau (L3) définit le cylindre du microdispositif et la languette. De même, pour le microdispositif, nous avons établi des zones de chevauchement d'adhésion d'une longueur >30µm entre le deuxième et le troisième niveau. En ce qui concerne la version pliable, une zone de chevauchement a également été définie pour relier les rabats et la languette de maintien. Grâce à cette technique, nous avons pu fabriquer des lots de plus de 300 pièces dans un délai de 3 jours. Le processus de fabrication détaillé se trouve dans la version anglaise de ce manuscrit.

3.1.5 Assemblage et pliage de dispositifs microfabriqués

Après avoir libéré les micropièces du substrat, ces dernières ont été rincées abondamment à l'eau et isolées manuellement. En ce qui concerne la version à assembler, les microdispositifs de capture ont d'abord été placés manuellement dans un support sur-mesure sous contrôle optique. Dans une deuxième étape, les ouvertures de la languette ont été faites pour coïncider avec les languettes d'insertion, et en appliquant une légère pression sur celle-ci, les microdispositifs et la languette ont été verrouillés mécaniquement. Afin d'assurer la fixation, une goutte de colle EP 630 (rapport 100:35) a été déposée sur la jointure.

En ce qui concerne la version pliable, un seul microdispositif a d'abord été placé sur le bord d'une surface plane, afin de la suspendre et de permettre un libre accès verticalement. Ensuite, sous contrôle optique et à l'aide d'une pince, nous avons appliqué manuellement une légère pression directement sur le bord extérieur du microdispositif afin de le faire se plier à 90° environ.

3.1.6 Capture cellulaire à l'aide de microdispositifs en nickel : évaluation in vitro

3.1.6.1 Capture cellulaire à partir d'un milieu de culture cellulaire

Afin d'évaluer la capacité de capture cellulaire de cette nouvelle génération de microdispositifs, nous avons d'abord évalué son intégration à des consommables médicaux commerciaux. Les microdispositifs en nickel ont été conçus à l'origine pour être insérés à travers des cathéters en plastique. Cependant, étant donné les tolérances restreintes que nous avons établies dans les dimensions pendant le processus de conception, les microdispositifs ne s'adaptaient pas facilement à la lumière du cathéter correspondant. Nous avons donc décidé de continuer à utiliser le système d'insertion à double aiguille introduit au début du chapitre II, suivant la même stratégie d'assemblage. Cette configuration permet de travailler directement avec la version 20G et la 22G et avec la 18G dans une moindre mesure.

Compte-tenu des limites susmentionnées, nous nous sommes particulièrement concentrés sur l'utilisation d'un modèle de petite taille, c'est-à-dire le 22G, pour un premier système expérimental in vitro, et pour une utilisation in vivo dans des modèles animaux à terme. Pour cet ensemble d'expériences, nous avons utilisé un seul microdispositif métallique sur chaque languette en gardant v_{min} comme condition d'écoulement pendant 10 min, dans le canal en PDMS de 3 mm. Nous avons décidé de préparer des suspensions de PC3-GFP en dessous de 5000 par mL en concentration cellulaire en utilisant le colorant Hoechst comme deuxième marqueur nucléaire.

Nous avons observé que les cellules capturées adhèrent à la membrane trouée en gardant une forme sphérique et en développant des protubérances ou pseudopodes. De plus, les cellules sont également restées attachées à la surface de la membrane trouée pendant le retrait à partir du canal fluidique, la fixation des cellules et les étapes de caractérisation après le piégeage. En accord avec les observations précédentes, la plupart des cellules piégées sont situées à la surface de la membrane trouée et non dans les pores.

Pour les cellules en suspension à une concentration inférieure, soit 1000 cellules par mL, nous avons constaté que le nombre moyen de cellules capturées était de C_C=11,2 ± 6,38 (moyenne ± écart-type, n=5). Nous avons simplement considéré les cellules exprimant à la fois la GFP et la coloration Hoechst, puis nous les avons identifiées par MEB. Nous avons également été en

mesure d'isoler des cellules à partir d'une suspension de 100 cellules par mL où le nombre moyen était C_C=6 ± 1,73 (n=3). De la même manière, nous avons également essayé des concentrations plus faibles, de l'ordre de 10 cellules par mL, mais aucune des expériences n'a clairement mis en évidence le piégeage de cellules PC3.

3.1.6.2 Capture cellulaire à partir de sang complet

Avant d'évaluer la capture des cellules, nous avons d'abord évalué le degré de contamination à l'intérieur de la membrane trouée lors du traitement d'échantillons de sang total sans cellules cancéreuses. Nous avons surtout observé des plaquettes adhérant à la surface trouée de la membrane et quelques cellules sanguines s'accumulant dans certains pores, correspondant probablement à des GB. Lorsque l'étape de rinçage a été mal effectuée, c'est-à-dire en utilisant un volume de milieu plus faible, on a observé un degré relativement plus élevé de contamination par des cellules sanguines. Dans le cas des BRC, nous croyons que cela résulte principalement de l'accumulation résiduelle et non du piégeage physique.

Dans une deuxième série d'expériences, nous nous sommes penchés sur la performance de capture d'un seul microdispositif métallique 22G à partir de cellules ajoutées à du sang total. En utilisant une concentration cellulaire de 1000 cellules PC3 par mL dans le sang total, nous avons identifié une valeur moyenne de C_C=2.83 ± 2.45 (n=5), où ces cellules ont d'abord été identifiées par microscopie à fluorescence, GFP et émission Hoechst, et ensuite par MEB.

Nous avons également évalué la capture de PC3 à partir de sang total à des concentrations cellulaires plus faibles, soit 100 cellules par mL. Ces expériences n'ont pas révélé la capture de cellules cancéreuses. Nous croyons qu'à cette gamme de concentrations, un durée expérimentale plus importante est nécessaire. Malheureusement, des expériences plus longues n'ont pas été réalisées, et des études supplémentaires sont donc encore nécessaires. Ces résultats pris dans leur ensemble, nous avons conclu que le seuil de sensibilité pour un seul microdispositif métallique 22G est de 1000 cellules PC3 par mL de sang.

3.1.6.3 Capture de cellules à partir de sang total à l'aide de plusieurs microdispositifs par languette

Dès la phase de conception, nous avons envisagé de placer plusieurs microdispositifs par languette afin d'augmenter la probabilité de capture cellulaire. La version assemblée permet l'évaluation de cette caractéristique ; par conséquent, nous avons assemblé des languettes ayant trois microdispositifs en série. Trois microdispositifs 22G ont été placés sur la languette avec un espacement de 2 mm. Nous avons utilisé une concentration de 1000 cellules cancéreuses par mL de sang, dans les conditions d'écoulement utilisées comme référence tout au long de ce manuscrit. A partir de cette expérience, nous avons identifié une quantité totale de cellules C_C=7 PC3 réparties entre les trois microdispositifs.

Une comparaison directe entre des microdispositifs simples et multiples, avec C_C=2,83 ± 2,45 et C_C=7 respectivement, suggère que l'intégration de plusieurs dispositifs par languette pourrait potentiellement entraîner la capture d'une plus grande quantité de cellules cancéreuses. Cependant, les données préliminaires présentées ici ne permettent pas de le prouver quantitativement, d'autres expériences sont donc nécessaires.

3.1.7 Capture de cellules à l'aide de dispositifs métalliques : évaluation in vivo

Comme dernière étape de cette partie du projet, nous avons programmé une nouvelle série d'expériences in vivo. Notre objectif principal était de démontrer la capture de cellules cancéreuses véritablement en circulation, entraînées dans la circulation sanguine par le cœur. Un deuxième objectif était de confirmer la robustesse des microdispositifs de capture métalliques pour résister à l'ensemble de la procédure. Un troisième était de déterminer si nos résultats in vitro seraient transposables à un environnement in vivo, en termes de capture cellulaire.

Pour cet ensemble, quatre rats mâles ont été soumis à une intervention chirurgicale. Les expérimentations animales ont été menées dans le cadre des directives de soins aux animaux, sur la plateforme de zootechnie du CHU de Rangueil à Toulouse, et avec le soutien de Denis Calise pour l'intervention chirurgicale.

Les microdispositifs de capture utilisés pour cet ensemble provenaient de la version assemblée, plaçant trois microdispositifs sur chaque languette. Les languettes ont été adaptées au système d'insertion à double aiguille tel qu'il a été réalisé in vitro. Ci-après, cet assemblage sera appelé dispositif intravasculaire (DIV).

Initialement, nous voulions injecter des cellules PC3 en suspension dans le corps de l'animal afin d'obtenir une concentration approximative de 25 000 cellules par mL de sang en circulation. Pour ce faire, nous avons préparé des suspensions cellulaires de cellules cancéreuses PC3-GFP marquées au Hoechst à ~$1x10^6$ cellules par mL dans du milieu de culture dans un volume total de 500 µL.

Tous les animaux ont été soumis indépendamment à une préparation pré-chirurgicale et une laparotomie xyphopubienne a été pratiquée, les détails sont donnés dans la version anglaise de ce manuscrit. Une fois l'intervention chirurgicale effectuée, la veine cave a été perforée avec l'aiguille externe du système d'insertion à double aiguille. Immédiatement après, la suspension de cellules PC3 a été injectée dans la région sélectionnée comme indiqué ci-dessus. Environ une minute après la perfusion cellulaire, les microdispositifs de capture ont été exposés au flux sanguin à l'aide du piston de la seringue pendant 3 minutes. Après ce temps d'exposition, les microdispositifs ont été rétractés dans l'aiguille de ponction et le dispositif intravasculaire a été retiré de la veine cave.

Pour tous les animaux, nous avons confirmé la présence de cellules PC3 dans le système circulatoire. Cependant, des quatre dispositifs intravasculaires utilisés chez les animaux, il a été possible d'identifier la capture de cellules PC3 dans le DIV-4. En utilisant la microscopie à fluorescence, nous avons quantifié un total de cellules C_C=4 PC3 dont une a été trouvée en D1, deux en D2 et une en D3.

3.1.8 Conclusions de la partie I

La première partie de ce chapitre présente la stratégie principale suivie pour fournir un microdispositif de capture de cellules 3D robuste et mécaniquement résistant, afin de relever les défis mis en évidence dans le chapitre II. Nous avons conçu des microdispositifs ayant un nombre maximisé de pores pour augmenter la probabilité de capture cellulaire. Nous avons également décrit deux stratégies simples pour former des microdispositifs de capture métalliques de type 3D à partir de techniques de fabrication planaire, qui, à l'instar de la conception présentée au chapitre II, ont été conçues pour répondre aux exigences médicales de l'accès intraveineux. Dans cette première section, nous avons détaillé la conception technique et le processus de fabrication ainsi que les défis rencontrés.

Nous avons évalué la performance de capture cellulaire de ces microdispositifs métalliques, montés dans le système d'insertion veineuse à façon présenté au chapitre II, à la fois dans un fluide idéal et dans du sang total. Il est intéressant de noter que la limite de détection des cellules cancéreuses dans le sang total se situe dans une plage de concentration cellulaire similaire à celle du microdispositif 3D présenté au chapitre II. Compte-tenu de ces résultats et en combinaison avec des simulations informatiques, nous avons identifié des variables géométriques du microdispositif qui pourraient améliorer la stabilisation de l'écoulement dans la zone d'intérêt. Cependant, nous croyons qu'une meilleure compréhension de la dynamique des fluides, fondée sur des données numériques et expérimentales, fournirait des voies d'amélioration du dispositif intravasculaire.

Nous avons suggéré l'utilisation de plusieurs microdispositifs de capture par languette unique, ce qui a permis d'établir expérimentalement les premières preuves d'une amélioration de la performance globale de capture des cellules. Suite à cette stratégie de microdispositifs multiples, nous avons démontré avec succès, pour la première fois, la capture de cellules cancéreuses dans le sang d'un modèle animal. Globalement, ces résultats fournissent des preuves solides de l'utilisation potentielle des microdispositifs 3D pour isoler des CTC de la circulation sanguine. Nous sommes conscients qu'une étude beaucoup plus systématique et approfondie de la performance de capture des cellules est encore nécessaire, en particulier dans la gamme des concentrations rapportées dans la littérature dans le sang des patients atteints d'une maladie cancéreuse. Par conséquent, le développement technologique, les protocoles et les résultats préliminaires présentés ici pourraient servir de point de départ pour de futurs essais cliniques.

Comme l'application du concept de filtration in vivo représente un défi majeur, nous avons proposé un concept alternatif ex vivo, qui est également basé sur la microfiltration du sang pour l'isolement des cellules cancéreuses sur la base de leurs propriétés physiques intrinsèques dans des conditions d'écoulement physiologiquement pertinentes. Ce concept alternatif pourrait être facilement intégré par la communauté médicale au chevet du patient. C'est pourquoi la deuxième partie de ce chapitre est consacrée à son introduction.

3.2 Partie II : Filtres portatifs à base de métal pour le sondage du sang ex vivo à haut débit

3.2.1 Concept général : la transcendance d'un filtre portable

Comme présenté dans le chapitre II, en utilisant le banc d'essai, l'occlusion partielle d'un canal fluidique par un microdispositif de filtration permet la capture de cellules cancéreuses à un niveau relativement bas ΔP dans un système fluidique en boucle fermée. Suivant le principe d'isolement de cellules cancéreuses à partir de sang total dans des conditions d'écoulement physiologiquement pertinentes, nous avons envisagé une approche ex vivo innovante dans laquelle un filtre, ayant des dimensions de l'ordre du millimètre, pourrait effectuer la capture des cellules cancéreuses avec une performance améliorée tout en conservant des conditions de fonctionnement à basse pression. Contrairement à l'approche in vivo où les dimensions globales étaient limitées à quelques centaines de micromètres, par la taille de la veine et la stratégie de ponction veineuse, cette approche ex vivo n'a pas de contraintes dimensionnelles.

Nous avons également conçu ce filtre comme portable, ce qui signifie qu'il pourrait être intégré dans des consommables en contact avec le sang disponibles dans le commerce utilisés en routine clinique, ou toute autre plateforme similaire, afin d'effectuer la capture des cellules cancéreuses et ensuite retiré du consommable pour une caractérisation cytomorphologique. De plus, la portabilité de ce filtre pourrait potentiellement permettre d'effectuer une analyse fonctionnelle in situ du matériel biologique capturé. Le concept d'adaptabilité est une perspective innovante, prévoyant, par exemple, un filtre effectuant un sondage sanguin continu par dérivation ex vivo similaire aux systèmes d'hémodialyse, mais surtout, sans l'utilisation d'un pompage externe. Une autre application alternative du concept d'adaptabilité peut être d'effectuer la capture des cellules cancéreuses en même temps que la prise de sang de routine, en tirant partie du vide des tubes sous vide comme système de pompage.

Cette approche pourrait permettre un suivi plus systématique de l'évolution de la maladie en routine clinique. De plus, elle pourrait potentiellement répondre aux exigences d'un dispositif au chevet du patient. Les travaux présentés dans les sous-sections suivantes sont préliminaires et visent principalement à démontrer la faisabilité technologique plutôt qu'à offrir une preuve quantitative des concepts susmentionnés.

3.2.2 Conception du filtre portable

Nous avons utilisé une tubulure à double extrémité (BD Vacutainer) comme support pour le filtre portable. Ce support est un consommable disponible dans le commerce et est utilisé de manière standard en routine clinique pour la collecte de sang dans les tubes sous vide. Nous avons envisagé de placer le dispositif portable dans la lumière d'un raccord Luer Slip mâle. Afin de permettre un positionnement correct du filtre, nous avons usiné quatre rainures sur le raccord d'origine.

La lumière du connecteur Luer mâle a un diamètre d'environ 2,3 mm, c'est pourquoi nous avons choisi comme diamètre principal du filtre portable D=2,2 mm. Afin d'éviter le colmatage, nous avons conçu un filtre équipé de grandes ouvertures permettant une circulation continue d'une partie du fluide, pendant que le reste du courant est filtré. Nous avons placé quatre ouvertures symétriques représentant environ 25 % de la section transversale de la lumière du connecteur.

Les pores ont été placés au centre du dispositif portable avec une distribution uniforme et symétrique. La zone de filtration est définie par des puits de 200 µm, ce qui confère au filtre une topographie en 3D. Au début de ce projet, deux designs ont été proposés : a) un filtre contenant cinq puits indépendants et b) un filtre contenant cinq puits interconnectés. A ce stade initial, nous avons fixé le diamètre du pore à 10 µm pour les deux designs. La surface totale de la région filtrante représente moins de 2 % de la section transversale de la lumière.

L'approche technologique utilisée pour leur fabrication a également été mise en œuvre en utilisant l'électrodéposition multicouche de métal, présentée dans la première partie de ce chapitre. Deux dépôts de nickel ont été mis en œuvre. L'épaisseur de L1 a été fixée à 5 µm tandis que l'épaisseur de L2 correspondant au support a été fixée à 150 µm.

3.2.3 Capture de PC3 à partir de sang complet à travers le filtre portable

Nous avons évalué les capacités de capture des cellules cancéreuses de ces modèles à l'aide de suspensions de cellules cancéreuses PC3-GFP colorées au Hoechst dans le sang total. La rotation a été adaptée afin d'obtenir une vitesse à l'intérieur du support similaire à la vitesse minimale trouvée in vivo, v_{min}=0,072 m s^{-1}.

Les premières expériences ont montré que le design à cinq puits interconnectés a permis d'obtenir un plus grand nombre de cellules capturées. Nous pensons que cela est lié au nombre élevé de pores. En utilisant ce design, nous avons réussi à détecter des cellules PC3 à partir de suspensions cellulaires à une concentration de 10 cellules PC3 par mL de sang total seulement. Comme prévu, l'utilisation de suspensions plus concentrées a permis d'obtenir une plus grande quantité de cellules capturées. Il est intéressant de noter que les cellules capturées étaient réparties uniformément sur toute la surface filtrante. Cet ensemble préliminaire de résultats suggère que pour capturer un plus grand nombre de cellules cancéreuses, la surface filtrante doit être maximisée sur toute la surface de soutien disponible. Sur la base de ces prémisses, nous avons conçu une nouvelle génération de dispositifs portables.

3.2.4 Filtres portables avec une surface de filtration maximisée

Comme mentionné ci-dessus, nous avons envisagé de fabriquer des filtres portables avec une couverture maximale des pores. En conservant les mêmes dimensions d'encombrement, nous avons réduit l'ouverture de moitié par rapport aux designs précédents, ce qui donne environ 12 % de la section transversale de la lumière. La surface filtrante représente environ 5 % de la section transversale de la lumière.

Les résultats préliminaires, utilisant des cellules PC3-GFP colorées au Hoechst en suspension dans un milieu de culture cellulaire à une concentration de 2000 cellules par mL, ont démontré que ces prototypes ont été en mesure d'isoler plus de 400 cellules dans une expérience de 10 minutes. Il est intéressant de noter que les cellules capturées se trouvent principalement à la surface du filtre et que leur morphologie semble être préservée.

Les données obtenues jusqu'à présent ne permettent pas de conclure sur le rapport de surface optimal entre les zones traversantes et les zones filtrantes. Nous croyons qu'il existe un seuil pour lequel la capture des cellules cancéreuses peut être maximisée sans que le filtre représente une résistance significative à l'écoulement, dans les conditions d'écoulement actuelles. Il est

nécessaire de mieux comprendre la dynamique des fluides pour laquelle des simulations informatiques sont actuellement effectuées.

3.2.5 Viabilité cellulaire des PC3 dans les substrats en Nickel

Nous avons utilisé un test colorimétrique, le test MTT, pour évaluer la viabilité des cellules PC3 en culture directement en contact avec des substrats de nickel. Dans cette expérience, nous avons évalué la viabilité cellulaire par rapport à différents substrats de Ni et matériaux de revêtement de surface. Pour ce faire, nous avons utilisé des filtres portables fabriqués en Nickel et ensuite recouverts d'héparine et/ou d'or (<50 nm). De plus, et à des fins de comparaison, nous avons également fabriqué des filtres portables fabriqués avec un polymère photosensible (DryFilms Resist).

Les expériences ont été réalisées en triplicats et ont été suivies pendant 72 heures.

À partir de ces expériences, nous avons observé que le nickel pur présente des niveaux de viabilité plus élevés que les autres conditions évaluées. De manière surprenante, le revêtement Or présente les niveaux de viabilité les plus bas. Nous pensons que c'est le résultat du processus de dépôt puisque le bain d'électrodéposition utilisé contient un complexe cyanuré, connu pour être cytotoxique. De plus, pour les échantillons de nickel pur, nous avons observé une forte adhérence des cellules sur l'ensemble de la surface, ce qui suggère la compatibilité cellulaire de ce matériau. D'autres expériences sont nécessaires pour confirmer ces données préliminaires.

3.2.5 Conclusions de la partie II

Dans la deuxième partie de ce chapitre, nous avons introduit un filtre portable qui, compte-tenu de ses dimensions et de sa conception, peut être facilement intégré à des consommables médicaux en contact avec le sang utilisés comme standard en routine clinique. Le filtre a été conçu et envisagé comme une plateforme potentielle pour des études in situ du matériel biologique capturé.

Sur la base de l'optimisation technologique réalisée pour la fabrication de microdispositifs métalliques de type 3D présentés dans la première partie de ce chapitre, nous avons également fabriqué les filtres portables proposés. Ces filtres ont détecté des concentrations de cellules cancéreuses de 10 cellules cancéreuses par mL de sang total seulement. Sur la base de ces résultats, nous étudions actuellement la performance de capture de la deuxième génération de filtres portables, où la surface de filtration a été maximisée. D'autres expériences et perspectives en cours concernant cette approche de capture sont présentées dans la section correspondant aux conclusions et perspectives de ce manuscrit.

Author: Alejandro Kayum JIMENEZ ZENTENO

Title: Engineered micro-devices for the isolation of circulating tumor cells in clinical routine

Thesis director: Christophe VIEU and Aline CERF

Date and place of the defense: 21st September 2018, LAAS-CNRS

Summary

Circulating tumor cells (CTCs) are believed to represent the main pathway of cancer dissemination in the human body through the circulatory system. These cells have the ability to detach from the primary tumor, enter into the bloodstream, and survive in this environment. A specific subpopulation of these cells possesses the capacity of colonizing new tissues and forming metastases. The relevance of these rare cells in the bloodstream has been intensively investigated during the last decades, finding that phenotypic and genomic information they carry could be correlated with that of solid biopsies. Moreover, the number and incidence of CTCs in metastatic patients could be used as an indicator for prognosis. Thus, their isolation from blood samples and analysis has been proposed as a surrogate to solid biopsies, having the added value of being a less invasive procedure and allow a more repeated measure. In fine, the routine analysis of CTCs in clinical practice could be used for the real-time monitoring of therapies and the adaptation of treatment in order to improve the outcome of patients, a step forward towards so-called precision medicine. In this PhD project, we have developed novel micro-devices for the capture, in flow conditions, of tumor-derived cells from human whole blood. CTCs being larger and less deformable than normal blood cells, we exploited theses physical traits to discriminate them. Sieve-like micro-devices were engineered to selectively sort out tumor-derived cells having as a priority the preservation of cell integrity and viability. In addition, devices were designed to allow direct access to the isolated biological material and thus perform in situ cell identification, such as immunocytochemistry, but also to potentially serve as a platform for functional analysis. We proposed two approaches compatible with clinical routine. The first approach consists in a customized guiding-strip equipped with integrated microfilters, designed to be introduced directly within the bloodstream through a conventional medical catheter to perform the capture of tumor-derived cells in vivo. The second approach aims to perform CTC isolation ex vivo through the integration of microfilters into a platform compatible with blood collection medical sets. Both technological developments were validated using a cancerous cell line suspended in either cell culture medium or whole blood. Our in vivo approach was optimized using a customized fluidic bench mimicking an artificial human vein and was tested successfully in an animal model. This prototype demonstrated its robustness and capability to capture tumor-derived cells in concentrations within the range found in metastatic patients. This sensitivity appraisal was carried out for the ex vivo approach, demonstrating analogous capture performances. We believe that these technologies could enable repeated and reliable CTC detection for prognosis and monitoring of treatment efficiency in metastatic patients.

Keywords: liquid-biopsy, CTCs, cancer-monitoring, microfabrication, microfiltration, 3D-microdevices

---

Discipline: Nanophysics

Auteur: Alejandro Kayum JIMENEZ ZENTENO
Titre: Micro-dispositifs pour l'isolement des cellules tumorales circulantes en routine clinique
Directeur de thèse: Christophe VIEU and Aline CERF
Lieu et date de soutenance: 21 Septembre 2018, LAAS-CNRS

Résumé

Les cellules tumorales circulantes (CTCs) sont la principale voie de dissémination du cancer dans le corps humain au travers de la circulation sanguine. Ces cellules ont la capacité de se détacher de la tumeur primaire, de rejoindre la circulation sanguine et de survivre dans cet environnement. Une sous-population spécifique de ces cellules a la capacité de coloniser de nouveaux tissus et de former des métastases. L'importance de ces cellules rares dans la circulation sanguine a été intensément étudiée au cours des dernières décennies, et il a été constaté que les informations phénotypiques et génomiques qu'elles contiennent pourraient être corrélées avec celles obtenues à partir d'une biopsie tissulaire. De plus, le nombre et l'incidence des CTC chez les patients métastatiques pourraient être utilisés comme indicateurs pronostics. Ainsi, leur isolement à partir d'échantillons sanguins et leur analyse a été proposé en remplacement des biopsies conventionnelles, comme une alternative moins invasive et permettant un échantillonnage plus répété. In fine, la détection et l'analyse des CTC en routine clinique pourraient être utilisées pour le suivi en temps réel des thérapies et de leur efficacité pour améliorer la prise en charge des patients, un pas de plus vers une médecine de précision. Dans ce projet de thèse, nous avons développé de nouveaux micro-dispositifs pour la capture, sous flux, de cellules cancéreuses à partir de sang complet humain. Nous avons exploité les propriétés physiques des CTC, plus grandes et moins déformables que les cellules sanguines normales, pour discriminer ces cellules rares (<1 cellule par mL aux premiers stades de la maladie). Des micro-dispositifs ont été conçus tels des tamis à trois dimensions pour filtrer sélectivement les cellules cancéreuses tout en préservant l'intégrité et la viabilité des cellules. De plus, les dispositifs ont été conçus pour permettre l'accès au matériel biologique isolé et effectuer ainsi une identification des cellules in situ, e.g. par immunocytochimie, mais aussi potentiellement pour servir de plateforme pour une analyse fonctionnelle de ces cellules. Nous avons proposé deux approches totalement compatibles avec la routine clinique. La première consiste en un guide équipé de microdispositifs, conçu pour être introduit directement dans la circulation sanguine au travers d'un cathéter médical et effectuer la capture des cellules cancéreuses in vivo. La deuxième approche vise à réaliser l'isolement des CTCs en utilisant des microdispositifs intégrés à des plateformes ex vivo compatibles avec les consommables médicaux de prélèvement sanguin. Les deux développements technologiques ont été validés en utilisant des cellules issues de lignée cancéreuse en suspension dans un milieu de culture cellulaire ou dans du sang complet Notre approche in vivo a été optimisée sur la base d'observations réalisées à l'aide d'un banc fluidique mimant une veine artificielle et a été testée avec succès in vivo dans un modèle animal. Ce prototype a démontré sa robustesse et sa capacité à capturer des cellules cancéreuses à des concentrations proches des concentrations en situation métastatique. Une évaluation de la sensibilité a été réalisée de la même manière pour l'approche ex vivo, démontrant des performances de capture analogues. Nous croyons que ces technologies pourraient permettre des prélèvements de CTC de manière répétée et fiable pour le pronostic et le suivi thérapeutique des patients métastatiques.

Keywords: biopsie liquide, CTCs, surveillance du cancer, microfabrication, microfiltration, microdispositifs 3D

Discipline: Nanophysique